

**University of Strathclyde**  
**Department of Pure and Applied Chemistry**

**Development of Small Molecule  
Colorimetric Sensors for the  
Determination of Mercury in Aqueous  
Media**

By

**Klthom M. A. Nshnsh**

A thesis submitted to the Department of Pure and Applied Chemistry,  
University of Strathclyde in partial fulfilment of the requirements for the  
degree of Doctor of Philosophy

September 2018

‘This thesis is the result of the author’s original research. It has been composed by the author and has not been previously submitted for examination which has led to the award of a degree.’

‘The copyright of this thesis belongs to the author under the terms of the United Kingdom Copyright Acts as qualified by University of Strathclyde Regulation 3.50. Due acknowledgement must always be made of the use of any material contained in, or derived from, this thesis.’

## **Dedication**

To my dear parents, who have been always a source of encouragement and inspiration to me throughout my life, a very special thanks for your support and unconditional love.

To my dear husband Khaled, for his continued love, practical and emotional support, and understanding during my pursuit of my PhD degree. You were always around at times I thought that it is impossible to continue. I greatly value your contribution and deeply appreciate your belief in me.

To my angels Bessan, Omar and Mohamed, for being so supportive, patient - even when being there 'without Mum' was hard. I consider myself the luckiest in the world to have such lovely kids in my life.

This work is for you and because of you. Thanks for always being there for me.

## **Acknowledgements**

All praise to Allah, the Almighty, for giving me the strength and the composure to prepare and complete this dissertation with good health and sound mind.

First and foremost, I would like to express my deepest gratitude to my supervisor, Dr Christine M Davidson. Her support, encouragement, expertise and patience provided me necessary insight at every phase of my work. Without her kind supervision and proper guidance, this project would simply not have been completed perfectly.

My special gratitude goes also to Dr Lorraine T Gibson (second supervisor) for her valuable support and guidance throughout this study.

I also extend my thanks to the Ministry of Higher Education and Scientific Research/Libya for their financial support all the way through this work.

I acknowledge my indebtedness to Dr Mark Spicer, for his assistance and helping out during the synthesis stage.

My appreciation goes to the UK National Crystallography Service and Dr Alan Kennedy for the use of the crystallography service.

I also owe a great deal of gratitude to Dr Mark Dunlop, senior lecturer in computer science, for his valuable contribution and assistance in the development of the mobile system.

Finally, special thanks go to my colleagues and office mates in the Analytical Chemistry Research Group, all the staff, trainers, who spared their time generously, namely; Mr Alex Clunie, Mr Craig Irving and Mrs Mara Knapp for their guidance, help and suggestion whenever needed.

# Table of Contents

<b>Abbreviations</b> .....	xi
<b>Abstract</b> .....	xiii
<b>1. Introduction</b> .....	1
1.1. Mercury in the environment.....	1
1.2. The chemistry of Hg .....	2
1.3. Biogeochemical cycling of Hg in the environment.....	3
1.4. Bioaccumulation of Hg in the food chain .....	5
1.5. Human exposure and health effects associated with Hg exposure.....	7
1.5.1. Routes of human exposure.....	7
1.5.2. Toxicity of Hg in humans .....	9
1.6. The regulation of Hg exposure.....	13
1.7. Analytical methods for sensitive determination of Hg .....	14
1.8. Mercury screening methods .....	15
1.8.1. The need for Hg screening methods.....	15
1.8.2. Portable X-ray fluorescence spectroscopy .....	16
1.8.3. Colorimetric sensors of Hg detection.....	17
1.8.3.1. Organic dye-based sensors.....	17
1.8.3.2. Complex-based sensors.....	22
1.8.3.3. Polymer-based sensors.....	25
1.8.3.4. Nanoparticle-based sensors.....	28
1.9. Immobilisation of the colorimetric sensors in solid supports .....	33
1.9.1. Paper-based colorimetric sensing.....	35
1.9.2. Microfluidics paper-based devices ( $\mu$ PAD).....	36
1.10. Aim of the study.....	38
<b>2. Theory of applied analytical techniques and statistical analysis</b> .....	40
2.1. Ultraviolet-visible reflectance/transmittance spectroscopy .....	40
2.1.1. The principle of ultraviolet-visible spectrophotometry.....	40
2.1.2. The absorption spectrum.....	41
2.1.3. Absorbance law .....	43
2.1.4. Components of a spectrophotometer.....	44
2.2. Charge-coupled devices (CCDs).....	46
2.2.1. Basic of operation .....	46

2.2.2.	Colour CCD image sensors.....	47
2.3.	Data handling approaches .....	47
2.3.1.	The arithmetic mean.....	47
2.3.2.	Measures of spread.....	48
2.3.3.	Accuracy and precision of analysis.....	48
2.3.4.	Limit of detection.....	49
2.3.5.	Correlation coefficient and the coefficient of determination .....	49
2.4.	Statistical analysis of data .....	50
2.4.1.	Significance testing.....	50
2.4.1.1.	F-test .....	50
2.4.1.2.	T-test .....	51
<b>3.</b>	<b>General experimental procedures .....</b>	<b>53</b>
3.1.	Cleaning procedure .....	53
3.2.	Determination of Hg <sup>2+</sup> based on the reaction with copper iodide (CuI) .....	53
3.2.1.	Reagents and apparatus.....	53
3.2.2.	Procedures.....	54
3.2.2.1.	Solutions preparation .....	54
3.2.2.2.	Conditioning of detecting papers .....	54
3.2.2.3.	Determination of Hg <sup>2+</sup> as spot test .....	54
3.2.2.4.	Determination of Hg <sup>2+</sup> using the Hg bubbler apparatus of Yallouz <i>et al.</i> .....	55
3.3.	Determination of Hg <sup>2+</sup> based on the reaction with diphenylcarbazone (DPC)... ..	56
3.3.1.	Reagents and apparatus.....	56
3.3.2.	Procedures.....	56
3.3.2.1.	Solutions preparation .....	56
3.3.2.2.	Determination of Hg <sup>2+</sup> in solution phase.....	57
3.3.2.3.	Determination of Hg <sup>2+</sup> as spot test .....	57
3.4.	Determination of Hg <sup>2+</sup> based on the reaction with rhodamine 6G (R6G).....	57
3.4.1.	Reagents and apparatus.....	57
3.4.2.	Procedures.....	58
3.4.2.1.	Solutions preparation .....	58
3.4.2.2.	Determination of Hg <sup>2+</sup> in solution phase.....	59
3.4.2.3.	Determination of Hg <sup>2+</sup> as spot test .....	59
3.5.	Determination of Hg <sup>2+</sup> based on the reaction with rhodamine B thiolactone .....	59
3.5.1.	Reagents and apparatus.....	59

3.5.2.	Procedures.....	60
3.5.2.1.	Synthesis of rhodamine B thiolactone.....	60
3.5.2.2.	Identification of rhodamine B thiolactone .....	61
3.5.2.3.	Solutions preparation .....	67
3.5.2.4.	General procedure for Hg <sup>2+</sup> determination in aqueous solution.....	68
3.5.2.5.	Determination in anti biotic assay discs.....	68
3.6.	Immobilisation of rhodamine B thiolactone in solid matrices and determination of Hg <sup>2+</sup> on the coloured membranes.....	68
3.6.1.	Reagents and apparatus .....	68
3.6.2.	Procedures.....	69
3.6.2.1.	Solutions preparation .....	69
3.6.2.2.	Preparation of sol-gel membrane .....	69
3.6.2.3.	Preparation of agar-agar gel membrane .....	69
3.6.2.4.	General procedure for colour development.....	70
3.6.2.5.	Data processing and analysis .....	71
<b>4.</b>	<b>Characterisation and application of small molecule colorimetric sensors for Hg<sup>2+</sup> determination .....</b>	<b>72</b>
4.1.	Introduction.....	72
4.2.	Aim .....	76
4.3.	Experimental.....	77
4.3.1.	Reagents and apparatus.....	77
4.3.2.	Solutions preparation .....	77
4.3.3.	Determination of Hg <sup>2+</sup> based on the reaction with CuI.....	77
4.3.3.1.	Determination of Hg <sup>2+</sup> as spot test .....	77
4.3.3.2.	Determination of Hg <sup>2+</sup> using the Hg bubbler apparatus.....	77
4.3.3.3.	Method characterisation.....	78
4.3.4.	Determination of Hg <sup>2+</sup> based on the reaction with DPC .....	79
4.3.4.1.	Determination of Hg <sup>2+</sup> in solution phase.....	79
4.3.4.2.	Determination of Hg <sup>2+</sup> as spot test .....	79
4.3.4.3.	Determination of Hg <sup>2+</sup> using the Hg bubbler apparatus.....	79
4.3.5.	Determination of Hg <sup>2+</sup> based on the reaction with R6G .....	79
4.3.5.1.	Determination of Hg <sup>2+</sup> in solution phase.....	80
4.3.5.2.	Determination of Hg <sup>2+</sup> as spot test .....	80
4.3.5.3.	Determination of Hg <sup>2+</sup> using the Hg bubbler apparatus.....	80
4.4.	Results and discussion .....	80

4.4.1.	Determination of $\text{Hg}^{2+}$ based on the reaction with CuI.....	80
4.4.1.1.	Assessment of $\text{Hg}^{2+}$ detection in spot test mode .....	80
4.4.1.2.	Determination of $\text{Hg}^{2+}$ using the Hg bubbler apparatus.....	81
4.4.1.3.	Standard concentration differences for colour discrimination .....	82
4.4.1.4.	Visual evaluation of the effect of storage conditions on the colour fading.....	83
4.4.1.5.	UV-visible diffuse reflectance spectra of $\text{Cu}_2[\text{HgI}_4]$ complex.....	83
4.4.1.6.	UV-visible reflectance spectra for characterisation of $\text{Cu}_2[\text{HgI}_4]$ colour fading.....	85
4.4.1.7.	Within-sample variability of quantitative measurements.....	86
4.4.1.8.	Stability of CuI detecting papers.....	88
4.4.2.	Determination of $\text{Hg}^{2+}$ based on the reaction with DPC .....	89
4.4.2.1.	Determination of $\text{Hg}^{2+}$ in solution phase.....	89
4.4.2.2.	Determination of $\text{Hg}^{2+}$ as spot test .....	90
4.4.2.3.	Determination of $\text{Hg}^{2+}$ using the Hg bubbler apparatus.....	93
4.4.3.	Determination of $\text{Hg}^{2+}$ based on the reaction with R6G .....	93
4.4.3.1.	Determination of $\text{Hg}^{2+}$ in solution phase.....	93
4.4.3.3.	Determination of $\text{Hg}^{2+}$ using the Hg bubbler apparatus.....	99
4.5.	Conclusion .....	100
<b>5.</b>	<b>Rhodamine B thiolactone-based naked-eye sensor for rapid determination of <math>\text{Hg}^{2+}</math> in natural waters .....</b>	<b>104</b>
5.1.	Introduction.....	104
5.2.	Aim .....	106
5.3.	Experimental.....	107
5.3.1.	Reagents and apparatus .....	107
5.3.2.	Synthesis of rhodamine B thiolactone.....	107
5.3.3.	Solutions preparation .....	107
5.3.4.	General procedure for $\text{Hg}^{2+}$ determination in aqueous solution.....	107
5.3.5.	The determination on antibiotic assay discs.....	108
5.3.6.	Stability of solid rhodamine B thiolactone.....	108
5.3.7.	Optimisation of sensing conditions.....	108
5.3.8.	Limit of detection and range of method.....	108
5.3.9.	Interferences of other ions.....	108
5.3.10.	Method application in seawater .....	109
5.3.11.	Assessment of $\text{Hg}^{2+}$ detection in spot test mode .....	109

5.4.	Results and discussion .....	109
5.4.1.	Stability of solid rhodamine B thiolactone.....	109
5.4.2.	Optimisation of sensing conditions.....	111
5.4.3.	Limit of detection and range of method.....	115
5.4.4.	Interferences of other ions.....	117
5.4.5.	Method application in artificial seawater.....	121
5.4.6.	Assessment of Hg <sup>2+</sup> detection in spot test mode .....	122
5.5.	Conclusion .....	124
<b>6.</b>	<b>Immobilisation of rhodamine B thiolactone in solid matrices and determination of Hg<sup>2+</sup> on the coloured membranes .....</b>	<b>126</b>
6.1.	Introduction.....	126
6.2.	Aim .....	129
6.3.	Experimental.....	129
6.3.1.	Reagents and apparatus.....	129
6.3.2.	Solutions preparation .....	130
6.3.3.	Preparation of sensing gel membranes.....	130
6.3.4.	General procedure for colour development and data analysis .....	130
6.3.5.	Selection of agar-agar membrane strength.....	130
6.3.6.	Optimisation of water sample .....	131
6.3.7.	Optimisation of colorant reagent.....	131
6.3.8.	Membrane stability and reactivity.....	131
6.3.9.	Method application .....	132
6.3.10.	Recycling of sensor discs with KI.....	132
6.4.	Results and discussion .....	133
6.4.1.	Chromogenic analysis of the colorimetric responses.....	133
6.4.2.	Optimisation of sensing response on the agar-agar membrane.....	135
6.4.2.1.	Selection of agar-agar gel colloid concentration.....	135
6.4.2.2.	Optimisation of sample volume pumped through agar-agar papers .....	140
6.4.2.3.	Optimisation of colorant reagent volume added to 5 mL agar colloid....	142
6.4.3.	Analytical performance.....	143
6.4.3.1.	Sol-gel membrane detection limit and linear range .....	144
6.4.3.2.	Agar-agar gel membrane detection limit and linear range.....	145
6.4.4.	Membrane stability and reactivity.....	149
6.4.4.1.	Sol-gel membrane stability and reactivity.....	149
6.4.4.2.	Agar-agar membrane stability and reactivity .....	151

6.4.5.	Method application .....	153
6.4.5.1.	Investigation of the signal suppression .....	155
6.4.5.2.	Investigation of the effect of dissolved organic carbon (DOC) on sensor uptake.....	161
6.4.5.3.	Treatment of sample with AgNO <sub>3</sub> to remove Cl <sup>-</sup> .....	163
6.4.6.	Recycling of agar-agar membrane with KI.....	165
6.5.	Conclusion .....	166
<b>7.</b>	<b>Development of a portable smartphone colorimetric readout device .....</b>	<b>168</b>
7.1.	Introduction.....	168
7.2.	Aim .....	169
7.3.	Experimental .....	170
7.3.1.	Reagents and apparatus .....	170
7.3.2.	Solutions preparation .....	170
7.3.3.	Preparation of agar-agar membranes .....	170
7.3.4.	General procedure for colour development and data analysis .....	170
7.4.	Results and discussion .....	171
7.4.1.	Lightproof box design and Hg-Sense App data processing .....	171
7.4.2.	Evaluation of the proposed portable method .....	172
7.4.2.1.	Method performance with and without homemade lightproof box.....	172
7.4.2.2.	Comparison of the portable smartphone reader with use of a scanner....	175
7.4.2.3.	Evaluation of the portable peristaltic pump .....	177
7.4.3.	Sensitivity of Hg <sup>2+</sup> quantitation using iPhone Hg-Sense App .....	178
7.4.4.	Recovery of developed portable method for Hg <sup>2+</sup> detection.....	181
7.5.	Conclusion .....	182
<b>8.</b>	<b>Conclusions and further work .....</b>	<b>184</b>
8.1.	Conclusion .....	184
8.2.	Further work.....	188
	References.....	191
	Appendix 1.....	202
	Appendix 2.....	207
	Appendix 3.....	211
	Appendix 4.....	213
	Appendix 5.....	224

## Abbreviations

[ <i>bis</i> (2,2'-bipyridyl-4,4'-dicarboxylate)ruthenium (II) <i>bis</i> (tetrabutylammonium) <i>bis</i> (thiocyanate)]	N719
[(2,2':6',2''-terpyridine-4,4',4''-tricarboxylate)ruthenium(II) tris(tetrabutylammonium) tris(isothiocyanate)]	N749
2,2'-azino- <i>bis</i> (3-ethylbenzothiazoline-6-sulfonic acid) diammonium salt	ABTS
Boron-dipyrromethene	BODIPY
Charge coupled devices	CCD
Colorimetric-solid phase extraction	C-SPE
Complementary colours; cyan, magenta, yellow, and green	CMYG
Cuprous iodide	CuI
Cuprous mercury iodide	Cu <sub>2</sub> [HgI <sub>4</sub> ]
Diphenylcarbazone	DPC
Diphenylcarbazide	DPCI
Diphenylcarbadiazone	DPCDO
Dissolved gaseous mercury	DGM
Dissolved organic carbon	DOC
Environmental protection agency	EPA
Gold nanoparticles	AuNPs
Gold nanorods	AuNRs
Grey in the green channel	GG
Grey in the red channel	GR
Grey in the blue channel	GB
High dynamic range	HDR
Inductively coupled plasma mass spectrometry	ICP
Intermolecular charge transfer	ICT
Lactone	L form
Limit of detection	LOD
Localised surface plasmon resonance	LSPR
Metal-oxide-semiconductor	MOS
Microfluidics paper-based devices	μPAD
Minimal risk level	MRL
Papain coated-gold nanoparticles	P-AuNPs
Portable network graphic	PNG
Portable X-ray fluorescence spectroscopy	pXRF
Potentially toxic elements	PTE
Primary colours; red, green and blue	RGB
Reference dose	R <sub>d</sub>
Rhodamine 6G	R6G
Rhodamine B base 3',6'- <i>bis</i> (diethylamino)-2-(2-oxoethylideneamino)-spiro[isoindoline-1,9'-xanithen]-3-one	RHO

Semi-squaraine dye	SSQ
Semi-quantitative method	SQM
Silver nanoparticles	AgNPs
Silver nanoplates	AgNPLs
Si-rhodamine B thiolactone	Si-RBS
Specific UV absorbance at 254 nm	SUVA <sub>254</sub>
Surface plasmon resonance	SPR
World health organisation	WHO
Zwitterion	Z form

## Abstract

While a number of colorimetric sensors are available for the detection of  $\text{Hg}^{2+}$ , lack of sensitivity or selectivity, complicated synthetic routes and difficulty in adaptation for field application, are common drawbacks. Consequently, this thesis describes the development of readily synthesised, robust, selective, sensitive, cost-effective, small molecule colorimetric sensors for  $\text{Hg}^{2+}$  detection in water.

The reaction between  $\text{Hg}^{2+}$  and off-the-shelf chromogenic reagents, cuprous iodide (CuI), diphenylcarbazone (DPC) and rhodamine 6G (R6G), was studied in solution; in spot test mode (as wet reagents and dried onto filter papers); and in a Hg-bubbler apparatus. Both DPC and R6G produced a colorimetric response in solution and wet spot test mode, but bleaching and oxidation affected the response in dry spot mode. The Hg-bubbler apparatus was found applicable to R6G and CuI. However, reduction of reagents in the field is proved difficult.

Rhodamine B thiolactone (RBT) was synthesised. It exhibited high selectivity for  $\text{Hg}^{2+}$ , with reasonable visual and spectrophotometric detection limits. A disadvantage was that the solid was undergo ring-opening reaction unless stored at low temperature away from light. The RBT was immobilised in sol-gel and agar-agar matrixes with filter paper substrate. Pumping  $\text{Hg}^{2+}$  solutions through these membranes changed their colour. Images of the membranes were recorded and analysed using a flatbed scanner and ImageJ software. Based on the grayscale intensity in the green channel, the detection limits were 0.4 and 0.2  $\mu\text{g/L}$  for the sol-gel and agar-agar membranes, respectively. The method was used to quantify  $\text{Hg}^{2+}$  in real water samples. Interference due to the presence of  $\text{Cl}^-$  was noted.

Finally, a portable platform was developed. Images of RBT doped agar-agar membranes were captured using the camera of a mobile phone, together with a homemade lightproof box, and a bespoke “Hg-Sense” app. Results were generally acceptable and can be applied by regulation authorities.

# 1. Introduction

## 1.1. Mercury in the environment

Potentially toxic elements (PTEs) exist in the environment through natural processes. However, environmental contamination by PTE as a result of the rapid development of agriculture, traffic, and modern industries is a significant concern. Due to their hazardous nature, many PTE are investigated in research dealing with environmental safety, health-related issues in humans and food quality. In common with other PTE, As, Cd, Hg and Pb, are not biodegradable, and cannot be easily detoxified. Consequently, they can contaminate humans and animals as a result of accumulating in the environment.<sup>1</sup> According to the Agency for Toxic Substances and Disease Registry (ATSDR), Hg is one of the most dangerous and toxic elements.<sup>2</sup> Mercury is a pollutant of global concern that rapidly spreads all over the environment from its natural and anthropogenic sources. Natural inputs to the atmosphere include weathering of rocks and dust particles from mercuriferous areas, volcanic gases, forest fires, as well as oceanic emission.<sup>3, 4</sup> The common anthropogenic sources of Hg include fossil fuel combustion, gold production, coal mining, chemical manufacturing and solid waste incineration.

Almost half of the Hg produced from natural sources is released from the oceans, approximately  $2.68 \times 10^6$  kg of Hg per year.<sup>5</sup> In addition, 13% of Hg emissions from natural sources is emitted from biomass combustion, e.g., forest fires, which is responsible for about 675 tons of Hg per year.<sup>5</sup>

The anthropogenic Hg emission in 2015 was very similar to that in 2010.<sup>6</sup> Artisanal and small-scale gold mining (ASGM) and coal combustion are the largest anthropogenic sources of Hg pollution as they are responsible for about 38% and 21% of anthropogenic emissions, respectively. These are followed by non-ferrous metal production emission (about 15%) and cement production (about 11%).<sup>6, 7</sup> The global atmospheric Hg emission by sector is illustrated in Fig. 1.1.

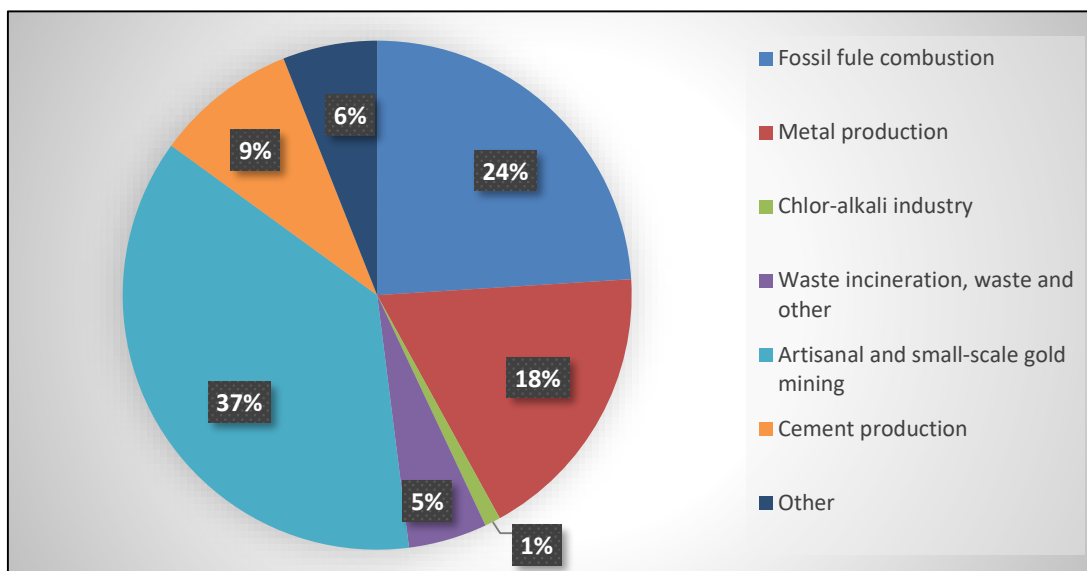


Figure 1.1: Global atmospheric Hg emissions by sector.

## 1.2. The chemistry of Hg

Mercury is the only liquid metal at ambient temperature and pressure. It is a heavy, silvery-white metal. It is rarely found as a pure element in nature.<sup>8</sup> It can exist in three valence states, elemental  $\text{Hg}^0$ , mercurous  $\text{Hg}^+$ , and mercuric  $\text{Hg}^{2+}$ . The  $\text{Hg}^0$  has several commercial applications including dental fillings and thermometers. It is easily evaporated into  $\text{Hg}^0$  vapour. Elemental mercury is more common in the atmosphere while  $\text{Hg}^{2+}$  is more common in aquatic systems. Mercurous ion is rare in the environment as a result of its chemical instability. The  $\text{Hg}^{2+}$  valence state of Hg is the most stable and can complex strongly with organic and inorganic ligands.<sup>9</sup>

Mercury complexes with a variety of ligands ( $\text{Cl}^-$ ,  $-\text{SH}$ ,  $\text{S}^{2-}$ ,  $\text{OH}^-$ , organic matter) influence its mobility and availability. The common forms of inorganic Hg are mercuric chloride and mercuric sulfide. Among the organic compounds of Hg, such as ethylmercury and phenylmercury, the common forms in the environment are methylmercury compounds,  $\text{CH}_3\text{Hg}^+\text{X}^-$ , which are often collectively referred to as methylmercury (MeHg). The MeHg is the most toxic form of Hg and is more easily bioaccumulated due to being lipid soluble.<sup>5</sup> Methylmercury is formed under reducing conditions, primarily by sulfate-reducing bacteria.<sup>10</sup>

### 1.3. Biogeochemical cycling of Hg in the environment

The different forms of Hg are widely spread and cycle through all phases of the environment (in air, sediment, soil, water). Once Hg is released to the atmosphere in gaseous form by either natural or anthropogenic sources, it may be transported great distances and can be deposited immediately or retained for several months in the atmosphere prior to deposition on the Earth's surface through a process known as the mercury cycle.<sup>11</sup> A portion of Hg emissions is attached to suspended mineral particles from soil and rocks and these too can remain in the atmosphere. After circulation through the atmosphere, Hg is deposited in both wet and dry forms. Dry deposition occurs by removing the Hg from the atmosphere through the settling of non-soluble material, e.g., dust. Wet deposition occurs through precipitation of Hg by either rain or snow. Wet and dry depositions occur in both aquatic and terrestrial situations.

The deposited Hg settles underwater or on land by gravity. However, wet and dry deposition from the atmosphere is the greatest source of Hg in the aquatic system (90%).<sup>12, 13</sup> Once Hg enters a body of water, it is subject to various biogeochemical processes. This includes oxidation-reduction reactions, precipitation-dissolution, complexing with various ligands, methylation-demethylation, desorption-adsorption to suspended particulate matter, sedimentation-resuspension, leaching and transport to other destinations through streams, and uptake by aquatic biota.<sup>14</sup> Although there are many studies on the behaviour of Hg in the water column, the levels of different Hg species, as well as their concentration profiles are still limited.

Mercury species in the aquatic environment include dissolved  $\text{Hg}^{2+}$ , dissolved gaseous Hg (DGM), and particulate Hg species ( $\text{Hg}_p$ ).<sup>15</sup> Generally,  $\text{Hg}^{2+}$  is the predominant form found in water. It can undergo photochemical reduction to  $\text{Hg}^0$ , present as inorganic and organic complexes.

The DGM is mainly (>90%) composed of  $\text{Hg}^0$  in the surface water.<sup>16</sup> In surface water,  $\text{Hg}^0$  undergoes volatilisation through the water-air exchange and this mechanism is a significant part of the Hg cycle.<sup>17</sup> The oxidation of  $\text{Hg}^0$  to  $\text{Hg}^{2+}$  can occur both photochemically and biologically. Additionally, DGM may also include MeHg and ethylmercury. However, the concentrations of these forms are not significant in surface waters.

In addition to undergoing redox transformations,  $\text{Hg}^{2+}$  can transform to MeHg by the action of methylating microorganisms at low oxygen and pH levels and in the presence of high amounts of organic matter. This process is known as biomethylation. Methylmercury rather than  $\text{Hg}^{2+}$  is bioconcentrated, it is taken up by organisms at various levels in the food chain. Demethylation also occurs both biologically and photochemically.<sup>16</sup> The sedimentation process traps particles rich in  $\text{Hg}_p$  within layers, and the sediment with the trapped  $\text{Hg}_p$  can be transported to other destinations through streams. The trapped  $\text{Hg}_p$  in sedimentary rocks can be washed away or carried to other destinations as a result of the erosion of the rock layers. It also can be re-suspended into the water or diffuse out of the sediment. Subsequently, Hg can both return to the atmosphere through volatilisation and/or begin to accumulate in the food chain; thus the Hg cycle continues on.<sup>8, 18</sup> A general scheme of Hg transformations in the environment,<sup>19</sup> is shown in Fig. 1.2.

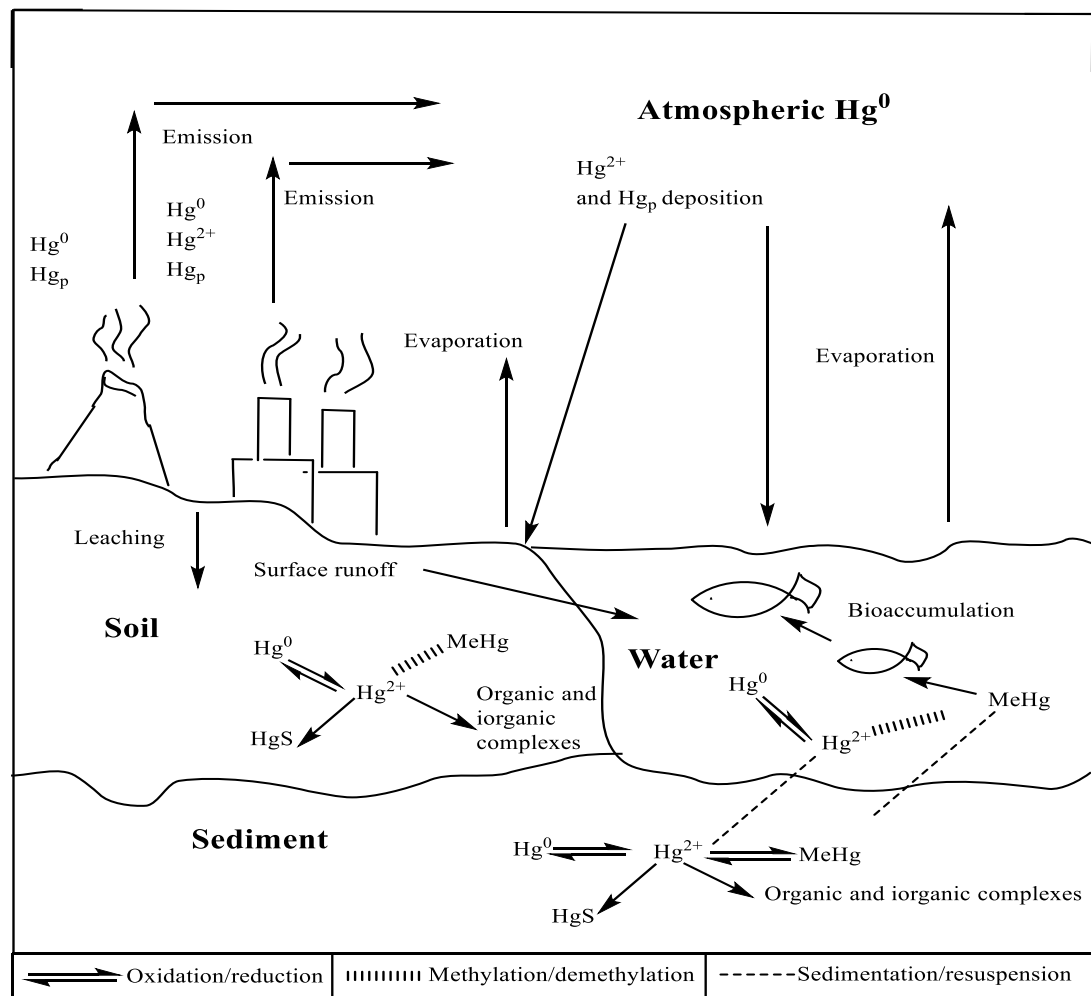
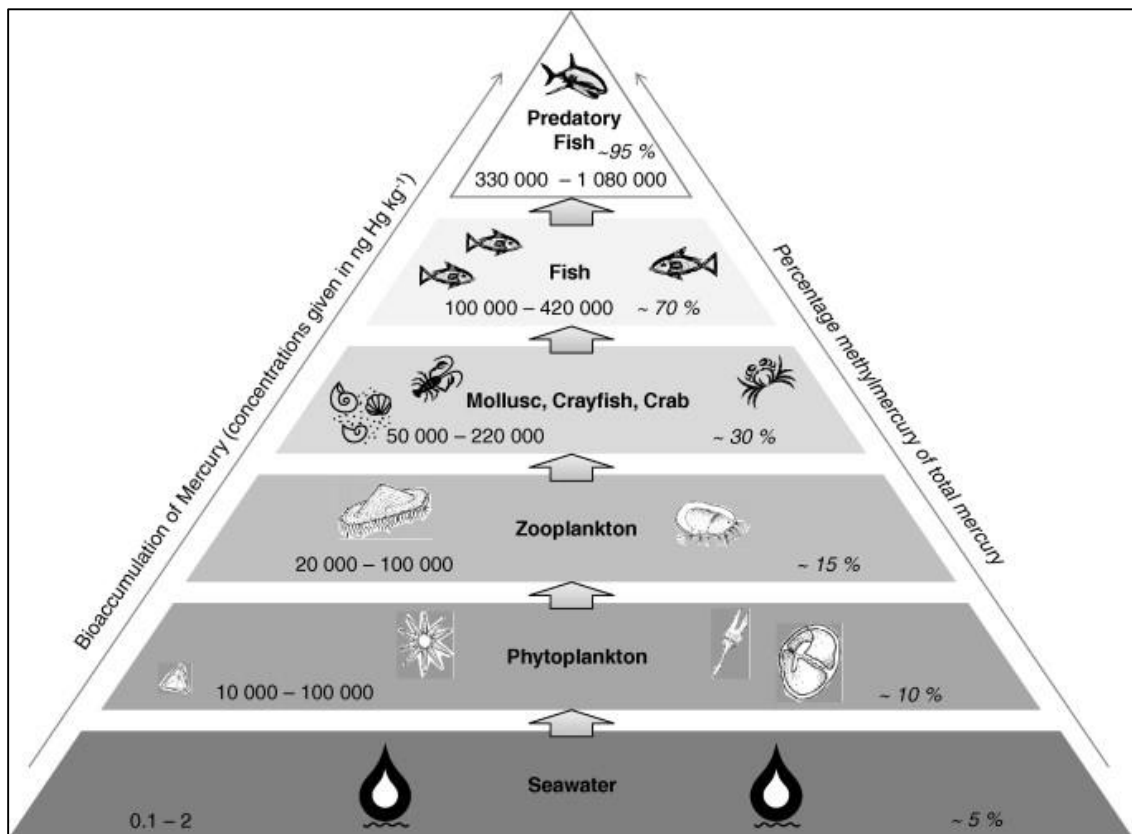


Figure 1.2: The biogeochemical cycling of Hg in the environment.

#### **1.4. Bioaccumulation of Hg in the food chain**

Human population, animals and plants are exposed to Hg during its cycle by direct contact and by consumption of Hg-contaminated food. The health effects of Hg exposure vary depending on its speciation, with each species targeting different organs. In higher animals,  $\text{Hg}^0$  is poorly absorbed in the digestive tract. Indeed, less than 0.01% of  $\text{Hg}^0$  that passed through the digestive system is absorbed and even that is rather quickly eliminated. Large quantities of  $\text{Hg}^{2+}$  would require to be swallowed to cause toxicity.<sup>20</sup> When it enters the environment,  $\text{Hg}^{2+}$  can be bio-transformed by bacteria to MeHg which is absorbed completely within the digestive system and hence bioaccumulated efficiently through the food chain.<sup>21</sup> Accumulation of Hg in living tissue occurs when the rate of uptake exceeds the rate of elimination. Significantly, MeHg requires several months or even years to be eliminated from living tissues. The absorption of MeHg can be connected to the daily diet, such as consumed Hg-contaminated fish.

Fish are exposed to MeHg mainly through their diet, bioaccumulation occurs as a result of assimilation of MeHg into their tissues. Following absorption through the digestive system MeHg enters the bloodstream and is distributed to organs and tissues in the body. Liver, kidney and spleen are the first places that MeHg accumulates, then redistribution to the brain tissue and muscle occurs later. In birds and mammals, most of the Hg in the kidney and liver is in a form of  $\text{Hg}^{2+}$  because they are capable of detoxifying MeHg through demethylation. However, MeHg can be found in the brain and skeletal muscle. The concentration of Hg is typically higher in larger and older individual animals as those tend to eat higher trophic position prey.<sup>4, 22, 23</sup> Fig. 1.3 shows the bioaccumulation of Hg in the food chain.



**Figure 1.3: Bioaccumulation of Hg in marine food chain.<sup>22</sup>**

Another source of MeHg accumulation in the food chain is agriculture. During the biogeochemical cycle, Hg is deposited by wet and dry processes to the land. The surface layers of the soil can become enriched with Hg as it can be trapped by organic matter. The background concentration of Hg in soil ranges from between 0.03 to 0.1 mg/kg, with an average concentration of 0.06 mg/kg. Soil can become heavily polluted in areas such as Hg mining districts. Crops grown in Hg-contaminated soil uptake the Hg from the soil to their tissues, thus Hg can be accumulated in the human body through the food chain. Studies have shown that MeHg can be absorbed strongly and accumulate in rice seed to unsafe levels. In rice, the concentration of MeHg can be as high as 174 µg/kg. Thus, crops contaminated with Hg are considered to be a significant route of Hg exposure to local residents at contaminated sites.<sup>11, 24</sup>

## 1.5. Human exposure and health effects associated with Hg exposure

### 1.5.1. Routes of human exposure

Inhalation of Hg vapour, dental amalgam and medical treatments, drinking water and ingestion of Hg-contaminated food are the most common potential sources of exposure to Hg in the general population.<sup>25</sup> Consumption of MeHg-contaminated fish is the most important route of non-occupational exposure to Hg. However, other foodstuffs contribute to MeHg exposure in some individual contaminated areas, which include ingestion of contaminated vegetables, cereals, or meat.<sup>26</sup> Exposure to Hg<sup>0</sup> in the general population is relatively low, but some groups experience higher non-occupational exposure, often related to dental amalgams, cultural practices or occupational exposures.<sup>27</sup> Although most Hg present in dietary uptake is in the form of MeHg, some Hg<sup>2+</sup> may also exist. Non-occupational sources causing exposure to Hg<sup>2+</sup> may include consuming contaminated fish, drinking water, ingestion or contact with contaminated soil.<sup>26</sup> Average non-occupational exposure is summarised in Table 1.1.

**Table 1.1: Estimated average of non-occupational exposure and daily intake of Hg.<sup>26</sup>**

Source of exposure	Daily intake and retention (µg/day) for various types of Hg		
	Hg <sup>0</sup>	Hg <sup>2+</sup>	MeHg
<b>Air</b>	0.04-0.2 (0.03-0.16)	Minimal	0.008 (0.0069)
<b>Dental amalgam</b>	1.2-27 (1.0-21.6)	0	0
<b>Food</b>			
<b>-Fish (100 g/week containing 0.2 mg Hg/kg)</b>	0	0.60 (0.06)	2.4 (2.3)
<b>- Other</b>	0	3.6 (0.36)	0
<b>Drinking water</b>	0	0.05 (0.005)	0
<b>Total</b>	1.2-27 (1-22)	4.3 (0.43)	2.41 (2.31)

Inhalation of Hg vapour in the workplace is considered as the main source of occupational exposure to Hg<sup>0</sup>.<sup>28</sup> Individuals and workers in industries involving the processing or dealing with the element are at the highest risk of Hg exposure. Those

include workers manufacturing fluorescent lights, thermometers, house painters, dental staff, individuals involved in recycling or disposal of Hg-contaminated wastes and chemists analysing environmental samples containing Hg.<sup>29</sup> Gold extraction by Hg-amalgamation also involves another population at risk of exposure to Hg. Studies found that the exposure to Hg is not found only in the gold mine workers, who are exposed frequently to Hg vapour during amalgamation, but all the communities of gold mining areas have a high risk of exposure to Hg<sup>0</sup>, Hg<sup>2+</sup> and MeHg.<sup>30, 31</sup>

Two significant examples of non-occupational exposure of the general public to Hg occurred in Minamata, Japan and in Iraq.<sup>32</sup> Poisoning with MeHg was recognised in Minamata, Japan between 1932 and 1968. A local chemical plant's acetaldehyde production factory discharged Hg effluent into Minamata Bay. In the 1950s the local residents, fisher folk and their families who depended on the fish and shellfish in the bay were poisoned by MeHg that accumulated in the fish. High level of Hg exposure contributed to at least 50,000 people being affected with a serious neurological disease, about 50 deaths and more than 2000 cases of Minamata disease in infants born to mothers with high Hg levels. Infants born with Minamata disease were suffering from blindness, brain damage, cerebral palsy and incoherent speech.<sup>33</sup> However, as a result of negligible Hg monitoring at that time, information on the effects, exposure biomarkers and risk assessment were not provided.<sup>27</sup>

In 1971 and 1972, epidemics of Hg poisoning occurred in Iraq as a result of consumption of grain that had been treated with organomercurial fungicides.<sup>27</sup> These were the largest outbreak of MeHg poisoning that has ever occurred. Barley and wheat seeds treated with seed dressing agents containing Hg were distributed in Iraq. An unknown quantity of these seeds was used to feed sheep and to make bread. The first person was admitted to hospital in December 1971 who was suffering from MeHg poisoning.<sup>34</sup> Four months later, 6530 patients had been admitted to hospitals across the country, and there were 459 deaths as a result of poisoning by MeHg.<sup>35</sup> However, because the hospitals became overcrowded and there were no effective treatments offered, these numbers are an underestimate of the total number of cases.

### 1.5.2. Toxicity of Hg in humans

All forms of Hg are toxic and harmful to wildlife and humans. The nature of this hazard is represented in the obstructing of thiol groups in enzymes and proteins as a result of Hg's strong affinity for S-containing ligands. There is not enough data available for all Hg forms to conclude that they cause cancer in humans. However, the United States Environmental Protection Agency, U.S. (EPA) has determined that MeHg and Hg<sup>2+</sup> are a possible human carcinogen.<sup>36</sup> A list provided by the ATSDR for the substances that can cause major human health problems indicates that As, Cd, Hg, and Pb are the most toxic PTE, as well as being among the most toxic substances, Table 1.2. This substance priority list classified the harmful substances according to both their toxicity and through potential human exposure.<sup>37</sup>

**Table 1.2. The ATSDR substance priority list of some PTE**

2017 Rank	Substance
1	As
2	Pb
3	Hg
7	Cd

Substances (4 to 6) are organic compounds not PTE.

The toxic influence of Hg on human health is well documented.<sup>38, 39</sup> The hazards associated with Hg depend on the level of exposure, the form of Hg, and the effects on target cells. There are two different types of toxicity: acute toxicity and chronic toxicity. Acute toxicity is caused by sudden exposure to a large dose, whereas chronic toxicity is attributable to low dose exposure over a long time. However, each type causes different effects and symptoms. Generally, Hg acute toxicity symptoms include vomiting, severe abdominal pain, muscular weakness, headaches, mood swings, sleep disturbance, depression, and slowed nerve functions or memory loss. These symptoms are likely to be reversible after termination of exposure. Permanent damage of the digestive system, kidneys and nervous system are the most reported chronic toxicity effects of Hg.<sup>40</sup>

Approximately 80% of  $\text{Hg}^0$  is absorbed through inhalation, while only 0.01% is absorbed following the oral digestion.<sup>31</sup> On absorption in the human body,  $\text{Hg}^0$  is widely distributed to fat-rich tissues. The absorbed  $\text{Hg}^0$  may be oxidised to  $\text{Hg}^{2+}$  which binds to thiol groups in proteins and enzymes and interferes with their function causing toxicity and damage to the target organs.<sup>26</sup> The oxidised  $\text{Hg}^{2+}$  accumulates primarily in the kidneys. Exposure to  $\text{Hg}^0$  gives rise to lung and kidney damage. Although dermal absorption is reported to be limited, direct contact with  $\text{Hg}^0$  may cause eczema. Also, it has been reported that the  $\text{Hg}^0$  from amalgam dental filling may cause several symptoms known as amalgam disease.<sup>41</sup>

Ingestion is the most common route of exposure to  $\text{Hg}^{2+}$ . High doses on a single occasion are associated with symptoms including diarrhoea, necrosis of the gastrointestinal tract, and severe abdominal pain leading to death.<sup>25</sup> Within 24 hours after ingestion, damage in the stomach and intestines, and kidney failure may occur. However, occasional effects have been reported in lung, liver, and heart function.<sup>31</sup>

Methylmercury is associated with acute nephron-neurotoxicity in humans. Poisoning with MeHg has a period of 2-4 weeks following severe exposure which may lead to death. Consumed MeHg-contaminated food is the main exposure route as about 95% of MeHg is absorbed through the gastrointestinal tract.<sup>24, 31</sup> The fatal doses in human are not known, however a value of 10 to 60 mg/kg body weight has been estimated.<sup>25</sup> After entering the bloodstream, MeHg tends to form small molecular weight thiol complexes that allow its transportation into cells and distribution to all tissues including the brain. Like  $\text{Hg}^0$ , MeHg may be oxidised in the body to  $\text{Hg}^{2+}$ . The accumulated Hg in the human body can cause disruption in adrenal and thyroid hormone systems, damage to the central nervous system, DNA, and motor disorders.<sup>41</sup>

In general, two groups are likely to be more affected by Hg exposure: foetuses and pregnant women who consume Hg-contaminated fish and shellfish. The most famous example of chronic exposure to MeHg is Minamata disease. Methylmercury moves easily through the placenta into the blood of the foetus, then distributes to the child's brain and other tissues.<sup>25</sup> The foetus's nervous system and brain can be affected adversely by MeHg exposure. Symptoms related to fine motor skills, constriction of

the visual field, irregular gait, cognitive thinking, and loss of memory and coordination in children may be attributed to those who were exposed to MeHg as foetuses.<sup>32</sup>

The second group is people who are regularly exposed to high levels of Hg; those include people who are occupationally exposed or populations that mainly rely on fish consumption. The accumulation of Hg in the food chain is a global concern and studies of selected subsistence fishing populations showed the association between cognitive impairment in children and the consumption of MeHg contaminated fish.<sup>32</sup> A summary of toxicity associated with exposure to different forms of Hg can be found in Table 1.3.

**Table 1.3. The toxicity associated with the different Hg forms.**<sup>42, 31, 26</sup>

Parameter	Hg <sup>0</sup>	Hg <sup>2+</sup>	MeHg
<b>Inhalation</b>	Approximately 80% absorption	Uncertain	Approximately 95% absorption
<b>Oral absorption</b>	Poor absorption approximately 0.01%	2-38% depend on Hg <sup>2+</sup> compounds	High absorption 95%
<b>Dermal absorption</b>	Average rate of absorption = 2.6%	Limited absorption. 2-3% depending on Hg <sup>2+</sup> compounds	Uncertain
<b>Distribution</b>	Because it is lipophilic, rapidly distributed throughout the body. Penetrates through blood-brain, and placental barriers readily	Highly accumulated in kidney. Does not penetrate through blood-brain or placental barriers readily	Because it is lipophilic 1-10% of the oral absorbed content distributes to blood; 90% of blood MeHg in RBCs. Penetrate through blood-brain, and placental barriers readily
<b>Biotransformation</b>	In tissue and blood Hg <sup>0</sup> oxidised to Hg <sup>2+</sup> by catalase and hydrogen peroxide	Following oral administration of Hg <sup>2+</sup> , Hg <sup>0</sup> vapour exhaled	Demethylation of MeHg slowly to Hg <sup>2+</sup> . Mechanisms of demethylation unknown
<b>Target organ</b>	Brain and kidney	Kidney	Brain, (adult and foetus )
<b>Causes of toxicity</b>	Oxidation of Hg <sup>0</sup> to Hg <sup>2+</sup>	Hg <sup>2+</sup> binds to thiol groups in proteins and enzymes and interferes with their function	Demethylation of MeHg to Hg <sup>2+</sup> and natural toxicity of MeHg
<b>Half-life elimination</b>	Approximately 60 days	Approximately 25 days, depends on Hg <sup>2+</sup> compounds	Approximately 70-80 days, depends on dose, species and sex
<b>Excretory route</b>	Excreted in faeces >50% and urine <50% as Hg <sup>2+</sup> . Excreted in exhalation, saliva, sweat and trans-placental transfer	Mainly excreted in faeces and urine; also excreted in exhalation, saliva, sweat, breast milk and trans-placental transfer	Major excretory rote is faeces approximately 90% as Hg <sup>2+</sup> , urine 10% as Hg <sup>2+</sup> , 16% in breast milk as MeHg. Also it is excreted in exhalation, saliva, sweat and trans-placental transfer

## 1.6. The regulation of Hg exposure

After the Minamata and Iraq incidents, global awareness has been raised concerning Hg exposure. The exposure level and the associated health effects of the Iraq incident were used to generate risk assessment data based on analytical results obtained from patients' hair as the main biomarker. Several environmental and health organisations have since contributed to defining the acceptable level of Hg exposure. However, each of these organisations assesses the exposure limit according to their individual parameters, resulting in disagreement about which study should be used.

For example, the EPA considered a value known as a reference dose ( $RfD$ ) which is the quantity of chemical ingested every day that does not cause harmful health effects.<sup>43</sup> In 2001 an  $RfD$  value of  $0.1 \mu\text{g}/\text{kg bw}/\text{day}$  (where bw is body weight) for MeHg was adopted by EPA based on the oral route data.<sup>43</sup> The ATSDR derived two minimal risk levels (MRLs) for inhalation and oral exposure, which are defined as the estimated daily human exposure to a chemical that is likely to be without adverse health effects over a duration of time. In 1999 the ATSDAR derived an MRL value of  $0.0002 \text{ mg}/\text{m}^3$  for inhalation exposure to  $\text{Hg}^0$  vapour, and an MRL of  $0.3 \mu\text{g}/\text{kg bw}/\text{day}$  for oral exposure to MeHg.<sup>25</sup> A number of international organisations have proposed tolerable daily intake (TDI) values for Hg inhalation and oral exposure route.

Based on a 70 kg adult inhaling  $20 \text{ m}^3$  of air a day, an intake of  $0.06 \mu\text{g}/\text{kg bw}/\text{day}$  for  $\text{Hg}^0$  was recommended as the tolerable daily intake TDI.<sup>31</sup> For  $\text{Hg}^{2+}$ ,  $2 \mu\text{g}/\text{kg bw}/\text{day}$  is recommended as the TDI by the International Programme on Chemical Safety and the World Health Organisation (WHO). A TDI of  $0.23 \mu\text{g}/\text{kg bw}/\text{day}$  for MeHg is recommended by the Joint FAO/WHO Expert Committee on Food Additives and the Committee on Toxicity of Chemicals in Food, Consumer Products and the Environment [UK].<sup>31</sup> However, these guideline values for the protection of human health cannot be applied to protect organisms that are exposed to Hg in the environment.

Because aquatic systems are the principle source for Hg re-emission, deposition and accumulation in living species, the potential effect of Hg on humans and the environment can be considered by monitoring the Hg concentration in water. Toxicity research efforts were directed towards defining an upper limit of allowable Hg

concentration in the water. The European Union and China regulated a  $\text{Hg}^{2+}$  level of  $1 \mu\text{g/L}$ ,<sup>25</sup> whereas EPA has set a maximum limit of  $2 \mu\text{g/L}$   $\text{Hg}^{2+}$  in drinking water,<sup>44</sup>  $1.4 \mu\text{g/L}$  in freshwater and  $1.8 \mu\text{g/L}$  in saltwater.<sup>45</sup> In 2004, WHO recommended a new guideline concentration for  $\text{Hg}^{2+}$  in drinking water of  $6 \mu\text{g/L}$  based on the theory that “almost all mercury in uncontaminated drinking-water is thought to be in the form of  $\text{Hg}^{2+}$ . Thus, it is unlikely that there is any direct risk of the intake of organic mercury compounds, especially of alkylmercurials, as a result of the ingestion of drinking-water”.<sup>46</sup>

Concern about human exposure to Hg *via* a variety of routes that include consumption of fish, dental amalgam and the workplace environment contributed to international effort to address Hg health and environmental effects. The Minamata Convention on Mercury in 2013 is a global treaty designed to provide international action to control and reduce Hg use and emission.<sup>47</sup> This includes controls on Hg emissions to the atmosphere and on releases to water, banning new Hg mines and phasing-out the existing ones, regulating the use of Hg in artisanal and small-scale gold mining, manufacturing processes, and the production of everyday items such as cosmetics, energy-saving light bulbs, batteries, dental amalgams, thermometers, cements, *etc.* The Minamata Convention provided that the Convention entered into force on August 2017.<sup>48</sup>

### **1.7. Analytical methods for sensitive determination of Hg**

Several traditional instrumental techniques have been applied for Hg identification and quantification, including atomic absorption spectrometry,<sup>49</sup> inductively coupled plasma mass spectrometry,<sup>50</sup> and cold vapour atomic fluorescence spectrometry.<sup>51</sup> Although several of these techniques have the advantage of low detection limit, excellent performance and accuracy, they are: expensive to both buy and run; not capable of on-site testing as they are too large to be field portable; and specialised personnel are required to carry out the operational procedure and interpret the data. Also, they generally need static infrastructure such as mains electricity. In addition to these issues, collection and transport of the sample to the laboratory, sample pre-treatment, and sometimes pre-concentration of the target elements in the sample, are required prior to the detection procedure being carried out. To protect human health

and the environment from the adverse effects of Hg, and support the requirements of developing legislation, advances in methods capable of Hg detection in environmental and biological samples are needed.

Inexpensive, lightweight, and rapid on-site analytical technologies are widely developed for *in-situ* detection of PTE in several environmental samples. In this regard, screening methods present an attractive option for cheap, sensitive, and qualitative detection for target analytes without the requirement to use expensive equipment.

## **1.8. Mercury screening methods**

### **1.8.1. The need for Hg screening methods**

Monitoring and quantitative determination of total Hg concentration are necessary to allow an assessment of the overall contamination. However, time consumption and cost can limit the use of several classical Hg detection techniques in many countries within Africa and Asia.<sup>32</sup> Further, in developing countries Hg is widely used in gold mining by ASGM communities. On a global basis, ASGM is the largest source of Hg pollution in air and water. During extraction, amalgam is formed which consists of approximately equal parts of Hg and gold. Following heating of the amalgam, Hg is evaporated into the atmosphere, leaving the gold. Eventually, the vaporised Hg settles in the soil and sediment of lakes, rivers, and oceans resulting in contamination of the food chain. Exposure to Hg in ASGM communities is associated with adverse health effects which not only affect ASGM workers, but also those in the communities surrounding the processing centres. According to the WHO, approximately 15 million people participate in the ASGM industry in 70 countries across Sub-Saharan Africa, East and Southeast Asia, and South America.<sup>52</sup> However, assessment of Hg contamination is not carried out regularly due to the expensive of analysis and limited resources. To overcome these limitations, there is a requirement for Hg screening methods. These methods involve less complicated sample preparation, together with rapid, inexpensive, and portable instrumentation. Therefore, the analysis can be carried out in the field which means a reduction in time and cost.

Over the last few decades, several sensors have attracted particular attention by offering rapid, on-site qualitative and quantitative information on Hg contamination. Three different types of sensors have been adopted, these are:

- Fluorescence sensors
- Electrochemical or potentiometric sensors
- Colorimetric sensors

Reviews can be found by Kim *et al.*<sup>53</sup>, Nolan *et al.*<sup>54</sup> and Choi *et al.*<sup>55</sup>.

Although highly sensitive determination of Hg can be achieved using fluorescence and electrochemical sensors, the latter has an interference issue between some ions.<sup>56</sup> Screening methods vary in cost, accuracy and limit of detection. Some of these techniques merely provide information on the presence or absence of Hg; others can give a semi-quantitative determination. Two screening methods that can easily be applied to environmental samples are portable X-ray fluorescence spectroscopy (pXRF), and colorimetric sensors.

### **1.8.2. Portable X-ray fluorescence spectroscopy**

portable X-ray fluorescence spectroscopy is a non-destructive technique that can be applied to a range of samples. This technique involves irradiating the material to be analysed with X-rays. When the energy of the X-ray is greater than the energy binding an electron to the nucleus, the electron is emitted from one of the atoms' inner shells. To become stable again, an electron from a higher energy level drops to the lower energy level, emitting the difference in energy as an X-ray.<sup>57</sup> Each atom emits a unique set of X-ray from which it can be identified. The number of X-rays counted is proportional to the concentration of the element. The technique is rapid and involves no extraction or digestion of the sample. Also, the use of portable instrumentation allows the technique to be implemented in the field giving a rapid screening result. However, the pXRF instruments are more expensive than colorimetric sensors, measure only discrete points where the beam focuses, and do not take matrix or surface variation into account. Dussubieux *et al.*<sup>58</sup> describe the capability of pXRF as “semi-quantitative at best”.

### 1.8.3. Colorimetric sensors of Hg detection

In general, colorimetric sensors are one of the most attractive approaches providing rapid and simple determination of Hg. Detection can be achieved through the correct combination of chromophores and receptors. The development of Hg receptors involves adapting selective indicators into strips, test papers and membranes without the requirement to use expensive equipment. The change in colour can be easily registered by the naked eye. A review of recent colorimetric sensors can be found in Yan *et al.*<sup>59</sup>, Chen *et al.*<sup>60</sup> and Wu *et al.*<sup>61</sup>

A wide range of colorimetric sensors have been developed for Hg<sup>2+</sup> detection, based on a specific chemical reaction between a highly selective sensor molecule and the target species. However, further study is required to ensure such sensors are stable, sensitive, and selective to the target element. The following sections highlight recent developments in colorimetric sensors for Hg<sup>2+</sup> determination according to their receptors.

#### 1.8.3.1. Organic dye-based sensors

Because most of the organic dye based sensors possess the advantages of scalable and facile synthesis, photophysical properties, and solution processability, several organic dye materials with tunable optical properties have attracted attention and been used as colorimetric chemosensors. These include squaraine, rhodamine and polyether based sensors.

Squaraine and its derivatives are one of the most attractive colorimetric molecules that are applied for detecting PTE. In particular, the molecules can absorb strongly in the red to near IR region as a result of their rigid D- $\pi$ -A- $\pi$ -D conjugation. Excluding absorption in the visible region can improve the sensitivity of detection in the near IR region. For example, the implementation of semi-squaraine dye (SSQ) has been demonstrated by Avirah *et al.*<sup>62</sup> as a novel sensor for Hg<sup>2+</sup> determination, (Fig. 1.4). On addition of Hg<sup>2+</sup> to a SSQ solution, the colour changes from deep yellow to colourless.

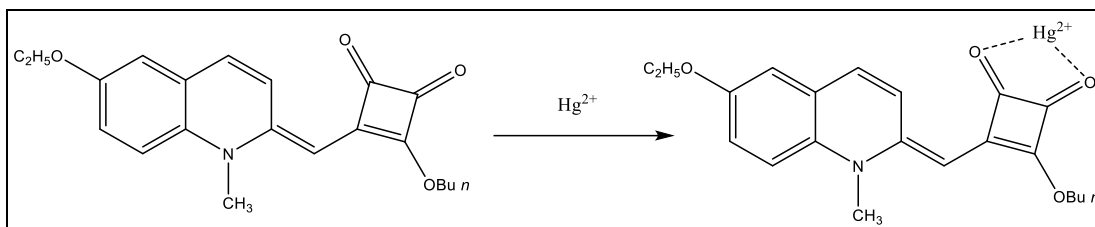


**Figure 1.4: Proposed mechanism of formation for SSQ-Hg<sup>2+</sup>.**

Chen *et al.*<sup>63</sup> developed a probe based on a Hg<sup>2+</sup>-mediated squaraine dye disaggregation mechanism, Fig. 1.5. The sensor is non-fluorescent due to the formation of an H-aggregate. However, upon addition of Hg<sup>2+</sup>, an obvious colour change from light-blue to intense purple takes place.

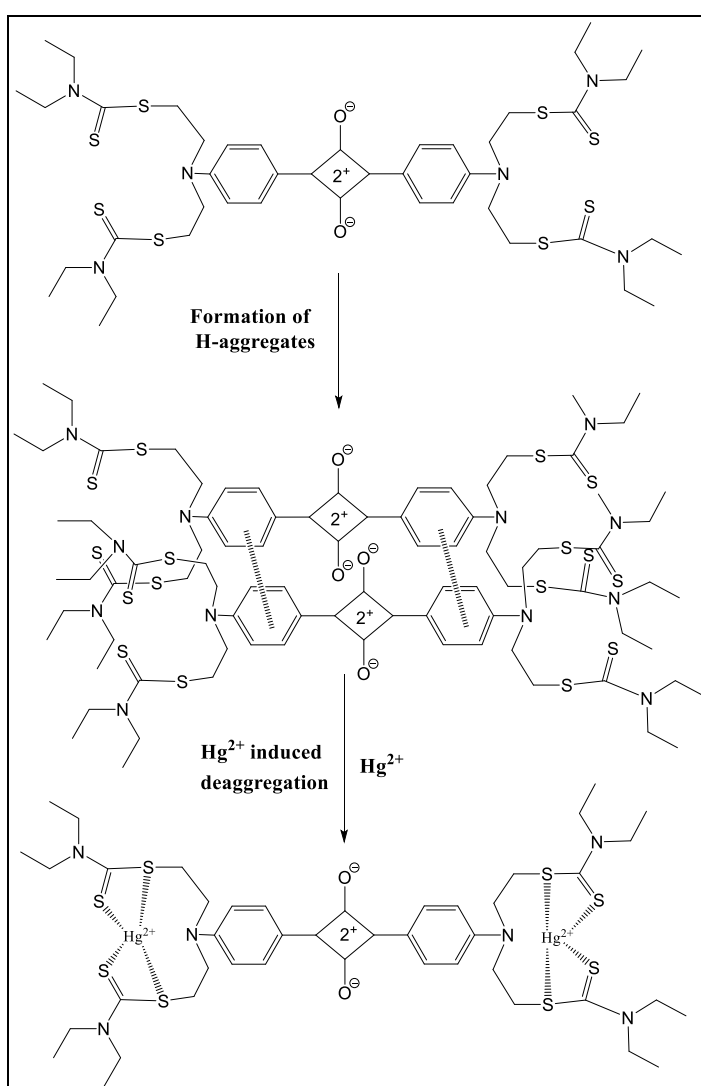


**Figure 1.5: The proposed binding model of Hg<sup>2+</sup>-SQ1.**

An unsymmetrical squaraine dye that operates by a similar mechanism was synthesised by the same group.<sup>64</sup> It also displayed a good selectivity and sensitivity. The addition of  $\text{Hg}^{2+}$  caused a colour change from lilac to brilliant blue.

Rhodamine and its derivatives are well known as organic indicator sensors for the determination of Hg.<sup>65-69</sup> The sensing mechanism for Hg detection depends on the ability of  $\text{Hg}^{2+}$  to open the spirolactam ring of the rhodamine moiety. As a result, a Hg-rhodamine complex has been formed with a strong fluorescent emission and vivid colour change. Wang *et al.*<sup>66</sup> described a novel rhodamine derivative bearing 2, 4-dichloroquinazoline as a selective chemosensor for  $\text{Hg}^{2+}$ . The addition of  $\text{Hg}^{2+}$  to the dye solution cause ring-opening combined with a strong yellow fluorescence and a change in the colour to the pink, Fig. 1.6. The fluorescence and colorimetric changes of the rhodamine sensor were specific for  $\text{Hg}^{2+}$  detection in buffer solution.

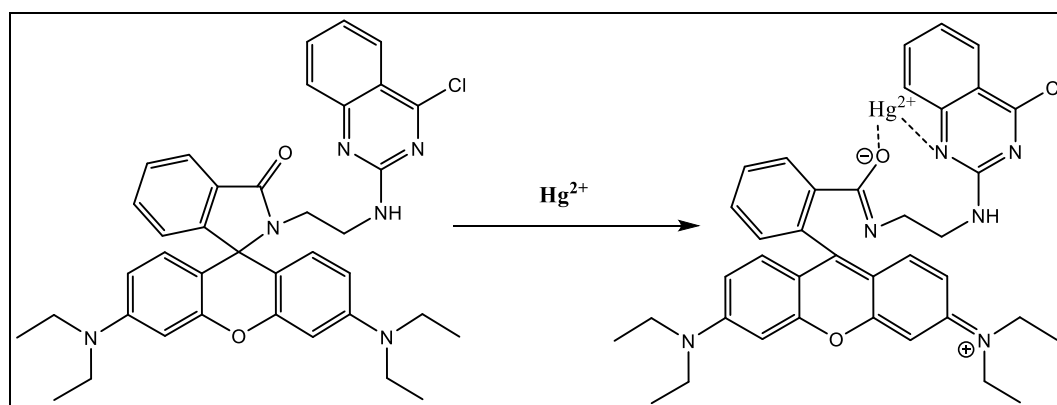


**Figure 1.6:**  $\text{Hg}^{2+}$ - induced ring opening of rhodamine derivative bearing 2, 4-dichloroquinazoline.

A rhodamine B derivative, bearing mono and bis-boronic acid was demonstrated by Kim *et al.*<sup>70</sup> as the first reversible fluorescent chemosensor for  $\text{Hg}^{2+}$ . The colour change from colourless to dark pink in the presence of  $\text{Hg}^{2+}$  had a detection limit of 6000  $\mu\text{g/L}$ . A novel rhodamine B base 3',6'-bis(diethylamino)-2-(2-oxoethylideneamino)-spiro[isindoline-1,9'-xanithen]-3-one (RHO) for  $\text{Hg}^{2+}$  detection was prepared by Ni *et al.*<sup>71</sup> The RHO gave high sensitivity and selectivity towards  $\text{Hg}^{2+}$  in the presence of other metal ions based on the ability of  $\text{Hg}^{2+}$  to stimulate hydrolysis in ethanol-water mixtures, Fig. 1.7. The presence of  $\text{Hg}^{2+}$  induced an increase in the absorbance and fluorescent bands accompanied by an

obvious colour change from colourless to pink, with a concentration of 0.54  $\mu\text{g/L}$  as detection limit.

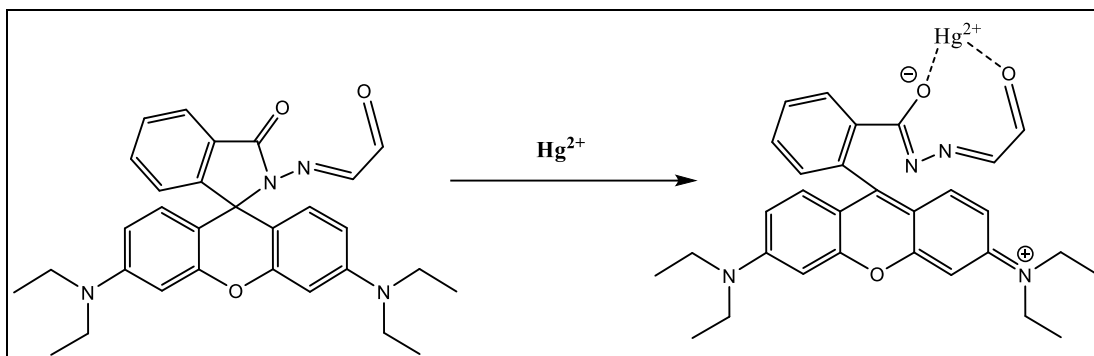


**Figure 1.7:** The proposed mechanism of RHO binding with  $\text{Hg}^{2+}$ .

Si-rhodamine B thiolactone Si-RBS has been successfully synthesised by Tao *et al.*<sup>72</sup>, Fig. 1.8. The addition of  $\text{Hg}^{2+}$  changed the Si-RBS solution colour from colourless to light blue. Importantly, a detection limit down to 0.05  $\mu\text{g/L}$  was noted for quantitative determination of  $\text{Hg}^{2+}$ .

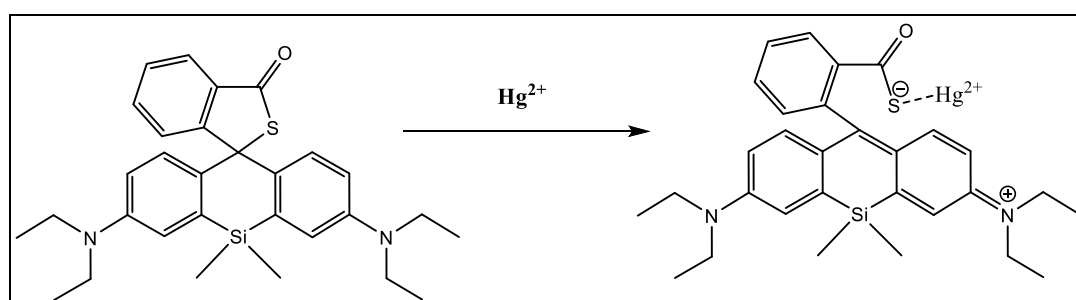


**Figure 1.8:** The proposed binding model of  $\text{Hg}^{2+}$  with Si-rhodamine B thiolactone.

Polyether organic sensors molecules with more than one ether group, incorporated with N, O, or S atoms as multidentate ligands, are able to coordinate strongly to  $\text{Hg}^{2+}$ . A qualitative receptor reported by Sancenon *et al.*<sup>73</sup> containing azo-oxa binding sites could be selective for  $\text{Hg}^{2+}$  with an obvious change in colour from yellow to red.

Zhang *et al.*<sup>74</sup> developed sensors based on 4-(bis (2-(ethylthio) ethyl) amino)-*N*-n-butyl-1,8-naphthalimide (BTABN) that combined with  $\text{Hg}^{2+}$  and a complex was produced in a ratio of 1:1, Fig. 1.9. In the presence of  $\text{Hg}^{2+}$ , the change in colour can be captured by the naked eye as the solution changed from bright yellow to colourless.

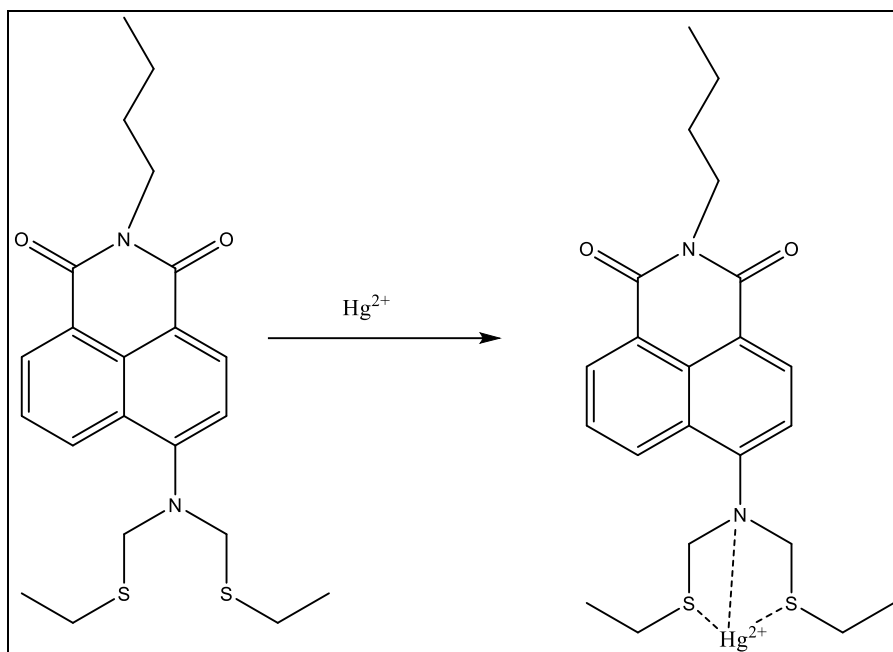


**Figure 1.9: Proposed complexation of BTABN with  $\text{Hg}^{2+}$  in ratio of 1:1.**

Choi *et al.*<sup>55</sup>, designed a novel sensor 2-((E)-(3-(1H-imidazole-1-yl) propylimino) methyl)-5-(diethylamino) phenol as selective  $\text{Hg}^{2+}$  colorimetric chemosensor, Fig. 1.10. It was based on the combination between imidazole groups and diethylaminosalicylaldehyde. In the presence of  $\text{Hg}^{2+}$ , the colour of the sensing system changed from colourless to yellow.

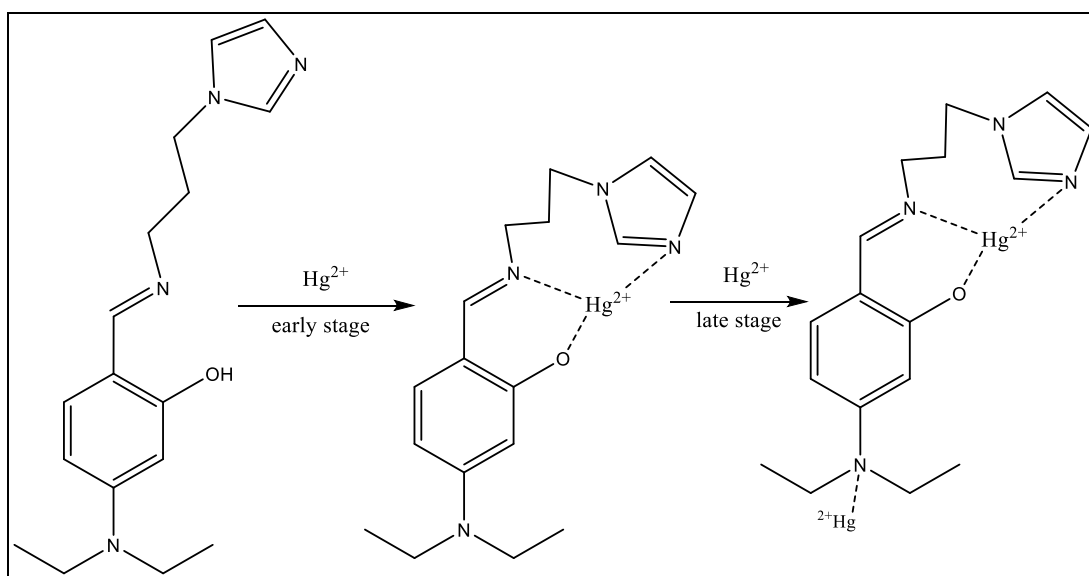


**Figure 1.10: Proposed a 1:2 formation of complex with  $\text{Hg}^{2+}$ .**

Another imidazole derivative 6-(Pyren-1-yl)-2-(1,4,5-triphenyl-1H-imidazol-2-yl)quinoline probe was synthesised by Harsha *et al.*<sup>75</sup> It selectively changed from colourless to yellow in the presence of  $\text{Hg}^{2+}$ . Minimum detectable limit of  $\text{Hg}^{2+}$  was found to 19.6  $\mu\text{g/L}$ .

Further organic colorimetric chemosensors for  $\text{Hg}^{2+}$  detection not involving squaraine, rhodamine and polyether sensors, were reported.<sup>21, 76</sup> Two highly selective colorimetric chemosensors, S1 and S2, for  $\text{Hg}^{2+}$  were based on the action of the aldehyde group as the electron acceptor and the azobenzene as the electron donor, Fig. 1.11. Both sensors S1 and S2 changed colours from light yellow to deep red in the presence of 4000  $\mu\text{g/L}$   $\text{Hg}^{2+}$ , which can easily be observed by the naked eye.<sup>19</sup> Indeed, the advantage of these sensors is that they involve high selectivity for  $\text{Hg}^{2+}$  using intramolecular charge transfer (ICT) as the signalling mechanism.

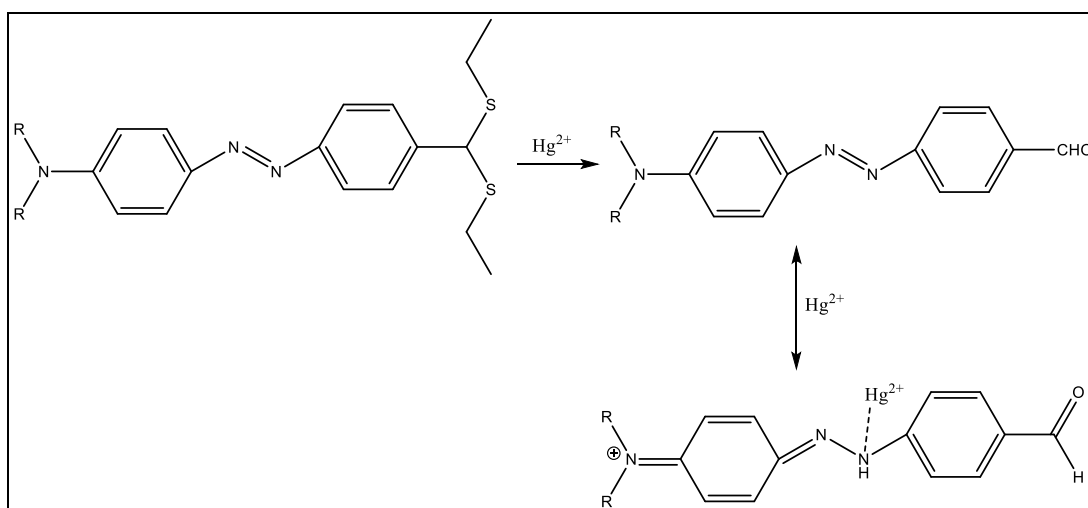


**Figure 1.11:** proposed  $\text{Hg}^{2+}$  sensing process of S1 and S2.

### 1.8.3.2. Complex-based sensors

Two selective and sensitive colorimetric sensors based on the ruthenium complexes [bis(2,2'-bipyridyl-4,4'-dicarboxylate)ruthenium (II) bis(tetrabutylammonium) bis(thiocyanate)]N719 and [(2,2':6',2''-terpyridine-4,4',4''-tricarboxylate)ruthenium(II) tris(tetrabutylammonium) tris(isothiocyanate)] N749 were developed by Coronado *et al.*<sup>77</sup>, Fig. 1.12. A reversible interaction occurred between  $\text{Hg}^{2+}$  and the S atom of NCS groups in the ruthenium N719 and N749 which induced an obvious colour change of the dye from dark red-purple to orange. Detection limits were reported as 20  $\mu\text{g/L}$

using N719, and 150  $\mu\text{g/L}$  using N749. By adsorbing these dyes onto specific mesoporous metal oxide films, such as mesoporous  $\text{TiO}_2$  films, an easy-to-use reversible sensing of  $\text{Hg}^{2+}$  in aqueous solution could be obtained. Films were recycled by washing with an aqueous solution of potassium iodide, which removes  $\text{Hg}^{2+}$  from the film surface and forms a stable iodide complex instead.

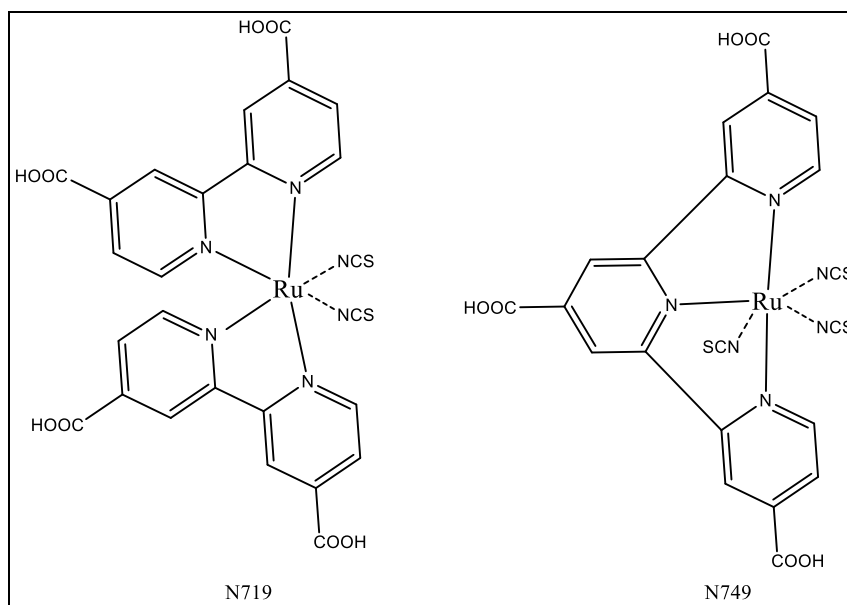


**Figure 1.12: Chemical structure of the molecular probes N719 and N749.**

A sub-micromolar sensitivity sensor based on a ruthenium dye (N719) synthesised with a mesoporous  $\text{TiO}_2$  film was used to detect  $\text{Hg}^{2+}$  in aqueous solutions.<sup>78</sup> The resulting rapid colorimetric detection for  $\text{Hg}^{2+}$  can be observed by the naked eye with a detection limit of 4  $\mu\text{g/L}$ . The loss of the S atoms from the complex, instead of forming a complex with  $\text{Hg}^{2+}$ , can cause the colour of the film to change from red-purple to yellow. This observation suggested that the process responsible for the colour change of the N719 dye could be a chemical transformation of the thiocyanate ligands accelerated by the  $\text{Hg}^{2+}$ .

Sun *et al.*<sup>79</sup> designed an excellent fluorescent and colorimetric probe for  $\text{Hg}^{2+}$  detection based on a boron-dipyrromethene (BODIPY) dye containing a benzo [2, 1, 3] thiadiazole (BDT) bridge as a receptor, Fig. 1.13. The interaction between the S atom in the BDT and  $\text{Hg}^{2+}$  affects the energy level of the molecular orbitals, allowing naked

eye detection as the change of solution colour from purple to yellow can be observed. A detection limit as low as 100  $\mu\text{g/L}$  was achieved.

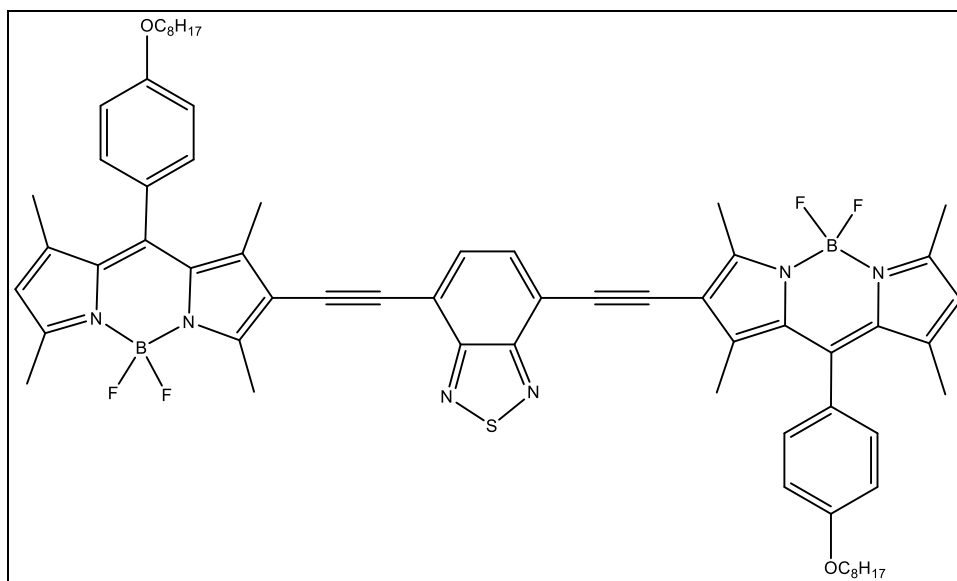


**Figure 1.13: Chemical structure of BODIPY dyes.**

A novel monostyryl BODIPY chemosensor containing two triazole units as receptor was designed for  $\text{Hg}^{2+}$  determination.<sup>80</sup> This sensor was based on the ICT mechanism. The  $\text{Hg}^{2+}$  binding with the N atom in the triazole ring inhibited ICT from N to boron in the BODIPY, resulting in colour change from blue to purple, with a detection limit of 45  $\mu\text{g/L}$ , Fig. 1.14.

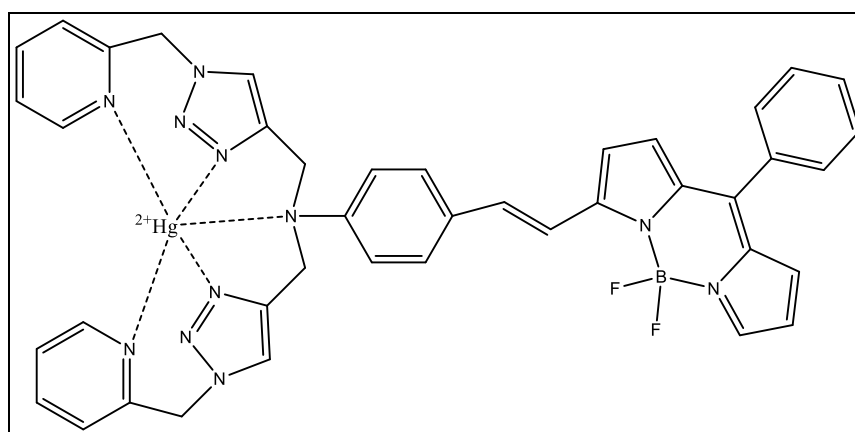


**Figure 1.14: Sensing process of  $\text{Hg}^{2+}$ - monostyryl BODIPY.**

The BODIPY fluorescent dyes have been widely used in various fields including as  $\text{Hg}^{2+}$  chemosensors. In recent years, aza-BODIPY dyes are emerging as a promising class of NIR emitting dyes.<sup>81, 82</sup> The C atom of the BODIPY core is replaced by an N atom. The absorption and emission bands can be modulated by introducing various substituents into the aza-BODIPY core. However, the reported applications and spectral characteristics of aza-BODIPY dyes are few.

### 1.8.3.3. Polymer-based sensors

Natural polymers such as DNA, cellulose and protein are rich in N, O and sometimes small proportions of S. They are able to strongly bind with Hg ions, resulting in effects in their visual characteristics. Because of the strong interaction of oligonucleotides with  $\text{Hg}^{2+}$ , two thymine bases of DNA could bind to generate stable base pairs of T- $\text{Hg}^{2+}$ -T. Such sensing systems have been employed as tools for  $\text{Hg}^{2+}$  selectivity detection.<sup>83-89</sup> For the first time, Li *et al.*<sup>90</sup> utilised the  $\text{Hg}^{2+}$  moderated T-T base pair in order to inhibit the DNAzyme activity and modify the proper folding of G-quadruplex DNAs; therefore colorimetric detection of  $\text{Hg}^{2+}$  could be established, Fig. 1.15. Two bimolecular DNA G-quadruplexes containing several T residues were adopted, which functioned well in low and high salt conditions, respectively. In the folded state, two bimolecular DNA G-quadruplexes with many T residues are able to bind hemin to form the G-quadruplex-based DNAzymes with the peroxidase-like activities. However, in the presence of  $\text{Hg}^{2+}$ , and as a result of the formation of T- $\text{Hg}^{2+}$ -T complex, the proper folding of DNAzymes was prevented. Therefore, a sharp decrease in the catalytic activity toward the  $\text{H}_2\text{O}_2$  oxidation of 2,2'-azino-bis(3-ethylbenzothiazoline-6-sulfonic acid) diammonium salt (ABTS) is observed, with a change in solution colour. The  $\text{Hg}^{2+}$  detection limit was as low as 10  $\mu\text{g/L}$ .

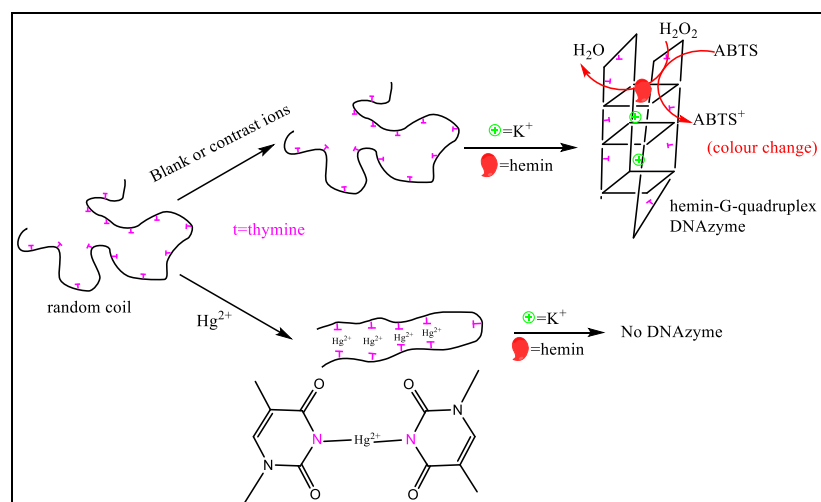


Figure 1.15: Proposed mechanism for the T- $\text{Hg}^{2+}$ -T in the DNA.

Cellulose is another significant natural polymer that has recently attracted attention to provide qualitative and semi-quantitative determination of  $\text{Hg}^{2+}$  in aqueous solutions. Diez-Gil *et al.*<sup>91</sup> reported cellulose-based colorimetric  $\text{Hg}^{2+}$  detection by a simple procedure, surface-confined coating of the selective Hg indicator directly on cellulose substrates without using any further matrix. Particularly, a paper-based analytical test was produced by incorporating a highly selective sensor for  $\text{Hg}^{2+}$  based on the 1,4-disubstituted azine bearing two ferrocene groups, Fig. 1.16. Depending on the amount of  $\text{Hg}^{2+}$  in contact with the sensing cellulose probes colour change was produced. Such functionalised cellulose probes opened a modern route for disposable solid phase sensors for simple detection by the naked eye, with a detection limit of 10  $\mu\text{g/L}$ .

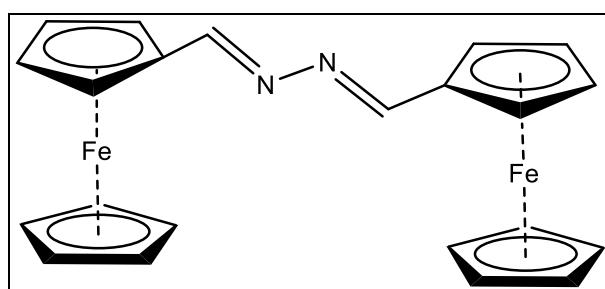


Figure 1.16: Chemical structure of 1,4-disubstituted azine.

Liu *et al.*<sup>56</sup> employed a novel cellulose-based sensing system for Hg. Rhodamine B thiolactone which is known to be selective for Hg detection was captured on a silica matrix, and a silica layer was impregnated in a filter paper. The  $\text{Hg}^{2+}$  ions were

entrapped by the rhodamine B thiolactone in the silica matrix when an aqueous sample containing  $\text{Hg}^{2+}$  flowed through the membrane. An optical change could be observed instantly with the naked eye as the membrane colour changed from white to purple-red, with a  $\text{Hg}^{2+}$  detection limit of  $0.24 \mu\text{g/L}$ .

A series of ICT molecules was designed by Cheng *et al.*<sup>92</sup>, relying on thiophene groups as electron donors attached to a triphenylamine backbone integrated with an electron acceptor aldehyde group, Fig. 1.17. The corresponding compounds S1, S2 and S3 were prepared to serve as novel dual-channel chemosensors for  $\text{Hg}^{2+}$  based on the protective reaction between ethanethiol and an aldehyde. Upon addition of  $\text{Hg}^{2+}$  to the dithioacetals compound the colour was changed from blue to green, with a limit of  $\text{Hg}^{2+}$  detection as low as  $2 \mu\text{g/L}$ .

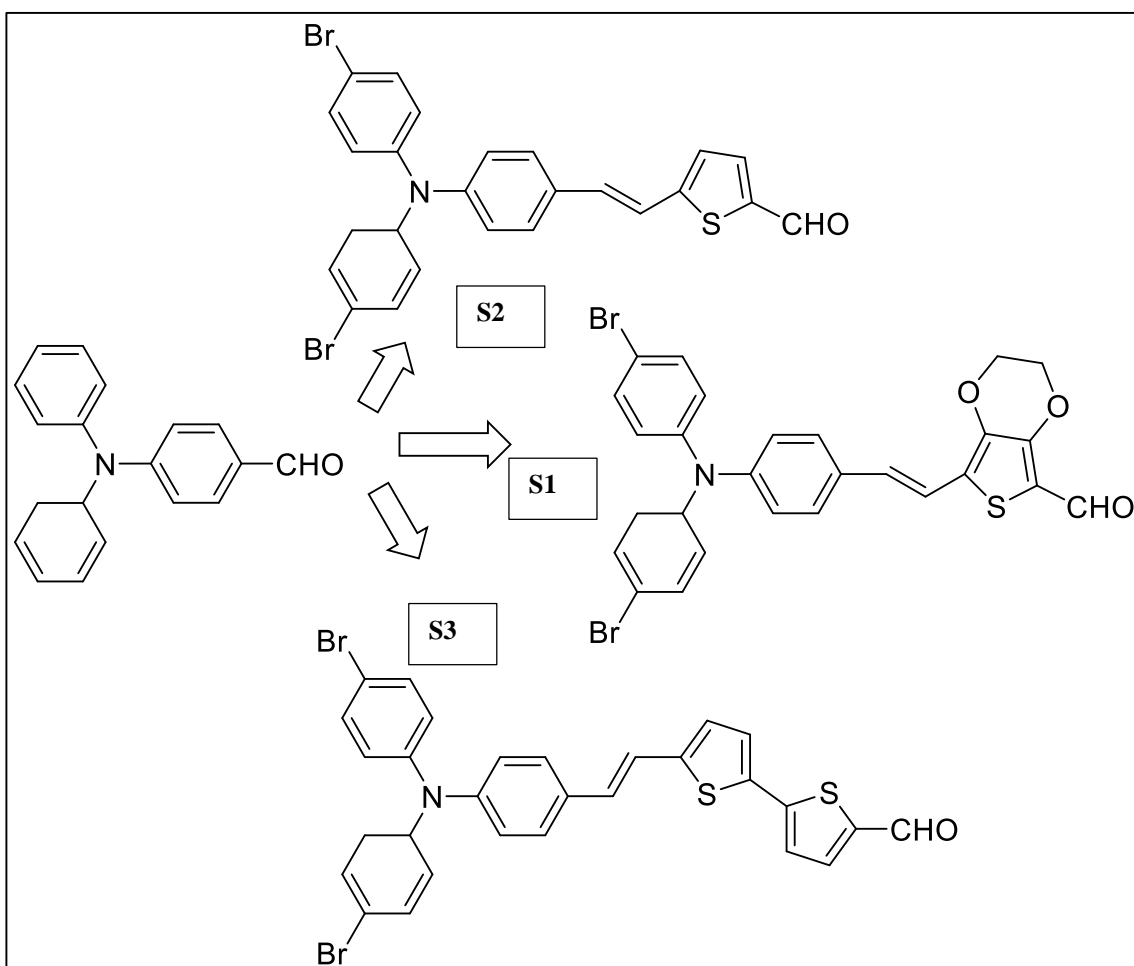


Figure 1.17: The structures of ICT molecules series, S1, S2, and S3.

Another complex polymer incorporating oligopyrene derivative, oligo (*N'*, *N'*, *N'*, *N4,N4,N4,N4*-hexamethyl-2-(4-(pyren-1-yl)butanoyloxy)butane-1,4-diaminium - bromide), and oligothymine was developed by Chen *et al.*<sup>93</sup> as a fluorescent and colorimetric sensor for Hg detecting in aqueous media. Upon addition of Hg, a T-Hg-T complex resulted, which leads to chain aggregation, fluorescence and colour change in the complex polymer. The change in colour can be distinguished with the naked eye and the detection limit of Hg<sup>2+</sup> was 1000 µg/L.

Pyrene derivative<sup>94, 95</sup> and terpyridine derivative-based polymers<sup>96</sup> as a colorimetric Hg<sup>2+</sup> sensor were developed. Terpyridine, Fig. 1.18 provided the ability to selectively and sensitively detect Hg<sup>2+</sup> over a number of environmentally relevant ions especially Cd<sup>2+</sup>, Cu<sup>2+</sup>, Ni<sup>2+</sup>, Pb<sup>2+</sup> and Zn<sup>2+</sup>. The addition of Hg<sup>2+</sup> into the polymer solution caused a change of colour from colourless to pink with a detection limit of 5 µg/L.

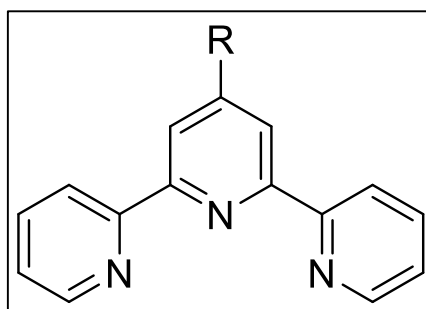


Figure 1.18: The chemical structure of terpyridine.

#### 1.8.3.4. Nanoparticle-based sensors

Over the past decades, various nanomaterials have been developed that have the advantage of high surface to volume ratio, so as to supply a large area of interaction with the target analyte. As a result of intensive surface plasmon resonance (SPR), nanoparticles provide rapid, sensitive and specific analysis. These nanomaterials include silver nanoparticles (AgNPs), and gold nanoparticles (AuNPs). A review of the recent AgNPs and AuNPs Hg-based sensors can be found in Zarlaida *et al.*<sup>97</sup>

Several recent studies have utilized AgNPs as colorimetric sensors for the detection of Hg<sup>2+</sup> with high sensitivity and selectivity.<sup>98-102</sup> Because of their lower cost compared with AuNPs, AgNPs have become more popular. A sensitive and selective

colorimetric  $\text{Hg}^{2+}$  detection method reported by Wang *et al.*<sup>103</sup> was based on  $\text{Hg}^{2+}$  specific oligonucleotides (MSO). On addition of  $\text{Hg}^{2+}$  the conformation transformed from random coil MSOs to a hairpin structure, as the presence of  $\text{Hg}^{2+}$  would result in the generation of stable T-Hg-T bonds. An innovative dual-function colorimetric sensor for  $\text{Hg}^{2+}$  was documented by Wang *et al.*,<sup>104</sup> Fig. 1.19. In the presence of  $\text{H}_2\text{O}_2$ , AgNPs could reduce  $\text{Hg}^{2+}$  to  $\text{Hg}^0$  within several seconds. This catalysed reduction reaction made AgNPs aggregate and the colour changed from light yellow to deep yellow with a limit of detection less than  $0.40 \mu\text{g/L}$ .

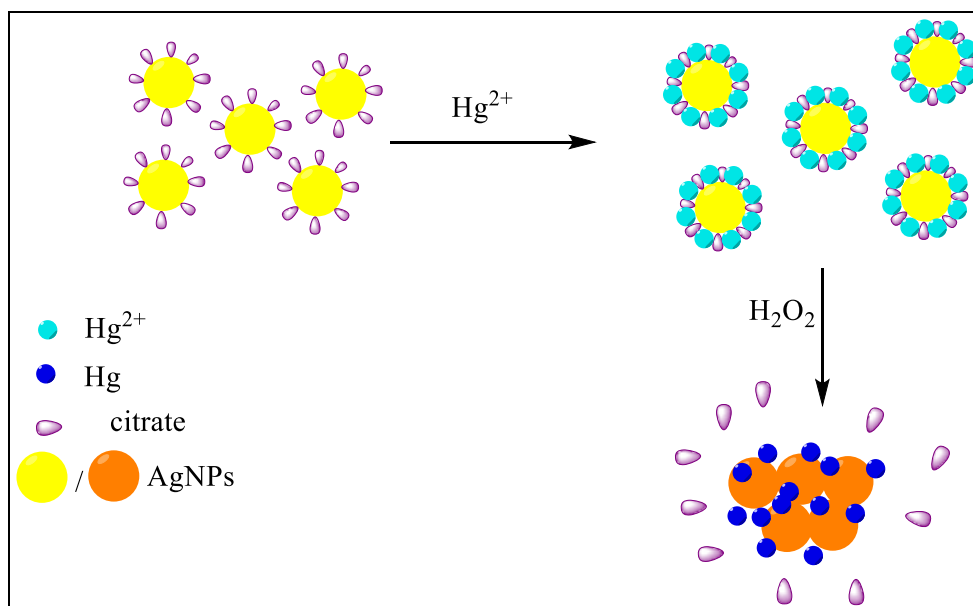


**Figure 1.19: Proposed mechanism for the induced  $\text{Hg}^{2+}$ -AgNPs in the presence of  $\text{H}_2\text{O}_2$ .**

Apilux *et al.*<sup>105</sup> employed a simple and rapid detection method for  $\text{Hg}^{2+}$  dependant on a combination of nanoparticle science with lab-on-paper methodology. Particularly, using AgNPs and Ag nanoplates (AgNPLs) made it possible to undertake  $\text{Hg}^{2+}$  measurements with only  $2 \mu\text{L}$  of the sample. With the addition of  $\text{Hg}^{2+}$ , the paper's colour changed immediately from yellow to light yellow. This colour change resulted from the changes in SPR of the AgNPs and AgNPLs. The linear detection range was  $5000\text{-}75000 \mu\text{g/L}$   $\text{Hg}^{2+}$  with a limit of detection of  $120 \mu\text{g/L}$ .

Gold nanoparticles have been widely considered as colorimetric sensors to provide detection methods for Hg based on the advantages of the specific surface conjugation features, the tunable SPR, and the high molar absorptivity over the visible spectrum.

In this respect, various sizes and shapes of AuNPs can be surface-modified with several functionalities of recognition unit including oligonucleotides<sup>106-108</sup>, small thiolate ligands,<sup>109-111</sup> peptides and proteins<sup>112-115</sup> to induce aggregation.

➤ ***Nucleotide-functionalised AuNPs***

Lee *et al.*<sup>106</sup> designed a Hg detection sensor which employed a combination of two complementary DNA-AuNPs, each functionalised with different thiolated-DNA sequences 5'HS-C<sub>10</sub>-A<sub>10</sub>-T-A<sub>10</sub>3' and 5'HS-C<sub>10</sub>-T<sub>10</sub>-T-T<sub>10</sub>3' to form DNA-linked aggregates that exhibit a T-T mismatch. The T-T mismatch is bridged by the AuNPs aggregate and the T-Hg<sup>2+</sup>-T in the presence of Hg. At a specific temperature or the melting temperature (*T<sub>m</sub>*) of the DNA-AuNP aggregates, the sensing system can become dissociated with a purple to red colour change depending on Hg<sup>2+</sup> concentrations in aqueous solution.

➤ ***Thiol-functionalised AuNPs***

Developing colorimetric sensors for detecting Hg<sup>2+</sup> based on the interaction between Hg<sup>2+</sup> and thiol-functionalised nanoparticles has been widely considered as a result of the strong tendency of Hg<sup>2+</sup> to interact with thiols such as protein, cysteine and other mercapto derivatives. An example of such sensors, reported for the first time by Tan *et al.*,<sup>109</sup> involved the cloud point extraction of AuNPs modified with homocysteine (HCys) and 3-mercaptopropionic acid (MPA) in the presence of 2, 6-pyridinedicarboxylic acid as a colorimetric sensor for Hg<sup>2+</sup> detection. The colour changed from colourless to red, which is unusual compared to the other AuNP methods where the change in colour was from red to blue. This method combined the advantages of the colour change with the selective function of the cloud point extraction to provide an ultrahigh sensitivity.

A rapid and simple colorimetric sensor for Hg<sup>2+</sup> detection in aqueous solution was developed by Zhou *et al.*<sup>110</sup> based on the ability of Hg<sup>2+</sup> to prevent the aggregation of AuNPs generated by 4-mercaptophenylboronic acid (MPBA). In the absence of Hg<sup>2+</sup>, MPBA can bind to the AuNPs *via* Au-S bonds resulting in aggregation of AuNPs by self-dehydration condensation of boronic acid groups resulting in a visible colour

change of the AuNPs solution from red to blue, Fig. 1.20. However, in the presence of  $\text{Hg}^{2+}$ , MPBA loses the ability to induce aggregation of AuNPs because the  $\text{Hg}^{2+}$  binds to the thiol group, with a change of solution colour from blue to red.

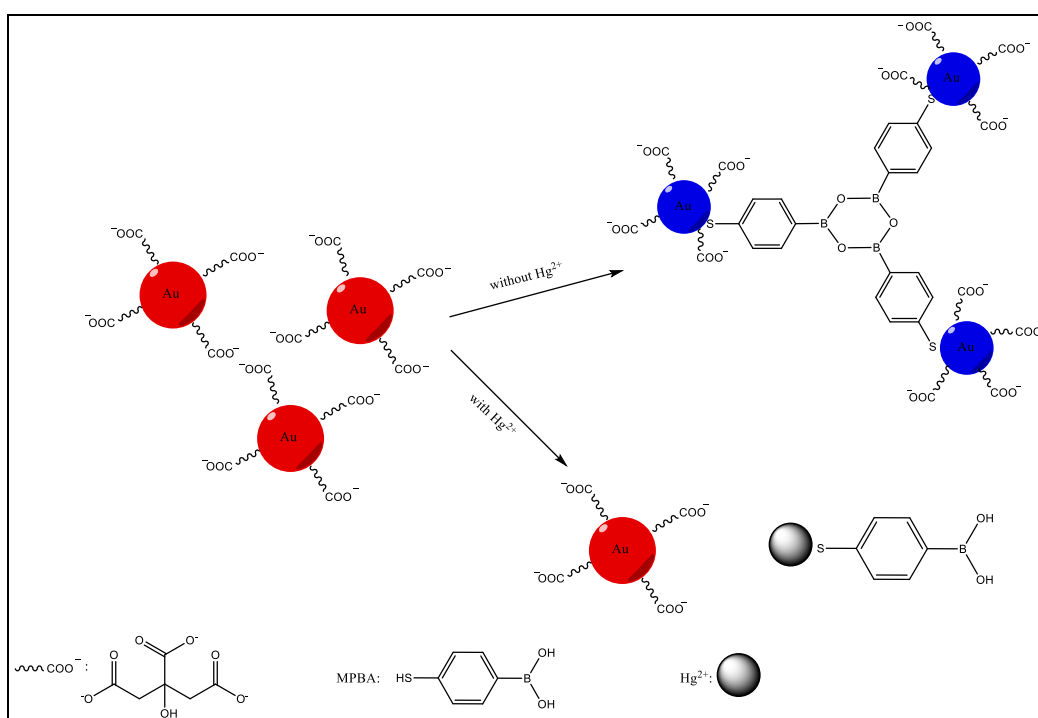


**Figure 1.20: The AuNPs colorimetric mechanism for  $\text{Hg}^{2+}$  detection.**

### ➤ *Au-amalgam based-sensors*

The ability of  $\text{Hg}^{2+}$  to deposit on the AuNPs surface to form a solid amalgam-like structure, which can affect the surface molecular conjugation, plasmonic resonance, and therefore colloid stability is well known.<sup>116-118</sup> The formation of Hg-Au alloy on the Au surface resulted in a new colorimetric sensor for Hg detection. In this respect, the use of Tween 20-modified AuNPs was developed by Lin *et al.*<sup>116</sup> as a homogeneous and rapid sensor for the highly selective detection of  $\text{Hg}^{2+}$ , Fig. 1.21. It was found that when the citrate-capped AuNPs were modified with Tween 20, the citrate ions were still adsorbed on the Au, thus stabilising the citrate-capped AuNPs under high ionic strength conditions without  $\text{Hg}^{2+}$ . However, in the presence of  $\text{Hg}^{2+}$ , citrate ions reduced  $\text{Hg}^{2+}$  to form Hg-Au alloys on the surface of the AuNPs, resulting in Tween 20 being removed from the NP surface. Therefore, the AuNPs became unstable under high ionic strength, and aggregation occurred. Tween 20-AuNPs could

detect  $\text{Hg}^{2+}$  selectively at concentrations as low as  $20 \mu\text{g/L}$  and provide instant colour change from red to purple.

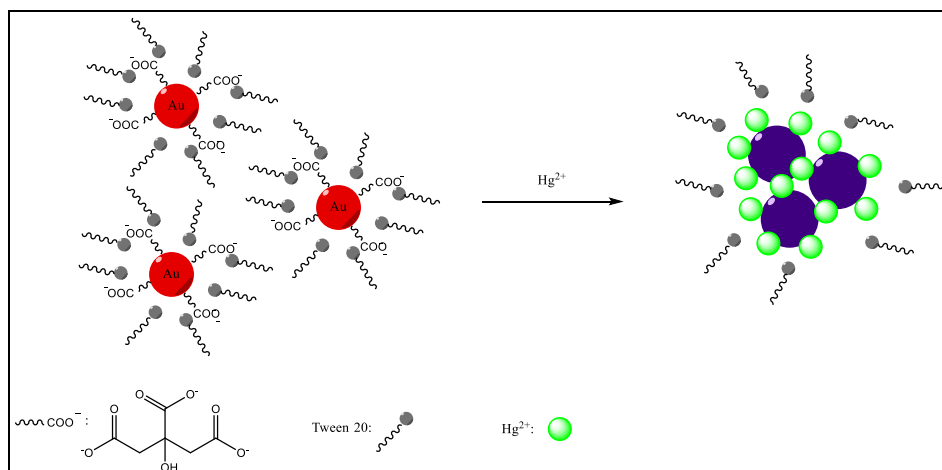


**Figure 1.21: The proposed mechanism of  $\text{Hg}^{2+}$  sensing by Tween 20-AuNPs.**

Based on their chemical redox surface chemistry, mesoporous silica-coated gold nanorods (MS AuNRs) were employed by Wang *et al.*<sup>119</sup> as a non-aggregation-based colorimetric sensor for  $\text{Hg}^{2+}$  detection. Particularly,  $\text{Hg}^{2+}$  ions were reduced to  $\text{Hg}^0$  and placed on the surface of MS AuNPs in the presence of ascorbic acid. The MS AuNRs generated a colour change from purple to blue-green and  $2000 \mu\text{g/L}$  was the lower limit of detection.

### ➤ *Protein-functionalised AuNPs*

Protein is a natural polymer containing many functional groups, which has been employed widely for colorimetric determination of  $\text{Hg}^{2+}$ . In 2011, a simple colorimetric system for Hg detecting based on papain coated-gold nanoparticles (P-AuNPs) in aqueous solution was developed.<sup>112</sup> Papain is a single polypeptide chain having seven cysteine residues, and could be adsorbed directly on the AuNPs surfaces, forming P-AuNPs that could be used selectively to detect  $\text{Hg}^{2+}$ , Fig. 1.22. Upon the addition of  $\text{Hg}^{2+}$ , the aggregation of the 13 nm AuNPs created by the binding between papain and the ions occurred, resulting in the colour of P-AuNPs changing from red to blue, with a detection limit of  $800 \mu\text{g/L}$ . The concentration of P-AuNPs solution, pH, and the size of the AuNPs could affect the detection sensitivity of this method: the larger AuNPs were associated with more sensitive  $\text{Hg}^{2+}$  detection.

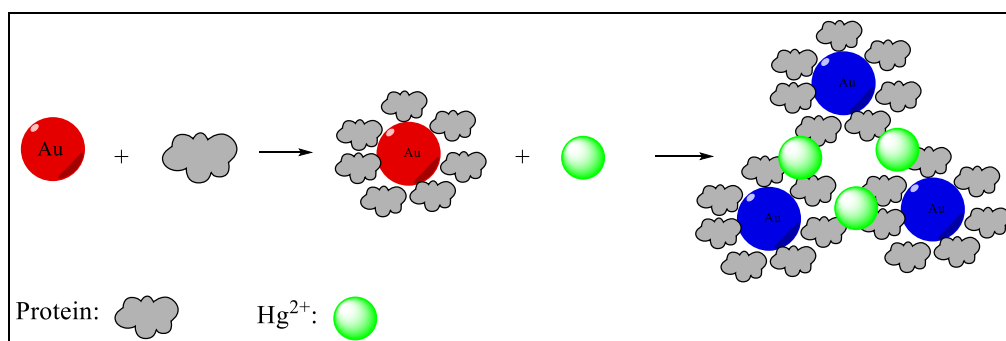


**Figure 1.22: The induced interaction between Hg<sup>2+</sup> and P-AuNPs.**

Tripathi *et al.*<sup>113</sup> demonstrated a rapid and simple sensor for Hg<sup>2+</sup> colorimetric detection using AuNPs combined with fungal biomass of *Trichoderma harzianum* (*T. harzianum*). In the presence of Hg<sup>2+</sup> in AuNPs solution, the colour changed from pink-red to greyish blue, combined with a shift in the SPR of nanoparticles to a higher wavelength. The minimum concentration that would be detected was 0.5 µg/L. Tripathi *et al.*<sup>113</sup> explained the potential detection mechanism based on the fact that the fungi synthesise cysteine in order to avoid the toxic effect of Au ions under metal stress condition. Cysteine is a thiol-containing amino acid that can bind with Hg<sup>2+</sup> to form metal complexes resulting in destabilisation of the AuNPs leading to aggregation.

### 1.9. Immobilisation of the colorimetric sensors in solid supports

Although several molecules have been successfully used for Hg<sup>2+</sup> ion sensing, only a few of them are available to be anchored to a solid substrate. Firm fixation of active indicators on solid substrates has been undertaken by several procedures. Compatible polymer, membrane or template are used to hold the active agents before immobilising on microtiter plates, films, glasses, sol-gel, and paper strips.<sup>120</sup>

In microtiter plates devices, the reagent can be arranged in the wells either as a solution placed in vials or as a membrane at the bottom before obtaining the analytical signal. The format requires a small volume of the sample, even at submicroliter level.<sup>120</sup>

A number of films have been employed for Hg<sup>2+</sup> detection with varying degree of success. The adsorption of molecular dyes to the surface of specific mesoporous metal

oxide films such as mesoporous TiO<sub>2</sub> films, has led to applications such as described by Coronado *et al.*<sup>77</sup> and Palomares *et al.*<sup>78</sup>

Paper-based and membrane-based colorimetric sensors provide additional advantages of pre-concentration and lowering of the detection limit. Based on filtration on sol-gel membrane, a simple colorimetric sensor array to distinguish PTE ions was developed by Feng *et al.*<sup>121</sup>. The PTE ion indicators with S, N, or O ligands were incorporated in the macroporous silica matrix in the presence of a considerable number of free hydroxyl groups which help immobilise the indicators in the silica and prevent leaching, Fig. 1.23. Moreover, the indicator-doped sol-gel colloid was coated on a cellulose acetate/nitrate membrane. A clear difference in the colorimetric responses demonstrated the ability of this technique in detecting Hg<sup>2+</sup>.

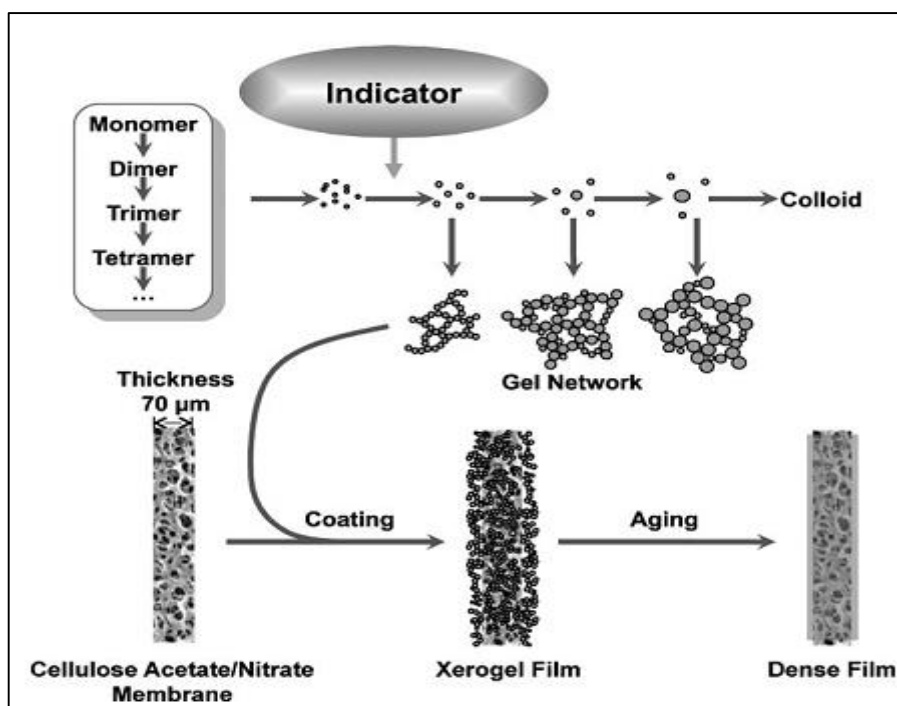


Figure 1.23: The silica sol-gel matrix formation.<sup>121</sup>

Jayabal *et al.*<sup>122</sup> developed a simple optical and colorimetric sensor for Hg<sup>2+</sup> detection based on the localised surface plasmon resonance (LSPR) of AuNRs. The sensor was prepared by fixing AuNRs in an amine-functionalized silicate sol-gel matrix (Au-TPDT NRs). It was observed that the LSPR band intensity decreased with a blue shift

upon addition of  $\text{Hg}^{2+}$  into the Au-TPDT NRs, combined with colour change as a result of the formation of an Au-Hg amalgam.

### **1.9.1. Paper-based colorimetric sensing**

Paper-based sensors are widely used to provide low cost and simple means of on-site analysis. The advantage of using paper is well documented.<sup>123</sup> Analogous to litmus paper, paper-based sensors are manually cut into strips or sections and soaking in chemical reagent(s) that change colour on exposure to a specific pollutant; the change in colour relates to the pollutant concentration and can be estimated by the naked eye or read out by an electronic device.

Such a method for screening Hg has been optimised and applied by Yallouz *et al.*<sup>124</sup> to develop a semi-quantitative method (SQM) for Hg analysis in fish. The colorimetric screening test based on the reaction of copper iodide with Hg is one of the simple and inexpensive methods that can be applied to Hg screening in the environment.

Colorimetric  $\text{Hg}^{2+}$  ion detection using spot test, paper strips containing the active indicator have been widely developed.<sup>125-128</sup> However, they have some disadvantages which need to be overcome. The detection limits of the paper-based colorimetric sensors are usually high making them unsuitable for monitoring very low concentrations of  $\text{Hg}^{2+}$  in the environment. Although paper-based sensors are inexpensive, the incorporation of nanoparticle materials into paper-based sensors increases their cost relatively. The colour change in some sensors could be only observed under a UV lamp. Additionally, interpretation of colour intensity differs for each individual, ambient light condition and the condition of the paper substrate (wet or dry). Furthermore, the leakage of reagent could also occur. Therefore, further attention was given to the paper-based sensor array design.

### 1.9.2. Microfluidics paper-based devices ( $\mu$ PAD)

As an alternative to traditional paper-based devices, Whitesides and co-workers<sup>129</sup> introduced microfluidics paper-based devices ( $\mu$ PAD). The  $\mu$ PAD represent a novel sensing process for fluid analysis and handling for a variety of applications including health diagnostics, and environmental monitoring. The reasons behind using paper as the substrate for such screening systems include that it possesses the advantages of being lightweight, flexible, readily available, disposable, compatible with many biological and chemical indicators and use capillary forces to transports liquids without the requirement of external forces.<sup>130</sup> Fabrication of  $\mu$ PAD is based on patterning sheets of paper into hydrophilic channels bounded by hydrophobic barriers; the resulting channels either can be left open to the atmosphere or sealed to thin polymer sheets.<sup>123</sup> A review of common fabrication methods can be found in Cate *et al.*<sup>131</sup> Various types of paper-based devices have been described: Hossain and Brennan used a flower design with wax-printed hydrophobic channels and inkjet-printed detection areas.<sup>132</sup> An eight detection area wheel design paper device with a sampling area in the middle which improves the pre-concentration was described by Feng *et al.*<sup>133</sup>. Another design based on a 3 $\times$ 3 membrane array with a wax-printed technique for the pattern was presented by Feng *et al.*<sup>134</sup>, Fig. 1.24.

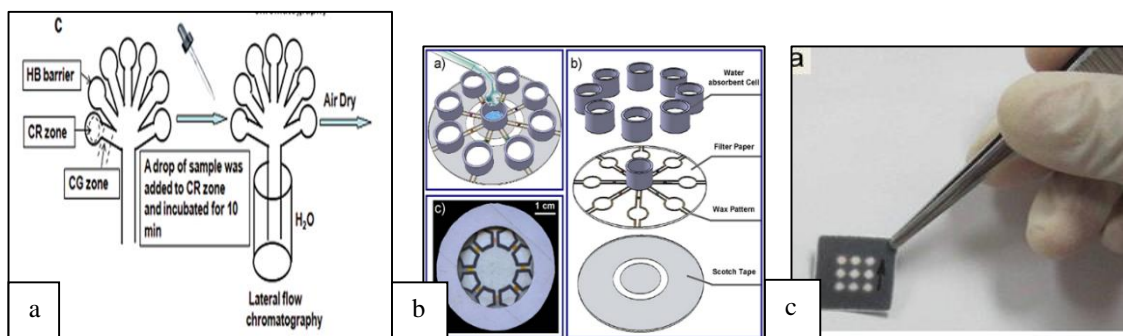


Figure 1.24: The design of multiplexed array paper, (a): flower design, (b): wheel design, (c): 3 $\times$ 3 membrane array design.<sup>132-134</sup>

The basic system in such array devices consists of various colorimetric indicators (dyes, pH indicator, chromogenic sensors, *etc.*), each selective and sensitive to a specific analyte, that can give rise to a colour change response. The colorimetric reagents can be used alone or in combination with an enzymatic test such as a  $\beta$ -galactosidase-based test.<sup>132</sup> However, in other cases, the array is composed of reagents

that combine receptor and chromophores in the molecule. Examples of such arrays include reagents based on oligonucleotide sequences as receptor attached to unmodified AuNPs to provide rapid Hg<sup>2+</sup> sensing,<sup>93</sup> and rhodamine derivatives bearing 2,4-dichloroquinazoline as receptor for Hg<sup>2+</sup> detection.<sup>66</sup> A summary of the  $\mu$ PADs developed for the determination of Hg<sup>2+</sup>, along with other PTE, can be found in Almeida *et al.*<sup>135</sup> Although  $\mu$ PADs have the advantage of multi-analyte capability, low cost, low sample volume, and portability, they possess some limitations, which are associated with the fabrication techniques, the material properties of paper, and the performance of the colorimetric detection methods incorporated into the devices.<sup>130</sup> The combination of optical methods of pattern recognition and inexpensive sensor array device has been applied for the rapid detection of Hg<sup>2+</sup>. Imaging devices such as digital cameras, scanners, and more recently digital cameras in portable devices such as smartphones, are one of the most interesting approaches to obtain qualitative and quantitative information on water quality.

In the preceding literature review a number of colorimetric sensors for the detection of Hg<sup>2+</sup> ion have been presented. A summary of these sensors can be found in Table A1.1 in Appendix 1. Rapid colour change, simplicity and detection limit are the main discussions in the literature. A variety of remarkable probes based on organic molecules, polymeric materials, and nanoparticles have been developed for Hg<sup>2+</sup> detection over the past decades, which have provided considerable quantitative information on dissolved Hg<sup>2+</sup> in water. However, most of the examples are not well suited for in-field analysis or rapid screening. Additionally, the ability to detect MeHg or total Hg in food and biological samples have not been much discussed.

In most cases of DNAzymes-based sensors, an appropriate probe, e.g., AuNPs or fluorophore is combined with oligonucleotides to indicate the colour change. Although this offers some advantages, it is costly and time-consuming. The instability and the requirement for enzyme-like activity are challenging in a label-free approach. These detection systems are still difficult and complicated to implement in a field setting.

Modified or functionalized Au/Ag nanoparticles have attracted lots of attention in recent years because of their optical properties. Although these methods seem highly stable, they suffer from the drawback of the high cost of ligands used and long detection

times. The amount of Au/Ag metal solution needed even for single detection use is still considered expensive. Furthermore, distinguishing colour by the naked eye is not accurate comparable to spectrophotometer reading. This has resulted in lower visual detection limit.

A variety of small-molecule organic dye-based sensors have been utilised in the monitoring of  $\text{Hg}^{2+}$ . They are designed to give optical read-out of  $\text{Hg}^{2+}$  upon complexation. Dyes can be immobilised into assay kits, portable fiber devices, membranes and paper-based indicators, facilitating rapid  $\text{Hg}^{2+}$  detection. However, their sensitivity, complexity of synthesis and preparation, solubility, and assay range are factors that should be further considered. Importantly, most of the determinations using a dye-based sensor involved relatively difficult preparation procedures, using organic solvents. The drawback is the fact that organic solvents have low solubility in water. This limits the availability of the reactive reagent for the interaction, thus, reduction on the detection sensitivity.

More factors must be considered in the preparation and immobilisation of paper-based colorimetric sensors. The immobilised dyes are often sensitive to light. The light has enough energy to change the molecular structures of the dyes and their chromophoric properties. Thus, dye-based molecules sensors may need to be kept in controlled storage conditions. However, there is barely any discussion in the literature on sensor stability for long-term uses.

### **1.10. Aim of the study**

The overall aim of this project was to develop a lab-on-paper based colorimetric sensor for determination of  $\text{Hg}^{2+}$  in aqueous environmental samples. A sensor meets the requirements of high sensitivity, excellent selectivity, stability, low cost, ease of use, long shelf life and adaptation for field application. These specifications are the key components in the ideal colorimetric sensors. The specific objectives selected were thus:

- To evaluate commercially available small molecule sensors for the determination of  $\text{Hg}^{2+}$ . Therefore, the conditions under which the coloured Hg-

complexes produced were discussed for three colorimetric reagents; copper iodide, diphenylcarbazone and rhodamine 6G (Chapter 4).

- To assess the reproducibility and analytical capability of rhodamine B thiolactone as a potential chemosensor for  $\text{Hg}^{2+}$  determination in aqueous solution (Chapter 5).
- To immobilise rhodamine B thiolactone on the surface of filter paper coated with silica and agar-agar matrices, and create a chromogenic analysis model based on the RGB colour (Chapter 6).
- To introduce a built-in digital camera in a smartphone to analyse  $\text{Hg}^{2+}$ -exposed agar-agar membranes developed in Chapter 6. The built-in camera within the smartphone was selected to facilitate the development of a portable field device (Chapter 7).

## 2. Theory of applied analytical techniques and statistical analysis

### 2.1. Ultraviolet-visible reflectance/transmittance spectroscopy

Because of the simple operation procedure and relatively inexpensive instrumentation, spectrophotometry has been widely used for quantitative analysis of  $\text{Hg}^{2+}$  in solution. Relatively, poor sensitivity is the significant drawback of this techniques as it normally can only detect Hg at mg/L levels.<sup>136</sup> Since Hg usually exists in the environment at  $\mu\text{g/L}$  levels, and in a complicated matrix, preconcentration procedure are often required prior to analysis. As mentioned before paper-based colorimetric methods possess the merits of preconcentration and lowering of the detection limit. They can sometimes be coupled with techniques such as ultraviolet-visible spectrophotometry, or the spectrophotometry can be used to assess the performance of the proposed field sensor. In this study, paper-based screening tests with a colorimetric reagent were used and their performance assessed using UV-vis reflectance/transmittance spectroscopy.

#### 2.1.1. The principle of ultraviolet-visible spectrophotometry

When a beam of light comes into contact with a solid surface and the photons enter an object, some may be reflected from the object surface, transmitted, absorbed, refracted or polarized,<sup>137, 138</sup> Fig. 2.1.

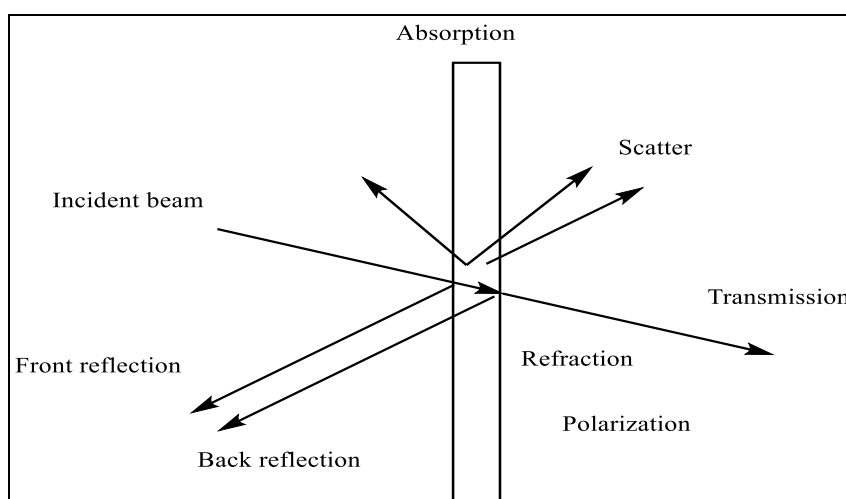


Figure 2.1: Schematic diagram of interactions of light with solid surfaces.

### 2.1.2. The absorption spectrum <sup>139</sup>

In a molecule, the sum of electronic, vibrational, and rotational energies represents its total potential energy. Light is a form of energy, and when absorbed by matter, the molecule's energy increases. Among the different states, the differences in energy are in the order:

$$E_{\text{electronic}} > E_{\text{vibrational}} > E_{\text{rotational}}$$

When photons of UV-vis light have enough energy, a transition between different electronic energy levels occurs where an electron moves from a lower energy level to a higher energy level. The differences in energy levels involved in electronic transitions are at highly characteristic wavelengths, have fixed values, and it would be expected that the resulting absorption bands would be very narrow and sharp, as depicted in Fig. 2.2.

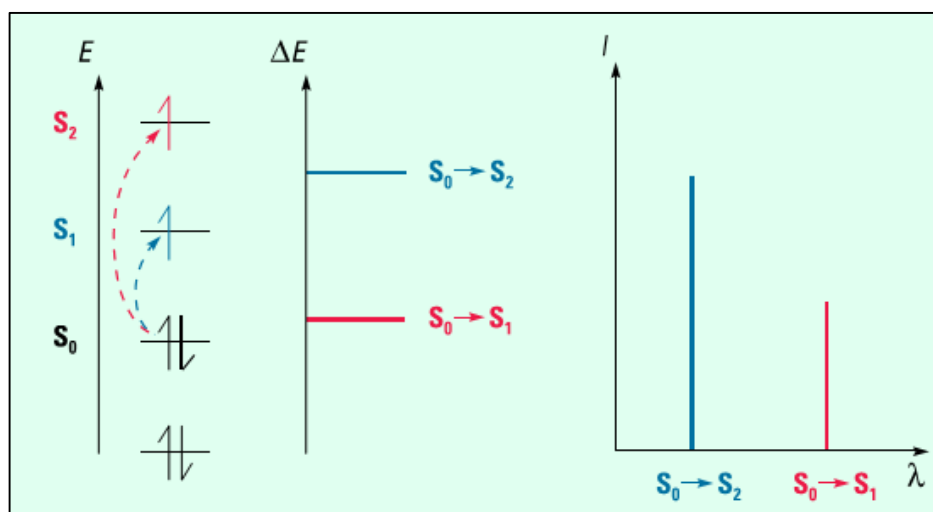


Figure 2.2: Electronic transitions and spectra of atoms.<sup>139</sup>

However, for molecules this is rarely observed. Broadened absorption bands are seen, instead. A large number of vibrational and rotational energy levels are superimposed on each electronic energy level, and many transitions with different energies result in peak broadening, Fig. 2.3.

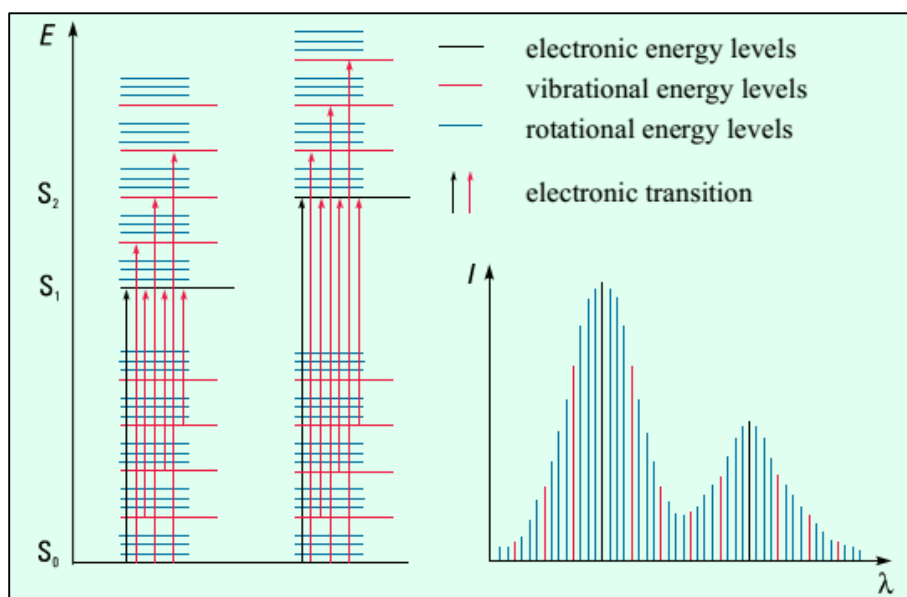


Figure 2.3: Electronic transitions and UV-vis spectra in molecules.<sup>139</sup>

When light passes through or is reflected from a sample, an excitation occurs as the valence electrons will absorb some of the energy from the light source. The absorbance is the difference between the transmittance radiation ( $I$ ) and the incident radiation ( $I_0$ ), which can be expressed as either transmittance ( $T$ ), Equation 2.1 or absorbance ( $A$ ), Equation 2.2.

$$T = I/I_0 \text{ or } \%T = (I/I_0) \times 100 \quad \text{Equation 2.1}$$

$$A = -\log T \quad \text{Equation 2.2}$$

For most applications, absorbance values are used to measure concentration in accordance with the Beer-Lambert law since the relationship between absorbance and concentration is linear.<sup>139</sup>

### 2.1.3. Absorbance law <sup>140</sup>

When the radiation comes into contact with the atoms or molecules, the intensity of the incident (exciting) light is reduced, raising them to higher energy levels. The extent of attenuation depends on the path length through the sample and on the concentration of the absorbing species, as shown in Fig. 2.4.

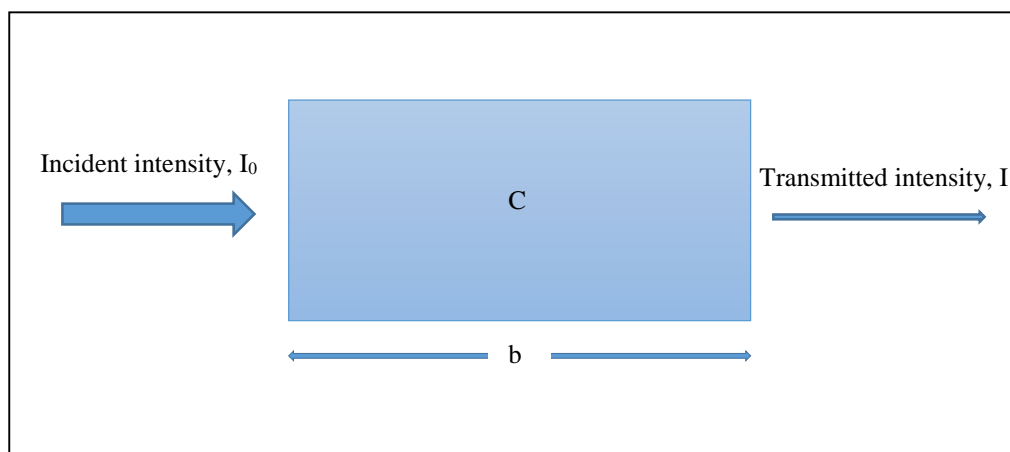


**Figure 2.4: The absorption of electromagnetic radiation by a sample.**

As the intensity decreases exponentially when the radiation of a particular wavelength passes through the sample, Lambert's law indicated that the fraction of light absorbed is depended on the path length. The mathematical formulation is expressed as in Equation 2.3:

$$T = I/I_0 = e^{-kb} \quad \text{Equation 2.3}$$

Where,  $e$  is the base of natural logarithms,  $k$  is a constant and  $b$  is the path length.

Beer's law indicated that absorption is proportional to the number of absorbing molecules. Combining these two laws, gives the Beer-Lambert Law, Equation 2.4:

$$T = I/I_0 = e^{-kbc} \quad \text{Equation 2.4}$$

Where,  $c$  is the concentration of the absorbing molecules. By taking the logarithm this equation can be transformed into a linear expression, Equation 2.5:

$$A = -\log T = -\log(I/I_0) = \log(I_0/I) = \epsilon bc \quad \text{Equation 2.5}$$

Where,  $\epsilon$  is the molar absorptivity.

Since the absorbance is proportional to the concentration, quantification can be carried out by comparing the absorbance of the sample with the absorbance of standards at known concentrations.

#### 2.1.4. Components of a spectrophotometer <sup>140-142</sup>

An UV-vis spectrophotometer is an instrument for measuring the reflectance, transmittance or absorbance of a sample as a function of the wavelength of incident light. A typical system contains the following key components: a source of light, a monochromator, a sample compartment, a detector and a display or data processor, as shown in Fig. 2.5.

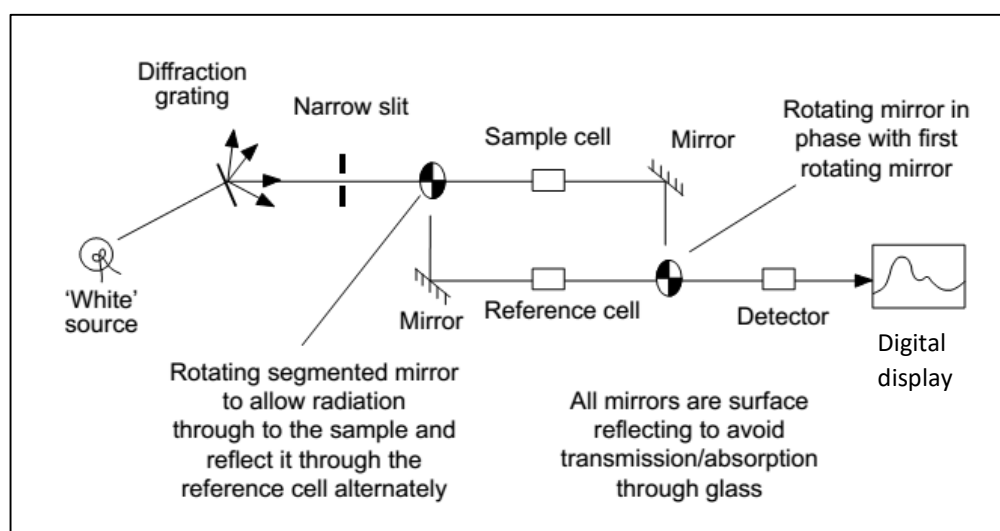


Figure 2.5: Schematic diagram of UV-vis spectrometer.<sup>140</sup>

Most spectrophotometers used to measure the UV-vis range contain some combination of a deuterium arc lamp, a tungsten filament lamp and a tungsten halogen bulb as sources of light. Xenon arc lamps may also be used. No single lamp can provide radiation across the whole range required. A tungsten filament lamp or a tungsten halogen lamp is typically the source of visible light (400-800 nm). The source most

often used for the UV range (200-400 nm) is a deuterium lamp. Arrangements are made to switch between these sources at an appropriate wavelength, often around 380 nm. The power output of the light source must be high enough to produce reflected signals sufficiently stronger than the background noise signal. A constant intensity over the wavelength range, and long term stability are required for an ideal light source, which unfortunately does not exist.

Dispersion devices cause different wavelengths of light to be dispersed at different angles and collect the reflected signal. Diffraction gratings and silica glass prisms are the typical dispersive elements. These devices can be used to select a narrow wavelength band of light for quantitative analysis when combined with an appropriate exit slit filter. Light from the source passes down the slit and is reflected equally onto a set of mirrors so that beams pass through the sample and reference cells.

In transmittance mode, the sample is generally a dilute solution. In a transmittance spectrometer, the sample solution is typically contained in a square thin-walled silica glass cell with optical path lengths of 1 cm. The solvent alone or another sample blank contained in a matched reference cell. The sample compartment can be replaced to convert the instrument to reflectance mode for analysis of solid samples. Reflectance measurements are made on opaque surfaces, such as thin layer chromatography plates or materials with surface coatings.

The final major component of a UV-vis spectroscopy system is the detector that converts photons of radiation into tiny electrical currents. Either a photomultiplier tube detector or photoelectric devices are used. A multi-channel diode array detector may also be used in some instruments to detect all the wavelengths simultaneously with a resolution of about  $\pm 1$  nm. This provides a faster analysis and an improved signal/noise ratio.

Some visual presentation or display is needed in order to observe and record the spectrometric results. The recorded spectrum is generally displayed by plotting absorbance against wavelength.

## **2.2. Charge-coupled devices (CCDs)**

A charge-coupled device (CCD) is a circuit, light-sensitive detector initially conceived to operate as a memory device. They were invented in the late 1960s at Bell Laboratories by Willard S. Boyle and George E. Smith.<sup>143, 144</sup> In recent years, CCDs have become a major technology for digital imaging. The CCDs are now used as the image sensor in digital and video cameras, modern scanners and photocopiers. They are also used in bar code readers, medical imaging devices, spectroscopic detectors, astronomical telescopes and other devices.<sup>145</sup>

### **2.2.1. Basic of operation**

Technically, generating an image with a CCD image sensor can be divided into four primary functions:

1. Charge generation
2. Charge collection and storage
3. Charge transfer
4. Charge measurement.

Detailed discussions of these operation functions can be found in several textbooks and reviews.<sup>146-151</sup> A brief introduction to each function is given below.

In the CCD, the data for an image is represented in such a way that each pixel in the image is converted into a corresponding number of electrons. The stronger the light, the more electrons are generated. When photon falls onto one of the circuit' pixels, charges are released from atoms in the pixel. These charges are stored in the depletion region of a metal-oxide-semiconductor (MOS) capacitor. By placing the MOS capacitors very close to one another the charges are allowed to move within the CCD circuit and manipulate on the gates of the capacitors. Thus, the charge is transfer from one MOS capacitor to the next on a parallel sequence. In order to measure the amount of light that fell onto each pixel, a charge detection amplifier is used to detect the presence of the charge on the pixel at the end of the last row in the grid. As a result, an output voltage is generated for each pixel proportional to the signal charge

transferred. The charge is then dumped onto a small capacitor connected to an output amplifier, and the next charge in line is measured. This process is repeated until all the charges in that row have been measured. Then all the charges in all the remaining rows are made to shift over one row, and the whole process is repeated.

### 2.2.2. Colour CCD image sensors

The analytical data that a CCD image sensor returns are depending on the amount of light from bright to dark with no colour information.<sup>152</sup> Since CCD image sensors are ‘colour blind’, a colour filter in front of the sensor allows the sensor to convert the electrical charge to colour tones. The intensity of this is related to a colour in the colour spectrum. There are two common methods for colour registration. Red, green, and blue (RGB) and cyan, magenta, yellow, and green (CMYG).<sup>153</sup>

The primary colours RGB with 8 bits each are mixed in different combinations to produce most of the colours recognisable by the human eye. Hence, a value is returned to the user ranging from 0 to 255 for each channel. The most common RGB colour filter is a Bayer array, which arrange RGB in a square grid has alternating rows of red-green and green-blue filters. This arrangement of colour filter is particularly used in most digital cameras, video cameras and scanners to create a colour image.<sup>154, 155</sup>

Complementary colours CMYG filter is another way to filter colour on CCD image sensors. Due to its broader spectral band pass, the CMYG system basically offers higher pixel signals. However, because the signals must then be converted to RGB, this implies more processing and added noise.<sup>153, 156</sup>

## 2.3. Data handling approaches <sup>157-161</sup>

### 2.3.1. The arithmetic mean

**The arithmetic mean,  $\bar{x}$**  - also called the average - is the average quantity of a discrete set of measurements. The mean can be calculated using Equation 2.6:

$$\bar{x} = \frac{\sum_{i=1}^n x_i}{n} \quad \text{Equation 2.6}$$

Where, n is the number of independent measurements, and x is the measurements for observation i.

### 2.3.2. Measures of spread

**The standard deviation, S** is a numerical value used to indicate how the individual measurements spread about the mean. The standard deviation is calculated as the square root of variance, as indicated in Equation 2.7:

$$S = \sqrt{\frac{\sum_{i=1}^n (x_i - \bar{x})^2}{n-1}} \quad \text{Equation 2.7}$$

Where,  $x_i$  is one of n individual measurements, and  $\bar{x}$  is the mean.

Frequently, **the relative standard deviation, RSD** is reported, which can be calculated by using Equation 2.8.

$$\%RSD = \frac{s}{\bar{x}} \times 100 \quad \text{Equation 2.8}$$

### 2.3.3. Accuracy and precision of analysis

**Accuracy** is a measure of how close a measure of mean value is to the true value ( $\mu$ ), or expected value. Accuracy is usually calculated using Equation 2.9.

$$E_r = \frac{\bar{x} - \mu}{\mu} \times 100 \quad \text{Equation 2.9}$$

**Precision** is a measure of the variability or closeness within a set of replicate measurements. It may be expressed as the range, the standard deviation, or the relative standard deviation. Precision is commonly determining the repeatability and reproducibility. Repeatability is the precision obtained when a sample is repeatedly analysed under identical circumstances during a single period of laboratory work, using the same solutions and equipment. Reproducibility is the precision obtained under any other set of circumstances, including that between samples, or between laboratory sessions for a single sample.

#### 2.3.4. Limit of detection<sup>159</sup>

**The limit of detection, LOD** is the lowest concentration of an analyte that can be detected, but not necessarily quantified, to be statistically different from an analyte blank. **The limit of quantification LOQ** is the lowest concentration of an analyte that can not only be reliably detected, but at which acceptable precision and accuracy are met. The LOQ may be equivalent to the LOD or it could be at a much higher concentration. To calculate the instrumental LOD and LOQ, Equation 2.10 can be used.

$$LOD \text{ or } LOQ = \frac{F \times s}{\text{slope of calibration curve } S} \quad \text{Equation 2.10}$$

Where F is Factor of 3.3 and 10 for LOD and LOQ, respectively; s is standard deviation of the blank and S is the slope or sensitivity of the calibration curve.

However, other commonly methods are used to express the detection limit, one such method is based on the visual evaluation. Because of its simplicity, the visual detection limit is determined by the analysis of standards with known concentrations and by establishing the minimum level at which the analyte can be reliably detected by the naked eye. Additionally, the response signals of replicate measurements of a serial number of diluted standards are measured, then a calibration curve is prepared. The regression line passes through the representative points. This line affords a prediction that any new standard will give a signal falling in the neighbourhood of this obtained line. The lowest response distinguished from the blank is then detected from the calibration line as the limit of detection.<sup>162</sup> The latest methods were used in this thesis.

#### 2.3.5. Correlation coefficient and the coefficient of determination

The common method to evaluate the linear relationship between variables x and y is to calculate the Pearson product-moment correlation coefficient, r, which is referred to simply as the correlation coefficient. This statistic is calculated as in Equation 2.11:

$$r = \frac{\sum_i [(x_i - \bar{x})(y_i - \bar{y})]}{\sqrt{[\sum_i (x_i - \bar{x})^2][\sum_i (y_i - \bar{y})^2]}} \quad \text{Equation 2.11}$$

The values of  $r$  can only lie in the range of  $-1 \leq r \leq +1$ . When  $r = -1$  this indicated a perfect negative correlation between the variables. Similarly, when  $r = +1$  a perfect positive correlation is observed. If the variables  $x$  and  $y$  are not related, the value of  $r$  will be close to zero  $r = 0$ . The higher the values of  $r$ , the stronger the relationship between the two variables. Thus, when  $r$  value between 0.1 and 0.3, this indicates a weak relationship, a value between 0.4 and 0.6 indicates a moderate relationship, and a value between 0.7 and 0.9 indicates a strong relationship. By squaring the correlation coefficient, the resultant is the coefficient of determination  $r^2$  which describe the strength of the linear association between  $x$  and  $y$ .

## 2.4. Statistical analysis of data <sup>142, 158, 163</sup>

### 2.4.1. Significance testing

A significance test is designed to compare whether the difference between a calculated experimental factor and a tabulated factor is significant. A null hypothesis and an alternative hypothesis provide answers as to whether a difference is significant or not. The **null hypothesis** “is that indeterminate error is sufficient to explain any difference in the values being compared”.<sup>157</sup> The **alternative hypothesis** “is that the difference between values is too great to be explained by a random error and, therefore, must be real”.<sup>157</sup> Significance tests are carried out at a significant level,  $\alpha$ , that defines the probability of rejecting a null hypothesis that is true. Tabular values for some significance tests have been compiled for what are described as one-tailed and two-tailed tests. A one-tailed test is to establish whether one experimental value significantly greater than the other, while a two-tailed test is used to establish whether there is a significant difference between the two values being compared.

#### 2.4.1.1. F-test

The F-test is a test statistic that is used for comparing the precisions of two sets of data to see if their difference is or is not significant. Calculated F value,  $F_{\text{calc}}$ , is defined as the ratio of the two samples variances, as in Equation 2.12.

$$F_{\text{calc}} = \frac{s_A^2}{s_B^2} \qquad \text{Equation 2.12}$$

Where  $s^2_A$  is greater than or equal to  $s^2_B$ .

The  $F_{\text{calc}}$ , is calculated and compared with a critical F value,  $F_{\text{critical}}$ , at a defined confidence level, usually 95%, two-tailed, and for the number of degrees of freedom ( $v = n-1$ ), where n is the number of replicates. If  $F_{\text{calc}}$  is less than or equal  $F_{\text{critical}}$ , then the null hypothesis that there is no significant difference between the two variances stands. If  $F_{\text{calc}}$  is larger than  $F_{\text{critical}}$ , the F-test is failed and there is a significant difference between the two variances.

#### 2.4.1.2. T-test

The T-test is a test statistic that is used for comparing two mean values to see if their difference is or is not significant. This test is used to compare the experimental means of one set of data with a reference value or to compare the experimental means of two sets of data. The calculated t value,  $t_{\text{calc}}$ , is calculated, depending on the circumstances, by one of three alternative equations.

##### *Comparison of one experimental mean with a known value*

$$t_{\text{calc}} = \frac{[\bar{x} - \mu] \times \sqrt{n}}{s} \quad \text{Equation 2.13}$$

Where  $\mu$  is true mean value,  $\bar{x}$  is measured mean value, n is a number of replicates, and s is a standard deviation.

##### *Comparison of two experimental means*

Equation 2.14 is used when the F-test is passed;

$$t_{\text{calc}} = \frac{[\bar{x}_A - \bar{x}_B]}{s_{\text{pool}} \times \sqrt{(1/n_A) + (1/n_B)}} \quad \text{Equation 2.14}$$

Where  $\bar{x}_A$  and  $\bar{x}_B$  are measured means of samples A and B,  $n_A$  and  $n_B$  are a number of replicates, and  $s_{\text{pool}}$  is the pooled standard deviation, which it is calculated by Equation 2.15:

$$s_{\text{pool}} = \sqrt{\frac{(n_A - 1)s_A^2 + (n_B - 1)s_B^2}{n_A + n_B - 2}} \quad \text{Equation 2.15}$$

Equation 2.16 is used to calculate the t-test when the F-test is failed;

$$t_{\text{calc}} = \frac{[\bar{x}_A - \bar{x}_B]}{\sqrt{(s_A^2/n_A) + (s_B^2/n_B)}} \quad \text{Equation 2.16}$$

The  $t_{\text{calc}}$ , is calculated and compared with a critical t value,  $t_{\text{critical}}$ , at two-tailed 0.05  $\alpha$ , and for the number of degrees of freedom  $\nu$ .

If F-test is passed, the  $\nu$  value is calculated by Equation 2.17, while Equation 2.18 is used when the F-test is failed.

$$\nu = n_A + n_B - 2 \quad \text{Equation 2.17}$$

$$\nu = \frac{[(s_A^2/n_A) + (s_B^2/n_B)]^2}{\left[\frac{s_A^2/n_A}{n_A + 1}\right]^2 + \left[\frac{s_B^2/n_B}{n_B + 1}\right]^2} - 2 \quad \text{Equation 2.18}$$

### **3. General experimental procedures**

This chapter describes the experimental procedures used throughout the thesis. Some further specific procedures related to individual chapters will be described later.

#### **3.1. Cleaning procedure**

All glassware used during the experiments was first soaked in an acid bath filled with 10% (v/v) HNO<sub>3</sub> overnight. Then they were rinsed with distilled water and dried in a clean air environment before use.

#### **3.2. Determination of Hg<sup>2+</sup> based on the reaction with copper iodide (CuI)**

##### **3.2.1. Reagents and apparatus**

###### **Reagent**

All chemicals used were of analytical reagent grade. Mercury standard solution 10000 µg/mL, Hg(NO<sub>3</sub>)<sub>2</sub>, was purchased from QMX Laboratories Ltd. (Essex, UK). Nitric acid (HNO<sub>3</sub> > 65% for trace analysis), hydrochloric acid (HCl, 30% for trace analysis) and tin (II) chloride dihydrate, SnCl<sub>2</sub>·2H<sub>2</sub>O were obtained from Sigma-Aldrich Company Ltd. (Gillingham, UK). Magnesium sulfate dried (MgSO<sub>4</sub>) was obtained from BDH VWR International Ltd. (Poole, UK). Tin grains were purchased from BDH Laboratory Chemical Division (Poole, UK). Detecting papers coated with CuI emulsion (CuI: 5 g; 3% carboxymethylcellulose: 10 g; MgCl<sub>2</sub> moistening agent: 1.5 g) were purchased from Cetem, Centro de Tecnologia Mineral, Rio de Janeiro, Brazil.

###### **Apparatus**

Determination systems (3) each consisting of a conical flask, aeration duct (bubbler), aquarium pump (Elite Pro, Brazil), PVC paper support, mini condenser, acrylic support and plastic mould were obtained from Cetem, Centro de Tecnologia Mineral (Rio de Janeiro, Brazil). Mini aquarium pumps (3), AquaAir Mini were from Interpet (Surrey, UK). UV-vis reflectance spectrometer, CCD Array reflectance unit (S.I. Photonics, Inc. USA).

### **3.2.2. Procedures**

#### **3.2.2.1. Solutions preparation**

##### **50% (w/v) SnCl<sub>2</sub> solution**

A 50 g portion of SnCl<sub>2</sub>·2H<sub>2</sub>O was weighed into a 500 mL beaker, then 50 mL of HCl and 50 mL of distilled water were slowly added. The solution was stored in an amber storage bottle containing grains of metallic tin to maintain stability.

##### **Stock Hg<sup>2+</sup> standard solution (10 mg/L in 10% (v/v) HNO<sub>3</sub>)**

A 100 µL aliquot of a 10000 µg/mL Hg<sup>2+</sup> standard solution was pipetted into a 100 mL volumetric flask containing approximately 50 mL distilled water, followed by 10 mL of HNO<sub>3</sub>. The solution was made up to 100 mL with distilled water, stored at 4 °C and replaced monthly.

##### **Standard solutions of Hg<sup>2+</sup> at different concentration**

From the 10 mg/L Hg<sup>2+</sup> stock solution, standard solutions were prepared daily as required.

#### **3.2.2.2. Conditioning of detecting papers**

Since paper humidity affects Hg<sup>0</sup> capture,<sup>164</sup> the detecting papers were conditioned for at least 48 hours before use in a desiccator containing a saturated solution of MgSO<sub>4</sub> in order to produce 90-95 % atmosphere humidity.

#### **3.2.2.3. Determination of Hg<sup>2+</sup> as spot test**

A 75 ml aliquot of Hg<sup>2+</sup> standard solution was reduced to Hg<sup>0</sup> by 5 mL of SnCl<sub>2</sub>. The visual detection in the form of spot tests was carried out by adding dropwise approximately 100 µL of the reduced Hg standard solution onto the CuI detection paper. In the same manner, the spot test mode was also carried out using the non-reduced Hg standard solution.

#### 3.2.2.4. Determination of $\text{Hg}^{2+}$ using the Hg bubbler apparatus of Yallouz *et al.*<sup>165</sup>

Approximately 75 mL of  $\text{Hg}^{2+}$  standard solution was transferred into a 250 mL conical flask following which 5 mL of  $\text{SnCl}_2$  reductant was added. A two-armed aeration duct (bubbler) was inserted into the conical flask where the short arm of the bubbler was connected to the condenser at the back of the determination unit *via* suitable tubing and the long arm of the bubbler, that was immersed in the solution, was connected to an aquarium pump, Fig. 3.1. Once the connection was complete, the detecting paper was removed from the desiccator and cut to the required size by placing it on top of a mould and cutting around it, Fig. 3.2.

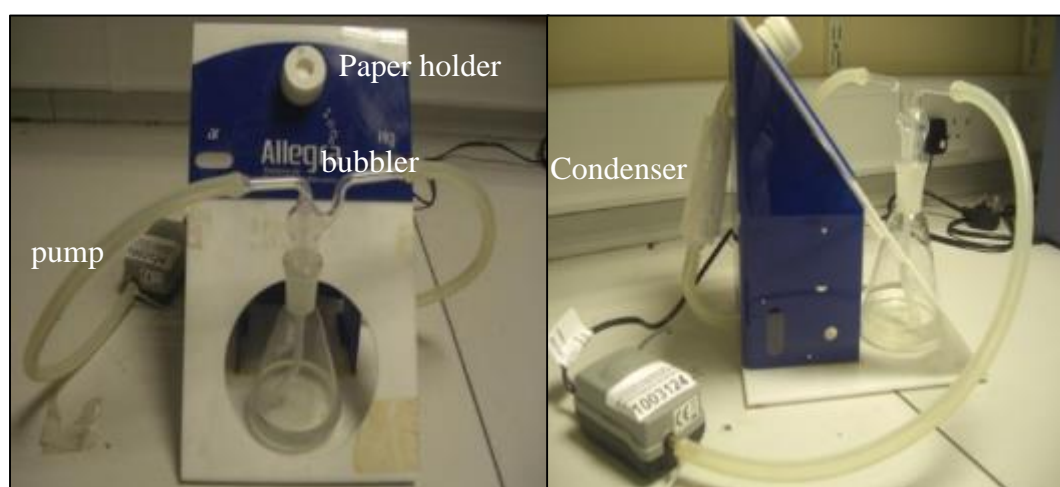


Figure 3.1: Set up of the Hg bubbler apparatus for the semi-quantitative determination of Hg.



Figure 3.2: Plastic mould and sheet consisting of six CuI detecting papers.

The detecting paper was then positioned inside the holder, Fig. 3.3. The aquarium pump was turned on and air was then bubbled through the sample. Mercury vapour was removed via the aeration duct and forced to pass through the paper where it reacted with the coating to produce the  $\text{Cu}_2[\text{HgI}_4]$  complex. The determination step was continued for 20 min. To avoid pump damage, the paper holder was opened and the paper removed before turning off the pump. Each standard was analysed at least twice to assess the results' quality.



Figure 3.3: Poly(vinyl chloride) paper holder.

### 3.3. Determination of $\text{Hg}^{2+}$ based on the reaction with diphenylcarbazone (DPC)

#### 3.3.1. Reagents and apparatus

Mercury standard solution 10000  $\mu\text{g}/\text{mL}$ ,  $\text{Hg}(\text{NO}_3)_2$ , was purchased from QMX Laboratories Ltd. (Essex, UK). Nitric acid ( $\text{HNO}_3 > 65\%$  for trace analysis), ethanol absolute  $> 99.8\%$  and diphenylcarbazone (DPC) were supplied by Sigma-Aldrich Company Ltd. (Gillingham, UK). Filter papers (qualitative Fisher brand) were obtained from Fisher Scientific (UK).

#### 3.3.2. Procedures

##### 3.3.2.1. Solutions preparation

### **1% (w/v) DPC solution in ethanol**

A 1 g portion of DPC was weighted in a 100 mL beaker followed by the addition of 50 mL ethanol. The mixture was transferred to a 100 mL volumetric flask and made up to the mark with ethanol. A fresh solution of DPC was prepared prior to the samples being analysed and stored in an amber storage bottle for up to two days.

### **Mercury stock standard solution (1000 mg/L, pH 4.6)**

A 1000  $\mu\text{L}$  aliquot of a 10000  $\mu\text{g}/\text{mL}$   $\text{Hg}^{2+}$  standard solution was pipetted into a 100 mL volumetric flask containing approximately 50 mL distilled water, followed by 1.274 mL of  $\text{HNO}_3$ . The solution was made up to 100 mL with distilled water after adjusting the pH carefully to 4.6 by use 1.0 Mol solution of NaOH, stored at 4 °C, and replaced monthly.

#### **3.3.2.2. Determination of $\text{Hg}^{2+}$ in solution phase**

A 1 mL aliquot of each  $\text{Hg}^{2+}$  standard solution was transferred to a mini centrifuge test tube, followed by the addition of 50  $\mu\text{L}$  of 1% ethanolic DPC solution.

#### **3.3.2.3. Determination of $\text{Hg}^{2+}$ as spot test**

Test papers of DPC were produced by immersing filter papers with a 1% ethanolic DPC solution. Immediately after the paper was produced, 100  $\mu\text{L}$  aliquot of  $\text{Hg}^{2+}$  standard solution was added dropwise on to the DPC test paper. The same procedure was performed after the test paper had completely dried under ambient conditions.

### **3.4. Determination of $\text{Hg}^{2+}$ based on the reaction with rhodamine 6G (R6G)**

#### **3.4.1. Reagents and apparatus**

##### **Reagents**

All chemicals used were of analytical reagent grade from Sigma-Aldrich Ltd. (Gillingham, UK), unless otherwise stated: hexamine, potassium iodide (KI), rhodamine 6G (R6G), gelatin, nitric acid ( $\text{HNO}_3 > 65\%$  for trace analysis and tin (II)

chloride dihydrate ( $\text{SnCl}_2 \cdot 2\text{H}_2\text{O}$ ). The mercury standard solution 10000  $\mu\text{g/mL}$ ,  $\text{Hg}(\text{NO}_3)_2$  was from QMX Laboratories Ltd. (Essex, UK). Filter papers (qualitative Fisher brand) were obtained from Fisher Scientific (UK).

### **Apparatus**

In addition to the apparatus listed in Section 3.2.1, a UV-vis spectrometer, Varian Cary 50 probe (Varian, Inc.) was used for transmittance measurements in solution.

### **3.4.2. Procedures**

#### **3.4.2.1. Solutions preparation**

##### **Stock $\text{Hg}^{2+}$ standard solution (10 mg/L in 10% (v/v) $\text{HNO}_3$ )**

Mercury stock solution and working standard solutions were prepared as described in Section 3.2.2.1.

##### **1 Mol/L Hexamine buffer, pH 5.0**

A 14.02 g mass of hexamine was weighed into a 100 mL beaker; then 50 mL of distilled water was slowly added. The pH of the solution was adjusted to  $\sim 5$  with 0.1 Mol  $\text{HNO}_3$ . The solution was transferred to a 100 mL volumetric flask and made up to the mark with distilled water.

##### **10% (w/v) KI solution**

A 10 g portion of KI was weighed into a 500 mL beaker, followed by the addition of 50 mL distilled water. The solution was transferred to a 100 mL volumetric flask and made up to the mark with distilled water.

##### **0.01% (w/v) R6G solution**

A 0.01 g portion of R6G was weighed into a 500 mL beaker, followed by the addition of 50 mL distilled water. The solution was transferred to a 100 mL volumetric flask and made up to the mark with distilled water.

### **1% (w/v) Gelatine solution**

A 1 g portion of gelatine was weighed into a 500 mL beaker, followed by the addition of 50 mL distilled water. The solution was transferred to a 100 mL volumetric flask and made up to 100 mL with distilled water.

### **50% (w/v) SnCl<sub>2</sub> solution**

A 50% (w/v) SnCl<sub>2</sub> solution was prepared as described in Section 3.2.2.1.

#### **3.4.2.2. Determination of Hg<sup>2+</sup> in solution phase**

A 4 mL aliquot of Hg<sup>2+</sup> standard solution and 1 mL of hexamine buffer were pipetted in to a 25 mL beaker. The pH was adjusted to  $5.2 \pm 0.2$  using HNO<sub>3</sub> or NaOH. A 2 mL aliquot of 5% KI, 2 mL of 0.01% R6G, followed by 1 mL of 1% gelatine were added to the beaker. The solution was transferred to a 25 mL volumetric flask and diluted to the mark with distilled water. Approximately 3 mL of the solution was added to a 1 cm<sup>2</sup> quartz cell. The absorbance was measured over a wavelength range of 390-700 nm using a UV-visible spectrophotometer.

#### **3.4.2.3. Determination of Hg<sup>2+</sup> as spot test**

Test papers of R6G were produced by immersing filter papers in a mixture of 1 mL hexamine buffer, 2.5 mL 10% KI, 5 mL 0.01% R6G and 1 mL 1% gelatin. Approximately 100  $\mu$ L of each Hg<sup>2+</sup> standard solution was added dropwise onto the surface of the R6G test paper either immediately after the papers were produced or after the test paper had completely dried under ambient condition.

### **3.5. Determination of Hg<sup>2+</sup> based on the reaction with rhodamine B thiolactone**

#### **3.5.1. Reagents and apparatus**

##### **Reagents**

All chemicals used were of analytical reagent grade. Mercury standard solution 10000  $\mu$ g/mL, Hg(NO<sub>3</sub>)<sub>2</sub>, and multi-element standard solution 10 mg/L each of As<sup>3+</sup>, Cd<sup>2+</sup>,

$\text{Co}^{2+}$ ,  $\text{Cr}^{3+}$ ,  $\text{Cu}^{2+}$ ,  $\text{Fe}^{3+}$ ,  $\text{Mg}^{2+}$ ,  $\text{Mn}^{2+}$ ,  $\text{Na}^+$ ,  $\text{Ni}^{2+}$ ,  $\text{Pb}^{2+}$  and  $\text{Zn}^{2+}$  in 2%  $\text{HNO}_3$  were purchased from QMX Laboratories Ltd. (Essex, UK). Nitric acid ( $\text{HNO}_3 > 65\%$  for trace analysis), acetonitrile ( $\text{CH}_3\text{CN}$ ), 1,2-dichloroethane ( $\text{ClCH}_2\text{CH}_2\text{Cl}$  for HPLC  $\geq 99.8\%$ ), dichloromethane ( $\text{CH}_2\text{Cl}_2$ ), ethyl acetate analytical standard ( $\text{CH}_3\text{COOC}_2\text{H}_5$ ), petroleum ether 40-60 °C, and phosphorus (V) oxychloride ( $\text{POCl}_3 > 99\%$  for trace analysis) were supplied by Sigma-Aldrich Company Ltd. (Gillingham, UK). Acetate buffer solution 1.0 M pH 5 sodium acetate / acetic acid solution ready for use, and sodium sulfide anhydrous ( $\text{Na}_2\text{S} > 99.99\%$  for trace analysis) were obtained from Alfa Aesar (Lancashire, UK). Rhodamine B base analytical standard 99% ( $\text{C}_{28}\text{H}_{30}\text{N}_2\text{O}_3$ ) was supplied by ACROS Organics (New Jersey, USA). Sea-salt was from Lake Products Company LLC (USA).

## **Apparatus**

Reflux apparatus consisted of a round-bottomed flask, a reflux condenser and a hotplate stirrer. Rotary evaporator, BUCHI (Switzerland). UV-vis spectrophotometer, Varian Cary 50 probe (Varian Inc.). pH meter, Mettler Toledo AG, Schwerzenbach (Switzerland). Norell® Standard Series™ 5 mm NMR tubes were obtained from Sigma-Aldrich Company Ltd. (Gillingham, UK). Nuclear magnetic resonance spectroscopy, NMR, AV3 400, 9.4 T Bruker UltraShield magnet, University of Strathclyde (Scotland, UK). X-ray generator, Rigaku HG Saturn724+ rotating anode instrument, Mo wavelength radiation ( $0.71075 \text{ \AA}$ ), National Crystallography Service, University of Southampton (Southampton, UK).

### **3.5.2. Procedures**

#### **3.5.2.1. Synthesis of rhodamine B thiolactone**

A 0.5 g portion of rhodamine B base was weighed and transferred into a 50 mL round-bottomed flask, and then 8 mL of  $\text{ClCH}_2\text{CH}_2\text{Cl}$  was added and stirred at room temperature. A 0.4 mL aliquot of  $\text{POCl}_3$  was added to the mixed solution dropwise over a period of 5 min. The mixed solution was refluxed at 83 °C for 4 h. The reaction mixture was allowed to cool and evaporated using a rotary evaporator to obtain crude rhodamine B acid chloride. A 3 mL aliquot of saturated  $\text{Na}_2\text{S}$  aqueous solution (1.95 g in 10 mL distilled water) was then added to the crude acid chloride, and the resulting

solution was stirred overnight at room temperature. Then the mixture solution was extracted with 25 to 50 mL of  $\text{CH}_3\text{COOC}_2\text{H}_5$ . The extraction product was concentrated under vacuum and purified by silica-gel column chromatography with  $\text{CH}_2\text{Cl}_2$ /petroleum ether (40-60°C) (1:1) as eluent. The components of the mixture ran down the column forming a separate yellow band. Once the yellow solution had eluted, the solvent was evaporated under vacuum using a rotary evaporator to afford a pale yellow solid rhodamine B thiolactone in 48% yield (0.25 g), as shown in Fig. 3.4.



**Figure 3.4: Solid rhodamine B thiolactone.**

### **3.5.2.2. Identification of rhodamine B thiolactone**

X-ray crystallography and NMR spectroscopy were used to confirm the structure of synthesised rhodamine B thiolactone. Single crystals of rhodamine B thiolactone that had grown from  $\text{CH}_2\text{Cl}_2$ - $\text{CH}_3\text{CN}$  (1:1) were suitable for X-ray crystallography. Crystallographic data for the rhodamine B thiolactone were collected by the UK National Crystallography Service. The sample had a structure that matched the one published by Shi *et al.*<sup>166</sup> The structure was solved by the Cambridge Structural Database System (CSD System) methods and refined on MERCURY software version 9.3. The thiospirocyclic structure of rhodamine B thiolactone is as illustrated in Fig. 3.5.

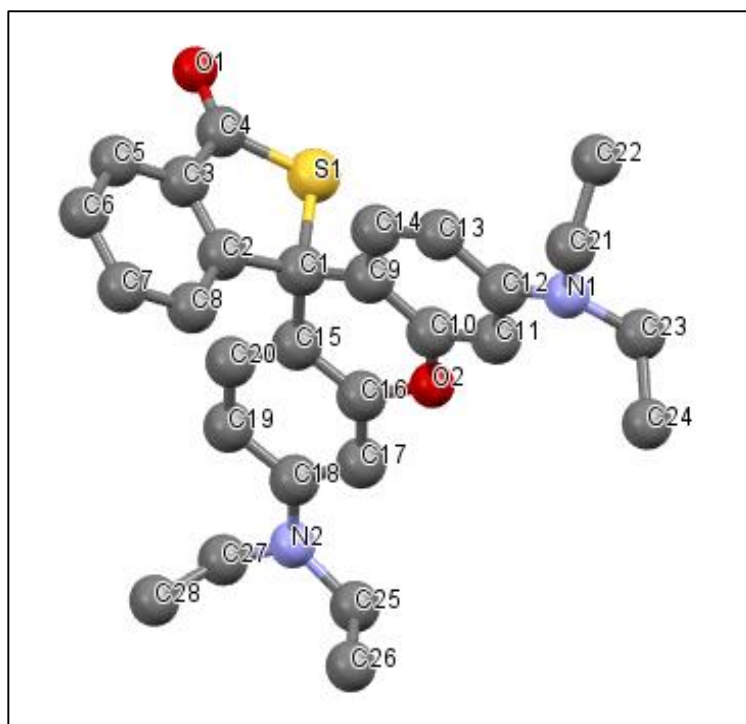


**Figure 3.5:** The molecular structure of rhodamine B thiolactone with the atomic-numbering scheme showing the spiro-ring structural fashion (hydrogen atoms were omitted for clarity, the S, O and N atoms were drawn in yellow, red and blue, respectively).

Hydrogen atoms were omitted for clarity. The two aromatic moieties of the rhodamine framework form vertical planes that break the conjugation of the system. The break of the conjugation system in the rhodamine framework leads to the characteristic colourlessness and non-fluorescence of the molecule and the stock solution thereof. The crystal data of the rhodamine B thiolactone compound are listed in Table A3.1, in Appendix 3.

For NMR spectroscopy measurements, a 10 mg portion of solid rhodamine B thiolactone was weighted, and 700  $\mu\text{L}$  of  $\text{CDCl}_3$  was then added. The resultant solution was transferred by pipette to a 5 mm NMR tube. The  $^1\text{H}$  NMR and  $^{13}\text{C}$  NMR spectra were measured on a Bruker AV3 400 spectrometer at 400 and 100 MHz. The  $^1\text{H}$  NMR and  $^{13}\text{C}$  NMR spectra of rhodamine B thiolactone are as shown in Fig. 3.6, 3.7 and 3.8, respectively.

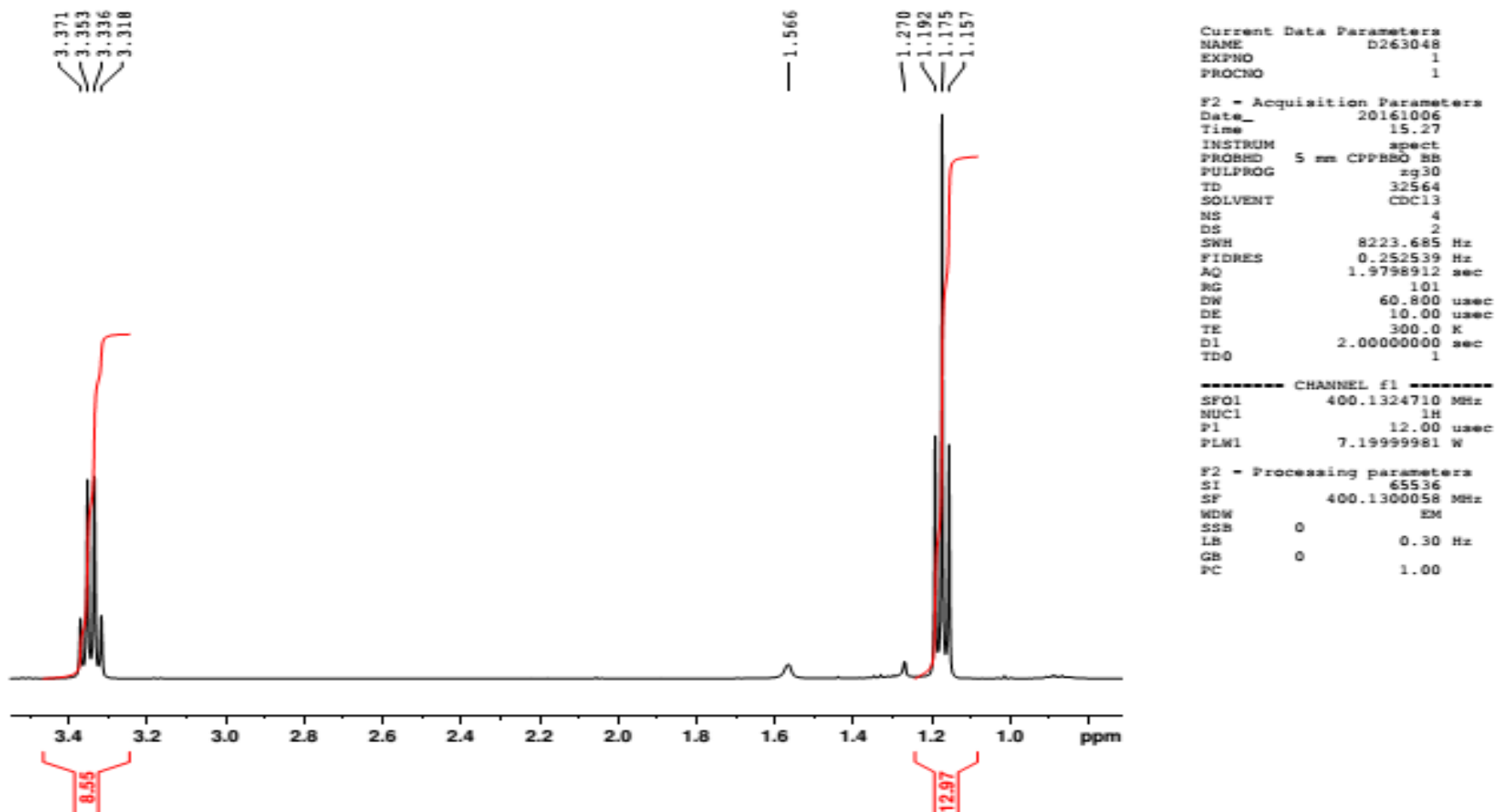


Figure 3.6:  $^1\text{H}$  NMR spectrum of rhodamine B thiolactone in  $\text{CDCl}_3$ .

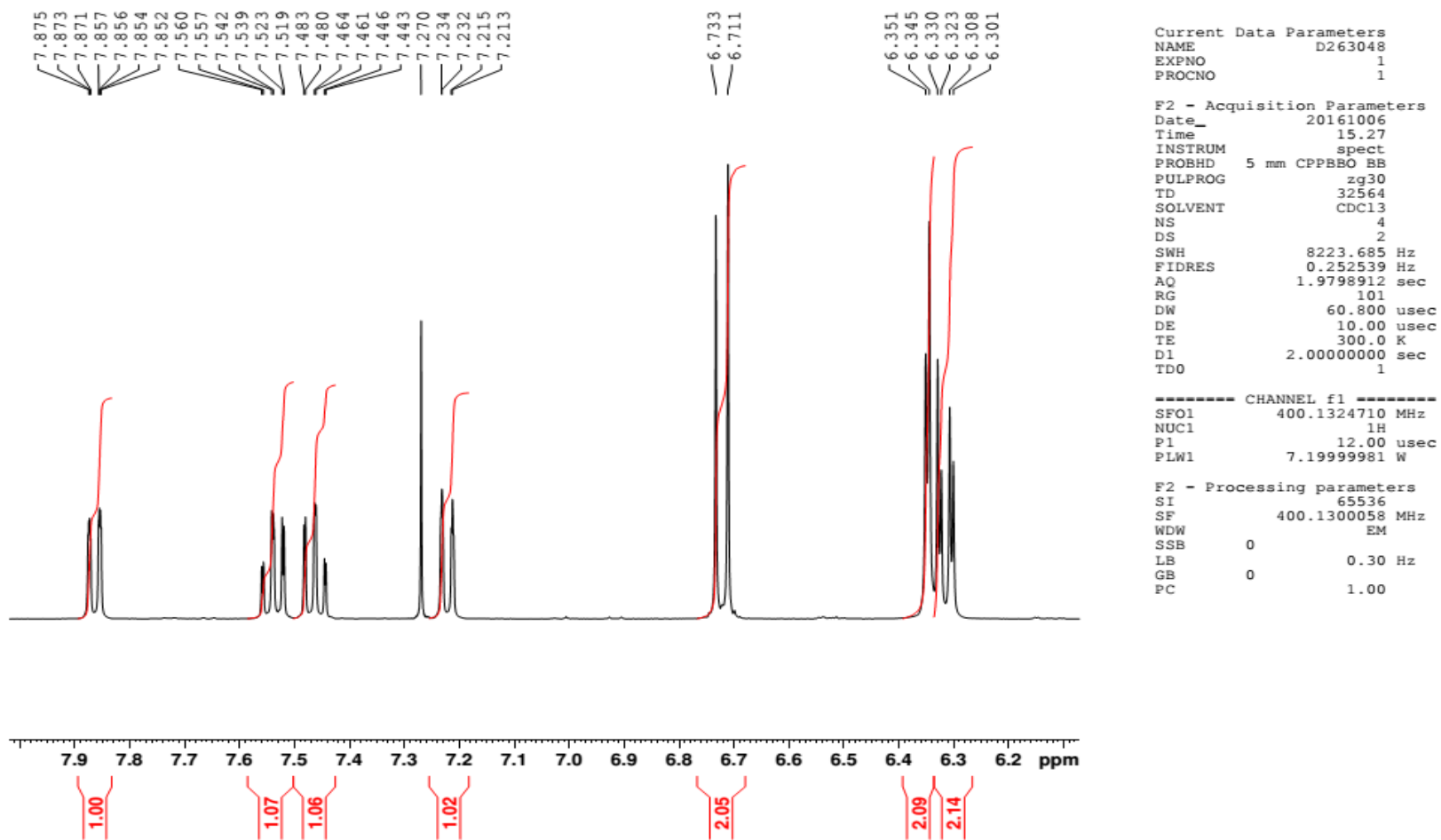
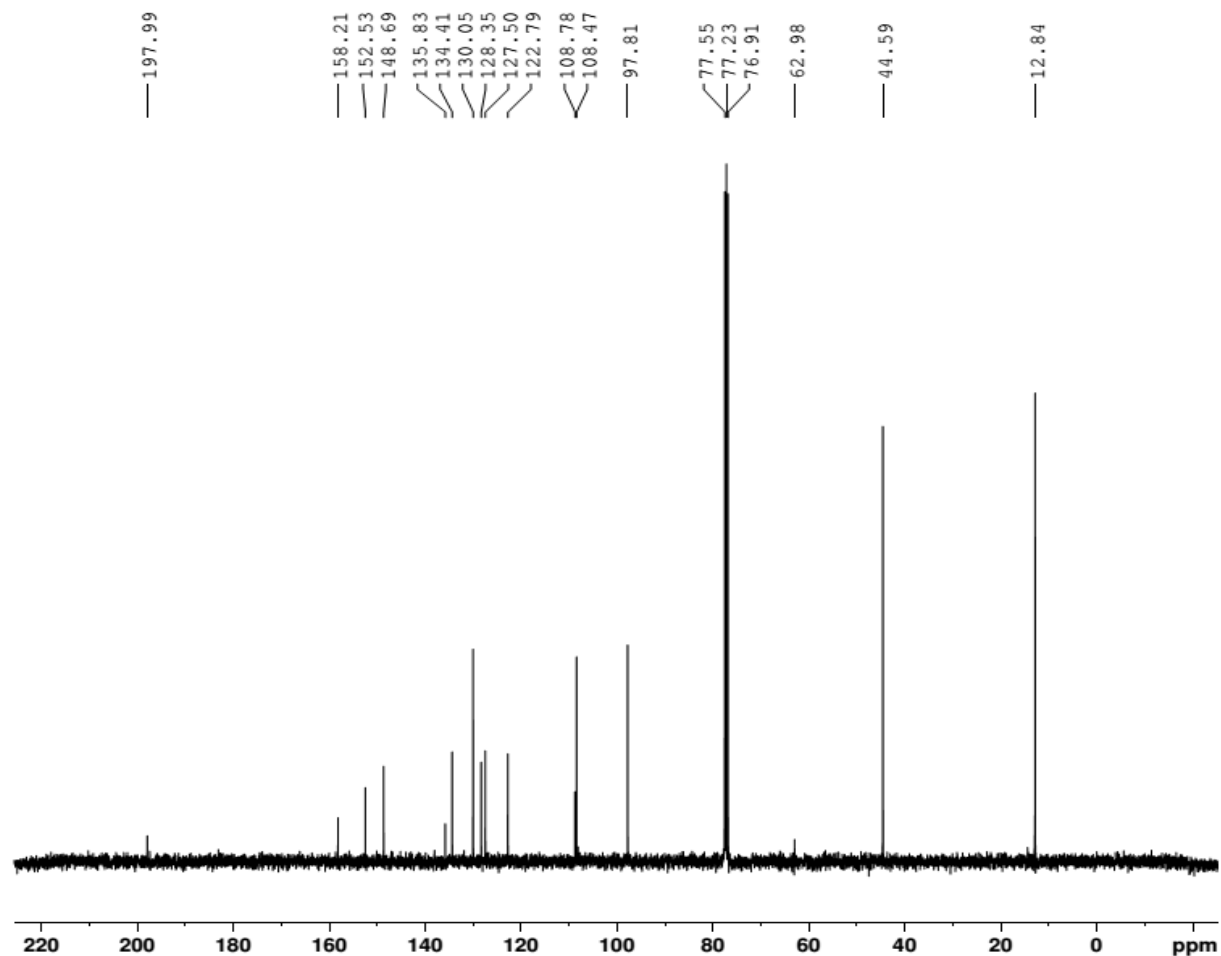


Figure 3.7:  $^1\text{H}$  NMR spectrum of rhodamine B thiolactone in  $\text{CDCl}_3$ .



```

Current Data Parameters
NAME          D263550
EXPNO         2
PROCNO        1

F2 - Acquisition Parameters
Date_         20161014
Time          15.47
INSTRUM       spect
PROBHD        5 mm CPPBBO BB
PULPROG       zgpg30
TD            16384
SOLVENT       CDC13
NS            64
DS            4
SWH           25252.525 Hz
FIDRES        1.541292 Hz
AQ            0.3244032 sec
RG            2050
DW            19.800 usec
DE            18.00 usec
TE            300.0 K
D1            0.69999999 sec
D11           0.03000000 sec
TD0           1

===== CHANNEL f1 =====
SFO1          100.6228298 MHz
NUC1          13C
P1            10.00 usec
PLW1          35.00000000 W

===== CHANNEL f2 =====
SFO2          400.1316005 MHz
NUC2          1H
CPDPRG[2]    waltz16
PCPD2        90.00 usec
PLW2          7.50000000 W
PLW12         0.16379000 W
PLW13         0.08238400 W

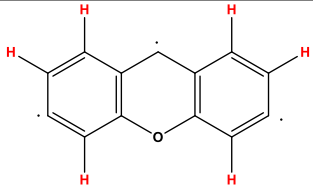
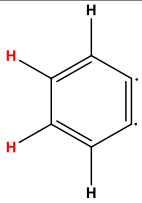
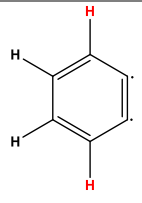
F2 - Processing parameters
SI            32768
SF            100.6127478 MHz
WDW           EM
SSB           0
LB            1.50 Hz
GB            0
PC            1.40

```

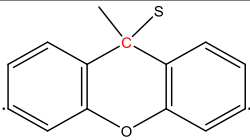
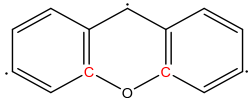
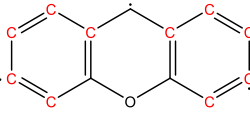
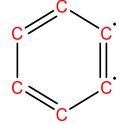
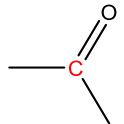
Figure 3.8:  $^{13}\text{C}$  NMR spectrum of rhodamine B thiolactone in  $\text{CDCl}_3$ .

The  $^1\text{H}$  NMR and  $^{13}\text{C}$  NMR spectra showed that the assignment of the peaks for both H and C were in agreement with the molecular structure. The chemical shifts of the signals fall in several well-defined regions, depending on the nature of the attached atoms and the substituents.  $^1\text{H}$  NMR and  $^{13}\text{C}$  NMR peak assignment data for rhodamine B thiolactone are shown in Table 3.1 and 3.2, respectively.

**Table 3.1:  $^1\text{H}$  NMR peak assignments of rhodamine B thiolactone**

Type of proton	Chemical shifts ppm	Splitting pattern	Integration
<b>-N-CH<sub>2</sub>-CH<sub>3</sub></b>	1.17	triplet	12H
<b>-N-CH<sub>2</sub>-CH<sub>3</sub></b>	3.34	quartet	8H
	6.30, 6.34 and 6.72	doublet	2H
	7.46 and 7.54	triplet	1H
	7.22 and 7.86	doublet	1H

**Table 3.2:  $^{13}\text{C}$  NMR peak assignments of rhodamine B thiolactone**

Type of carbon	Chemical shifts ppm
-N-CH <sub>2</sub> -CH <sub>3</sub>	12.8
-N-CH <sub>2</sub> -CH <sub>3</sub>	44.6
	63.0
	97.8
	108.5 - 128.4
	130.1 - 158.2
	198.0

### 3.5.2.3. Solutions preparation

#### Stock rhodamine thiolactone solution (5 mM)

The stock solution of rhodamine thiolactone was prepared by dissolving 22.95 mg of the solid in 10 mL CH<sub>3</sub>CN. It was stored at 4 °C.

#### Stock Hg<sup>2+</sup> standard solution (10 mg/L in 2% (v/v) HNO<sub>3</sub>)

A 100 μL aliquot of a 10000 μg/mL Hg<sup>2+</sup> standard solution was pipetted into a 100 mL volumetric flask containing approximately 50 mL distilled water, followed by 2 mL of HNO<sub>3</sub>. The solution was made up to 100 mL with distilled water, stored at 4 °C and replaced monthly.

### **Artificial seawater**

A 41.953 g portion of sea salt was weighed into a 500 mL beaker, and then 400 mL of distilled water was slowly added. The solution was transferred to a 1000 mL volumetric flask, followed by addition of 2 mL HNO<sub>3</sub>. The solution was made up to 1000 mL with distilled water.

#### **3.5.2.4. General procedure for Hg<sup>2+</sup> determination in aqueous solution**

To a 10 mL volumetric flask containing 5 mL of 1M pH 5.0 acetate buffer and 50 µL 5 mM rhodamine B thiolactone solution, an appropriate volume of 10 mg/L Hg<sup>2+</sup> standard solution was added directly with a micropipette. The final volume was made up to 10 mL with distilled water. Approximately 3 mL of the solution was then transferred to a 1 cm<sup>2</sup> quartz cell to measure the absorbance over a wavelength range of 400-700 nm against the reagent blank using a UV-vis spectrometer.

#### **3.5.2.5. Determination in anti biotic assay discs**

Detecting papers of rhodamine B thiolactone were produced by immersing 1 cm<sup>2</sup> antibiotic assay discs in a 5 mM stock solution of rhodamine B thiolactone. Then approximately 50 µL of each Hg<sup>2+</sup> standard solution pH 5.0 was added dropwise onto the surface of the detecting paper either immediately after the papers were produced, or after the detecting papers had completely dried under ambient condition.

### **3.6. Immobilisation of rhodamine B thiolactone in solid matrices and determination of Hg<sup>2+</sup> on the coloured membranes**

#### **3.6.1. Reagents and apparatus**

##### **Reagent**

All chemicals used were of analytical reagent grade. Mercury standard solution 10000 µg/mL, Hg(NO<sub>3</sub>)<sub>2</sub>, was purchased from QMX Laboratories Ltd. (Essex, UK). Tetraethyl orthosilicate (TEOS) 99.9% for trace metals basis, ethanol absolute >99.8% and hydrochloric acid (HCl, 30% for trace analysis) were obtained from Sigma-Aldrich Company Ltd. (Gillingham, UK). Agar-agar, granular powder was supplied

by Fisher Scientific (Loughborough, UK). Filter paper Whatman (ashless/white ribbon 12.7 mm) was purchased from GE Healthcare UK Ltd. (Buckinghamshire, UK).

## **Apparatus**

Mechanical flow device consisting of a multi-channel peristaltic pump, REGLO ICC and 0.51 mm extension tubing Tygon® LMT-55 was obtained from VWR International (Lutterworth, UK). 13 mm in-line polycarbonate filter holders were purchased from Cole-Parmer (St. Neots, UK). Colour image scanner, Canoscan LiDE 220 (Canon, UK).

### **3.6.2. Procedures**

#### **3.6.2.1. Solutions preparation**

Stock  $\text{Hg}^{2+}$  standard solution (10 mg/L in 2% (v/v)  $\text{HNO}_3$ ) and stock rhodamine B thiolactone solution (5 mM) were prepared as described in Section 3.5.2.3.

#### **3.6.2.2. Preparation of sol-gel membrane**

To prepare the sol-gel colloid formulation 1.2 mL of TEOS, 1 mL distilled water and 2 mL ethanol were mixed. In order to catalyse the hydrolysis of the silica precursors the pH of the mixture was adjusted to 2 by using 0.1 M HCl. After stirring for 3 h, an aliquot of 1.5 mL of 5 mM rhodamine B thiolactone was added and then the mixture was stirred for another 0.5 h. Using tweezers, filter papers were immersed in the sol-gel colloid solution for 5 min and then withdrawn. The coated papers were dried in air for 30 min prior to use.

#### **3.6.2.3. Preparation of agar-agar gel membrane**

A portion of 1 g agar-agar powder was dissolved in 100 mL distilled water using an electric steriliser unit to give a concentration of 1% (w/v) agar. Once the resulting solution was a clear, thin liquid it was allowed to cool slightly before the addition of 5 mM rhodamine B thiolactone. Agar colloid and rhodamine thiolactone were mixed in a 5:1 ratio. Filter papers were dipped in the colloid solution, withdrawn and dried in air for 30 min prior to use.

### 3.6.2.4. General procedure for colour development

The Hg-sensing membranes were fixed on a 13 mm in-line filter holder, as shown in Fig. 3.9. The holder was then fixed on the plastic rack using elastic bands. The inlet of the filter holder was connected to the outlet of the peristaltic pump using the 0.51 mm extension tubing. The outlet of the filter holder was connected to a tube, such that the Hg<sup>2+</sup> waste could be collected in the waste tray. The setup of the device for colorant procedure was as shown in Fig. 3.10. Mercury standard solutions were pumped through the membranes using the multi-channel peristaltic pump at a flow rate of about 17 mL/min. After the required volume of Hg<sup>2+</sup> standards were pumped through the membranes, then the exposed sensors were removed and immediately used for data analysis.

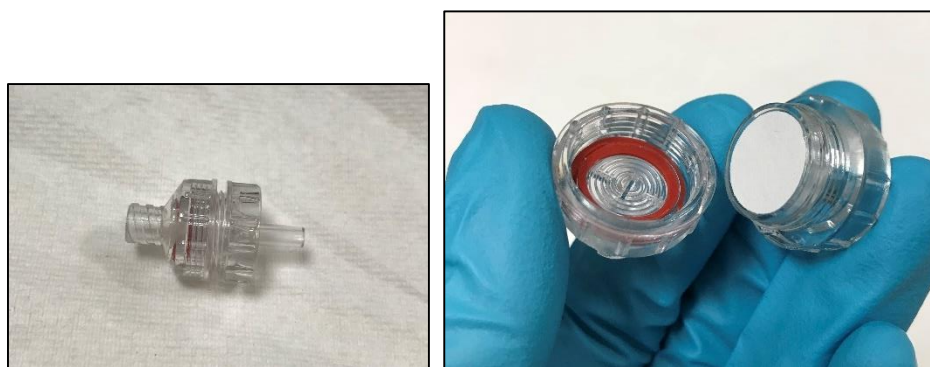


Figure 3.9: Fitting of the Hg-sensing membranes on a 13 mm in-line filter holder.

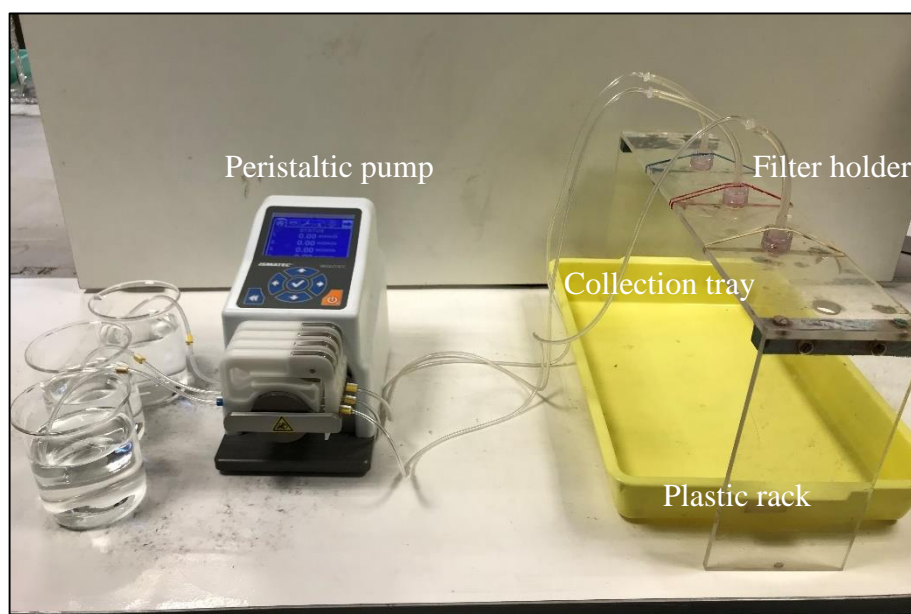


Figure 3.10: Set up of the mechanical flow device.

### 3.6.2.5. Data processing and analysis

After removal from the in-line filter holders, any excess reagent adhering to the surface of the exposed sensors was removed using tissue paper, then the coloured sensors were immediately scanned. A flatbed scanner was used to record the sensors' colour at 4960×7015 pixels (600 dpi resolution). The sensors were scanned with the exposed surface facing down. ImageJ software (ImageJ bundled with 64-bit Java 1.8.0-112) was used to display, edit, analyse and process the scanned images. For each image, a selection of processing steps that illustrate typical usage process were follow. The scanned image was opened as a virtual stack by dragging and dropping directory into ImageJ. The sides above and below the exposed sensor papers were cropped with ImageJ's rectangular region of interest tool and image → crop command.

The RGB channels were digitally separated using the command; image → colour → split channels. Three virtual slides that contributed to the RGB channels were produced. Following this, each slide was converted to a grayscale image with command; edit → invert. The converted images of all three channels were subjected to background correction, which was performed using a grayscale intensity value acquired from the blank (blank image) with the command; process → math → subtract → input the blank grayscale intensity value. The blank image was obtained by passing distilled water through the sensing membranes (the same volume as used for the Hg<sup>2+</sup> standard solution).

The average grayscale values of RGB were calculated from the centre of the sensor by defining the sensor area to contain only the region of interest with ImageJ's oval tool and running analyse → measure. Automatically, all the grayscale values were appended to a single row of the result table, labelled with the image's file name.

## 4. Characterisation and application of small molecule colorimetric sensors for Hg<sup>2+</sup> determination

### 4.1. Introduction

Several small molecule Hg<sup>2+</sup> detecting probes have been reported since the mid 2007<sup>54, 167-175</sup> that meet the demanding requirements for selectivity and sensitivity and have been employed with reasonable success in different environmental media. However, the majority of these molecules have not been adopted widely. The reason behind this is speculated to be difficulties in terms of synthesis, cost and convenience.

Colorimetric sensors with higher selectivity, sensitivity, accuracy and faster response times are preferable in the detecting of ultra-trace levels of target analytes. In a sensor's design several factors have to be considered, i.e., energy-transduction principles, sensor-fabrication, shelf life, manufacturability and availability of approaches that can be applied to shorten fabrication and analysis durations. Combining all of the aforementioned functions - composition, preparation and the end-use conditions of sensor materials - often make their design for real world applications difficult.<sup>176</sup>

Commercially available dipstick tests for Hg<sup>2+</sup> can provide simple procedures for daily monitoring and on-site analysis of water quality without using costly instruments. The commercial products consist of dyes or Hg<sup>2+</sup> detecting molecules as indicator, all of which is impregnated into filter paper. When this test strip is dipped into a water-based solution that contains Hg<sup>2+</sup>, a colour change indicates the presence/absence of Hg<sup>2+</sup>. The colour change can either be measured with a portable spectrophotometer or read visually by comparison with a provided reference chart. However, most of these kits have significant short-comings for their real application. Since the maximum allowable limit of Hg<sup>2+</sup> in the drinking water is remarkably low (2µg/L), the detection limits of commercial dipstick tests (mg/L) are insufficient to fulfil the required regulation. In addition, most of these kits are a single use kit with relatively high price ranging from £20.0 to £250.0. Lack of selectivity and leakage of reagent can also occur. Hence, reliability and sensitivity of detection are poor.

Therefore, still, there is a need for cheap, “off-the-shelf” probes whose changes in colour can be used to signal either qualitatively or quantitatively the presence of particular analytes of interest. Such indicators are especially valuable where they can be obtained readily without resort to customised synthesis. The utility of these probes is demonstrated by the fact that they mainly rely on simple chemical reactions and the produced results are visible and can be interpreted by the naked eye. No extensive training is required to perform the analysis. The reagents and laboratory materials needed to perform the tests are readily available and inexpensive. Also, in most approaches the amount of the reagents and materials required to employ the screening test is small.<sup>177-179</sup>

The work in this chapter presents the development of a semi-quantitative colorimetric method for  $\text{Hg}^{2+}$  determination by evaluation of three commercially available  $\text{Hg}^{2+}$  probes - CuI, DPC and R6G - that could be potentially used as “off-the-shelf” colour-based sensors in aqueous solutions. Because of their simplicity and ready availability, these indicators have been commonly used in the literature. Hence, they were chosen in this study.

The colorimetric screening test based on the reaction of CuI with Hg is one of the simple and inexpensive methods that can be applied to Hg screening in the environment. The reaction was first described by Gettler in 1937 as a simple colorimetric identification of Hg. Later in 1950, it was reported that this reaction is specific enough for Hg for use in semi-quantitative determination.<sup>180</sup> A salmon-pink colour develops as a result of the formation of cuprous mercury iodide,  $(\text{Cu}_2[\text{HgI}_4])$  complex if Hg is present in the analysed sample.

Yallouz *et al.*<sup>165</sup> described a low cost, semi-quantitative colorimetric method for Hg screening. The method has been successfully employed to determine Hg in fish, soil, fluvial and marine sediment and gold mining residues.<sup>124, 165, 181, 182</sup> A digestion step was carried out using acid for a number of real samples followed by  $\text{Hg}^0$  reduction and collection on a detecting paper containing CuI. The acid extraction was performed using *aqua regia* in a conical flask. Tin (II) chloride was then added as reductant to reduce  $\text{Hg}^{2+}$  to  $\text{Hg}^0$ , Equation 4.1.



A conical flask fitted with a two-armed aeration duct (bubbler) was used to conduct the determination step. One arm of the bubbler was connected to a condenser whereas the other arm of the bubbler was connected to an aquarium pump. Following connection, the air was bubbled through the sample using the aquarium pump, and  $\text{Hg}^0$  was removed to react with the coating on a detecting paper positioned in a PVC filter holder, according to Equation 4.2.



The coloured  $\text{Cu}_2[\text{HgI}_4]$  complex was formed and its colour intensity was proportional to the Hg concentration in the sample. By comparing the colour intensity obtained from screening the samples with the colour intensity obtained from Hg standard solutions analysed in the same manner (without digestion); a semi-quantitative determination of Hg concentration could be obtained.

An electrical supply, a pump in order to transfer  $\text{Hg}^0$  to react with the coating on the paper and a heating device for sample digestion were required in addition to common laboratory glassware and chemicals. The method is easily implemented and simple. However, some issues were not considered by Yallouz *et al.*<sup>165</sup> Since the detecting papers should be suitable for use worldwide in different climates, the stability of the detection papers before use should be assessed to determine if temperatures typical of different climates affects performance. The effect of storage condition on the exposed detection paper should be assessed to evaluate how quickly colour fading occurred. For more accurate quantitative assessment, the ability to incorporate the screening method with a portable spectrometer such as reflectance spectrometry should be considered. Also, the applicability of other small molecule sensors for  $\text{Hg}^{2+}$  determination instead of CuI should be examined, e.g., DPC and R6G.

Diphenylcarbazide (DPCI) and DPC belong to a group of chemicals derived from hydrazine and hydrazone and are used as ligands to form coloured complexes with various metal ions in acidic media.<sup>183, 184</sup> In comparison with other colorimetric screening method, DPC and DPCI, due to their simplicity, have been widely used as colorimetric dye indicator to determine Hg<sup>2+</sup> and other metal ion species<sup>185-191</sup>. Gerlach *et al.*<sup>185</sup> and Clarke *et al.*<sup>192</sup> indicated that the determination of Hg by DPC was first discovered by Dubsy and Trtilek in 1933 when the determination of the Cl<sup>-</sup> in a sample was carried out by titration with Hg(NO<sub>3</sub>)<sub>2</sub> in the present of DPC. A vivid purple colour was obtained as a result of producing the Hg-DPC complex. It was found that, instead of indirect detection of Cl<sup>-</sup>, direct detection of Hg could be performed during this procedure. Odegaard *et al.*<sup>193</sup> published a series of standard metal detection tests using DPC; the application of DPC for Hg detection involved preparation of a 1% DPC ethanolic solution that was applied to the contaminated objects. The DPC solution has a characteristic salmon-pink colour at pH 8, is pink at pH 7, and becomes colourless at pH 6 and lower. In an alkaline solution of DPC, an instant purple colour is observed on the addition of Hg<sup>2+</sup> salts which is a result of the formation of the Hg-DPC complex. The reaction of DPC with Hg can occur only within a specific pH range. The most accurate results were obtained when samples have a pH value from 4.5 to 6.0. At a pH value of 4.0 and lower, unreliable results were obtained; as the acidity increased, inconsistent result and loss of sensitivity were observed.<sup>194</sup>

Ramakrishna *et al.*<sup>195</sup> established a simple sensor for Hg colorimetric detection based on the reaction of rhodamine 6G with Hg<sup>2+</sup> and iodide. The reaction of rhodamine 6G with Hg<sup>2+</sup> and iodide can be generated under the influence of highly stable tetraiodomercurate (II) resulting in formation of pink coloured [(HgI<sub>4</sub>)<sup>2-</sup>][(Rhodamine 6G)<sup>+</sup>]<sub>2</sub> complex, Equation 4.3.



The stoichiometry was established by equilibrium shift methods and the mole ratio of Hg<sup>2+</sup> to iodide to rhodamine 6G is now known to be 1:4:2. This complex was produced

instantly within a pH range of 1 to 7 and the absorbance remained constant at 575 nm when the system was stabilised with gelatin.<sup>196-198</sup> In subsequential work, Prathish *et al.*<sup>199</sup> proposed a multi-visual detection of Hg<sup>2+</sup> in a mixture of other metal ions based on the sequential ligand exchange (SLE) mechanism without affecting the Hg-I-rhodamine 6G combination.

This chapter tests whether simple coating of “off-the-shelf” signalling reagents on an appropriate substrate (filter papers) is suitable for field Hg<sup>2+</sup> screening. Thus, the formation of Hg<sup>2+</sup> complexes with CuI, DPC and R6G - estimated by the naked eye and by spectrophotometric measurements - were investigated.

## 4.2. Aim

The aim of this part of thesis was focused on evaluation of commercially available small molecule probes for the determination of Hg<sup>2+</sup>. Therefore, in this chapter, results for three colorimetric reagents are reported: CuI, DPC and R6G.

Specific objects were:

- To compare the analytical performance of the selected reagents in solution phase, in spot test mode (as wet reagents and when dried onto filter papers) and their suitability to be used with the Hg bubbler apparatus recommended by Yallouz *et al.*<sup>165</sup>
- To assess the colorimetric screening method in terms of the ability of an entire experiment to be duplicated, the lower limit of detection, the differences in standard concentration that could be distinguished by the naked eye, the characterisation of colour fading and how the storage conditions could effect the performance.
- To test the overall method efficiency by comparison with UV-visible reflectance/absorbance spectroscopy techniques that give an accurate quantitative analysis of the coloured complexes produced.

### **4.3. Experimental**

#### **4.3.1. Reagents and apparatus**

The reagents and apparatus used for the determination of  $\text{Hg}^{2+}$  based on the reaction with CuI, DPC and R6G were as described in Sections 3.2.1, 3.3.1 and 3.4.1 respectively.

#### **4.3.2. Solutions preparation**

The solutions used for the determination of  $\text{Hg}^{2+}$  based on the reaction with CuI, DPC and R6G experiments were prepared as described in Sections 3.2.2.1, 3.3.2.1 and 3.4.2.1 respectively. To investigate the method's range and limit of detection standard solutions of  $\text{Hg}^{2+}$  at different concentrations were prepared from the  $\text{Hg}^{2+}$  stock solution daily as required.

#### **4.3.3. Determination of $\text{Hg}^{2+}$ based on the reaction with CuI**

This experiment was conducted to evaluate the formation of  $\text{Cu}_2[\text{HgI}_4]$  in spot test mode and in the screening method based on the Hg bubbler apparatus.

##### **4.3.3.1. Determination of $\text{Hg}^{2+}$ as spot test**

Determination of  $\text{Hg}^{2+}$  in spot test mode was carried out as has been described in Section 3.2.2.3. A series of reduced and non-reduced  $\text{Hg}^{2+}$  standard solutions were used to evaluate the conditions under which the  $\text{Cu}_2[\text{HgI}_4]$  can be formed on the CuI detecting papers.

##### **4.3.3.2. Determination of $\text{Hg}^{2+}$ using the Hg bubbler apparatus**

When the semi-quantitative screening method using the Hg bubbler apparatus was applied, each standard was analysed in triplicate. A 75 mL aliquot of  $\text{Hg}^{2+}$  standard solution was transferred into a 250 mL conical flask and then 5 mL of  $\text{SnCl}_2$  reductant was added. The detecting paper was placed into the holder, then the procedure was conducted as described in Section 3.2.2.4. The detecting papers were stored in a

desiccator containing a saturated solution of  $\text{MgSO}_4$  prior to use as was described in Section 3.2.2.2.

#### **4.3.3.3. Method characterisation**

##### **Limit of detection over the range tested**

A series of  $\text{Hg}^{2+}$  standard solutions with a concentration range from 5 to 75  $\mu\text{g/L}$  were tested using the Hg bubbler apparatus to evaluate the method range and estimate the LOD.

##### **Standard concentration differences for colour discrimination**

To determine the degree of colour discriminations that could be achieved by the naked eye, a series of  $\text{Hg}^{2+}$  standard solutions differing in concentration by 5  $\mu\text{g/L}$  and by 10  $\mu\text{g/L}$  were tested.

##### **Visual evaluation of the effect of storage condition on the colour fading**

To assess the effect of storage conditions on the colour developed on the exposed detection paper, a comparison of colour intensity was carried out under controlled storage conditions in terms of temperature and light. These papers were stored at ambient room temperature in daylight and in the dark and at around 4 °C in a refrigerator.

##### **UV-visible reflectance spectra for characterisation of $\text{Cu}_2[\text{HgI}_4]$ colour fading**

Quantification of the colour developed on the surface of the detecting papers was carried out using UV-visible reflectance spectrophotometry. Since the colour intensity of the coloured complex gradually disappeared, how fast this fading occurred was studied to determine the fading rate over a period up to two weeks.

##### **Within-sample variability of quantitative measurements**

The performance of UV-visible reflectance spectrophotometry for quantitative measurements was evaluated by a triplicate screening of the same concentration of  $\text{Hg}^{2+}$ . This was repeated periodically.

## **Stability of CuI detecting papers**

To assess the stability of the CuI detecting papers for use worldwide in different climates, the detection papers were stored at different temperatures (4 °C, 25 °C and 35 °C) for up to 20 weeks, before use.

### **4.3.4. Determination of Hg<sup>2+</sup> based on the reaction with DPC**

The determination of Hg<sup>2+</sup> by the reaction with DPC was carried out both in solution and on a spot test mode to assess the lower limit of detection, and under what conditions the Hg-DPC could be formed.

#### **4.3.4.1. Determination of Hg<sup>2+</sup> in solution phase**

To evaluate the method range and estimate the limit of detection, a series of Hg<sup>2+</sup> standard solutions with concentrations 5, 10 and 100 mg/L were tested as described in Section 3.3.2.2.

#### **4.3.4.2. Determination of Hg<sup>2+</sup> as spot test**

In order to compare the performance of the DPC test papers in wet and dry conditions, Hg<sup>2+</sup> standard solutions were applied as spot tests with concentrations 5, 10 and 100 mg/L as has been described in Section 3.3.2.3.

#### **4.3.4.3. Determination of Hg<sup>2+</sup> using the Hg bubbler apparatus**

Some DPC test papers were produced as before and then allowed to dry under ambient condition. After the test papers were completely dry, the determination of Hg<sup>2+</sup> was carried out using the Hg bubbler apparatus as described in Section 3.2.2.4.

### **4.3.5. Determination of Hg<sup>2+</sup> based on the reaction with R6G**

This experiment was carried out to investigate the reaction between Hg<sup>2+</sup> and R6G in solution phase and on a filter paper as spot test mode. The limit of detection and the ability to duplicate the screening method procedure were considered.

#### **4.3.5.1. Determination of Hg<sup>2+</sup> in solution phase**

The determination of Hg<sup>2+</sup> in solution phase was conducted as described in Section 3.4.2.2. Up to 4 mL of Hg<sup>2+</sup> standard solution was added to the reaction mixture, adjusted to pH 5.2 ± 0.2 and then diluted. The range of Hg<sup>2+</sup> concentrations tested, as confirmed by UV-vis transmitted spectrometer was between 2 to 80 µg/L.

#### **4.3.5.2. Determination of Hg<sup>2+</sup> as spot test**

Determination of Hg<sup>2+</sup> in spot test mode was carried out for both wet and dry R6G papers. A set of R6G test papers was prepared by immersing a 25 mm circular segment cut from a filter paper in the reaction mixture before Hg<sup>2+</sup> solutions were applied as described in Section 3.4.2.3.

#### **4.3.5.3. Determination of Hg<sup>2+</sup> using the Hg bubbler apparatus**

The R6G test papers were prepared and then allowed to dry under ambient condition. The determination of Hg<sup>2+</sup> was conducted using the Hg bubbler apparatus as described in Section 3.2.2.4.

### **4.4. Results and discussion**

#### **4.4.1. Determination of Hg<sup>2+</sup> based on the reaction with CuI**

##### **4.4.1.1. Assessment of Hg<sup>2+</sup> detection in spot test mode**

Discolouration of CuI detecting paper upon addition of both pre-reduced and non-reduced Hg<sup>2+</sup> standard solutions was observed, Fig. 4.1. This likely occurred as a result of bleaching of the cellulose fibres under the acidic condition<sup>200</sup> of the Hg<sup>2+</sup> and SnCl<sub>2</sub> mixture. It would seem that the course and kinetics of hydrolysis were influenced significantly by acid concentration.<sup>201, 202</sup>

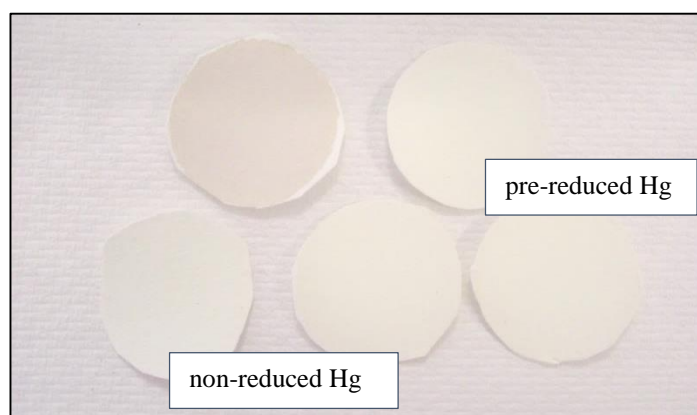


**Figure 4.1: Bleaching of CuI detection papers upon the addition of  $\text{Hg}^{2+}$  standard solutions, (reduced and non-reduced).**

The hydrolysis of cellulose with concentrated acid resulted in the formation of cellulose acid complexes; these occur only after the crystalline structure of cellulose is destroyed.<sup>200</sup> Thus, the primary course of degradation occurs in the amorphous cellulose under the impact of dissolution in the acid.<sup>202</sup> The CuI papers were not therefore considered suitable for use in spot-test mode.

#### **4.4.1.2. Determination of $\text{Hg}^{2+}$ using the Hg bubbler apparatus**

The colour intensity of the complex formed appeared to increase with an increase of the  $\text{Hg}^{2+}$  concentration in the standard solutions over the range tested, as shown in Fig.4.2.



**Figure 4.2: Increase in colour intensity of  $\text{Hg}^{2+}$  complex formed on detecting paper obtained using the Hg bubbler apparatus and  $\text{Hg}^{2+}$  standards with concentration of 25, 50 and 75  $\mu\text{g/L}$ .**

#### 4.4.1.3. Standard concentration differences for colour discrimination

Discrimination in colour intensity between standards could be difficult to see with a 5  $\mu\text{g/L}$  concentration difference over the range tested, Fig. 4.3. However, there was an obvious increase at a 10  $\mu\text{g/L}$  concentration difference, Fig. 4.4. Thus, higher difference in concentration between standards was required for colour discrimination to be observed with the naked eye. The minimum detectable concentration which could be discriminated by the naked eye from the blank was 5  $\mu\text{g/L}$ , making this the lower limit of detection.



Figure 4.3: Increase in colour intensity as the  $\text{Hg}^{2+}$  concentration increased with difference of 5  $\mu\text{g/L}$  in concentration 20, 25 and 30  $\mu\text{g/L}$ .

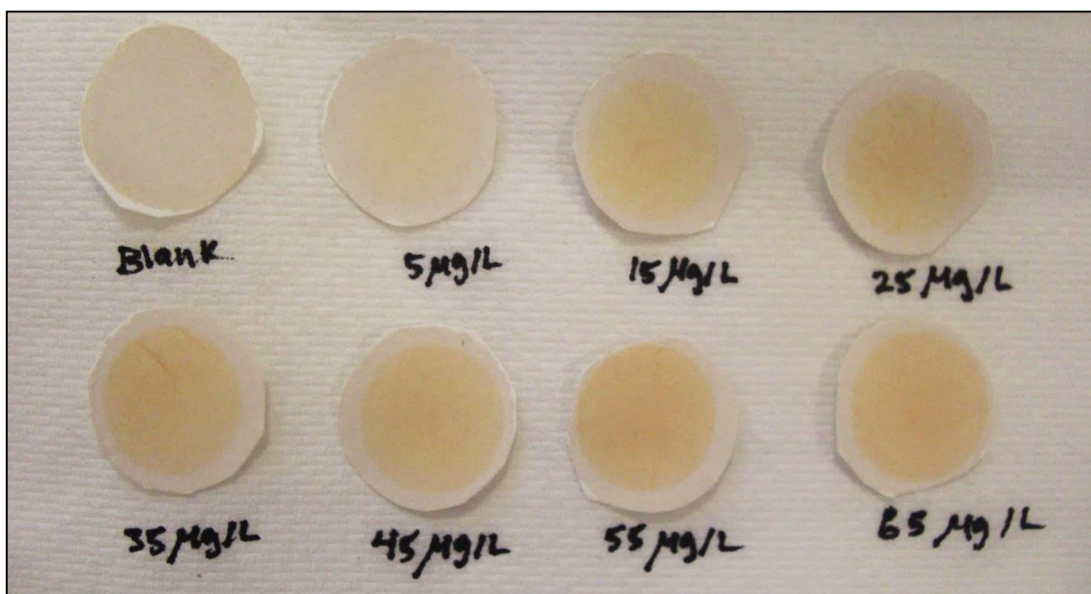
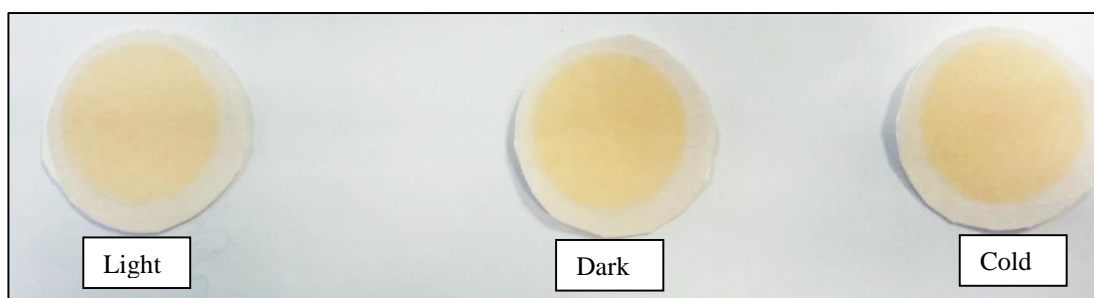


Figure 4.4: Increase in colour intensity as the  $\text{Hg}^{2+}$  concentration increased with difference of 10  $\mu\text{g/L}$  in concentration blank, 5, 15, 25, 35, 45, 55 and 65  $\mu\text{g/L}$ .

#### 4.4.1.4. Visual evaluation of the effect of storage conditions on the colour fading

The effect of storage condition on the detection paper after use in Hg screening was tested. The fading study was carried out by comparison of the colour intensity of the exposed papers obtained from the triplicate screening of a concentration of 75 µg/L. These papers were stored for one week in different environments; at ambient room temperature in direct sunlight in the laboratory and in the dark by wrapping them with aluminium foil, and at around 4 °C in a refrigerator. The results shown in Fig. 4.5 were observed by the naked eye and indicated that the intensity of the colour decreased in all the conditions. However, the detecting papers exposed to the light showed more colour loss than the others.

Exposure to direct light rapidly accelerated colour fading; in contrast, decreasing temperature had no effect. Since the colour loss is irreversible, the duration and intensity of light exposure should be carefully limited.



**Figure 4.5: Effect of storage conditions on the exposed detecting papers, illustrating that more fading occurred on the one stored in direct light.**

#### 4.4.1.5. UV-visible diffuse reflectance spectra of Cu<sub>2</sub>[HgI<sub>4</sub>] complex

A UV-vis reflectance spectrophotometer was employed to provide a more quantitative assessment than the naked eye of the success of formation of Hg complex on the exposed detection paper. The UV-vis reflectance spectra of Cu<sub>2</sub>[HgI<sub>4</sub>] complex on detecting papers was recorded in the range of 380-900 nm for different concentrations. The Cu<sub>2</sub>[HgI<sub>4</sub>] absorption peak can be located clearly at 434 nm, as shown in Fig. 4.6.

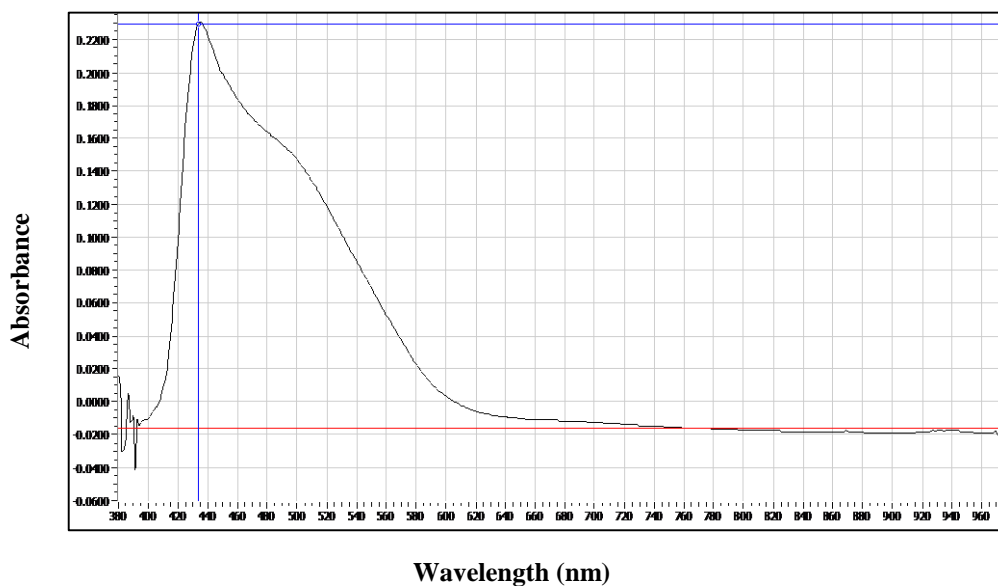
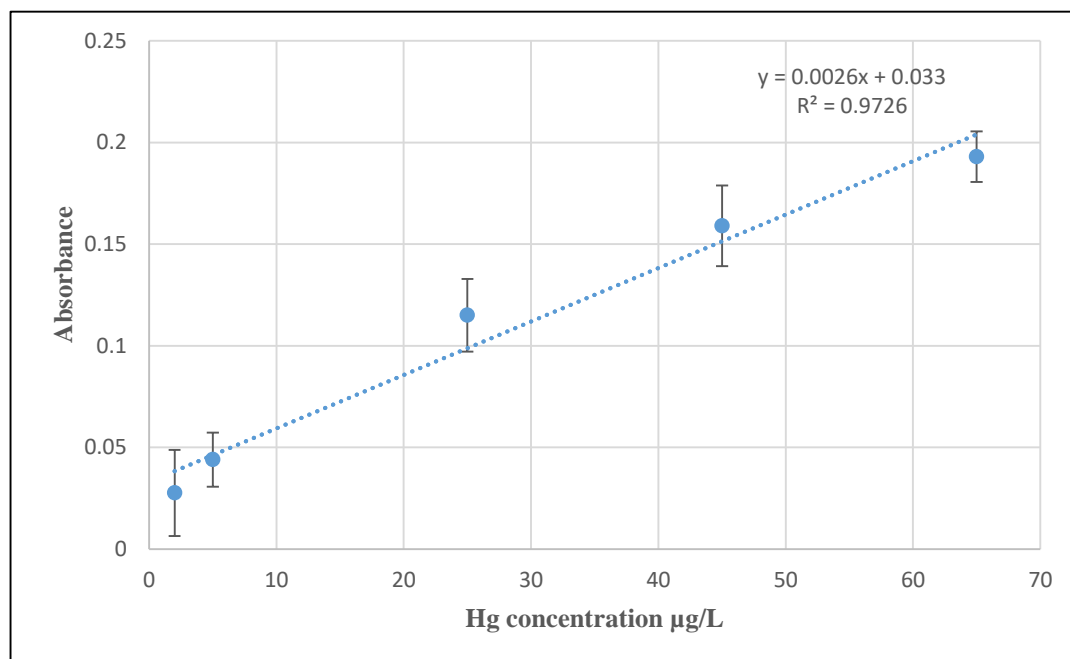


Figure 4.6: The reflection UV- vis spectrum of  $\text{Cu}_2[\text{HgI}_4]$  on the exposed detection paper.

The absorbance maximum was obtained at 434 nm against blank for a number of exposed detection papers. The blank paper was produced by exposure of CuI detecting paper using the bubbler apparatus to  $\text{SnCl}_2$  and distilled water without  $\text{Hg}^{2+}$ . This indicated that  $2 \mu\text{g/L}$  was the lower limit of detection. The results also indicated that the absorbance increased approximately linearly with the  $\text{Hg}^{2+}$  concentration in the standard solutions. A strong correlation ( $r^2=0.973$ ) was found between the absorbance and Hg concentration in the exposed papers, as illustrated in Fig. 4.7.



**Figure 4.7:** Calibration curve of the absorbance at 434 nm vs.  $\text{Hg}^{2+}$  concentration in CuI detecting papers; error bars represent one standard deviation ( $n=3$ ).

#### 4.4.1.6. UV-visible reflectance spectra for characterisation of $\text{Cu}_2[\text{HgI}_4]$ colour fading

The colour intensity of the coloured  $\text{Cu}_2[\text{HgI}_4]$  complex on the exposed papers gradually faded, and UV-vis spectrometry was also used to understand the characteristics of colour loses. The absorbance for a number of exposed papers that were stored in a dark place at room temperature was recorded for a period of 48 hours. From Fig. 4.8 the results showed that, although the colour fading occurred rapidly in the first 8 hours after the coloured complex was formed, this fading then decreased slightly for the next 48 hours. For the absorbance, statistical analysis (t-test at 0.05 significance level) (see Table A2.4 in Appendix 2) demonstrated that there was no significant difference between the results obtained at zero hour and the first hour after the coloured complex was formed. After this time, a significant difference for the rest of absorbance acquired. Therefore, it was recommended that absorbance values of colour should be read-out as soon as possible and certainly within the first hour.

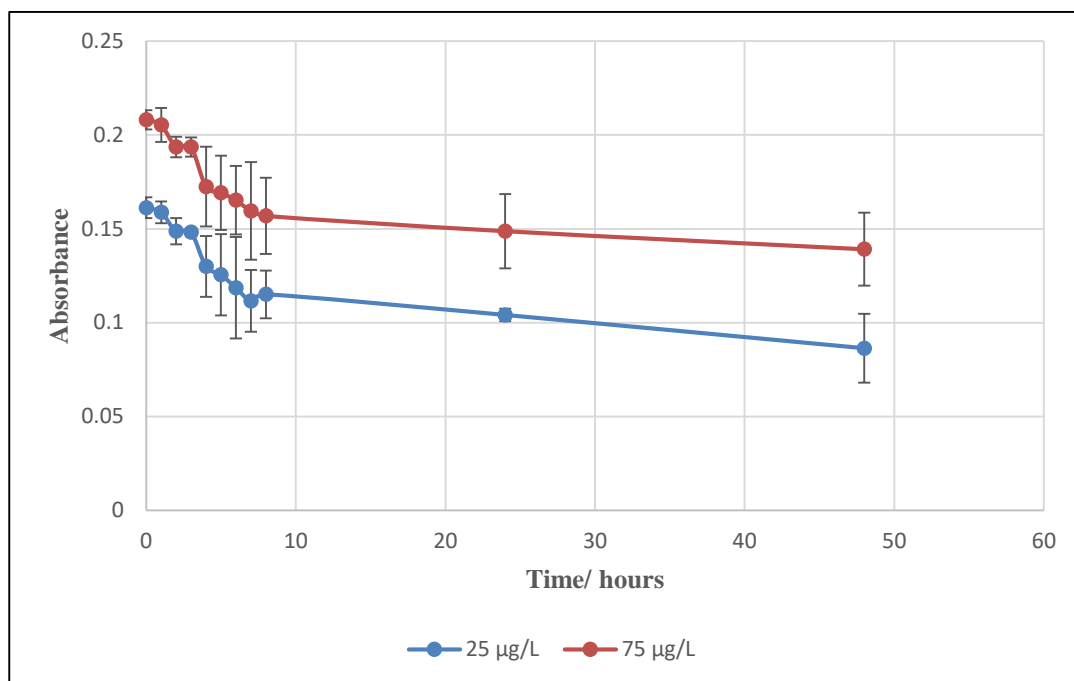


**Figure 4.8:** Decrease in the absorbance for  $\text{Cu}_2[\text{HgI}_4]$  complex with a concentration of 25 and 75  $\mu\text{g/L}$ , at  $\lambda = 434 \text{ nm}$  over the time; error bars represent one standard deviation ( $n=3$ ).

#### 4.4.1.7. Within-sample variability of quantitative measurements

To assess the reproducibility of quantitative analysis *via* UV-vis reflectance spectroscopy, triplicate screening of a 75  $\mu\text{g/L}$  concentration  $\text{Hg}^{2+}$  standard solution was carried out. Following this, the absorbance values were recorded at 434 nm at different positions within each exposed paper ( $n=5$ ), as shown in Fig. 4.9 and also between papers ( $n=3$ ), for a period of two weeks.

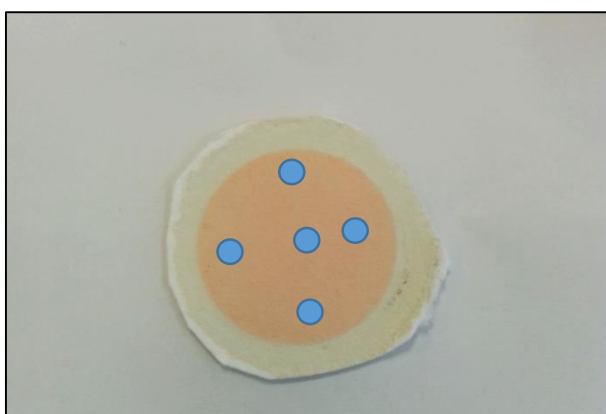


**Figure 4.9:** An example of the position of points where the absorbance has been taken.

A comparison between the absorbance values recorded for five different positions within each exposed paper and between the three exposed papers was carried out, as shown in Table 4.1.

**Table 4.1: The absorbance measurements for a triplicate screening of a Hg<sup>2+</sup> concentration of 75 µg/L.**

<b>Time elapsed</b>	<b>1 hour</b>	<b>1 day</b>	<b>1 week</b>	<b>2 weeks</b>
# 1, n=5	0.202 ± 0.028	0.186 ± 0.013	0.181 ± 0.012	0.178 ± 0.019
# 2, n=5	0.199 ± 0.014	0.188 ± 0.015	0.183 ± 0.011	0.180 ± 0.013
# 3, n=5	0.207 ± 0.019	0.187 ± 0.013	0.182 ± 0.020	0.179 ± 0.016
<b>Total, n=3</b>	0.203 ± 0.004	0.187 ± 0.001	0.182 ± 0.001	0.179 ± 0.001

Results are mean ± SD; n = number of replicate.

The results obtained revealed that the standard deviations of the five absorbance measurements conducted within a single exposed paper were between 0.011 and 0.028, and for the precision expressed as RSDs, approximately 75% of the RSDs values were < 10% and 25% of the values were between 10% and 15%, as shown in Fig. 4.10. This variability may be because of an uneven formation of Cu<sub>2</sub>[HgL<sub>4</sub>], leading to differences in colour across the surface. The higher absorbance values were recorded in the centre of the exposed paper, and the edges contributed the smallest values.

The results also indicated that similar absorbance readings were obtained from the triplicate screening measurement (SD=0.004). The colour faded over time as expected, but the absorbance values obtained after one day, one week and two weeks were similar across the three papers (SD=0.001). For the triplicate screening all RSDs values were less than ≤ 2%. Thus, the results indicated that the use of UV-vis reflectance spectroscopy technique for Hg<sup>2+</sup> quantitative analysis consistently provide precise and reliable measurements.

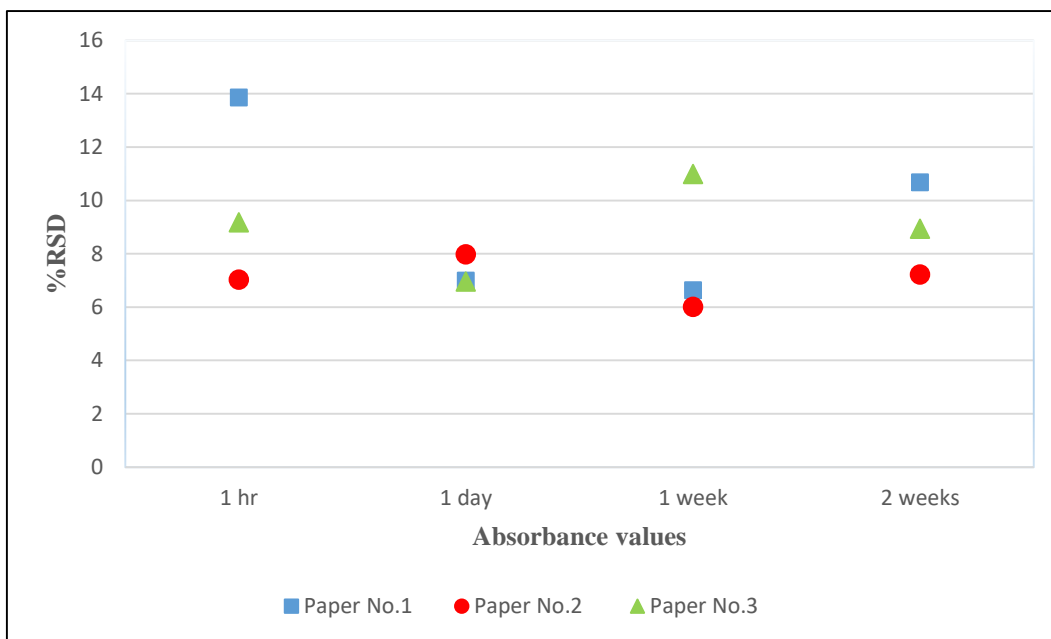


**Figure 4.10:** Values of the relative standard deviation (RSD) for the absorbance values recorded at 434 nm at different positions within each exposed paper (n = 5), after storage for a period of one hour, one day, one week and two weeks.

#### 4.4.1.8. Stability of CuI detecting papers

For worldwide practical applications, stability of the CuI detecting papers before use is required. Since this can affect the analysis performance. Environmental parameters such as temperature, lighting and humidity can affect the stability. Therefore, the effects of environmental factors on the paper's stability have been considered, Since the effect of humidity proved to be a key parameter for good repeatability, Yallouz *et al.*<sup>164</sup> suggested to store the papers in a 95% humidity atmosphere. The effect of temperature on the CuI papers has been studied in this work.

To investigate the effect of temperature, CuI detecting papers were stored at temperatures of 4 °C (in refrigeration), 25 °C and 35 °C (inside an incubator), for a period up to 20 weeks before use in Hg screening. The absorbance measurements were evaluated for a triplicate screening of 75 mg/L Hg<sup>2+</sup> standard solution every four weeks. Visual observations and absorbance measurements for this purpose were carried out in the 0, 4<sup>th</sup>, 8<sup>th</sup>, 12<sup>th</sup>, 16<sup>th</sup> and 20<sup>th</sup> weeks. On the timescale of the

measurements, the result revealed that the absorbance values given in Fig. 4.11 were stable and close to the result for the control sample.

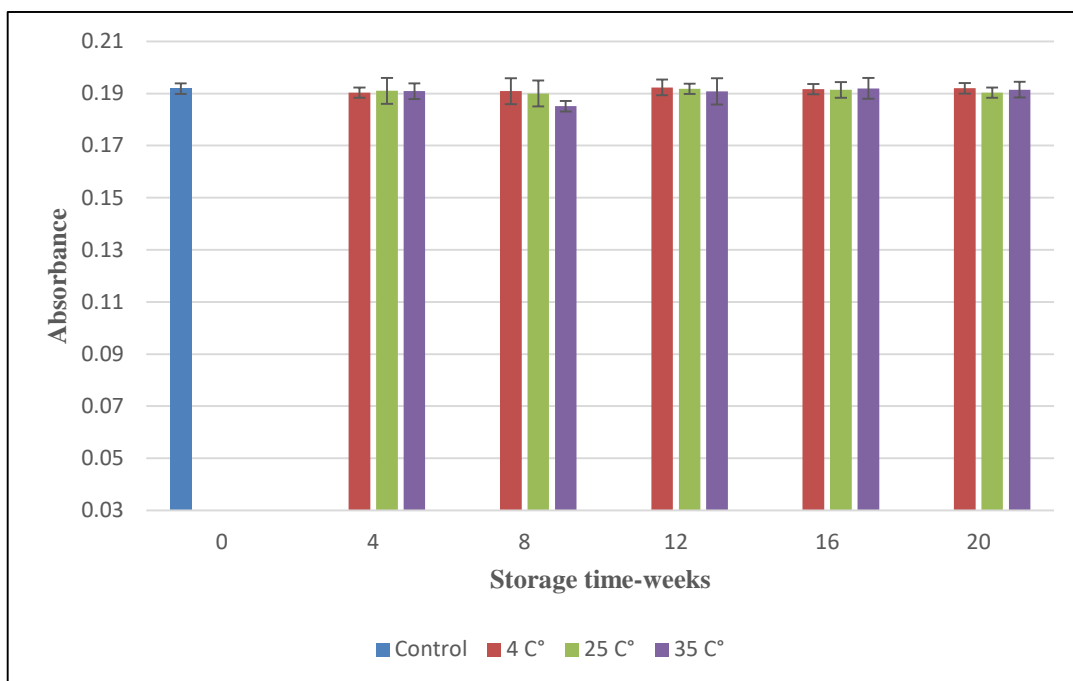


**Figure 4.11:** The absorbance measurements for triplicate CuI detecting papers that had been stored at 4 °C, 25 °C and 35 °C for up to 20 weeks before exposure to 75 µg/L Hg<sup>2+</sup> standard solution; error bars represent one standard deviation (n=3).

Analysis of absorbance data showed that the time and storage temperature had no significant impact on the performance of the CuI detecting papers within the duration of the experiment (up to 20 weeks). The CuI-impregnated Hg detecting papers appeared stable within the temperature range of 4 to 35 °C. Hence, the CuI detecting papers can be used worldwide in different climates without the negative influence on the performance.

#### **4.4.2. Determination of Hg<sup>2+</sup> based on the reaction with DPC**

##### **4.4.2.1. Determination of Hg<sup>2+</sup> in solution phase**

A vivid purple-coloured Hg complex was formed immediately upon the addition of DPC to Hg<sup>2+</sup> standard solutions. It has been suggested that Hg and DPC form two complexes, a 1:1 and a 1:2 complex (cation: carbazone).<sup>186</sup> The reaction of DPC with Hg<sup>2+</sup> was first studied by qualitative visual analysis. Visual observation concluded that

the intensity of colour produced appeared to increase with increasing  $\text{Hg}^{2+}$  concentration in the standards, as shown in Fig. 4.12. A concentration of 5 mg/L was observed to be the lower limit of visual detection.

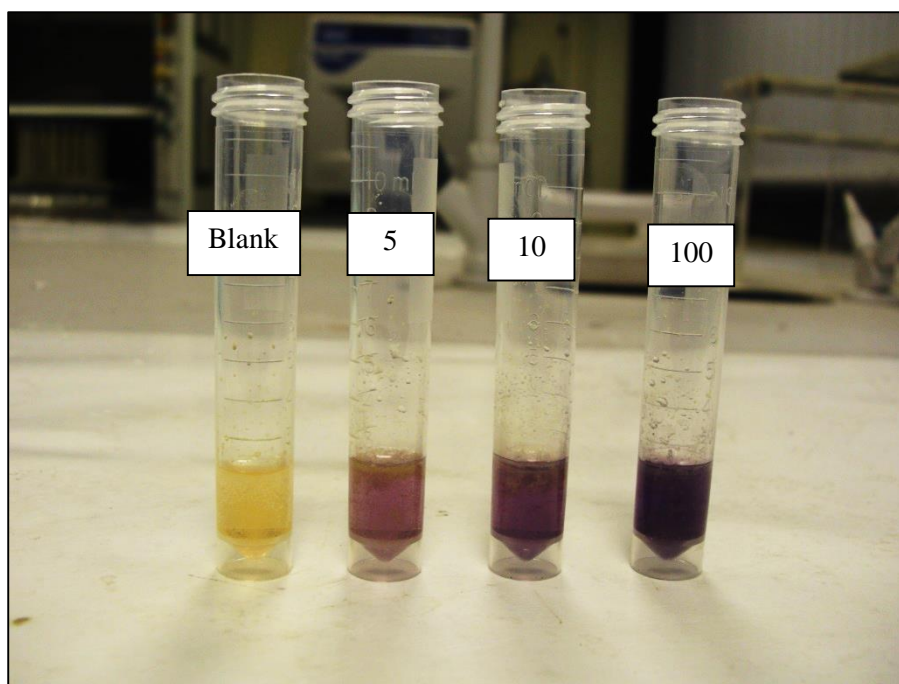


**Figure 4.12: Increase in purple Hg-DPC colour intensity as the  $\text{Hg}^{2+}$  concentration increased for 5, 10, and 100 mg/L standard solutions.**

The obtained complexes formed colloids in aqueous alcoholic solution. This was in agreement with the previous literature.<sup>186</sup> When the solutions were left to stand a precipitate formed, but colour reappeared in the solutions on shaking. However, decomposition of these complexes was accelerated by exposure to visible light.

#### **4.4.2.2. Determination of $\text{Hg}^{2+}$ as spot test**

##### **Wet paper condition**

As the  $\text{Hg}^{2+}$  standards were applied a purple colour was obtained immediately. The intensity of colour produced increased with increasing  $\text{Hg}^{2+}$  concentration in the standard solutions. A concentration of 5 mg/L would be considered as the lower limit of detection, Fig. 4.13. However, in the exposed DPC papers the colour started to fade almost immediately and continued for 1-3 hours, as shown in Fig. 4.14.

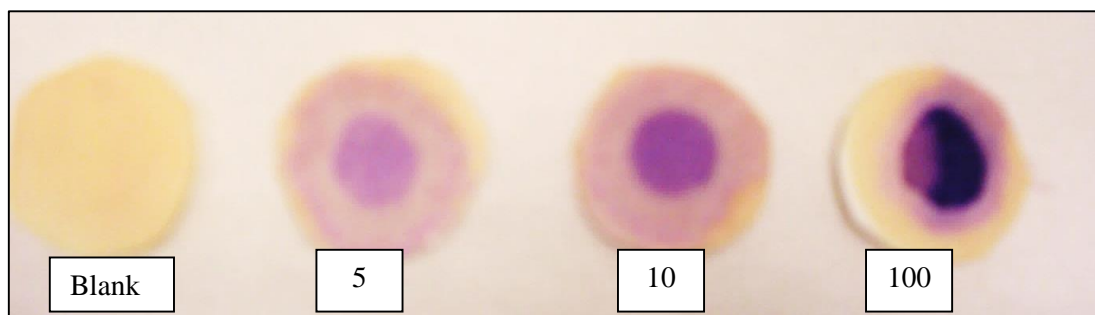


**Figure 4.13:** Increase in intensity of coloured Hg-DPC complex with  $\text{Hg}^{2+}$  concentrations of 5, 10, and 100 mg/L on the wet DPC papers.

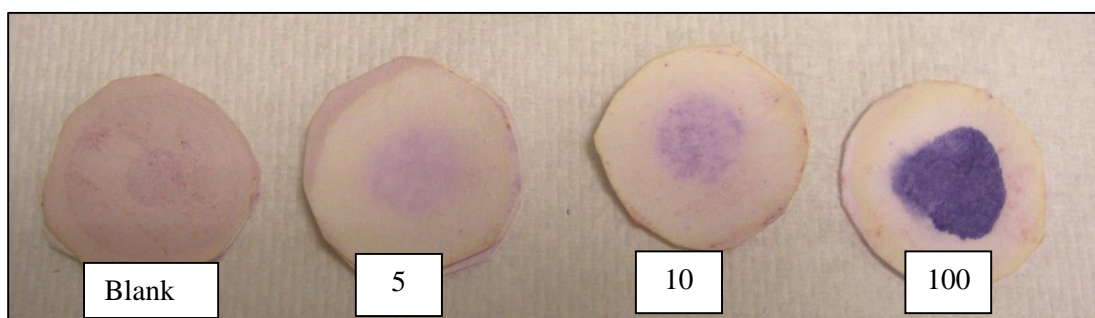


**Figure 4.14:** Intensity of coloured Hg-DPC complex with  $\text{Hg}^{2+}$  concentrations of 5, 10 and 100 mg/L after exposure to light for up to 3 hours.

The rapid fading of the colour formed on the DPC test papers was probably due to an increase in  $\text{HNO}_3$  concentration as a result of water evaporation. The Hg-DPC complex was produced by the addition of DPC to a dilute  $\text{HNO}_3$  solution of  $\text{Hg}^{2+}$ , adjusted to pH 4.6. However, when the concentrations of  $\text{HNO}_3$  increased due to evaporation of water, the formation of Hg-DPC complex was completely or partly prevented.<sup>203, 204</sup> Consequently, comparison of the intensity of colour between standards and samples should be performed as soon as the Hg-DPC forms.

#### **Dry paper condition**

Where DPC test papers were allowed to dry, a light pink colour developed on the test paper after 5-15 mins without the addition of  $\text{Hg}^{2+}$  solutions, as shown in Fig. 4.15. Further, completely dry spot test papers did not react with  $\text{Hg}^{2+}$  and there was no observation of a vivid purple colour. The Hg-DPC complex was not obtained with the dry DPC spots, as it was with the wet spots.

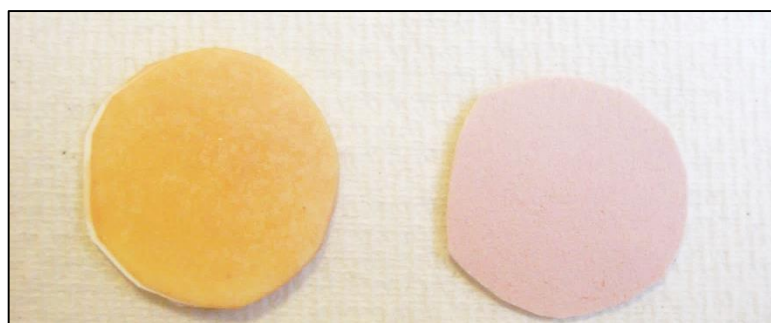


**Figure 4.15: Freshly prepared DPC test paper (left), and formation of light pink colour as a result of the compound oxidation after 5 min (right).**

It was suspected that this was likely to be as a result of oxidation of the compound and production of an inactive form of DPC. Kaparwan *et al.*<sup>205</sup> indicated that a stock solution of DPCI changed its colour from colourless to light pink when exposed to sun light as result of some photochemical reactions.

As the DPC was used as received, it contained approximately ~ 60% DPCI. Oxidation of DPCI to its second oxidation product diphenylcarbadiazone DPCDO could have occurred. The DPC was also oxidised to DPCDO. However, DPCDO was reduced to DPC and the later was further reduced to DPCI. A complete reversible oxidation-reduction reaction was possible giving the colour change of the dry DPC test papers. A proposed mechanism of the oxidation process is shown in Fig. 4.16.

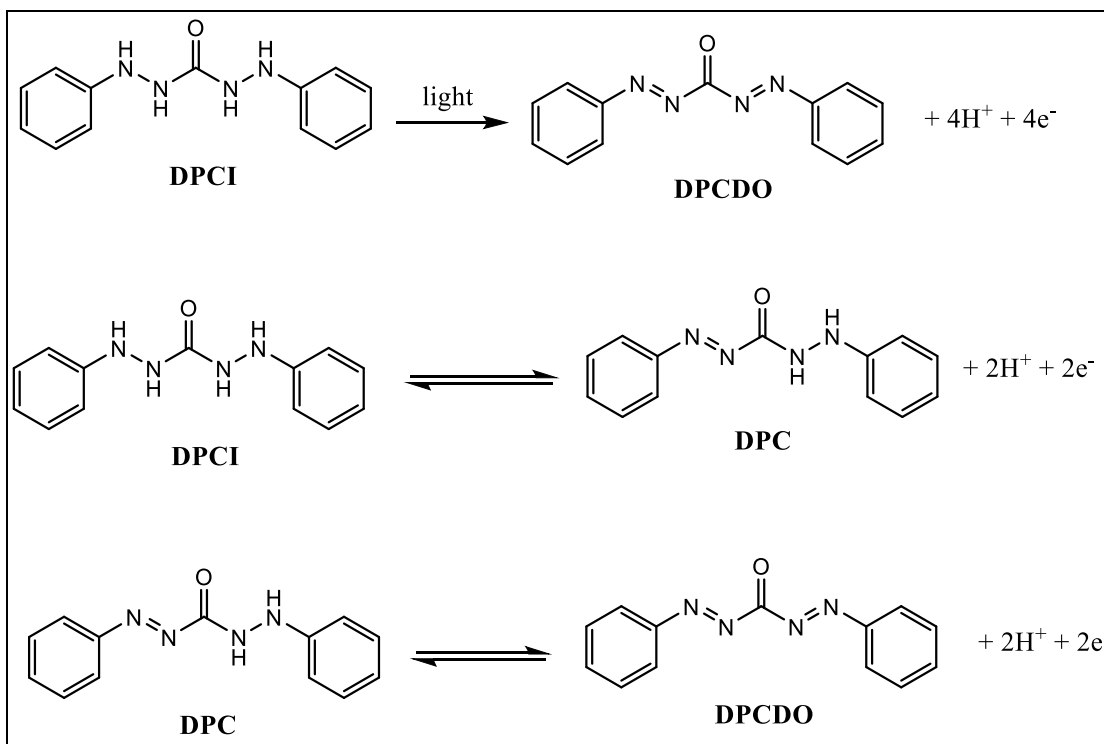


Figure 4.16: The proposed mechanism of oxidation-reduction of the DPC, (adapted).<sup>205</sup>

#### 4.4.2.3. Determination of $\text{Hg}^{2+}$ using the Hg bubbler apparatus

Because dry DPC test papers were found to be very sensitive towards sunlight, and the oxidation to an inactive form occurred very rapidly (5-15 mins) it was difficult to use them in the Hg screening apparatus described by Yallouz *et al.*<sup>165</sup>. It was decided not to pursue this avenue further due to the poor results and the lack of DPC test paper stability.

#### 4.4.3. Determination of $\text{Hg}^{2+}$ based on the reaction with R6G

##### 4.4.3.1. Determination of $\text{Hg}^{2+}$ in solution phase

A change of solution colour from orange red to pink was clearly noticed, which occurs as a result of R6G ion-associate in the presence of  $\text{Hg}^{2+}$ . However, it was observed that the blank also produced a pink colour, Fig. 4.17. Further investigation was carried out, and despite careful handling of the reagents and glassware washing regime, the reagent blank gave a pink colour each time upon the addition of KI to the reaction mixture. Therefore, it was necessary to check the reagent blank for possible

contamination by Hg. ICP-MS was used to evaluate the reagent blank by determining the purity of the reagents used to prepare the blank and the standards, separately.

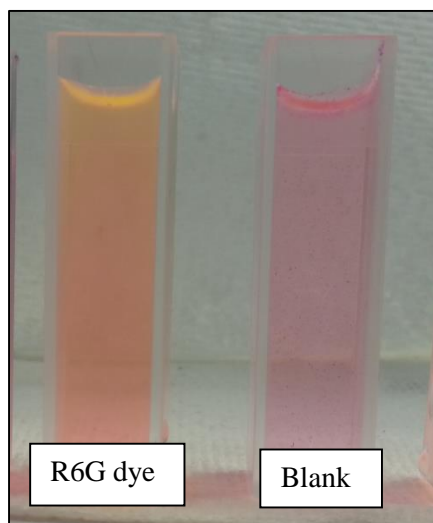


**Figure 4.17: Observation of the red-orange colour for the R6G dye and the formation of pink coloured  $[\text{HgI}_4][\text{R6G}]_2$  with the reagent blank.**

Results obtained initially from the ICP-MS revealed that the R6G dye solution contained  $27.5 \mu\text{g/L Hg}^{2+}$ . The analytical grade KI also contained traces of  $\text{Hg}^{2+}$  ( $1.32 \mu\text{g/L}$ ). The formation of the pink colour in the reagent blank was thus due to the fact that KI reacted with  $\text{Hg}^{2+}$  and produced tetraiodomercurate (II), with the presence of R6G dye then resulting in formation of pink coloured  $[(\text{HgI}_4)] [(\text{R6G})_2]$  complex.

To overcome this drawback, and find an appropriate observation regime, R6G dye alone was used as the blank for visual detection. However, in spectrometric analysis, a reagent blank solution containing all of R6G, KI, hexamine and gelatine, but without  $\text{Hg}^{2+}$ , was prepared with distilled water using the procedure described in Section 3.4.2.2 and measured under identical conditions.

For visual detection it was difficult to discriminate colour differences between standards at low concentrations ( $2 - 100 \mu\text{g/L}$ ) by the naked eye, although this was not the case at a concentration of  $800 \mu\text{g/L}$ , Fig. 4.18.

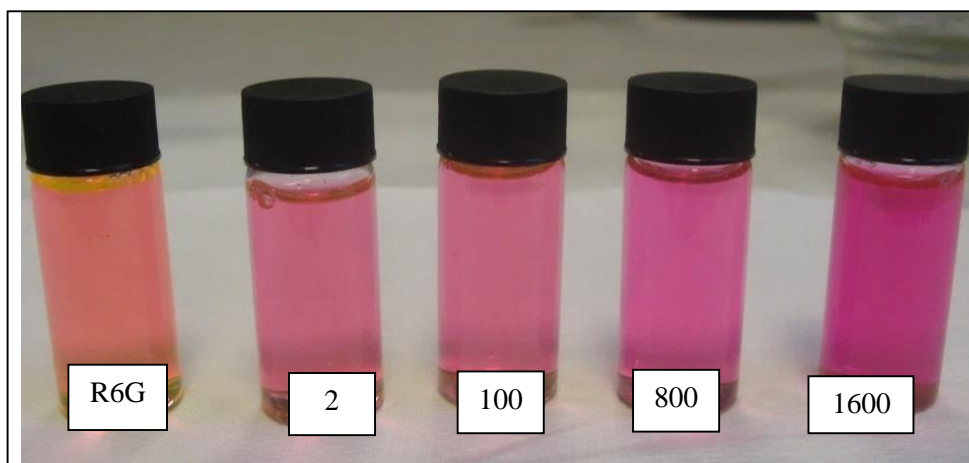


Figure 4.18: Formation of pink coloured  $[\text{HgI}_4][\text{R6G}]_2$  with Hg standard solutions of concentration 2, 100, 800 and 1600  $\mu\text{g/L}$ .

Spectrophotometry was performed using a transmittance UV-vis spectrophotometer over a wavelength range of 400-700 nm to evaluate the range of the method and the lower limit of detection. The absorbance was measured against distilled water, Fig. 4.19.

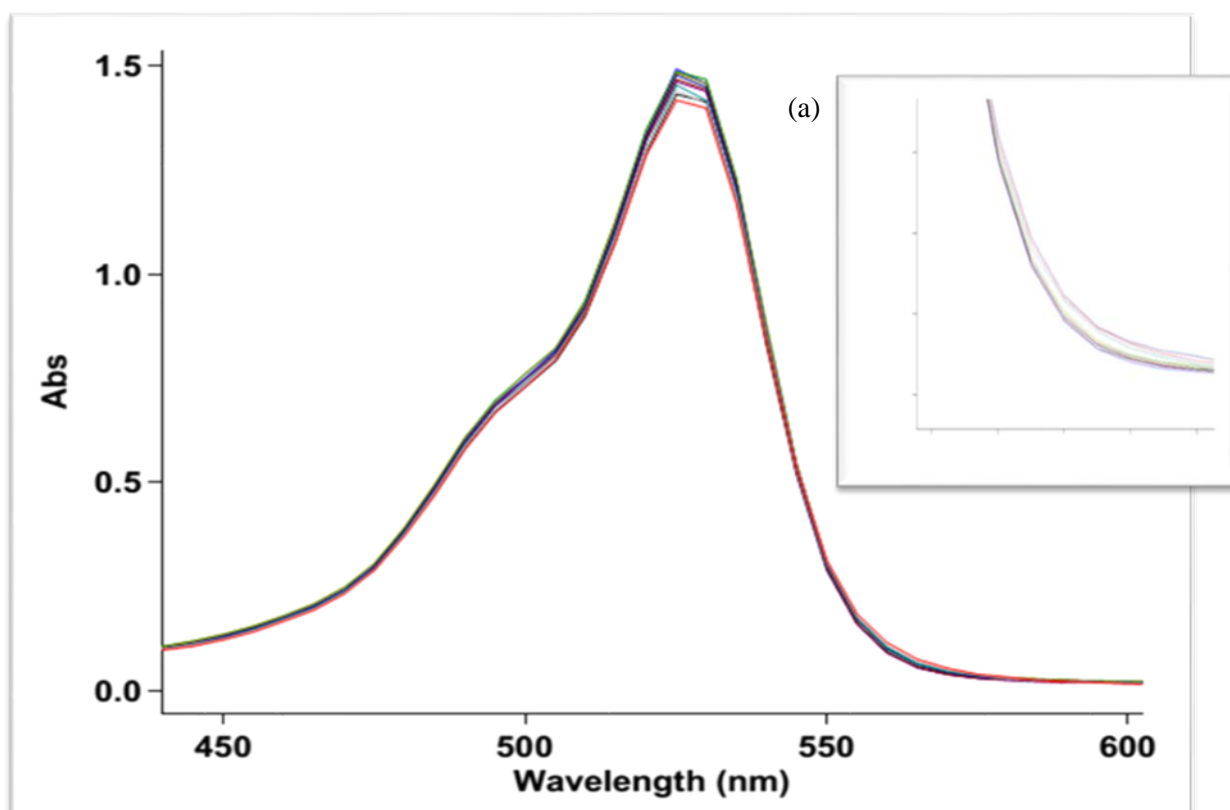
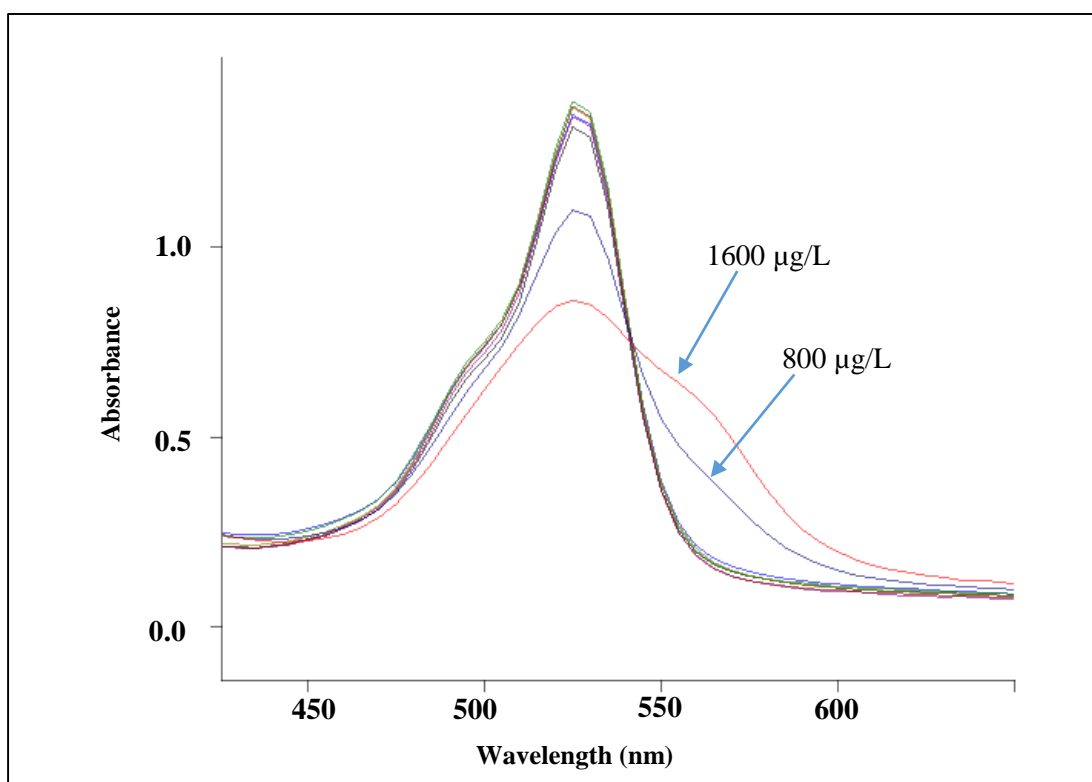


Figure 4.19: The transmission UV-vis spectra of R6G, R6G + Hg standard solutions with different concentration 2, 4, 8, 16, 32, 48, 64 and 80  $\mu\text{g/L}$ ; reference=water, inset (a) shows development of a new peak at about 570 nm associated with the formation of  $[(\text{HgI}_4)^2][(\text{R6G})^+]_2$ .

Spectral analysis (Fig. 4.19) showed that a new peak at about 570 nm corresponding to  $[(\text{HgI}_4)^{2-}][(\text{R6G})^+]_2$  was observed. The result indicated that the interaction of  $[(\text{HgI}_4)^{2-}]$  with R6G caused a bathochromic shift in the spectrum. The pink coloured  $[(\text{HgI}_4)^{2-}][(\text{R6G})^+]_2$  ternary complexes absorbed light at 570 nm, compared with the 530 nm absorbance maxima of the orange red coloured R6G dye.<sup>199</sup>

Further investigation was carried out for different concentration  $\text{Hg}^{2+}$  standards, which indicated that the absorbance of R6G at 530 nm diminished, while the absorbance at 570 nm corresponding to  $[(\text{HgI}_4)^{2-}][(\text{R6G})^+]_2$  increased, as  $\text{Hg}^{2+}$  concentration of the added standard solutions increased, Fig. 4.20. The absorbance spectrum was also measured at 570 nm against a reagent blank to more clearly illustrate the peak relating to formation of the  $[(\text{HgI}_4)^{2-}][(\text{R6G})^+]_2$ , Fig. 4.21. A concentration of 2  $\mu\text{g/L}$  could be considered as the lower limit of detection.



**Figure 4.20:** The transmission UV-vis spectra of the coloured  $[\text{HgI}_4][\text{R6G}]_2$  in solution, the new peak at 570 nm was observed clearly with higher  $\text{Hg}^{2+}$  concentration (800 and 1600  $\mu\text{g/L}$ ); reference = water.

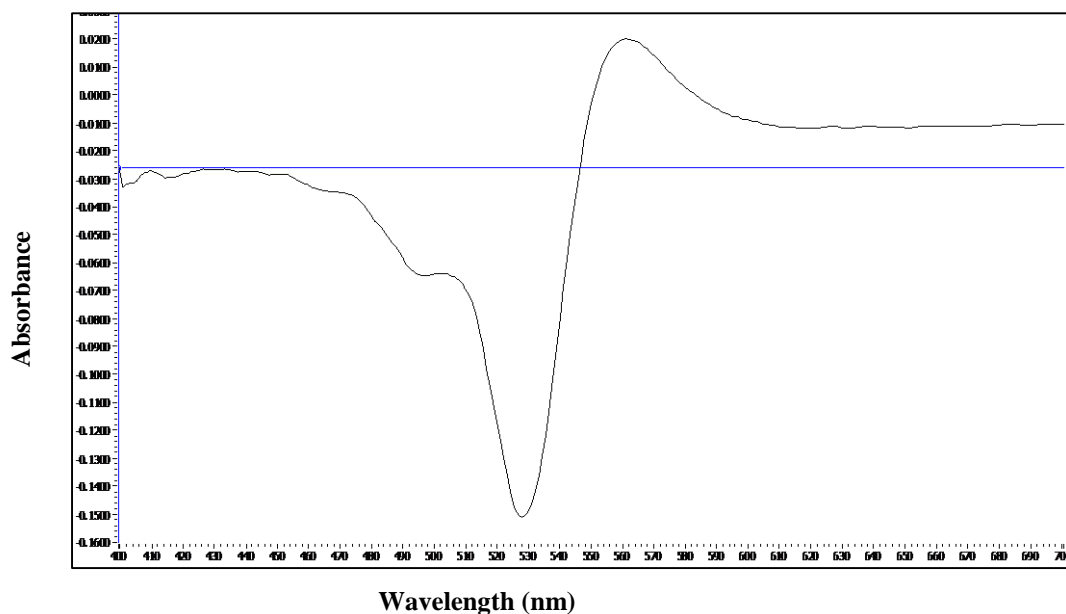


Figure 4.21: The transmission UV-vis spectrum of  $[\text{HgI}_4][\text{R6G}]_2$ ; reference = the reagent blank.

Calibration plots constructed for the absorbance obtained at 570 nm against  $\text{Hg}^{2+}$  concentration in the analysed standards indicated a strong correlation ( $r^2=0.9134$ ) between the absorbance and  $\text{Hg}^{2+}$  concentrations, Fig. 4.22. The absorbance of R6G

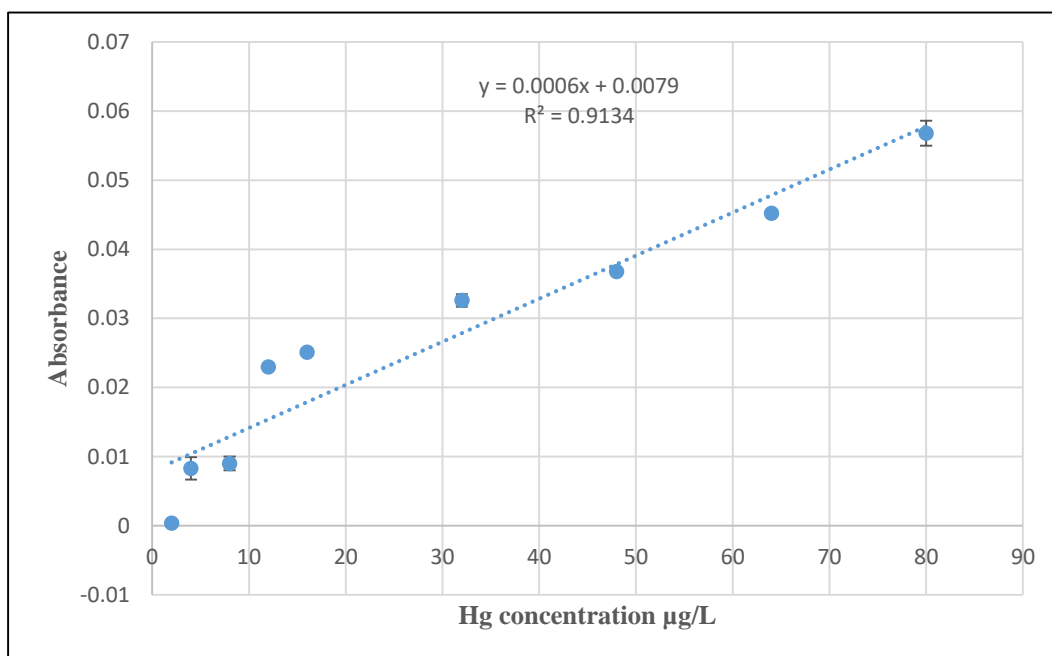
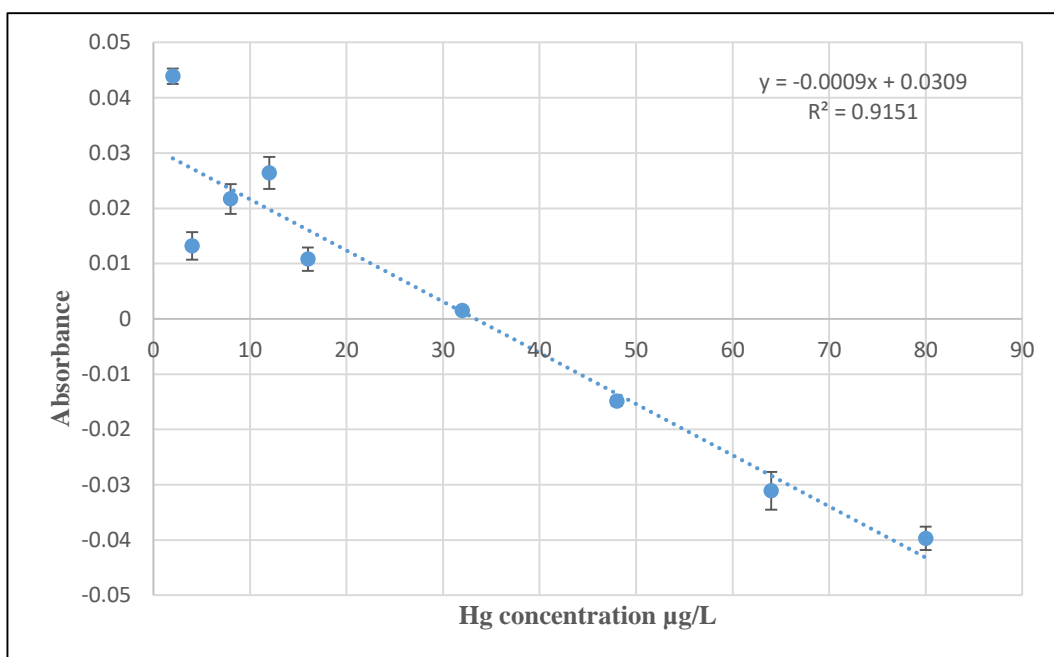


Figure 4.22: Calibration plots of the absorbance at 570 nm vs.  $\text{Hg}^{2+}$  concentrations; error bars represent one standard deviation ( $n=3$ ).

dye at 530 nm decreased upon the addition of  $\text{Hg}^{2+}$  solutions of increasing  $\text{Hg}^{2+}$  concentration, Fig. 4.23.



**Figure 4.23:** Calibration plots of the absorbance at 530 nm vs.  $\text{Hg}^{2+}$  concentrations; error bars represent one standard deviation ( $n=3$ ).

#### 4.4.3.2. Determination of $\text{Hg}^{2+}$ as spot test

A pink colour indicating the formation of  $[(\text{HgI}_4)^{2-}][(\text{R6G})^+]_2$  was produced immediately, on both wet and dried R6G test papers, when  $\text{Hg}^{2+}$  standard solutions with different concentrations were applied as spot test, Fig. 4.24. However, in the dry test papers, different colour zones were observed as R6G dye was leached out and spread across the papers, Fig. 4.25.

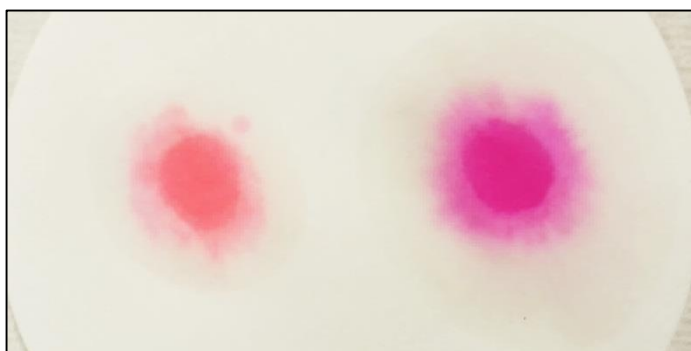


**Figure 4.24:** Formation of the pink coloured  $[(\text{HgI}_4)^{2-}][(\text{R6G})^+]_2$  complex in wet R6G papers.



Figure 4.25: Observation of lightening in colour intensity on the area of application of  $\text{Hg}^{2+}$  solution in dry R6G papers due to leaching and spreading.

#### 4.4.3.3. Determination of $\text{Hg}^{2+}$ using the Hg bubbler apparatus

The determination of  $\text{Hg}^{2+}$  was carried out using the Hg screening apparatus described in Section 3.2.2.4 and dried R6G test papers. The formation of the expected pink coloured ternary complex was observed. However, discrimination in colour intensity of the complex formed with different standards was difficult by the naked eye. The UV-vis reflectance spectrophotometer was employed to determine the lower limit of detection. The absorbance spectrum of the exposed R6G test papers with different concentration was measured against the R6G reagent blank. The  $[\text{HgI}_4][\text{R6G}]_2$  absorption peak could be obtained at 570 nm, Fig. 4.26.

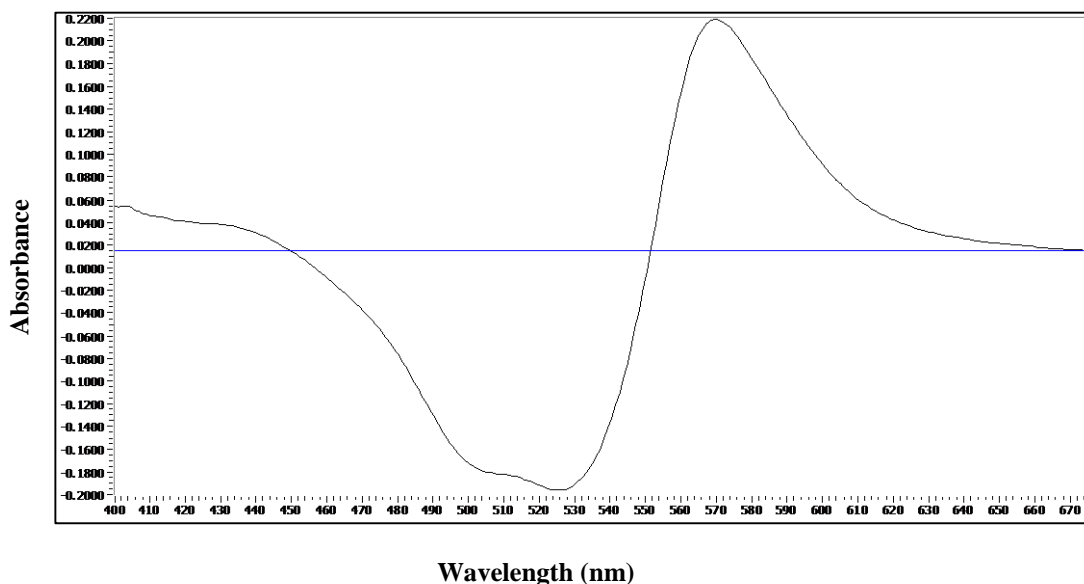
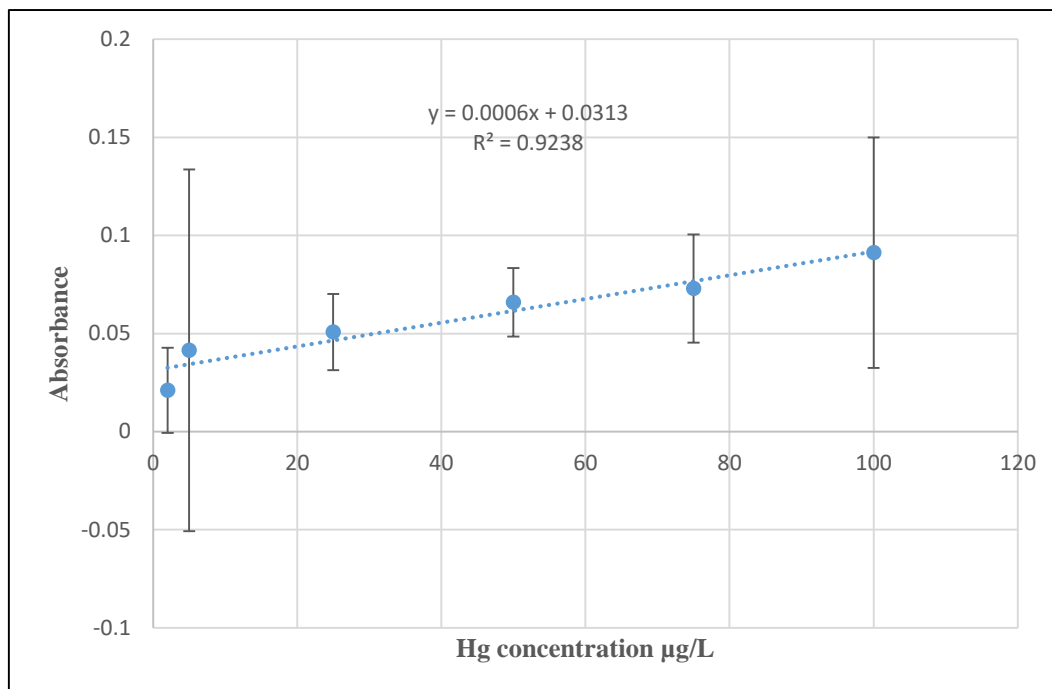


Figure 4.26: The reflection UV-vis spectrum of  $[\text{HgI}_4][\text{R6G}]_2$  on a paper support; reference= the reagent blank.

Calibration plots were established for the absorbance at 570 nm against  $\text{Hg}^{2+}$  concentration in the exposed papers. The results indicated a good linearity ( $r^2 = 0.9238$ ) between the absorbance at 570 nm and  $\text{Hg}^{2+}$  concentration in the range tested (2-100  $\mu\text{g/L}$ ), Fig. 4.27. The detection limit was founded to be about 2  $\mu\text{g/L}$ .



**Figure 4.27:** Calibration plots of the absorbance at 570 nm vs.  $\text{Hg}^{2+}$  concentrations; error bars represent one standard deviation ( $n=3$ ).

The absorbance profile for the complexes produced using CuI and R6G reagents can be found in Appendix 2.

#### 4.5. Conclusion

Three different chromogenic reagents for the detection of  $\text{Hg}^{2+}$  were selected and their analytical performance compared when used in solution, in spot test mode (both as wet reagents and when dried onto filter papers), and in the Hg bubbler apparatus recommended by Yallouz *et al.*<sup>165</sup> for semi-quantitative  $\text{Hg}^{2+}$  screening in environmental samples. A summary of the results is presented in Table 4.2.

**Table 4.2: Summary of the analytical performance of the small molecules reagents CuI, DPC and R6G for Hg determination.**

parameter	CuI	DPC	R6G
LOD	2 µg/L	5000 µg/L	2 µg/L
Formation of Hg-complex in solution phase	Was not attempted	Insoluble purple colour as a result of formation of Hg-DPC	Pink colour as a result of formation of [HgI <sub>4</sub> ][R6G] <sub>2</sub>
Formation of Hg-complex on filter paper as spot tests	Bleaching of CuI detecting papers upon addition of the reduced and non-reduced Hg standard solutions	A vivid purple coloured Hg-DPC complex in the wet test papers. No reaction with dry papers due to oxidation of the DPC	Pink colour in wet and dry R6G test papers. However, observation of leaching of R6G dye under dry test papers condition.
Adapting to the Hg bubbler apparatus developed by Yallouz <i>et al.</i> <sup>165</sup>	A salmon coloured Cu <sub>2</sub> [HgI <sub>4</sub> ] complex was formed	Not suitable for adapting with the semi-quantitative method	A pink coloured [HgI <sub>4</sub> ][R6G] <sub>2</sub> complex was formed
Colour read out with respect to standards	As soon as possible and certainly within the first 24 hours	As soon as the coloured complex produced	Not applicable
Incorporation with spectrophotometry	Yes	no	yes
Linearity of response	r <sup>2</sup> =0.972	Not applicable	r <sup>2</sup> =0.913, r <sup>2</sup> =0.923 in solution and spot test mode, respectively

The CuI detecting papers were not considered suitable in spot test mode as a result of colour bleaching of the papers upon the addition of  $\text{Hg}^{2+}$  standard solutions. In the Hg bubbler apparatus method, the intensity of  $\text{Cu}_2[\text{HgI}_4]$  coloured complex produced on CuI detecting papers increased with increasing  $\text{Hg}^{2+}$  concentration in the standards. Difference in colour intensity obtained with different  $\text{Hg}^{2+}$  concentration in standards could be seen with a 10  $\mu\text{g/L}$  concentration difference over the range of 5 to 75  $\mu\text{g/L}$ . As the coloured complex tended to fade from the detecting paper, it was important to compare the colour intensity between the standards and environmental samples as soon as possible and ideally within the first hour. The direct exposure of the exposed CuI detecting papers to light should be minimised as it causes an increase in colour fading. The absorbance spectra of the  $\text{Cu}_2[\text{HgI}_4]$  was measured directly on the surface of detecting papers using UV-vis reflectance spectroscopy. Although a concentration of 5  $\mu\text{g/L}$  was the lower detection limit that could be observed by the naked eye, 2  $\mu\text{g/L}$  was the lower limit of detection obtained by the spectrophotometric analysis. Linear calibration between the absorbance at 434 nm and  $\text{Hg}^{2+}$  concentrations was obtained with a strong correlation coefficient of  $r^2=0.972$ . The stability of the coating was not affected by the investigated temperatures 4 °C, 25 °C and 35 °C. Therefore, CuI detecting papers should be suitable for use worldwide in different climates.

The Hg-DPC compound formed with the coordination of DPC with  $\text{Hg}^{2+}$  was suitable for colorimetric determination of  $\text{Hg}^{2+}$  in solutions and wet paper conditions. The intensity of purple coloured complex obtained increased as the concentrations of  $\text{Hg}^{2+}$  in the standards increase. A concentration of 5 mg/L was the lower detection limit and could be observed rapidly and simply by the naked eye. The Hg-DPC coloured complex produced in solution phase was insoluble. Rapid fading of the Hg-DPC formed on the wet test papers occurred within 1-3 hours; thus, the colour intensity of standards and samples should be compared as soon as the Hg-DPC colour developed. Because of the oxidation-reduction of the DPC on the dried test papers, this reagent could not be adapted to the Hg screening method.

The presence of  $\text{Hg}^{2+}$  contamination in the R6G reagents was noted in this work. Although  $\text{Hg}^{2+}$  detection could be carried out, the results suggested that caution should be advised when visual and spectrometric analysis are conducted. It is strongly advised to check the purity of the reagents, as  $\text{Hg}^{2+}$  contamination critically impacts the results

obtained from the blank and the samples. Visual detection conducted using R6G dye only indicated that the reaction between  $[\text{HgI}_4]^{2-}$  and R6G was successfully achieved by producing an ion-associate that has a characteristic pink colour both in solution and wet spot test mode. Leaching of R6G was observed upon addition of  $\text{Hg}^{2+}$  standards under dry papers condition. The performance using the  $\text{Hg}^{2+}$  bubbler apparatus method was promising. Discrimination of the colour intensity produced was difficult to carry out by the naked eye, but spectrophotometric determination of the complex could be carried out in both solution and on the paper based support. The reagent blank was used as reference when the spectrometric analysis was conducted. The formation of  $[(\text{HgI}_4)^{2-}][(\text{R6G})^+]_2$  occurred with bathochromic shift at 570 nm. A concentration of 2  $\mu\text{g/L}$  was considered as the lower limit of detection. The absorbance values were proportional to  $\text{Hg}^{2+}$  concentration in the standards resulting in a linear calibration with strong correlation of  $r^2=0.913$  and  $r^2=0.923$  in solution and on the paper support, respectively.

When the Hg bubbler apparatus was used in combination with UV-vis reflectance spectroscopy, 2  $\mu\text{g/L}$  of  $\text{Hg}^{2+}$  could be detected with CuI and R6G probes. This detected value meets the EPA guideline for the maximum allowable  $\text{Hg}^{2+}$  level in drinking water. However, although the analytical equipment is simple, the transformation of the method from the current laboratory procedures to a field-based method is likely to prove difficult. Also, sample reduction in the field is undesirable and would require further development. The option of spot test would be simpler and more suitable for field use. The CuI impregnated papers did not work in spot test mode and were only sensitive to  $\text{Hg}^0$  vapour. Hence, these were not studied further. Rhodamine derivatives seem to have potential application for simple colorimetric  $\text{Hg}^{2+}$  determination, and so were chosen and explored in more detail in Chapter 5.

## 5. Rhodamine B thiolactone-based naked-eye sensor for rapid determination of Hg<sup>2+</sup> in natural waters

### 5.1. Introduction

The design and synthesis of simple, rapid and convenient chemosensors for environmental detection of Hg<sup>2+</sup> in aqueous media at trace levels are highly desirable for water quality monitoring. Significant advances in the development of spectroscopic sensing molecule probes based on fluorescence signaling and colorimetric changes have been made for the detection of metal ions including Hg<sup>2+</sup>. Their advantages relate to their low cost, high sensitivity and in particular their ability to be used for *in vivo* imaging applications.<sup>206-210</sup> In addition to those operate *via* chemical reactions, common photophysical mechanisms have been used advantageously in the design of these probes, that promote fluorescence and colorimetric changes, such as intramolecular charge transfer, photoinduced electron transfer, Förster resonance energy transfer, and chelation-induced enhanced fluorescence.<sup>61</sup> In this respect, large numbers of Hg<sup>2+</sup> detecting probes have been designed that can be categorised into two types, one based on a coordination-interaction<sup>81, 211-213</sup> with Hg<sup>2+</sup> and the other operating *via* chemical reactions.<sup>214-220</sup>

However, a number of reported synthesised chemosensors have limitations in terms of cross-interference towards other metal ions,<sup>199, 221</sup> poor aqueous solubility,<sup>222</sup> or complicated synthetic routes.<sup>78,223</sup> Recently, rhodamine B thiolactone has been proposed<sup>56, 166, 224</sup> as a reliable and simple chemosensor for naked eye detection of trace Hg<sup>2+</sup> in aqueous media.

Rhodamines are dyes particularly used as chemosensors in detecting certain metal ions, e.g., Cr<sup>3+</sup>, Cu<sup>2+</sup>, Fe<sup>3+</sup>, and Hg<sup>2+</sup>. Advantages include their high molar absorptivity, high fluorescence quantum yield and long wavelength absorption and emission.<sup>225</sup> Among rhodamine derivatives, rhodamine B exhibits an equilibrium between two main, well-defined molecular forms, the lactone (L) and the zwitterion (Z), as illustrated in Fig. 5.1. Generally, the L form is colourless and has very weak absorption and emission bands, while the Z form is highly coloured.<sup>226, 227</sup>

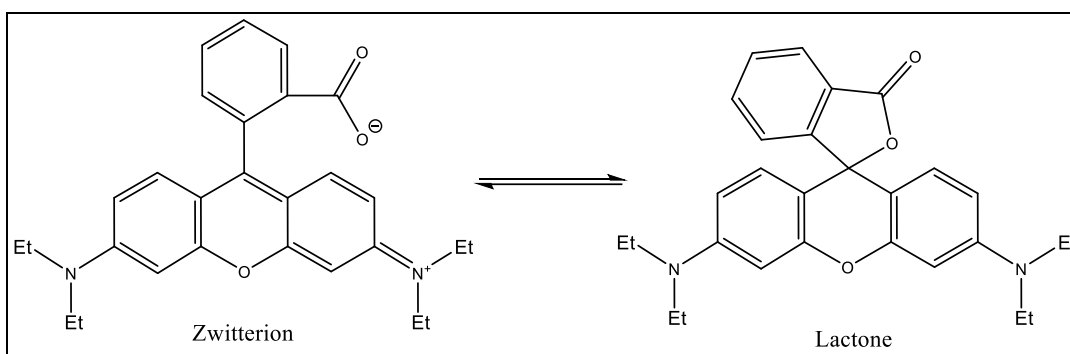


**Figure 5.1: Equilibria between zwitterion and lactone forms of rhodamine B.**

The position of the equilibrium between the L and Z forms is extremely sensitive to the local microenvironment. It has been found that the spectrum of the dye solution depends on solvent polarizability and hydrogen-bond donating ability, temperature and concentration.<sup>228</sup>

Most of the rhodamine B-based sensors reported contain a ‘soft’ ligand such as N or S atoms which can selectively bind to ‘soft’  $\text{Hg}^{2+}$ . Consequently, such coordination resulted in the opened-ring form and significant colour change.<sup>72, 229, 230</sup> However, due to the lack of stability, water solubility, insufficient sensitivity and pH independence, more improvements to these rhodamine-based sensors are still required.

To study the changes in the photophysical properties of rhodamine B probes upon interaction with  $\text{Hg}^{2+}$ , rhodamine B have been used to synthesise rhodamine B thiolactone.<sup>166, 224</sup> The sensing response was based on the ability of  $\text{Hg}^{2+}$  to induce a ring-opening reaction and trigger structural change from the colourless and nonfluorescent L form to the coloured and fluorescent open Z form.

Rhodamine B thiolactone was synthesised from commercially available rhodamine B base by a one-step reaction.<sup>224</sup> The reaction was based on the replacement of the O atom in the L form with a S atom. The synthetic route was as illustrated in Fig. 5.2. Rhodamine B was reacted with  $\text{ClCH}_2\text{CH}_2\text{Cl}$  and  $\text{POCl}_3$  to produce the intermediate rhodamine compound (1). The resultant mixture was stirred with saturated  $\text{Na}_2\text{S}$  aqueous solution at room temperature for 6 hrs. Then, the mixture was extracted and the solvent was removed under reduced pressure. The extracted product was separated

by silica-gel column chromatography with  $\text{CH}_2\text{Cl}_2$ /petroleum ether (1:1) as an eluent to afford the yellow solid rhodamine B thiolactone (2) in 48% yield (0.25 g).

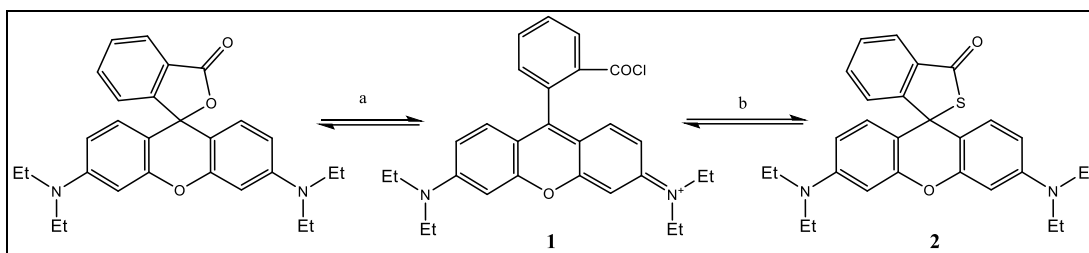


**Figure 5.2: Synthesis of rhodamine B thiolactone, (a)  $\text{ClCH}_2\text{CH}_2\text{Cl}$ ,  $\text{POCl}_3$ , reflux, 4 h, (b) excess  $\text{Na}_2\text{S}$  saturated aqueous solution.**

The rhodamine B thiolactone sensor has two advantages over the lactone. Firstly, the fact that  $\text{Hg}^{2+}$  is a thiophilic ion that has been used in desulfurization reactions for various S compounds such as thioacetal and different thiourea substituents.<sup>216, 231</sup> Based on this property the chemosensor was expected to provide high selectivity toward  $\text{Hg}^{2+}$ . Secondly, the thiol group is more nucleophilic than the hydroxyl group. Thus the benefit of S atom nucleophilicity served not only the condensation of thiol with acyl chloride but also as an enhanced centre for cyclisation with the electron-deficient benzylic carbon.

Chapter 5 examines if the one-pot synthesis route of rhodamine B thiolactone (a potential simple chemosensor for  $\text{Hg}^{2+}$  routine analyses) is readily carried out. It also addresses the conditions under which the spirocyclic structure is stable, and whether it is possible to obtain a sensor with a highly convenient, sensitive and selective spectral response toward  $\text{Hg}^{2+}$ .

## 5.2. Aim

The aim of this chapter was to assess the analytical capability of rhodamine B thiolactone as a chemosensor for  $\text{Hg}^{2+}$  determination in aqueous solution, specifically:

- To assess the reproducibility of the overall chemosensor synthesis.
- To determine the conditions under which the solid rhodamine B thiolactone molecule sensor is stable.
- To evaluate the method lower limit of detection and linear range.

- To assess interferences from ions potentially likely to coexist in the environment.
- To compare the method performance in distilled water and artificial seawater.
- To address the suitability of the reagent for immobilisation on a solid support such as an antibiotic assay disc.

### **5.3. Experimental**

#### **5.3.1. Reagents and apparatus**

The reagents and apparatus used for the determination of  $\text{Hg}^{2+}$  based on the reaction with rhodamine B thiolactone were as described in Section 3.5.1.

#### **5.3.2. Synthesis of rhodamine B thiolactone**

Rhodamine B thiolactone was synthesised from rhodamine B base and  $\text{Na}_2\text{S}$  by a one pot synthesis route<sup>224</sup>, as described in Section 3.5.2.1.

#### **5.3.3. Solutions preparation**

The stock solution of rhodamine B thiolactone (5 mM) was prepared in  $\text{CH}_3\text{CN}$ . Stock solutions of  $\text{Hg}^{2+}$  and multi-element standard solution (10 mg/L of  $\text{As}^{3+}$ ,  $\text{Cd}^{2+}$ ,  $\text{Co}^{2+}$ ,  $\text{Cr}^{3+}$ ,  $\text{Cu}^{2+}$ ,  $\text{Fe}^{3+}$ ,  $\text{Mg}^{2+}$ ,  $\text{Mn}^{2+}$ ,  $\text{Na}^+$ ,  $\text{Ni}^{2+}$ ,  $\text{Pb}^{2+}$  and  $\text{Zn}^{2+}$  in 2% (v/v)  $\text{HNO}_3$ ) were prepared in distilled water. The solution preparation procedures were as described in Section 3.5.2.3.

#### **5.3.4. General procedure for $\text{Hg}^{2+}$ determination in aqueous solution**

All the measurements were made according to the procedure described in Section 3.5.2.4. Before UV-vis spectroscopic measurements, the reaction mixture was freshly prepared and diluted. It was then transferred to a 1  $\text{cm}^2$  quartz cell to measure the absorbance within a wavelength range of 400 to 700 nm against the blank. The reagent blank solution containing acetate buffer, rhodamine B thiolactone and distilled water without  $\text{Hg}^{2+}$  was prepared and measured under identical conditions.

### **5.3.5. The determination on antibiotic assay discs**

Determination of  $\text{Hg}^{2+}$  was conducted in spot test mode for both wet and dry antibiotic assay discs. Rhodamine B thiolactone test papers were prepared by immersing antibiotic assay discs in the stock solution of rhodamine B thiolactone (5 mM) before  $\text{Hg}^{2+}$  solutions were added dropwise as described in Section 3.5.2.5.

### **5.3.6. Stability of solid rhodamine B thiolactone**

To assess the effect of storage conditions on the solid rhodamine B thiolactone compound, a comparison of colour was carried out under controlled storage conditions in terms of temperature and light.

### **5.3.7. Optimisation of sensing conditions**

In order to optimise the concentration of rhodamine B thiolactone in the reaction mixture to give a maximum and stable colorimetric response, a series of different volumes and concentrations of rhodamine B thiolactone stock solution were used for  $\text{Hg}^{2+}$  determination.

### **5.3.8. Limit of detection and range of method**

A series of  $\text{Hg}^{2+}$  standard solutions with different concentrations were tested to evaluate the method range and estimate the limit of detection.

### **5.3.9. Interferences of other ions**

To assess the selectivity of rhodamine B thiolactone toward  $\text{Hg}^{2+}$ , various ions potentially coexisting in the aquatic environment - both major and trace elements - were examined under the same conditions as described in Section 3.5.2.4. When the selectivity study was conducted, in parallel with the general procedure for  $\text{Hg}^{2+}$  detection, 50  $\mu\text{L}$  of the stock solution of rhodamine B thiolactone (5 mM) was mixed with an appropriate amount of a multi-element standard solution containing 10 mg/L each of  $\text{As}^{3+}$ ,  $\text{Cd}^{2+}$ ,  $\text{Co}^{2+}$ ,  $\text{Cr}^{3+}$ ,  $\text{Cu}^{2+}$ ,  $\text{Fe}^{3+}$ ,  $\text{Mg}^{2+}$ ,  $\text{Mn}^{2+}$ ,  $\text{Na}^+$ ,  $\text{Ni}^{2+}$ ,  $\text{Pb}^{2+}$  and  $\text{Zn}^{2+}$ . In the interference experiment, an appropriate amount of the 10 mg/L multi-element standard solution was added to a 10 mL volumetric flask containing 50  $\mu\text{L}$  5 mM

rhodamine B thiolactone stock solution, and an appropriate volume of 10 mg/L Hg<sup>2+</sup> standard solution.

#### **5.3.10. Method application in seawater**

The applicability of the rhodamine B thiolactone sensing was investigated by determining Hg<sup>2+</sup> in a spiked artificial seawater under the same conditions as described in Section 3.5.2.4.

#### **5.3.11. Assessment of Hg<sup>2+</sup> detection in spot test mode**

A series of detecting discs exposed to different Hg<sup>2+</sup> concentrations was evaluated by naked eye to find the lowest detectable concentration in both wet and dry paper conditions.

### **5.4. Results and discussion**

#### **5.4.1. Stability of solid rhodamine B thiolactone**

It was found that solid rhodamine B thiolactone changed colour from light yellow to pink over time at room temperature. Previous studies on rhodamine B thiolactone<sup>56, 166, 224</sup> have not highlighted this issue. Therefore, the effect of storage conditions on the synthesised chemosensor was investigated. The stability of the compound was investigated by a comparison of its colour change under different conditions. Rhodamine B thiolactone was stored in sealed containers for up to two weeks in different storage environments, at ambient room temperature (in the laboratory daylight and in the dark by wrapping the container with aluminium foil), and at around -18 °C in a freezer (in the dark and in the light by exposing the container to a small white light torch). It was observed clearly by the naked eye that the chemosensor changed its colour under all storage conditions except when stored in the dark at -18°C. Exposure to direct light at room temperature rapidly accelerated the colour change from yellow to dark pink within less than an hour. In contrast, storing the chemosensor in the dark at room temperature delays the change from yellow to pink by up to three to four hours, but it eventually changed to a light pink. At low temperature -18 °C in the light the yellow product retained its colour up to a week

before turning to light pink. It was concluded that the rhodamine B thiolactone was only stable at low temperature away from light, Fig 5.3.

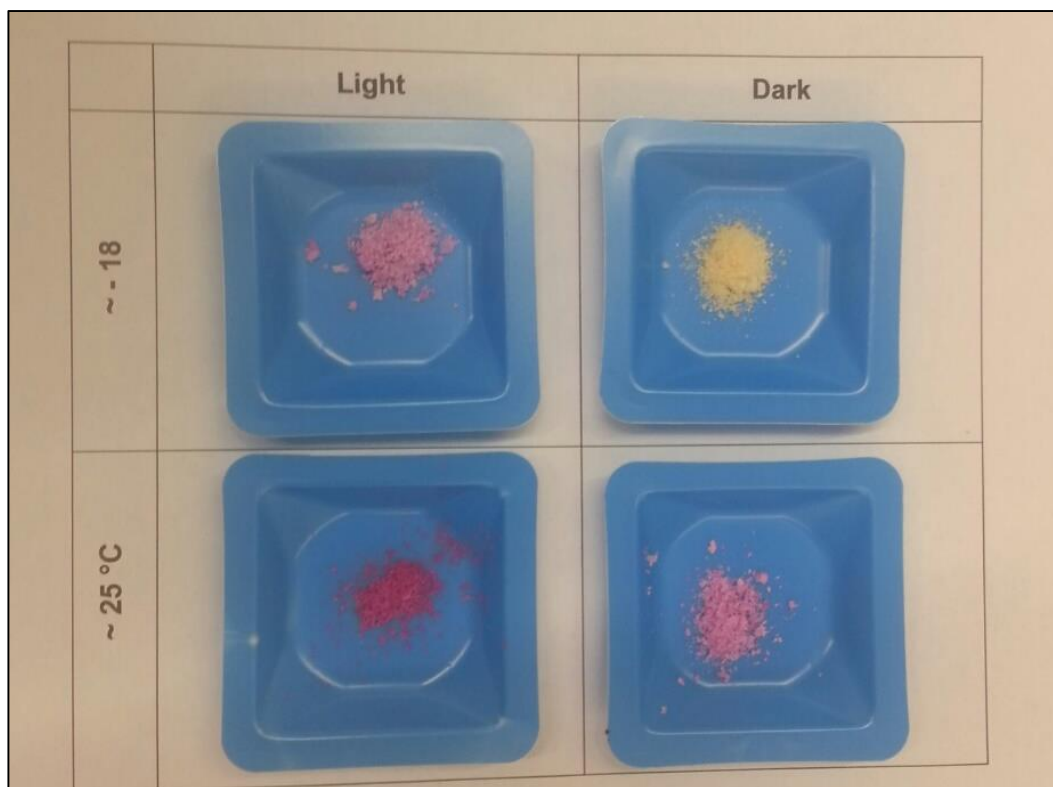


**Figure 5.3:** Effect of storage conditions on the stability of solid rhodamine B thiolactone.

Because the equilibrium between the L and Z forms is extremely sensitive to the local microenvironment, it was hypothesised that the action of light and temperature might induced ring opening of the solid rhodamine B thiolactone molecules and converted them into the Z form, which is highly coloured. To further study the colour change induced by exposure to light and temperature, the coloured product was observed using an optical microscope. A small sample of the product was separated, and the morphology of the material was studied under magnification. The microscope photo in Fig. 5.4 revealed colourless crystals surrounded by pink “branches” which might have indicated that the process of ring opening started from the outer layers of the crystals. Since the colour change was irreversible, temperature and light exposure should be minimised.

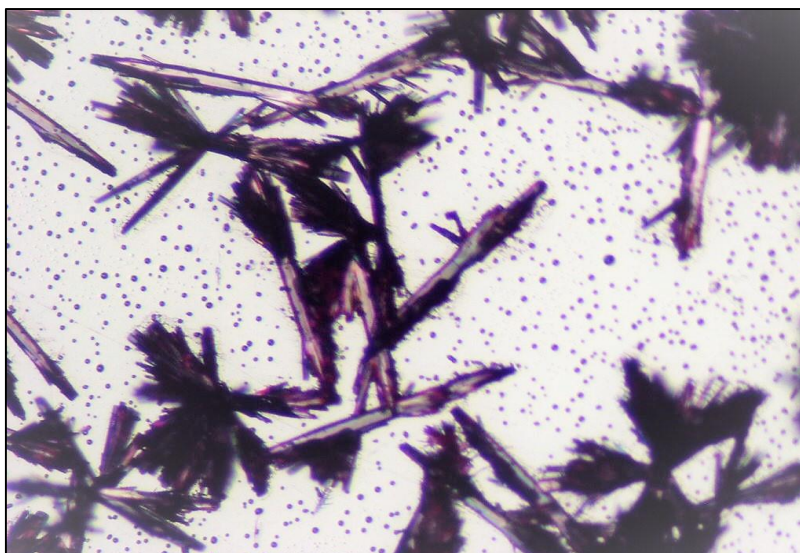


**Figure 5.4:** Microscope photo of the oxidised rhodamine B thiolactone.

#### **5.4.2. Optimisation of sensing conditions**

The colorimetric sensing was based on the complexation reaction between rhodamine B thiolactone and  $\text{Hg}^{2+}$ , with formation of a pink coloured complex. Shi *et al*<sup>166</sup> and Zhan *et al*<sup>224</sup> explored the reaction mechanism of rhodamine B thiolactone with  $\text{Hg}^{2+}$ . The resulted coloured product was subjected to electrospray ionization mass spectral analyses. Three major ion peaks were detected. One of the peaks was characterized to be rhodamine B as a final product. Another peak was proven to be a doubly charged ion product. They suggested that the possible reaction mechanism in this system may proceeded through the route illustrated in Fig 5.5. The reaction of  $\text{Hg}^{2+}$  with rhodamine B thiolactone leads to the formation of two kinds of complexes. Complex 3 is relatively stable in the solution, whereas the complex 4 can be further degraded to rhodamine B.<sup>224</sup>

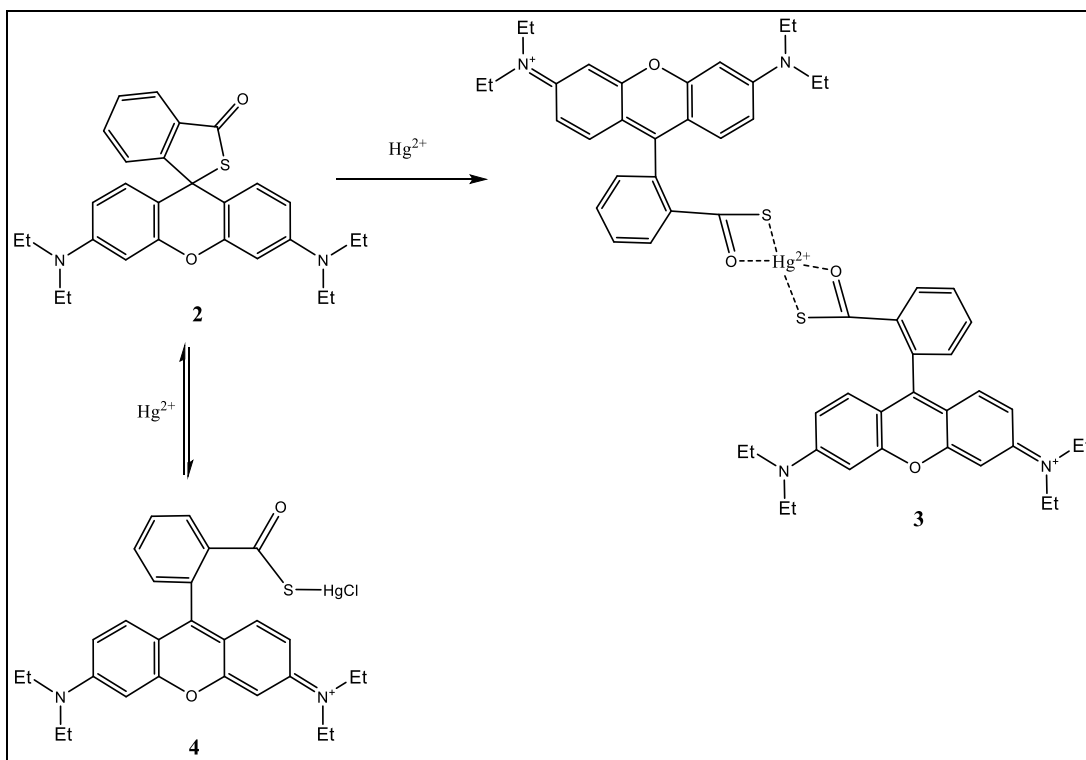


**Figure 5.5: The proposed reaction between  $\text{Hg}^{2+}$  and rhodamine B thiolactone.**

In order to optimise the concentration of rhodamine B thiolactone in the reaction mixture two strategies were followed;

- Firstly, the amount of 5 mM rhodamine B thiolactone stock solution added to a 10 mL reaction mixture was varied (10, 50, 100, 200, and 400  $\mu\text{L}$ ) corresponding to a total concentration of 5, 25, 50, 100, and 200  $\mu\text{M}$  respectively.
- Secondly, a parallel experiment, 50  $\mu\text{L}$  of different concentration of rhodamine B thiolactone stock solutions (5, 10, 15 and 20 mM) were added separately to the 10 mL reaction mixture corresponding to a total concentration of 25, 50, 75 and 100  $\mu\text{M}$  respectively.

A summaries of the findings are described in Table 5.1 and 5.2 respectively.

**Table 5.1: Optimisation in which different volumes of the reagent were added to the reaction mixture.**

Stock solution concentration (mM)	Volume added to a 10 mL reaction mixture ( $\mu\text{L}$ )	Final concentration of rhodamine B thiolactone in the reaction mixture ( $\mu\text{M}$ )	Visual observation
5	10	5	Pink colour formed
	50	25	More intense pink colour formed
	100	50	Similar colour intensity as before
	200	100	Similar colour intensity + cloudy solution formed
	400	200	Similar colour intensity + cloudy solution formed

**Table 5.2: Optimisation in which different concentrations of the reagent were added to the reaction mixture.**

Volume added to a 10 mL reaction mixture ( $\mu\text{L}$ )	Stock solution concentration (mM)	Final concentration of rhodamine B thiolactone in the reaction mixture ( $\mu\text{M}$ )	Visual observation
50	5	25	Intense pink colour formed
	10	50	Similar colour intensity as before
	15	75	Similar colour intensity + cloudy solution formed
	20	100	Similar colour intensity + cloudy solution formed

The colour intensity of the Hg-rhodamine B thiolactone complex produced increased with increasing volume of the colouration reagent from 10 to 50  $\mu\text{L}$ , however further addition seemed to show no significant difference in the colour intensity produced, as shown in Fig. 5.6 (a). Furthermore, cloudy suspended solutions were formed where the added volume was more than 100  $\mu\text{L}$ .

Similarly, the addition of 50  $\mu\text{L}$  of different concentrations of stock rhodamine B thiolactone showed similar colour intensity up to a concentration of 50  $\mu\text{M}$  in the mixture; however, again cloudy solutions were formed with concentrations 75 and 100  $\mu\text{M}$ , Fig. 5.6 (b).

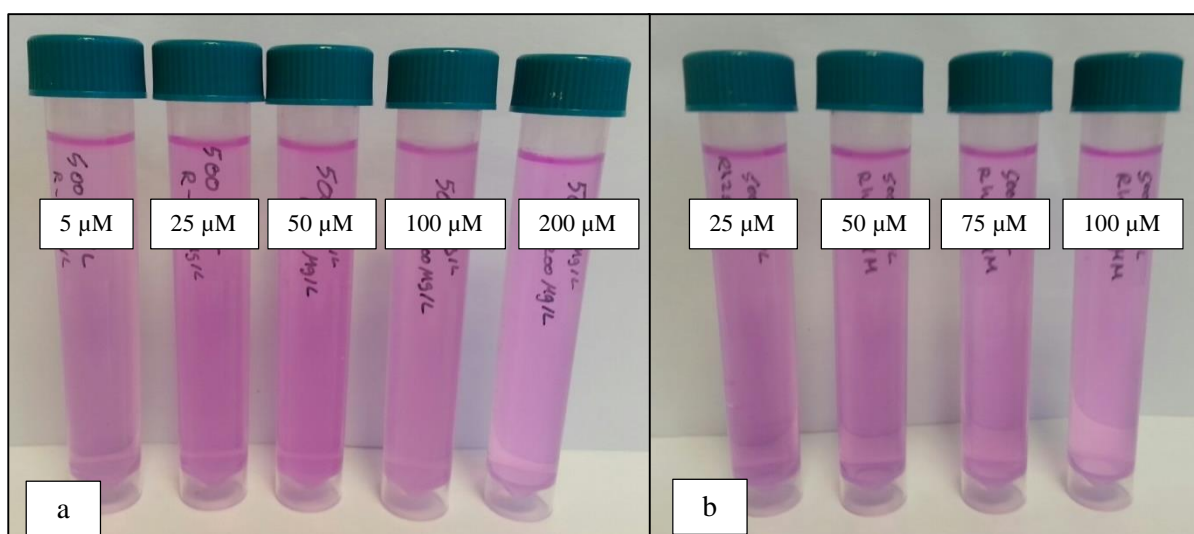


**Figure 5.6:** (a) The addition of 10, 50, 100, 200, and 400  $\mu\text{L}$  of 5 mM rhodamine B thiolactone stock solution to the reaction mixture. (b) The addition of 50  $\mu\text{L}$  of 5, 10, 15 and 20 mM rhodamine B thiolactone stock solution to the reaction mixture. The concentration of  $\text{Hg}^{2+}$  was 500  $\mu\text{g/L}$ .

It was likely that saturated solutions of rhodamine B thiolactone were starting to form with the addition of 100  $\mu\text{L}$  5 mM or 50  $\mu\text{L}$  10 mM to the 10 mL reaction mixture, making the final concentration of the reagent in the aqueous solution 50  $\mu\text{M}$ . Thus, any concentration above that remained insoluble and formed suspended particles in the aqueous solutions. However, as there was no difference in the colour intensity between the final concentration of 25 and 50  $\mu\text{M}$ , the use of 50  $\mu\text{L}$  of 5 mM rhodamine B thiolactone (which corresponding to a concentration of 25  $\mu\text{M}$  in the final reaction mixture) was selected as the optimal volume of the chromogenic reagent. The rhodamine B thiolactone could be used at this concentration in aqueous solutions with

no additional co-solvent except the introduction of 0.5% (v/v) of acetonitrile from the reagent stock solution, which would be favourable in improving the solubility.

#### 5.4.3. Limit of detection and range of method

Under the above optimised conditions, the concentration of  $\text{Hg}^{2+}$  that could be detectable by the naked eye was evaluated. As expected, rhodamine B thiolactone itself displayed a colourless solution. However, the addition of  $\text{Hg}^{2+}$  immediately produced a pink colour resulting from opening the rhodamine B thiolactone ring and formation of Hg-rhodamine B thiolactone complex. The intensity of the coloured product appeared to increase with increasing  $\text{Hg}^{2+}$  concentration in the standards, as shown in Fig. 5.7. A concentration of 50  $\mu\text{g/L}$  was the lower detection limit that could be observed rapidly and simply by the naked eye.

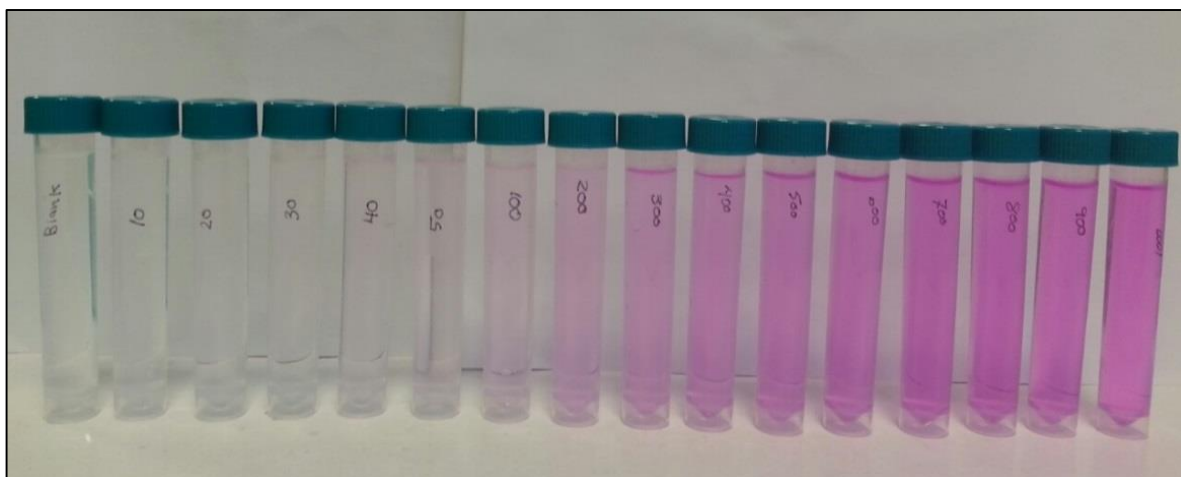


**Figure 5.7: Increase of pink colour intensity as the  $\text{Hg}^{2+}$  concentration increased for a range of 10 to 1000  $\mu\text{g/L}$  in the standard solutions.**

To evaluate the method's range and the instrumental limit of detection, spectrophotometric analysis was performed using a transmittance UV-vis spectrophotometer over a wavelength range of 400-700 nm. The absorbance was measured for a series of  $\text{Hg}^{2+}$  standard solutions with different concentration against the reagent blank (rhodamine B thiolactone, acetate buffer and distilled water without  $\text{Hg}^{2+}$ ), Fig. 5.8.

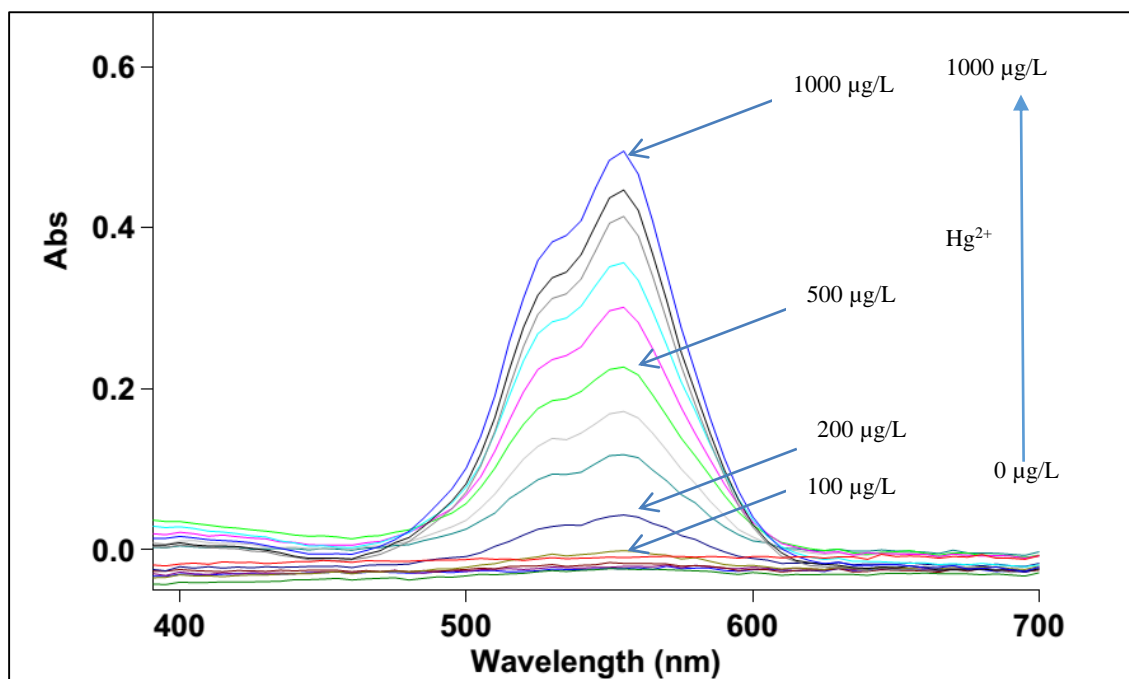
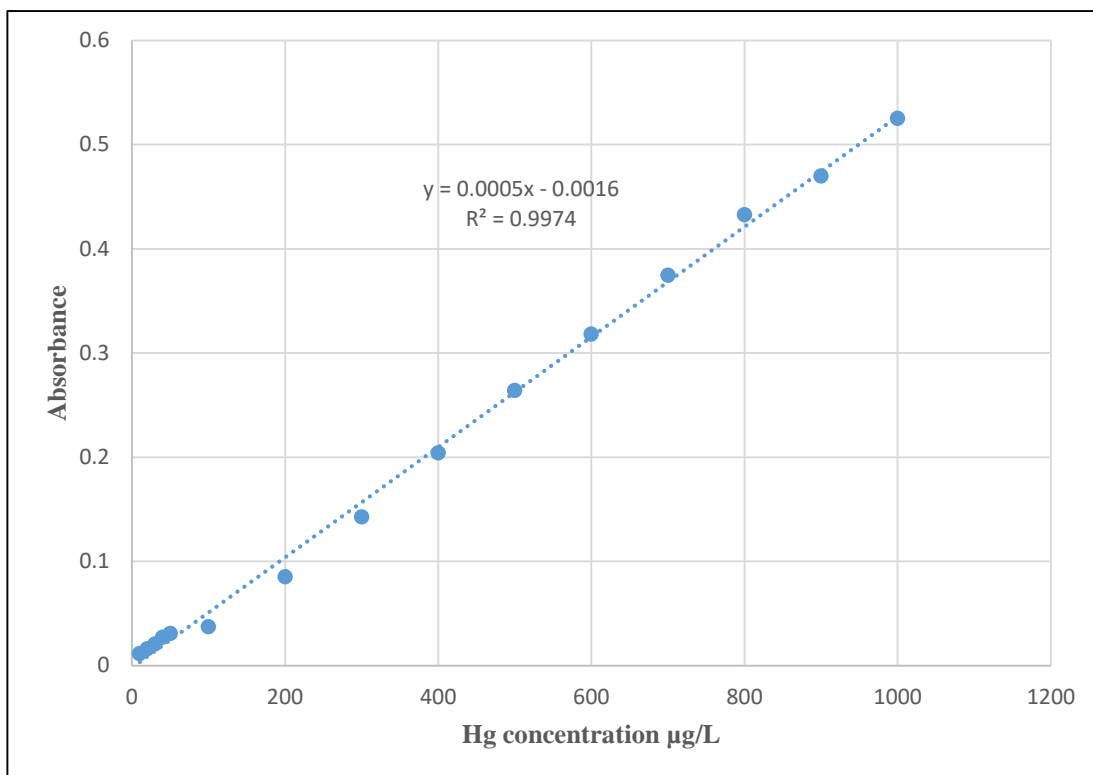


Figure 5.8: UV-vis absorbance titration spectra of rhodamine B thiolactone (25  $\mu\text{M}$ ) in 99.5: 0.5 % (v/v)  $\text{H}_2\text{O}-\text{CH}_3\text{CN}$  solution at pH 5 (acetate buffer) with  $\text{Hg}^{2+}$  from 0 to 1000  $\mu\text{g/L}$ .

From Fig. 5.8, UV-vis absorbance titration spectra of rhodamine B thiolactone with  $\text{Hg}^{2+}$  in the range from 0 to 1000  $\mu\text{g/L}$  showed that the colorimetric response increased with increasing  $\text{Hg}^{2+}$  concentration. The absorbance peak of the  $\text{Hg}$ -rhodamine B thiolactone complex formed could be clearly located at 559 nm.

Calibration plots constructed for the absorbance obtained at 559 nm against  $\text{Hg}^{2+}$  concentration in the analysed standards indicated a good linearity and strong correlation  $r^2=0.997$ , as shown in Fig. 5.9. A concentration of 10  $\mu\text{g/L}$  was considered as the instrumental lower limit of detection.



**Figure 5.9:** Calibration plots of the absorbance of Hg-rhodamine B thiolactone complex at 559 nm vs. Hg<sup>2+</sup> concentration; error bars (too small to observed) represent one standard deviation (n=3).

#### 5.4.4. Interferences of other ions

In environmental water samples, most of the coexisting ions are likely to have a concentration higher than the Hg<sup>2+</sup> concentration.<sup>232</sup> Natural waters contain a number of major dissolved mineral component ions including Ca<sup>2+</sup>, Mg<sup>2+</sup> and Na<sup>+</sup>, and smaller amounts of ions such as Fe<sup>3+</sup> and Mn<sup>2+</sup>. Trace metal ions also exist in natural water that have similar chemical reactivity to Hg<sup>2+</sup>; these include Cd<sup>2+</sup>, Pb<sup>2+</sup> and Zn<sup>2+</sup>. Therefore, it was necessary to evaluate the colorimetric response selectivity, i.e., the binding behaviour of the rhodamine B thiolactone toward Hg<sup>2+</sup> relative to the other competitive ions. The colorimetric response was examined in parallel under the same conditions by adding different ions to the reaction mixture containing the reagent, with and without Hg<sup>2+</sup>. The results showed almost no colour change in the presence of other examined ions. This was in agreement with the literature.<sup>166, 224</sup> The presence of even 5 mg/L of As<sup>3+</sup>, Cd<sup>2+</sup>, Co<sup>2+</sup>, Cr<sup>3+</sup>, Cu<sup>2+</sup>, Fe<sup>3+</sup>, Mg<sup>2+</sup>, Mn<sup>2+</sup>, Na<sup>+</sup>, Ni<sup>2+</sup>, Pb<sup>2+</sup> and Zn<sup>2+</sup> ions did not show any colorimetric response, except Ag<sup>+</sup> at 1 mg/L that gave minimal

response, as shown in Fig. 5.10. Furthermore, spectral analysis in Fig. 5.11, showed clearly that only  $\text{Hg}^{2+}$  caused strong absorbance.

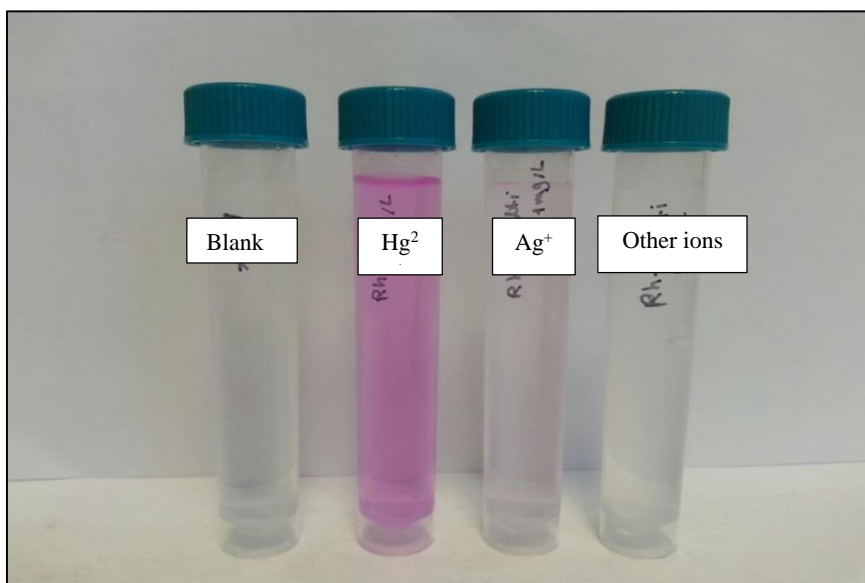


**Figure 5.10:** Colour changes observed for rhodamine B thiolactone (25  $\mu\text{M}$ ) in 99.5: 0.5 %(*v/v*)  $\text{H}_2\text{O}-\text{CH}_3\text{CN}$  solution at pH 5.0 (in 5.0 M acetate buffer) upon addition of 1 mg/L potentially interfering ions. From left to right: blank,  $\text{Hg}^{2+}$ ,  $\text{Ag}^+$ , and other mixed ions ( $\text{As}^{3+}$ ,  $\text{Cd}^{2+}$ ,  $\text{Co}^{2+}$ ,  $\text{Cr}^{3+}$ ,  $\text{Cu}^{2+}$ ,  $\text{Fe}^{3+}$ ,  $\text{Mg}^{2+}$ ,  $\text{Mn}^{2+}$ ,  $\text{Na}^+$ ,  $\text{Ni}^{2+}$ ,  $\text{Pb}^{2+}$  and  $\text{Zn}^{2+}$ ).

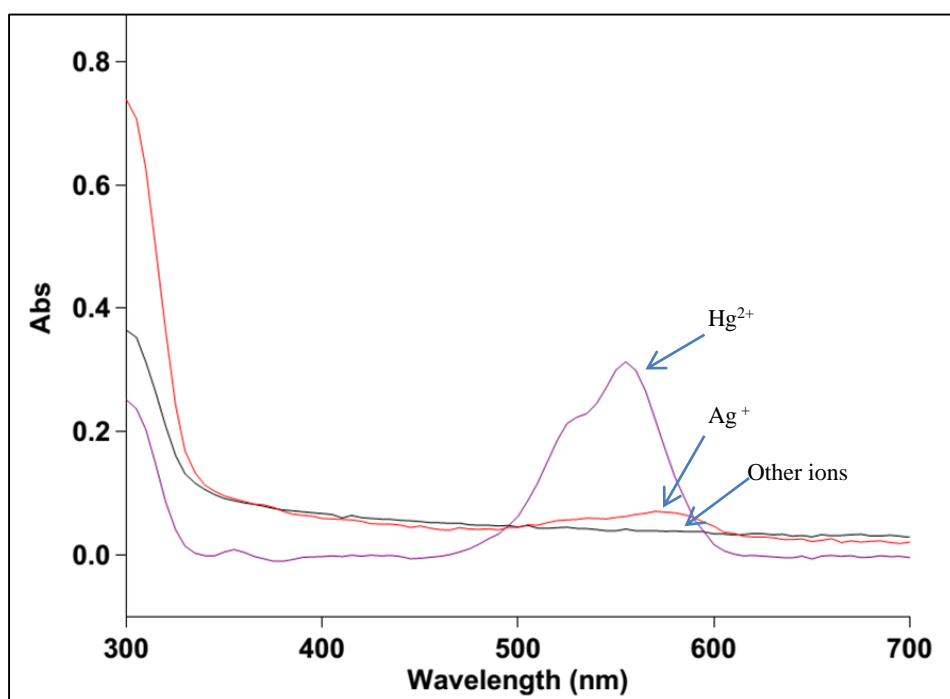


**Figure 5.11:** UV-vis absorbance spectra of rhodamine B thiolactone (25  $\mu\text{M}$ ) in the presence of 1 mg/L  $\text{Hg}^{2+}$ ,  $\text{Ag}^+$ , and other mixed ions ( $\text{As}^{3+}$ ,  $\text{Cd}^{2+}$ ,  $\text{Co}^{2+}$ ,  $\text{Cr}^{3+}$ ,  $\text{Cu}^{2+}$ ,  $\text{Fe}^{3+}$ ,  $\text{Mg}^{2+}$ ,  $\text{Mn}^{2+}$ ,  $\text{Na}^+$ ,  $\text{Ni}^{2+}$ ,  $\text{Pb}^{2+}$  and  $\text{Zn}^{2+}$ ) under the same condition.

According to the Pearson acid-base concept,<sup>233</sup> soft-soft and hard-hard interactions are more favourable than soft-hard ones. This concept was clearly noticed in the examined ions. Silver is a reasonably soft metal ion along with  $\text{Hg}^{2+}$  and  $\text{Cd}^{2+}$ , thus prefers coordination with soft S-containing donor group. The Ag-rhodamine B thiolactone coordination was, however, observed as a weak colorimetric and spectrometric response. Furthermore, it is unlikely to find such concentrations of  $\text{Ag}^+$  in environmental samples.

To explain why no response was obtained for  $\text{Cd}^{2+}$  it is important to consider the kinetic behaviour as well as thermodynamic properties relating to the interaction of  $\text{Cd}^{2+}$  with the donor ligands.<sup>234</sup> The stability of the  $\text{Cd}^{2+}$  complexes with ligands containing thioether-S donor atoms is much lower than those obtained for the thiol-S donor ligands.<sup>235</sup> Moreover, the various N and O donor ligands are also favourable competitive candidates for a stable interaction with  $\text{Cd}^{2+}$  ion in the order of (S,N,O) > (S,N) > (S,O,O) > (S,O) donor sets.<sup>236</sup> Finally, although the chemical properties of the 4d series are rather similar to those of the 5d elements for most of the transition elements, this is not true for the  $\text{Zn}^{2+}$  group elements investigated. There is a significant difference in the properties between  $\text{Cd}^{2+}$  and  $\text{Hg}^{2+}$  ions. Linear (2) and tetrahedral (4) coordination are the most preferred arrangements for  $\text{Hg}^{2+}$  complexes, while the major geometry of  $\text{Cd}^{2+}$  is octahedral.<sup>235</sup> It can be concluded that the contribution of the thioether moiety to  $\text{Cd}^{2+}$  binding was, however, rather weak. Thus, the thioether-S donor atom was likely in chelating position with both N and O atoms, which is more favoured for binding to  $\text{Cd}^{2+}$ . Because of the all aforementioned reasons  $\text{Cd}^{2+}$  was not observed to give a colorimetric response.

The colorimetric response of the potentially-interfering ions was also examined in the presence of  $\text{Hg}^{2+}$ . The result indicated that the ions did not interfere substantially with the detection of 1 mg/L  $\text{Hg}^{2+}$ , as shown in Fig. 5.12. A slight decrease in the colour intensity was observed both by the naked eye and spectroscopic analysis, Fig. 5.13, which is likely to be as a result of some ions having a reaction with  $\text{Hg}^{2+}$ .<sup>237</sup> As a consequence, the amount of free  $\text{Hg}^{2+}$  able to react with the reagent decreased.

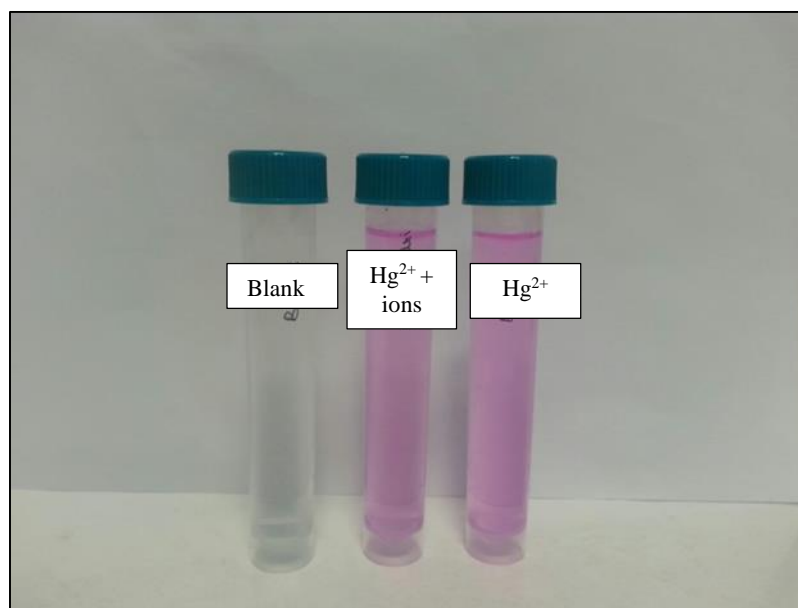


Figure 5.12: Colour change of rhodamine B thiolactone (25  $\mu\text{M}$ ) with various species. From left to right: blank, mixed ions ( $\text{As}^{3+}$ ,  $\text{Cd}^{2+}$ ,  $\text{Co}^{2+}$ ,  $\text{Cr}^{3+}$ ,  $\text{Cu}^{2+}$ ,  $\text{Fe}^{3+}$ ,  $\text{Mg}^{2+}$ ,  $\text{Mn}^{2+}$ ,  $\text{Na}^+$ ,  $\text{Ni}^{2+}$ ,  $\text{Pb}^{2+}$  and  $\text{Zn}^{2+}$  plus  $\text{Hg}^{2+}$ ) and only  $\text{Hg}^{2+}$ .

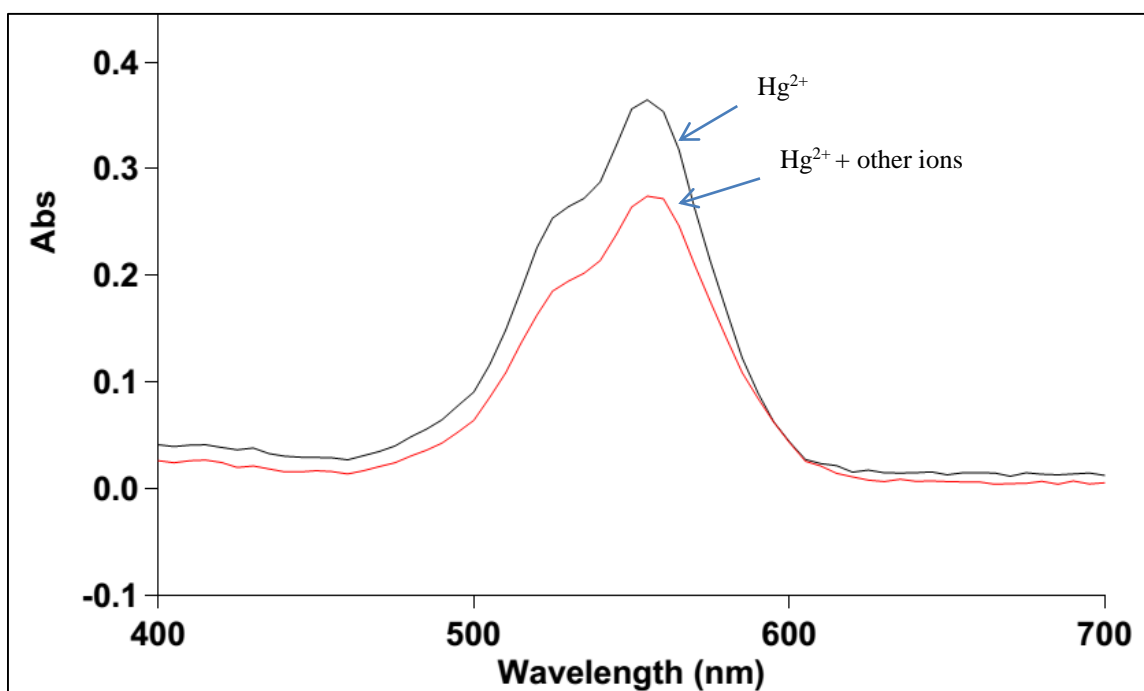
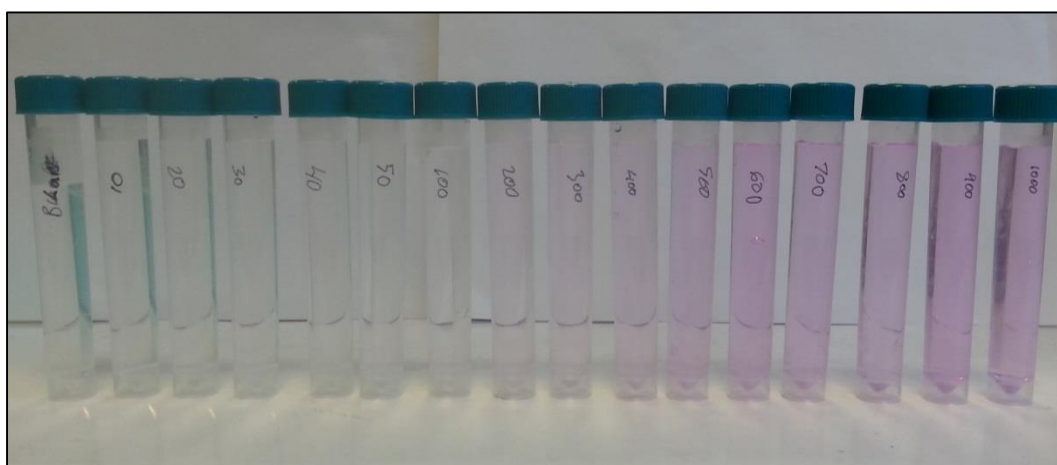


Figure 5.13: UV-vis absorbance spectra of rhodamine B thiolactone (25  $\mu\text{M}$ ) in the presence of 1 mg/L  $\text{Hg}^{2+}$ , and other mixed ions ( $\text{As}^{3+}$ ,  $\text{Cd}^{2+}$ ,  $\text{Co}^{2+}$ ,  $\text{Cr}^{3+}$ ,  $\text{Cu}^{2+}$ ,  $\text{Fe}^{3+}$ ,  $\text{Mg}^{2+}$ ,  $\text{Mn}^{2+}$ ,  $\text{Na}^+$ ,  $\text{Ni}^{2+}$ ,  $\text{Pb}^{2+}$  and  $\text{Zn}^{2+}$  plus  $\text{Hg}^{2+}$ ) under the same condition.

It could be concluded that rhodamine B thiolactone exhibited an extremely high selectivity toward  $\text{Hg}^{2+}$ , even in the presence of the other ions examined, which enables interference-free detection of  $\text{Hg}^{2+}$  in environmental samples directly by the naked eye.

#### 5.4.5. Method application in artificial seawater

The role of the seawater in the biogeochemical cycling of Hg is critical. It is well known that seawater influences the complexation reaction of Hg with other species. Furthermore, seawater acts both as a major Hg dispersion medium and as an exposure pathway.<sup>5, 12, 13</sup> Based on that, the applicability of the rhodamine B thiolactone sensing was examined by determination of  $\text{Hg}^{2+}$  in artificial seawater. The result indicated no significant colour change that could be observed in the blank artificial seawater. The colorimetric response was further tested for semi-quantitative detection of  $\text{Hg}^{2+}$  by spiking the artificial seawater with different concentration of  $\text{Hg}^{2+}$ . When spiked with  $\text{Hg}^{2+}$  concentrations ranging from 10 to 1000  $\mu\text{g/L}$ , a pink colour developed immediately. However, although the intensity of the colour produced appeared to increase with increasing  $\text{Hg}^{2+}$  concentration, the intensities were much less than those produced when distilled water was used, as shown in Fig. 5.14. A concentration of 200  $\mu\text{g/L}$  was considered the lower limit of detection that could be observed by the naked eye.



**Figure 5.14:** Increase of pink colour intensity as the  $\text{Hg}^{2+}$  concentration increased for a range of 10 to 1000  $\mu\text{g/L}$  in the spiked artificial seawater.

It was suggested that the reason might be the interaction of  $\text{Hg}^{2+}$  with the constituent ions of seawater, decreasing the free  $\text{Hg}^{2+}$  concentration, hence causing a decrease in the colorimetric response. This hypothesis was further discussed in Chapter 6, Section 6.4.5.1.

To assess this further, the absorbance spectrum was recorded in the range of 400-700 nm for a number of spiked seawater against seawater blank. As expected, when observing the intensities of the UV-vis absorbance peak at 559 nm, weak absorbance bands were quite clear on the spectrum. Furthermore, the absorbance peak increased with increasing  $\text{Hg}^{2+}$  concentration in spiked seawater, Fig. 5.15.

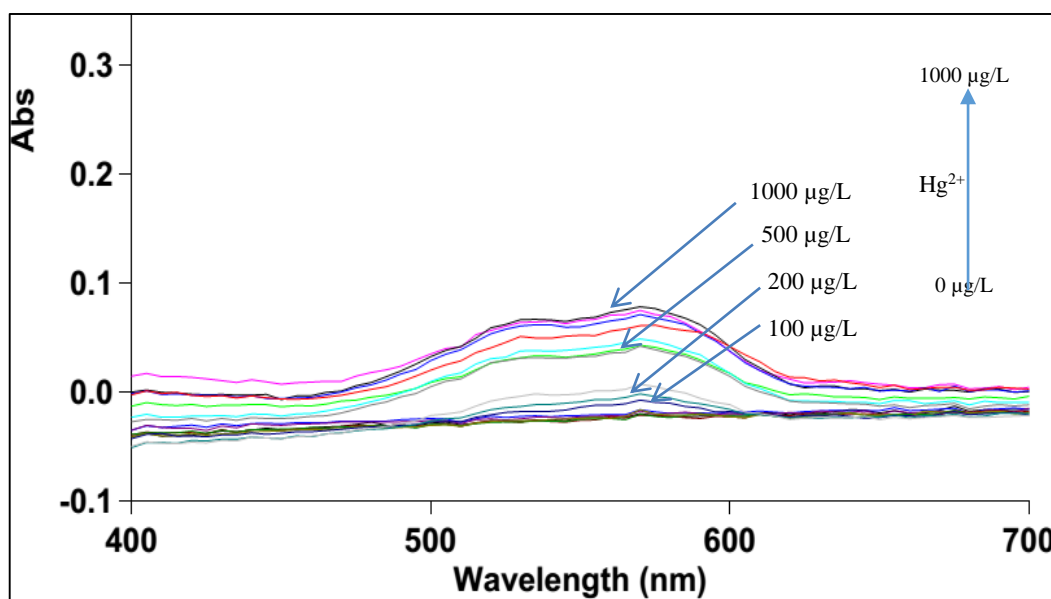
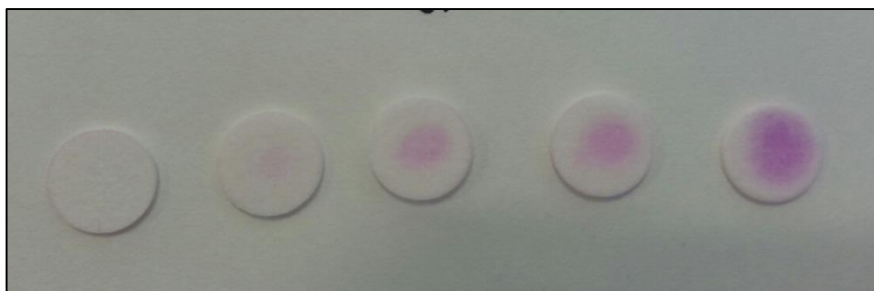


Figure 5.15: UV-vis absorbance titration spectra of rhodamine B thiolactone (25  $\mu\text{M}$ ) with  $\text{Hg}^{2+}$  spiked artificial seawater from 10 to 1000  $\mu\text{g/L}$ .

#### 5.4.6. Assessment of $\text{Hg}^{2+}$ detection in spot test mode

Under wet reagent conditions, a pink colour corresponding to the formation of  $\text{Hg}$ -rhodamine B thiolactone complex was obtained immediately when the  $\text{Hg}^{2+}$  standards were applied as a spot test. The intensity of the colour produced increased with increasing  $\text{Hg}^{2+}$  concentration in the standard solutions. A concentration of 100  $\mu\text{g/L}$  would be considered as the lower limit of detection that could be observed by the naked eye, Fig. 5.16.



**Figure 5.16: Increased intensity of coloured Hg-rhodamine B thiolactone complex with increasing  $\text{Hg}^{2+}$  concentrations under wet reagent conditions. From left to right: blank, 0.1, 0.5, 1, and 10 mg/L.**

As expected, a light pink colour developed before the addition of  $\text{Hg}^{2+}$  solutions when the detecting discs were allowed to dry completely, Fig. 5.17. The colour of the detecting discs changed to pink after 24 h even in the absence of  $\text{Hg}^{2+}$  as a result of the converting of rhodamine B thiolactone when the detecting discs were exposed to the air.



**Figure 5.17: Formation of light pink colour as a result of the reagent ring-opening after completely drying the discs for 24 hrs.**

Completely dry discs could still react with  $\text{Hg}^{2+}$  and there was an observation of a pink colour. However, the colour change produced may lead to misleading results in the  $\text{Hg}^{2+}$  colorimetric determination when observed by naked eye, Fig. 5.18. In this situation, and for more accurate quantitative measurements, the blank image should be recorded first. Then the sample images should also be recorded after the detecting discs were exposed to  $\text{Hg}^{2+}$ . The contrast image should be used for the assessment of  $\text{Hg}^{2+}$  concentration.

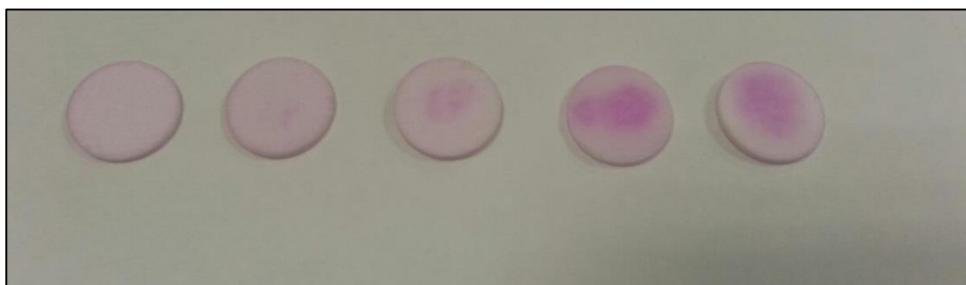


**Figure 5.18: Increased intensity of coloured Hg-rhodamine B thiolactone complex with increasing  $\text{Hg}^{2+}$  concentrations under dry reagent conditions. From left to right: blank, 0.1, 0.5, 1, and 10 mg/L.**

## 5.5. Conclusion

A convenient, sensitive and selective colorimetric sensor was successfully synthesised for naked eye determination and quantification of  $\text{Hg}^{2+}$ . Rhodamine B thiolactone was easily prepared from commercially available rhodamine B base in 48% overall yield by a “one pot synthesis”. The chemosensor was obtained as light yellow needles. The thiospirocyclic structure of rhodamine B thiolactone was confirmed by  $^1\text{H}$  NMR,  $^{13}\text{C}$  NMR and X-ray crystallography.

It was found that the chemosensor easily changed its colour from yellow to pink at room temperature. In order to prevent that, it was recommended that the solid rhodamine B thiolactone product had to be stored at  $-18\text{ }^\circ\text{C}$  away from light. The stock solution of it also needed to be stored at low temperature.

The stock solution of rhodamine B thiolactone was colourless, and the visual detection of  $\text{Hg}^{2+}$  was successfully achieved by inducing ring opening. The investigation on the effect of the colorant reagent concentration on the colorimetric response showed that for constant and maximum absorbance, the reaction mixture solution should contain a minimum of  $25\text{ }\mu\text{M}$  as an optimal value for the chromogenic reaction.

The produced Hg-rhodamine B thiolactone complex had a characteristic of pink colour. The intensity of the colour obtained was increased as the concentration of  $\text{Hg}^{2+}$  in the standards increased. A concentration of  $50\text{ }\mu\text{g/L}$  was the lower detection limit that could be observed visually. For more quantitative determination, UV-vis absorbance titration spectra of Hg-rhodamine B thiolactone with  $\text{Hg}^{2+}$  range from 0 to

1000  $\mu\text{g/L}$  showed an appearance of new peak at 559 nm. The spectroscopic response was increased with increasing  $\text{Hg}^{2+}$  concentration in the standards. A linear calibration was exhibited with a strong correlation of  $r^2=0.997$  over the  $\text{Hg}^{2+}$  range of 10 to 1000  $\mu\text{g/L}$ . A concentration of 10  $\mu\text{g/L}$  was considered as the lower limit of detection.

The chemosensor also showed good selectivity for  $\text{Hg}^{2+}$ . Only the presence of  $\text{Hg}^{2+}$  induced significant enhancement of the absorbance intensity of the rhodamine B thiolactone, whereas no colorimetric response occurred toward all the other tested ions, except that the presence of 1000  $\mu\text{g/L}$   $\text{Ag}^+$  showed a small response. It is, however, unlikely to find such concentrations of  $\text{Ag}^+$  in environmental samples.

The applicability of rhodamine B thiolactone was evaluated by determination of  $\text{Hg}^{2+}$  in artificial seawater. No significant colour change could be observed in the blank sample. The method was further tested for Hg-spiked samples. It was found that, although the intensities of the colour produced were less than those when distilled water was used, the colorimetric response of the spiked seawater still increased as the  $\text{Hg}^{2+}$  concentration increase. The reason for the low response may be that some ions could react with  $\text{Hg}^{2+}$ , thus the amount of free  $\text{Hg}^{2+}$  decreased. A concentration of 200  $\mu\text{g/L}$  was considered the limit of detection that could be observed by naked eye.

The visual detection of the reaction between  $\text{Hg}^{2+}$  and rhodamine B thiolactone was successfully achieved when used as wet and dry reagent in spot test mode. The intensity of the pink coloured complex obtained increased as the concentrations of  $\text{Hg}^{2+}$  in the standards increased. A concentration of 100  $\mu\text{g/L}$  was the lower detection limit that could be observed. However, because of the colour change of rhodamine B thiolactone on the dried discs even in the absence of a  $\text{Hg}^{2+}$  ion, misleading results could be obtained when an observation of  $\text{Hg}^{2+}$  concentration by naked eye took place.

To conclude, the characteristics of rhodamine B thiolactone show great potential in rapid detection of  $\text{Hg}^{2+}$ , however further studies to improve the sensitivity effectively by preconcentrate  $\text{Hg}^{2+}$  on sensing membrane and to investigate the reason for signal suppression in seawater analysis, will be discussed in detail in Chapter 6.

## 6. Immobilisation of rhodamine B thiolactone in solid matrices and determination of Hg<sup>2+</sup> on the coloured membranes

### 6.1. Introduction

Digital image analysis is a powerful tool used commonly nowadays for analysis without the requirement for complex instrumentation. The advantages of this type of analysis have been applied in different fields including medicine, biology, and materials science, alongside environmental sensing.<sup>238-240</sup> The captured images can be digitalised with appropriate photo processing applications to measure parameters such as shapes, areas and colour intensities.<sup>241</sup> Recent advances in digital image analysis technology have offered colour scanners, digital cameras, smartphones and video cameras (Webcams) based on CCD image sensor. They can be used as inexpensive and easily portable alternatives to a spectrophotometer, which may be used in field applications.<sup>129, 242-248</sup> These electronic devices are capable of capturing digital images and displaying the RGB system with a resolution up to 24 bits. The colours in the RGB colour system are combined in different intensities with values varying in the range of 0-255 per colour.<sup>249</sup>

It is well known that the theory of colorimetric sensor methods is based on the monitoring of colour change, which depends on the concentration of analytes and the intensity of the absorbed and/or transmitted light. However, the Beer-Lambert law is not expected to be universally applicable in chromatic analysis based on RGB data for coloured materials. Parameter such as the brightness, saturation and the G/R ratio can also produce empirical standard curves with a suitable resolution for a variety of colorimetric assays. In this regard, Birch *et al.*<sup>250</sup> initially proposed a consistent explanation of the colorimetric assay consisting of a scanner generating light and an RGB image processor; the incident light is enabled to pass twice through the target sample; first upwards through the sample to the reflecting white surface, and then downwards through the sample to the detector. Afterward, the light intensity is converted into an absorbance value.<sup>251</sup> Since then, the RGB chromatic analysis model has been further developed.<sup>252-254</sup>

Even with a portable device, performing a field test can be difficult, if it is still required to bring along numerous reagents, chemicals and sampling materials. Furthermore, several separations and preconcentration procedures may be required prior to the measurement of the analyte. However, many of these issues can be avoided by developing an assay that runs on a solid substrate, rather than in solution. An example of this is preconcentration on solid-phase extraction,<sup>255</sup> where the sample is simply added and allowed to flow through the substrate. The most commonly used substrate for colorimetric sensing is paper.

A combination of colorimetric detection and the application of solid phase extraction for preconcentration of trace metals resulted in a sorption-photometric method known as colorimetric-solid phase extraction (C-SPE).<sup>256-259</sup> This method is based on the selective preconcentration of an analyte on a colorimetric reagent-impregnated SPE membrane, followed by direct detection of the extracted coloured complex by either the naked eye or an optical instrument.

Liu *et al.*<sup>56</sup> designed and demonstrated a naked eye, C-SPE paper sensor for rapid determination of trace  $\text{Hg}^{2+}$  in water samples based on its reaction with rhodamine B thiolactone. In this approach, the Hg-sensing rhodamine B thiolactone was trapped inside a porous silica matrix. A piece of filter paper was coated with the colloid and the sol-gel membrane was then fitted onto a sintered glass filter. To avoid the structural change of rhodamine B thiolactone in the membrane from colourless and spirocyclic form to coloured open form, water samples were treated with an ascorbic acid solution and adjusted to pH 5.0 using acetate buffer before flowing through the sol-gel membrane. As the  $\text{Hg}^{2+}$  samples were passed through the sensor at a flow rate of ~30 mL/min using a vacuum pump, the membrane colour changed from white to magenta, which could be observed clearly with the naked eye.

The coloured membranes were scanned by a flatbed scanner. The images were then digitised and analysed using Adobe Photoshop software. The RGB chromatic analysis showed that the green channel contributed to almost 99% of the total colour change.

The sensitivity of the sensor was improved significantly, with a detection limit of 0.24  $\mu\text{g/L}$ , as a result of using the porous silica material, which serves as both a preconcentrator and a chromogenic reactor for  $\text{Hg}^{2+}$ . However, further study is still

needed since there are still issues to be addressed. For example, due to the hypothesised structural transformation of rhodamine B thiolactone, the membranes exposed to air changed to pink in the absence of Hg even after one day. Therefore, the stability of the sol-gel membrane was studied for a period of 40 days. It was found that the colorimetric change was minimised when the membranes were stored in a bottle filled with N<sub>2</sub> or in ascorbic acid solution. No studies have been conducted on the long term-storage of Hg<sup>2+</sup> sensor papers to determine the maximum storage time, neither has the use of different storage conditions been investigated. Furthermore, the reactivity of the stored sol-gel sensors with Hg<sup>2+</sup> was not tested. While the method has been applied to real samples and results agreed very well with the spiked level in tap water and mineral water, it was found that the spike recovery for pond water was only 41%. Sample matrix effects require further study. Additionally, the use of a more sustainable solid support, such as agar-agar gel, would be desirable because it is in accordance with the key principles of green analytical chemistry.<sup>260</sup> It would also be useful to simplify the sensor preparation procedure.

Agar-agar is a natural, unbranched polysaccharide obtained from the cell wall of some species of red algae (*Rhodophyta*). Chemically, agar-agar is a polymer made up of repeating units of D-galactose and 3,6-anhydro-L-galactopyranose. Agar-agar is considered as a sustainable, biocompatible, non-toxic and cost effective polymer. The robust gelling ability of agar-agar without interfering reactivity with other biomolecules makes it favourable for several commercial applications in pharmaceutical, food and biotechnological industries.<sup>261-264</sup> Furthermore, the agar-agar colloid exhibits remarkable stability at high temperatures up to 85 °C, even when a low concentration of 0.1% is used.<sup>265</sup> Because of all the aforementioned characteristics, the objective of this work was to encapsulate rhodamine B thiolactone within the polymeric network of agar-agar gel to shield the colorimetric sensor molecule from structural transformation and improve sensor robustness.

The hypothesis of this chapter is to investigate whether the rhodamine B thiolactone coated with agar-agar matrix serves as an alternative to, or advancement upon, the sol-gel matrix. Chapter 6 explores if the agar-agar sensor is robust, readily used, rapid and cost-effective.

## **6.2. Aim**

In this chapter, chromogenic analysis was carried out based on the RGB colour model in the grayscale mode with ImageJ processing for determination of the  $\text{Hg}^{2+}$  in water samples on the surface of filter paper coated with rhodamine B thiolactone immobilised in silica and agar-agar matrices. Specific objectives:

- Immobilisation of rhodamine B thiolactone was studied using silica sol-gel as a solid support carrier.
- A proposed immobilisation technique was utilised to preserve the sensing behaviour of rhodamine B thiolactone by using agar-agar colloid.
- Various concentrations of agar-agar were investigated in a suitable immobilisation media.
- Some experimental aspects were optimised including the volume of analysed samples and the colorant reagent concentration.
- Operational and storage stability was also explored under different environmental conditions to study the long-term usage of entrapped rhodamine B thiolactone.
- The colorimetric sensing activity of entrapped rhodamine B thiolactone was studied to observe the impact of storage conditions on efficiency and stability.
- The applicability of using the sensor in real environmental water samples was addressed using tap water, bottled water, stream water and seawater.
- Reuse and recycling of the membrane sensor was also tested by treatment of the exposed sensors with KI.

## **6.3. Experimental**

### **6.3.1. Reagents and apparatus**

The reagents and apparatus used for the determination of  $\text{Hg}^{2+}$  based on filtration through sol-gel and agar-agar gel matrices were as described in Section 3.6.1.

### **6.3.2. Solutions preparation**

The stock  $\text{Hg}^{2+}$  standard solution and stock rhodamine B thiolactone solution were prepared as described in Section 3.6.2.1. To investigate the method's range and limit of detection, standard solutions of  $\text{Hg}^{2+}$  at different concentrations were prepared from the  $\text{Hg}^{2+}$  stock solution daily as required.

### **6.3.3. Preparation of sensing gel membranes**

The sol-gel and agar-gel colloid solutions were prepared as described in Sections 3.6.2.2 and 3.6.2.3, respectively. The required amount of 5 mM rhodamine B thiolactone was added and then the mixture was stirred well. Filter papers were immersed in the colloid solutions with tweezers then withdrawn. The coated papers were dried in air for 30 min prior to use.

### **6.3.4. General procedure for colour development and data analysis**

The Hg-sensing membranes were fixed in a 13 mm in-line filter holder, and a peristaltic pump was connected as described in Section 3.6.2.4. An aliquot of the  $\text{Hg}^{2+}$  standard solution was transferred to a 500 mL conical flask. The procedure was then conducted and  $\text{Hg}^{2+}$  solutions were pumped through the membranes at a flow rate of 17 mL/min. Each standard was analysed simultaneously in triplicate using the multi-channel peristaltic pump. After completion, the exposed sensors were scanned immediately and used for data analysis. ImageJ was applied to analyse the developed colour of the sensors, through the grayscale system, as described in Section 3.6.2.5.

### **6.3.5. Selection of agar-agar membrane strength**

The degrees of stiffness of the agar membrane could significantly affect its air and water permeation, and thus the stability and Hg-rhodamine B thiolactone complex formation. To study the effect of different gel strengths, different agar membrane samples at concentrations of 1%, 2%, 3%, 4% and 5% (w/v) were prepared as described in Section 3.6.2.1.

### 6.3.6. Optimisation of water sample

An experiment was conducted to study the sensitivity of the sensor and investigate the optimal water sample volume required. Volumes varying from 50 to 1000 mL were pumped through the agar membrane, and the colorimetric responses were recorded at intervals as described in Sections 3.6.2.4 and 3.6.2.5.

### 6.3.7. Optimisation of colorant reagent

To determine the minimum amount of rhodamine B thiolactone needed to detect typical environmental  $\text{Hg}^{2+}$  concentrations an experiment was conducted in which different indicator volumes (0.5, 1.0, 1.5 and 2 mL) were added to the agar colloid following the procedure described in Section 3.6.2.3.

### 6.3.8. Membrane stability and reactivity

As mentioned in Chapter 5, rhodamine B thiolactone is likely to undergo ring opening reaction when exposed to air and converted into a Z form. In order to improve the storage stability and test the reactivity, the sol-gel membranes were evaluated by keeping them under various storage conditions:  $\sim 4\text{ }^{\circ}\text{C}$  in the refrigerator, in 0.1 mM ascorbic acid solution, stored in a dark place and by keeping them in a tightly sealed bottle containing sachets of oxygen absorber (Oxygen Absorber Ageless<sup>®</sup>, Mitsubishi Gas Chemical Company, Inc.). The stability of agar-agar membranes was also evaluated by storing them in a dark place and by covering them with 5% (w/v) agar colloid. The 5% (w/v) agar carrier support had to be peeled off the membranes before usage. The covering procedure was as shown in Fig. 6.1.



**Figure 6.1:** Covering procedure of the agar-agar membranes by 5% (w/v) agar colloid. (a) melted agar was poured in a petri dish to cover the bottom (about a quarter), (b) agar-agar membranes placed on the surface, (c) another layer of melted agar was poured in the top. The carrier support was cut and peeled off the membranes prior use.

In addition, reactivity of the sol-gel and agar-agar membranes was also tested after various storage time intervals up to 12 weeks. The sensing performance was conducted by pumping a 10  $\mu\text{g/L}$   $\text{Hg}^{2+}$  solution through the stored discs.

### **6.3.9. Method application**

The applicability of the sensing method was evaluated by determination of  $\text{Hg}^{2+}$  in real water samples, including seawater, bottled water, tap water and stream water. A seawater sample was obtained from Carradale Harbour, Carradale, Argyll, (55°35'32.7"N 5°27'48.4"W). Stream water 1 was collected from a stream at Carradale Village Hall, Carradale, Argyll (55°35'14.2"N 5°28'46.9"W), and stream water 2 was collected from the catchment of Gill Burn stream, East Kilbride, Glasgow (55°45'19.0"N 4°14'19.6"W). Bottled water 1 (Spa still mineral water, Belgium), bottled water 2 (Nestlé still spring water, England) and bottled water 3 (Evian® natural mineral water, France) were obtained from convenience stores. Tap water was collected from the water supply in the Department of Pure and Applied Chemistry, Thomas Graham Building, University of Strathclyde, Glasgow. The chlorine in the tap water was minimised by opening the tap water for 30 min prior to sample collecting. The water samples were filtered with 0.45  $\mu\text{m}$  cellulose acetate membranes (Sigma Aldrich, Gillingham, UK) and then acidified by the addition of 1.5 mL concentrated  $\text{HNO}_3$  per 1 L of water and were analysed within 48 h of sampling. The water samples were adjusted to pH 5.0 with 1.0 M acetate/acetic acid buffer solution prior analysis.

### **6.3.10. Recycling of sensor discs with KI**

An investigation into the re-usability of the colorimetric response of the agar membrane was conducted. The agar sensors were exposed to 10  $\mu\text{g/L}$   $\text{Hg}^{2+}$ . Then, KI was added dropwise to the surface of the exposed sensors; this was repeated several times. For each KI- $\text{Hg}^{2+}$  cycle, the membranes were scanned.

## 6.4. Results and discussion

### 6.4.1. Chromogenic analysis of the colorimetric responses

For the chromogenic analysis,  $\text{Hg}^{2+}$  standard solutions were pumped through the agar gel or sol-gel membranes. When the samples contained  $\text{Hg}^{2+}$  the sensors changed colour from white to pink. An image of the detection sensors was recorded using a flatbed scanner. The ImageJ software allowed the colours to be separated and converted into the grayscale intensities. The original image was decomposed into three images representing the grey in the red channel ( $G_R$ ), grey in the green channel ( $G_G$ ) and grey in the blue channel ( $G_B$ ) as shown in Fig. 6.2.

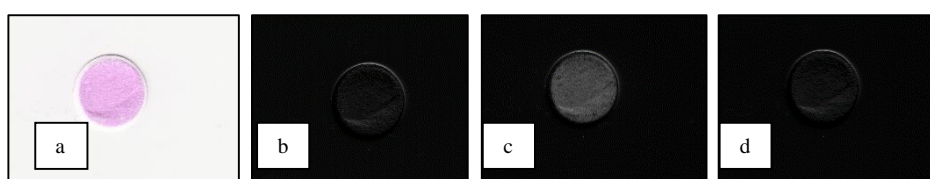


**Figure 6.2:** The image of a filter paper coated with rhodamine B thiolactone-agar colloid reacted with  $\text{Hg}^{2+}$ . The composition images showing (a) the original image, (b) grey in red channel ( $G_R$ ), (c) grey in green channel ( $G_G$ ) and (d) grey in blue channel ( $G_B$ ).

The sensitivity of the method was investigated for the signal intensities measured from the three decomposed images. In this study, only grayscale intensity in the green channel  $G_G$  of the exposed sensors was selected since this parameter showed the most sensitive response to the change of  $\text{Hg}^{2+}$  concentration. This is indicated by the high slope values compared with those obtained from the other channels in exposed sensors of both sol-gel and agar-agar membranes as shown in Fig. 6.3 and 6.4, respectively.

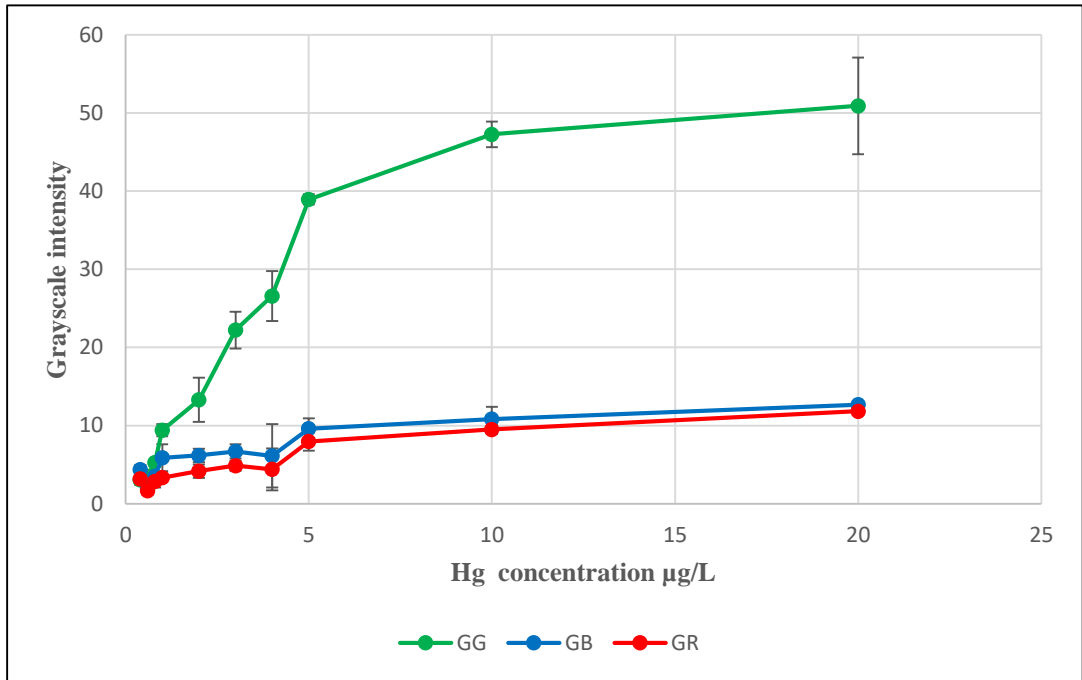


Figure 6.3: The relationship between the colorimetric response in  $G_R$ ,  $G_G$  and  $G_B$  and the concentration of  $Hg^{2+}$  on the exposed sol-gel membranes; error bars represent one standard deviation ( $n=3$ ).

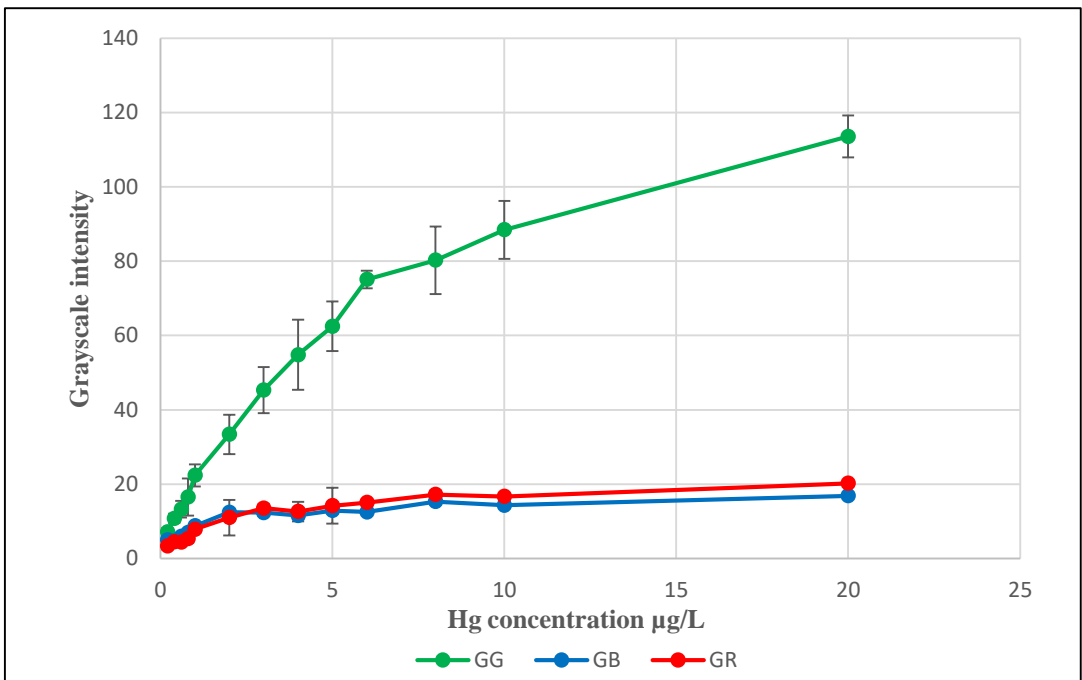


Figure 6.4: The relationship between the colorimetric response in  $G_R$ ,  $G_G$  and  $G_B$  and the concentration of  $Hg^{2+}$  on the exposed agar-agar gel membranes; error bars represent one standard deviation ( $n=3$ ).

The overall trend in the relationship between the intensities of the  $G_G$  and the  $Hg^{2+}$  concentrations from both sol-gel and agar-agar membranes was similar. The colorimetric responses of both were found to increase with changes in  $Hg^{2+}$  concentrations. Over a  $Hg^{2+}$  concentration range of 0.4 to 5  $\mu\text{g/L}$  and 0.2 to 6  $\mu\text{g/L}$ , the intensities of  $G_G$  were linear for sol-gel and agar-agar membranes, respectively. The colorimetric response was saturated above those concentrations for both membranes. After saturation, the responses flattened.

It is well known that the colours acquired from the RGB channels are additive colours. The red, green and blue spectral regions are roughly defined as the intervals 580-700, 500-580 and 400-500 nm, respectively. Each coloured object absorbs its complementary colour and transmits the rest of the visible range of the spectrum, hence affecting the colour seen. Thus the eye perceives the converse of the colour component that is primarily absorbed.<sup>149</sup> Therefore, the pink colour produced by increasing  $Hg^{2+}$  concentration was expected to reflect red and blue light and absorb green light. This finding was in agreement with the previous study reporting that the reaction between  $Hg^{2+}$  and rhodamine B thiolactone generated a subtractive colour in the colorimetric detection.<sup>56</sup> Because of the above, the selection of one particular colour component for quantification will often give better sensitivity.<sup>266</sup>

In addition, the inherent complexity level of grayscale images is lower than that of coloured images.<sup>267</sup> Thus to simplify the complexity of the mathematics and improve signal-to-noise ratio, grayscale intensity could be plotted directly for only single colour change channel ( $G_G$ ).

## **6.4.2. Optimisation of sensing response on the agar-agar membrane**

### **6.4.2.1. Selection of agar-agar gel colloid concentration**

The effect of various concentrations of agar-agar on the sensing activity of the immobilised rhodamine B thiolactone was examined. The quality of agar-agar gel colloid was reflected by its physical characteristics, e.g., gel strength, gel permeation and resistivity to a structural transformation of the reagent. A summary of such properties is shown in Table 6.1.

**Table 6.1: Physical characteristics of the immobilised agar-agar membranes with different agar concentrations.**

<b>Agar-agar concentration (w/v)</b>	<b>Membrane strength</b>	<b>Structural transformation of the reagent</b>	<b>Mechanical flow</b>	<b>Pink colour distribution</b>
<b>1%</b>	Soft	Within a week of preparation	Water pumped through the paper easily	Uniform, covered the whole membrane
<b>2%</b>	Soft	Within 2 weeks of preparation	Water pumped through the paper easily	The colour mostly covered the edges
<b>3%</b>	Slightly rigid	Within 3 weeks of preparation	Water pumped through with slight difficulty	The colour mostly covered the edges
<b>4%</b>	Rigid; membrane curled	Within 3 weeks of preparation	Water could not pass through	Not applicable
<b>5%</b>	Rigid; membrane curled	Within 3 weeks of preparation	Water could not pass through	Not applicable

A solidified matrix coating was generated as soon as the agar colloid was dried onto the surface of filter paper, resulting in a tough and rigid gel at higher agar-agar concentrations. Maximum stiffness was observed when 4% and 5% agar-agar was utilised for immobilisation of rhodamine B thiolactone. The coated papers started to curl as soon as the agar-agar colloid dried. This gradual curve of the papers might be due to the gel properties of the agar. The increase of agar concentrations increases the intermolecular glycosidic bonds between the D- and L-galactose to form an aggregate. Aggregation of galactose residues present within the agar gel alerts contraction of the polymer network, which decreases the interstitial space available to hold the water. As a result, shrinkage of the agar gel occurs over time.<sup>268,269</sup> Agar-agar membranes below these concentrations displayed a decline in the rigidity. A slight rigidity was observed in the 3% agar concentration, while 1% and 2% were soft and flexible.

The gel's ability to resist the ring opening of immobilised rhodamine B thiolactone over time was compared between different agar-agar concentrations (see Fig. 6.5). Compared with the sol-gel membranes, which were stable for less than one day in contact with air, the agar-agar colloid protected the reagent from structural

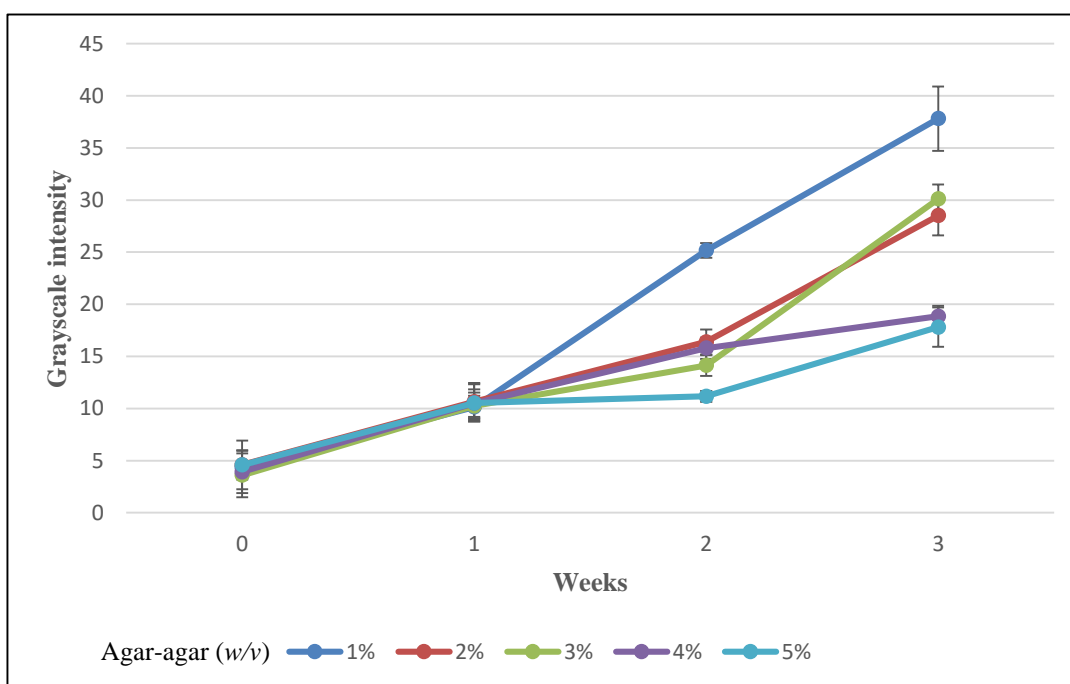


**Figure 6.5: Colour change monitoring of the immobilised agar-agar membranes kept in the open air at agar concentrations of 1%, 2%, 3%, 4% and 5% (w/v) for a period up to three weeks. Grayscale intensity indicates conversion process levels; error bars represent one standard deviation (n=3).**

transformation remarkably well. Although poorer resistance was detected with use of a concentration of 1% agar colloid, the transformation of immobilised rhodamine B thiolactone could still be restricted for up to one week.

As the agar concentration increased, the protective ability to delay the transformation of the reagent increased. In the case of concentrations 2% and 3%, the transformation was delayed by up to 2 weeks, while the 4% and 5% agar concentrations protected the reagent for up to 3 weeks. This increase in conversion resistance with concentration could be due to the fact that the air permeability of the gel was restricted. As the concentration increased, a longer time was required for penetration of air into the structure of the agar-agar matrix.

The mechanical flow characteristics are also important for determining whether the proposed agar-agar immobilising method was viable. A flow rate of 30 mL/min was the targeted flow rate for a water sample to pass through the sensing membranes.<sup>56</sup> In this study, it was found that such flow rate caused the agar-agar membrane to tear. Therefore, the flow rate was adjusted to 17 mL/min. The water permeation ability was evaluated by pumping a known volume of  $\text{Hg}^{2+}$  solution through a series of different concentration agar-agar membranes. No difficulty was observed when agar concentration of 1% and 2% were used. However, the permeability of 3% agar was much lower than that of 1% and 2% agar. As a result, the water flow was much slower with a high back pressure; this meant the flow rate needed to be further amended to only 5 mL/min. No water could be passed through the 4% and 5% agar membranes and, due to the high pressure produced, tubing detached from its fittings.

The 1%, 2% and 3% agar membrane papers were further investigated in terms of the distribution of the coloured Hg-rhodamine B thiolactone complex. It was found that the pink colour distributed finely and uniformly and almost covered the whole sensing membrane in the 1% agar concentration, while only the edges of the membranes changing colour with use of the 2% and 3% agar as shown in Fig. 6.6.

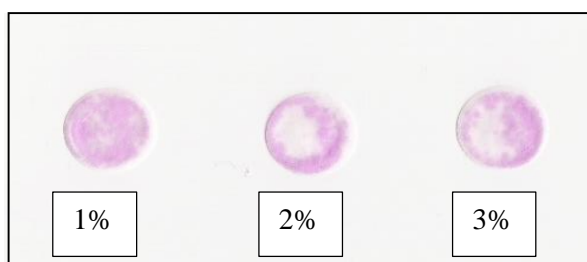


**Figure 6.6: Effect of agar-agar concentrations of 1%, 2% and 3% (w/v) on the distribution of the coloured Hg-rhodamine B thiolactone complex on the surface of agar-agar membranes.**

The reason behind this variation could be due to the effect of surface tension of the agar gel on the flow of water sample. In this study, subjected to mechanical compression, the surface of the gel became thicker and swollen, after which a hemispherical cap appeared on the surface, as illustrated in Fig 6.7. The higher the agar-agar concentration used the thicker the swelling produced.

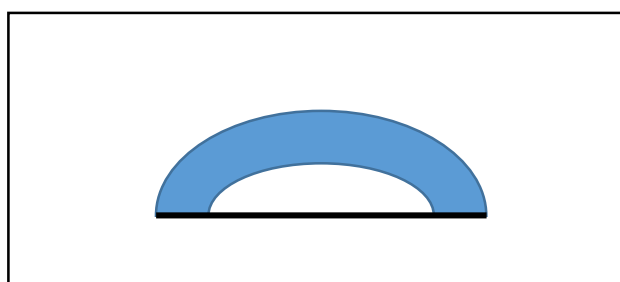


**Figure 6.7: Diagram represent the swelling behaviour of the agar-agar membrane during the process.**

The presence of the 3D swelling of gel particles is affected by surface tension as the molecules located on the surface are pulled inward and surface area increases. This creates some internal pressure and forces liquid surfaces to contract to the minimal area.<sup>270</sup> In this case, at the flow rate and sample volume used, the  $\text{Hg}^{2+}$  standard solution will flow gradually through the agar-agar membrane from the edges toward the centre. Because the 1% agar membrane was thinner than the others, the water sample could flow more easily giving the chance for all of the immobilised rhodamine B thiolactone to react with  $\text{Hg}^{2+}$ . As a result, a flow rate of 17 mL/min and agar-agar membrane of 1% (w/v) were chosen for further study.

#### 6.4.2.2. Optimisation of sample volume pumped through agar-agar papers

To test the sensitivity of the agar-agar sensor and select an appropriate volume of water sample for analysis, calibration curves were plotted for the colorimetric response against the volume of water samples from 50 to 1000 mL. Typical environmental  $\text{Hg}^{2+}$  concentrations of 5 and 10  $\mu\text{g/L}$  were used. The colorimetric response increased with sample volume as a result of the increase in the total amount of  $\text{Hg}^{2+}$  captured by the agar-agar sensor. As shown in Fig. 6.8, it was found that the colorimetric response flattened after around 300 mL of the water sample had been pumped through.

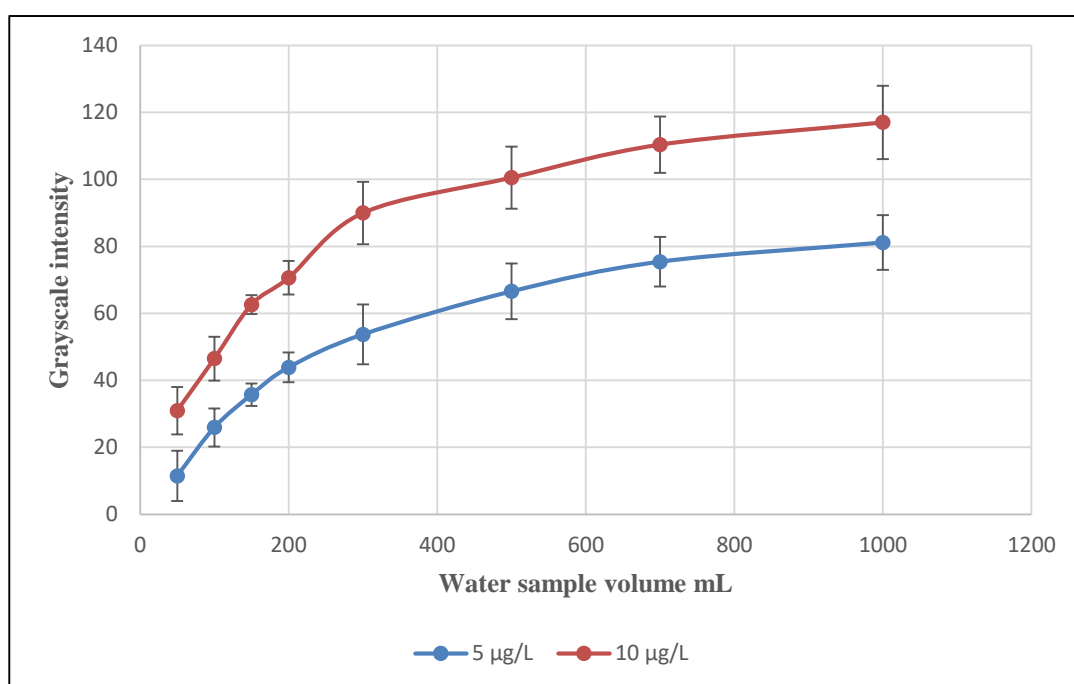


**Figure 6.8:** Effect of water sample volume on the colorimetric response in the  $G_G$  of the  $\text{Hg}$ -rhodamine B thiolactone complex compound. The concentration of rhodamine B thiolactone in the agar membrane was  $5.0 \times 10^{-6}$  mole. Typical  $\text{Hg}^{2+}$  concentrations used were 5 and 10  $\mu\text{g/L}$ ; error bars represent one standard deviation ( $n=3$ ).

The concentration of rhodamine B thiolactone in the agar-agar membrane was calculated to be  $5.0 \times 10^{-6}$  mole which corresponded to a mixing ratio of 1:5 (rhodamine thiolactone to agar-agar colloid). Further experiments were conducted using a different mixing ratio of rhodamine B thiolactone to agar colloid of 1.5:5 and 2:5 which corresponded to a concentration of  $7.5 \times 10^{-6}$  mole and  $1.0 \times 10^{-5}$  mole as shown in Fig. 6.9 and 6.10, respectively.

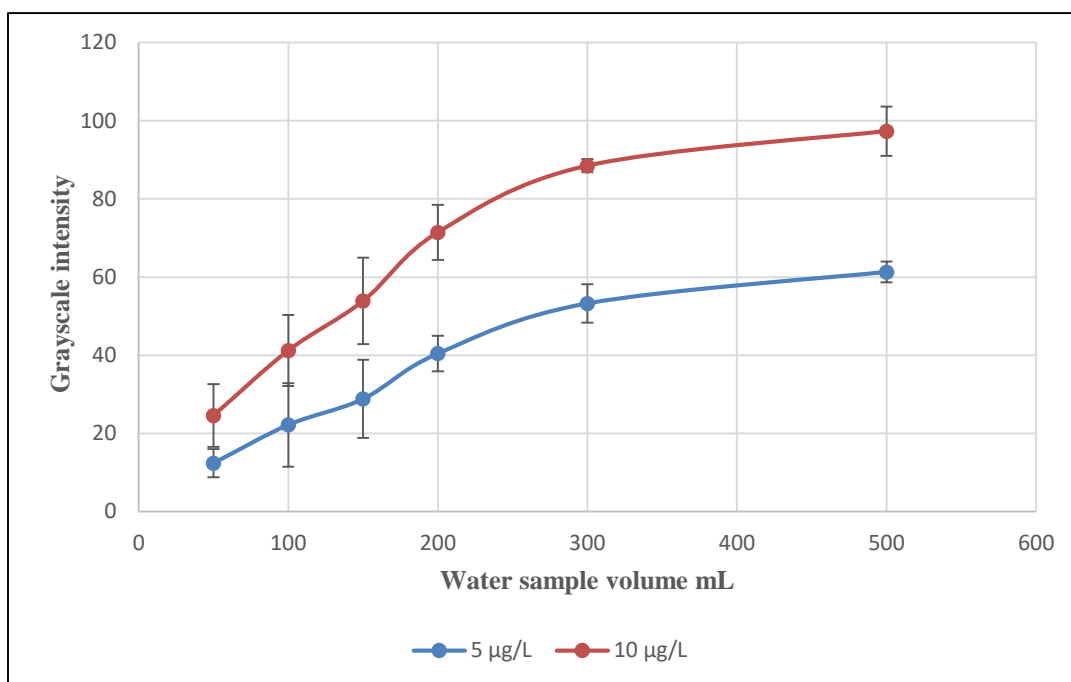


**Figure 6.9:** Effect of water sample volume on the colorimetric response in the  $G_G$  of the Hg-rhodamine B thiolactone complex compound. The concentration of rhodamine B thiolactone in the agar membrane was  $7.5 \times 10^{-6}$  mole. Typical  $Hg^{2+}$  concentration used was 5 and 10  $\mu g/L$ ; error bars represent one standard deviation ( $n=3$ ).

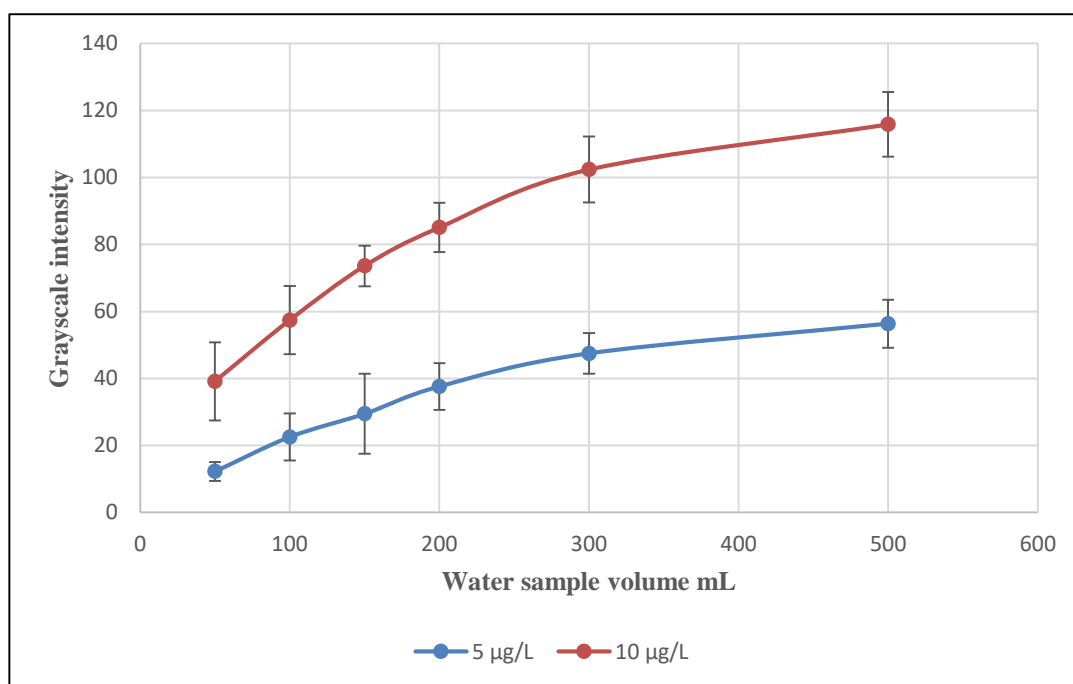


**Figure 6.10:** Effect of water sample volume on the colorimetric response in the  $G_G$  of the Hg-rhodamine B thiolactone complex compound. The concentration of rhodamine B thiolactone in the agar membrane was  $1.0 \times 10^{-5}$  mole. Typical  $Hg^{2+}$  concentration used was 5 and 10  $\mu g/L$ .

The results indicated that the colorimetric response was reasonable at 300 mL of water sample at a typical  $\text{Hg}^{2+}$  concentration used. Subsequently, although the colorimetric response seemed flattened, there was a slight increase. This could be as a result of saturating the exposed side of the agar membrane with  $\text{Hg}^{2+}$ , then any remaining  $\text{Hg}^{2+}$  could react with the other side of the membrane. Thus, the relationship between colorimetric response and sample volume kept increasing slightly until both sides of the membrane saturated, which consumed a large volume of water sample. The sample volume could be adjusted depending on the desired detection range of  $\text{Hg}^{2+}$ . However, considering the sensitivity at low  $\text{Hg}^{2+}$  concentration and the appropriate linear range for  $\text{Hg}^{2+}$  at such low concentration, a sample volume of 300 mL was selected for further use.

#### **6.4.2.3. Optimisation of colorant reagent volume added to 5 mL agar colloid**

The amounts of coloration reagent added to each 5 mL agar colloid were 0.5, 1, 1.5 and 2 mL, corresponding to  $2.5 \times 10^{-6}$ ,  $5.0 \times 10^{-6}$ ,  $7.5 \times 10^{-6}$  and  $1.0 \times 10^{-5}$  moles of coloration reagent loaded in the agar-agar membranes, respectively. A blank membrane exposed to distilled water without  $\text{Hg}^{2+}$  was used as a control for each concentration. The different loaded gels were exposed to 300 mL of 5 and 10  $\mu\text{g/L}$   $\text{Hg}^{2+}$  solutions separately.

Visual inspection of Fig. 6.11 shows that the colour intensity of the reagent-loaded gels increased slightly with increasing volume of the coloration reagent. However, this increase in the intensity was limited by the maximum added volume, which affects the gelling ability of agar colloid on the filter paper significantly.

The statistical results obtained (t-test at 0.05 significance level) (see Table A4.7 and A4.8 in Appendix 4) showed that there was no significant difference in colour intensity between the loaded gels when low  $\text{Hg}^{2+}$  concentration of 5  $\mu\text{g/L}$  was analysed. While there was a significant difference between the low loaded gel ( $2.5 \times 10^{-6}$  mole) and the other gels at high  $\text{Hg}^{2+}$  concentration of 10  $\mu\text{g/L}$ . This may be because the use of such small amount of rhodamine B thiolactone (0.5 mL) could not present enough moles to react with  $\text{Hg}^{2+}$  (15 nmole of  $\text{Hg}^{2+}$ ). Thus it was not sufficient enough for the formation of the coloured complex at high  $\text{Hg}^{2+}$  concentration. Because the minimum amount of

the colorant reagent was desirable, 1 mL of ( $5 \times 10^{-6}$  mole) rhodamine B thiolactone was chosen to be added to agar colloid as it gave sufficient colour intensity.

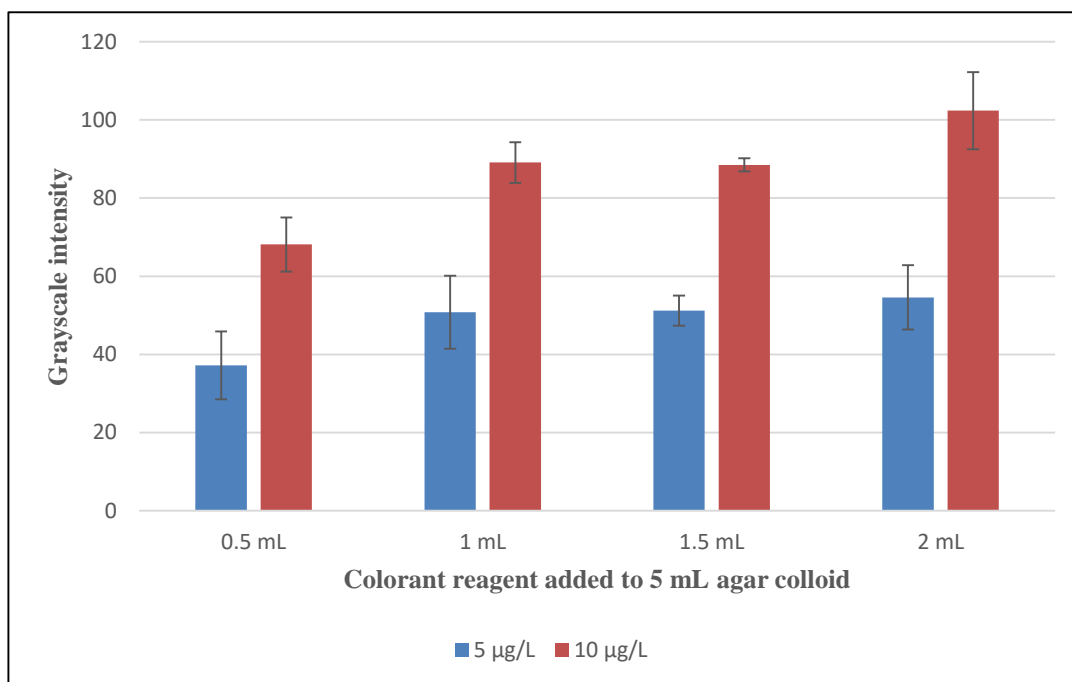


**Figure 6.11: Influence of colorant reagent volume on the colorimetric response in the  $G_G$  of the Hg-rhodamine B thiolactone complex compound. The concentrations of rhodamine B thiolactone in the agar membranes were  $2.5 \times 10^{-6}$ ,  $5.0 \times 10^{-6}$ ,  $7.5 \times 10^{-6}$  and  $1.0 \times 10^{-5}$  mole. Typical  $Hg^{2+}$  concentrations used were 5 and 10  $\mu g/L$ ; error bars represent one standard deviation ( $n=3$ ).**

### 6.4.3. Analytical performance

As discussed in Chapter 5, the colorimetric sensing relies on the ability of  $Hg^{2+}$  to induce a structural change in rhodamine B thiolactone. Compared with determination in solution phase and spot test mode, the sol-gel and agar-agar gel membranes serve as both a preconcentrator and a chromogenic reactor for  $Hg^{2+}$ . As a result, when the  $Hg^{2+}$  standard solutions were passed through the membranes, the filtration increases the probability of interaction between  $Hg^{2+}$  and rhodamine B thiolactone resulting in the formation of the pink product of Hg-rhodamine B thiolactone which could be discriminated clearly by the naked eye.

#### 6.4.3.1. Sol-gel membrane detection limit and linear range

Under the optimised sensing conditions mentioned in the previous study,<sup>56</sup> a series of sol-gel membrane sensors exposed to different  $\text{Hg}^{2+}$  standard solutions were evaluated. Pumping  $\text{Hg}^{2+}$  solutions through the sol-gel membranes immediately produced a pink colour resulting from opening the rhodamine B thiolactone ring and formation of Hg-rhodamine B thiolactone complex. The colour change from white to pink increased with increasing  $\text{Hg}^{2+}$  concentration in the standards. These results were in agreement with the literature.<sup>56</sup> Visual colour detection was found to occur at a concentration of  $1 \mu\text{g/L}$ , as shown in Fig. 6.12.

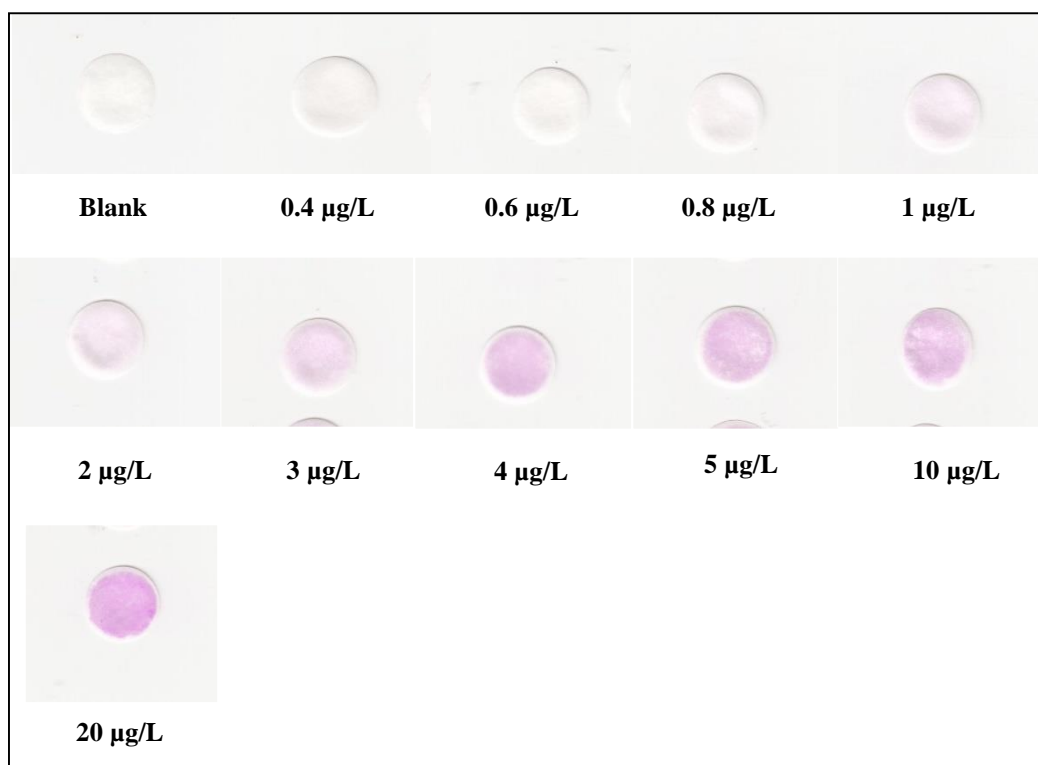


**Figure 6.12: Sequential increase of the colour intensity on the sol-gel membranes as a function of increased  $\text{Hg}^{2+}$  concentration: blank, 0.4, 0.6, 0.8, 1, 2, 3, 4, 5, 10 and 20  $\mu\text{g/L}$ .**

From the chromogenic analysis data in this experiment, a calibration plot was established for the  $G_G$  against  $\text{Hg}^{2+}$  concentration in the exposed membranes, as illustrated in Fig. 6.13. The results indicated good linearity ( $r^2=0.983$ ) over the range tested (0.4 to  $5 \mu\text{g/L}$ ). The minimum detectable  $\text{Hg}^{2+}$  concentration was found to be  $0.4 \mu\text{g/L}$ .

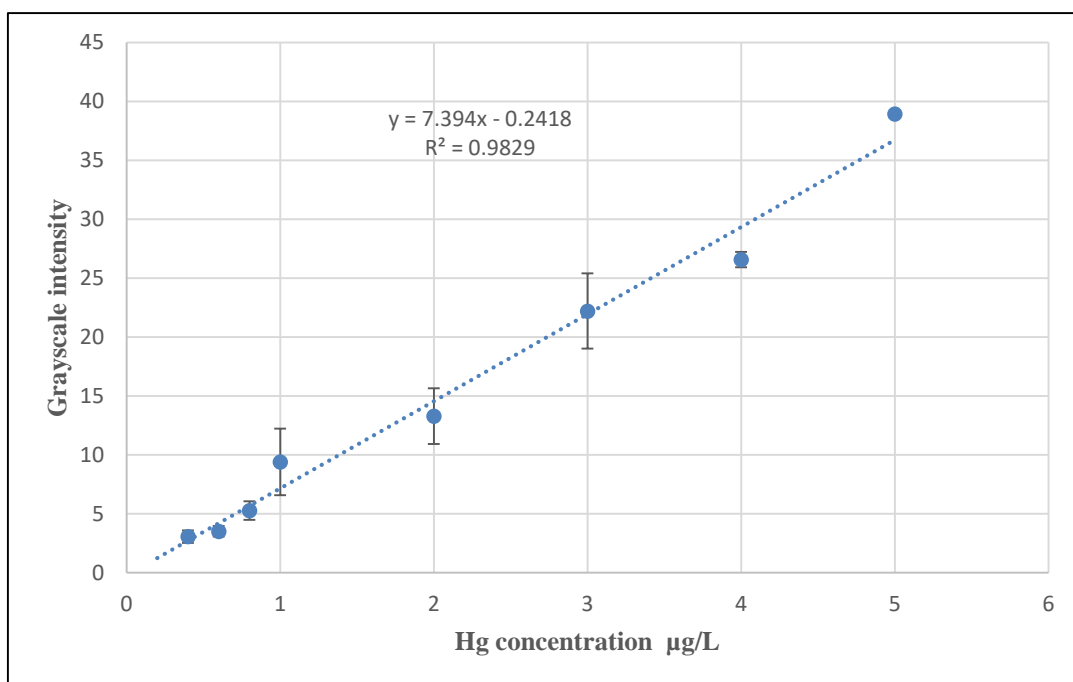


**Figure 6.13:** The linear correlation between the colorimetric response in  $G_G$  of the Hg-rhodamine B thiolactone formed on the sol-gel membranes and  $Hg^{2+}$  at the concentration range from 0.4 to 5  $\mu\text{g/L}$ ; error bars represent one standard deviation ( $n=3$ ).

#### 6.4.3.2. Agar-agar gel membrane detection limit and linear range

Upon the filtration of  $Hg^{2+}$  with concentrations ranging from 0.2 to 20  $\mu\text{g/L}$  through the agar-agar membrane under the optimised conditions developed, the colour intensity of the pink complex formed appeared to increase with increasing  $Hg^{2+}$  concentration in the standard solutions over the range tested. A concentration of 0.4  $\mu\text{g/L}$  could be easily distinguished by the naked eye, as shown in Fig. 6.14.

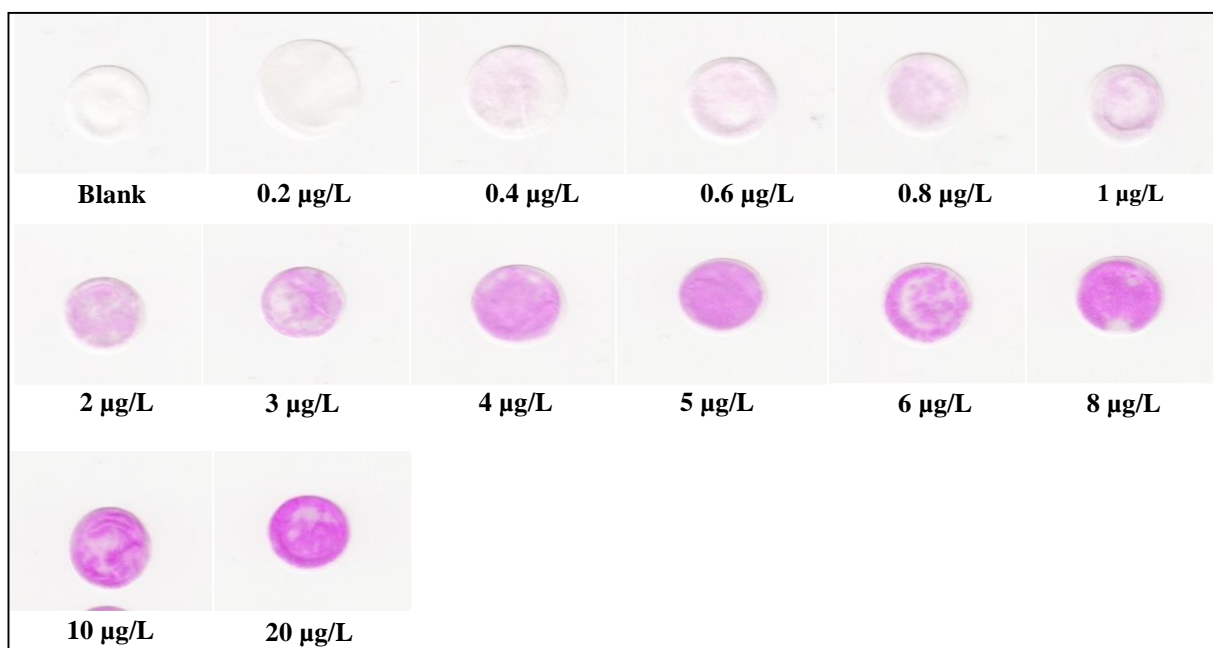


**Figure 6.14:** Sequential increase of the colour intensity on the agar-agar membranes as a function of increased  $\text{Hg}^{2+}$  concentration: blank, 0.2, 0.4, 0.6, 0.8, 1, 2, 3, 4, 5, 6, 8, 10 and 20  $\mu\text{g/L}$ .

The change in the  $G_G$  correlated well with  $\text{Hg}^{2+}$  concentration changes, as shown in Fig. 6.15. A good linear correlation ( $r^2=0.990$ ) existed between the  $G_G$  value and the concentration of  $\text{Hg}^{2+}$  over a range from 0.2 to 6  $\mu\text{g/L}$ .

The instrumental limit of detection was 0.2  $\mu\text{g/L}$  with good precision expressed as RSDs of 2.43 to 15.5% obtained with three experiments. Each experiment was repeated with three replicate agar-agar sensors at each  $\text{Hg}^{2+}$  concentration tested (see Table A4.10 in Appendix 4). The calibration curves of the individual experiments (from 0.2 to 6  $\mu\text{g/L}$ ) displayed good linear correlations of  $r^2=0.993$ ,  $r^2=0.985$  and  $r^2=0.964$ , as illustrated in Fig. 6.16. The small difference in slope from the three replicates indicated the good precision of the proposed method. Since the repeatability represented by RSDs for the three experiments was relatively low, thus, the results obtained from the proposed agar-agar method were reasonable and reliable.

Compared with the previously reported sol-gel membrane experiment, the preparation and use of the proposed agar-agar membrane was simple, straightforward, time-effective and consumed less reagents. Additionally, it provided a significantly lower limit of detection, with 0.4  $\mu\text{g/L}$  being sufficient for a visual  $\text{Hg}^{2+}$  determination with the naked eye.

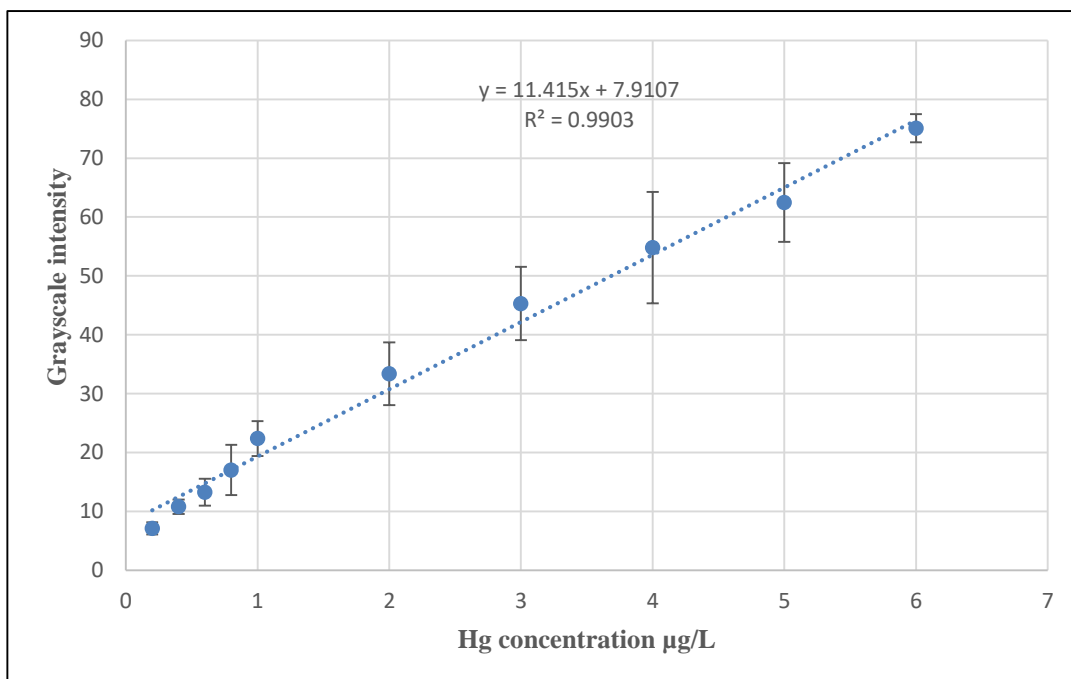


Figure 6.15: The linear correlation between the colorimetric response in  $G_G$  of the Hg-rhodamine B thiolactone formed on the agar-agar membranes and  $Hg^{2+}$  at the concentration range from 0.2 to 6  $\mu\text{g/L}$ ; error bars represent one standard deviation ( $n=3$ ).

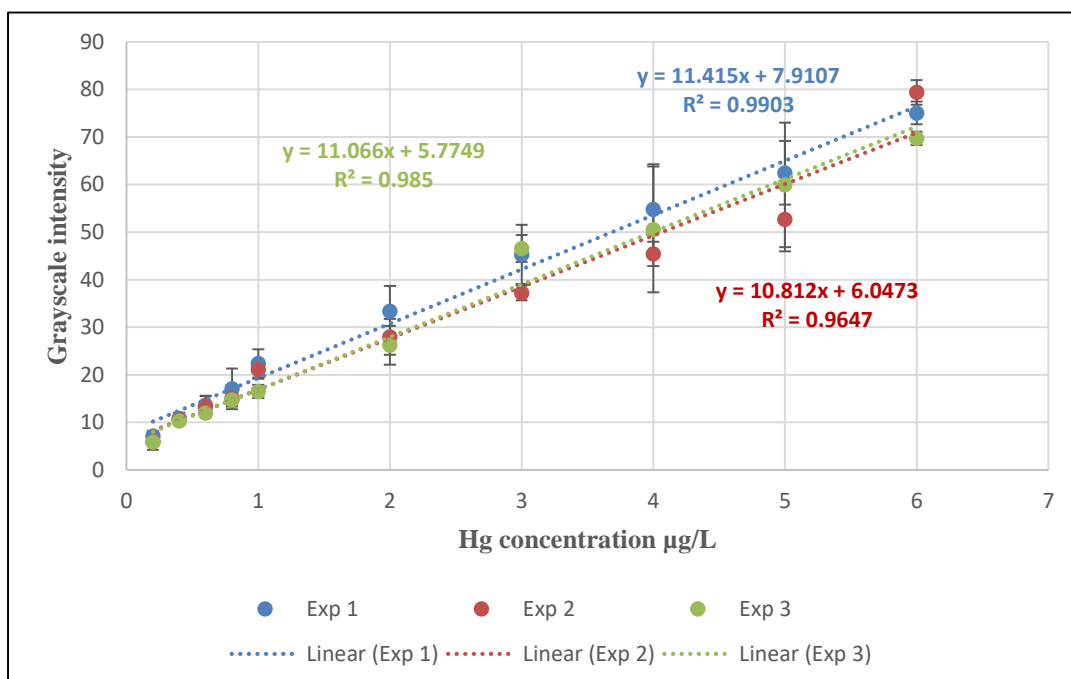


Figure 6.16: Calibration curves of the colorimetric response in  $G_G$  of the Hg-rhodamine B thiolactone complex formed on the agar-agar membranes in three repeated experiments ( $n=3$ ) versus the  $Hg^{2+}$  concentration range from 0.2 to 6  $\mu\text{g/L}$ ; error bars represent one standard deviation ( $n=3$ ).

## Accuracy and precision

The accuracy of the proposed agar-agar method was evaluated by spike recovery tests. The spike recovery study was done at three concentration levels where known amounts of  $\text{Hg}^{2+}$  concentrations were added to a known concentration of the sample (distilled water) in triplicate at low, medium and high concentration levels. The initial  $\text{Hg}^{2+}$  concentration was 1  $\mu\text{g/L}$  and the spiked concentrations were 1, 3 and 5  $\mu\text{g/L}$ . The spiked sample solutions were pumped through the sensors, then the exposed membranes were scanned for chromogenic analysis. After the intensities in  $G_G$  were measured, the  $\text{Hg}^{2+}$  concentrations were obtained from the corresponding regression equations and the percentage spike recoveries were calculated using Equation 6.1.

$$\begin{aligned} & \% \text{ spike recovery} \\ & = \frac{(\text{measured con. of } \text{Hg}^{2+} \text{ in spike reagent} - \text{measured con. of } \text{Hg}^{2+} \text{ in unspike reagent})}{\text{known con. of } \text{Hg}^{2+} \text{ in spiked reagent}} \times 100 \end{aligned}$$

### Equation 6.1

The results obtained were compared with the added amount, as given in Table 6.2. The RSD values were less than 10% and the spike recoveries were 99.1%, 103% and 97.7% for the low, medium and high concentration levels, respectively.

**Table 6.2: Accuracy/recovery study for the triplicate values of the colorimetric response in  $G_G$  recorded at three spiking levels.**

Initial $\text{Hg}^{2+}$ $\mu\text{g/L}$	$\text{Hg}^{2+}$ Spiked $\mu\text{g/L}$	$\text{Hg}^{2+}$ Found $\mu\text{g/L}$ n=3	% Recovery $\pm$ % RSD n=3
1	1	0.990 $\pm$ 0.089	99.1 $\pm$ 9.04
1	3	3.09 $\pm$ 0.144	103 $\pm$ 4.65
1	5	4.89 $\pm$ 0.438	97.7 $\pm$ 8.98

Results are mean  $\pm$  SD; n = number of replicates.

## 6.4.4. Membrane stability and reactivity

### 6.4.4.1. Sol-gel membrane stability and reactivity

Similar to findings reported previously,<sup>56</sup> the sol-gel membrane exposed to the open air at room temperature changed to pink even after one day. It was noticed that the acid catalysed sol-gel membrane underwent a fast curing process. Fast evaporation caused the formation of a membrane with high internal stresses. This led to shattering in the gel during the curing process, forming small cracks in the sol-gel membrane. Hence, the probability of the air penetration into the structure of the sol-gel matrix was increased, which might induce the structural transformation of rhodamine B thiolactone. Fig. 6.17 shows the stability of sol-gel membranes under different storage conditions. When the membranes were stored in ascorbic acid solution, the colour change was minimised up to 5 weeks, which was in agreement with the previous study. However, an obvious colour change was observed after that time. It was also noticed that the ascorbic acid solution started to change to a pink colour and had a more jelly-like constituency. The membranes stored in the open air in a dark place also changed their colour to pink markedly. In this study the membranes that were stored in a bottle

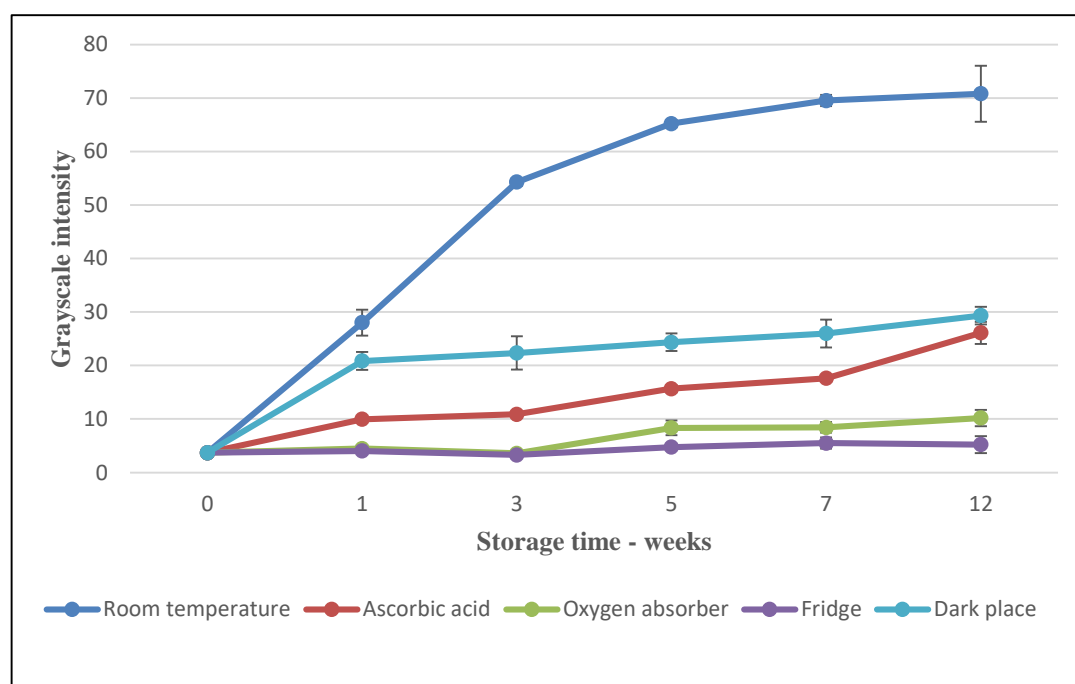


**Figure 6.17: Stability monitoring over time of the sol-gel membranes kept in open air, 1.0 mM of ascorbic acid, oxygen absorber, refrigerator and dark for a period up to 12 weeks; error bars represent one standard deviation (n=3).**

containing oxygen absorber or in a refrigerator revealed no change up to 12 weeks. Therefore, for long-term storage of the  $\text{Hg}^{2+}$  sensor, the membranes should be stored at low temperatures or in tightly sealed containers without oxygen.

The reactivity of stored membranes was also tested after various intervals of time, as shown in Fig. 6.18. The stored membranes were evaluated by exposure to  $10\ \mu\text{g/L}$   $\text{Hg}^{2+}$ . The control grayscale intensity (at 0 weeks) was recorded first. Then, after the stored membrane sensors were exposed to  $\text{Hg}^{2+}$ , the intensities were also recorded.

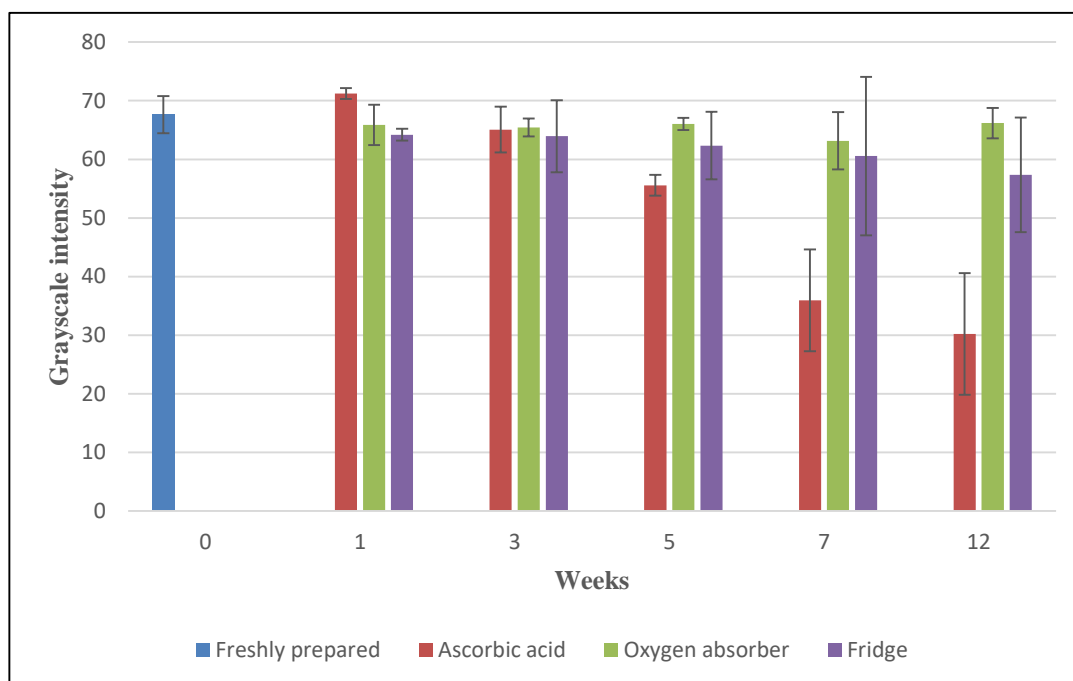


**Figure 6.18: Reactivity at different time intervals of the sol-gel membranes kept in 1.0 mM of ascorbic acid, oxygen absorber and refrigerator for a period up to 12 weeks. The membranes were exposed to  $10\ \mu\text{g/L}$   $\text{Hg}^{2+}$  solution; error bars represent one standard deviation (n=3).**

The sol-gel membranes stored in ascorbic acid displayed a significant decline in their response to  $\text{Hg}^{2+}$ , as indicated by the grayscale intensity, starting from week 5. This gradual decline might be due to the diffusion of rhodamine B thiolactone from the sol-gel to the solution of ascorbic acid during storage. The softening of the sol-gel substrate molecule into the ascorbic acid solution might also be a reason for formation of a jelly-like substance. Acid catalysed sol-gels have been studied widely for their excellent controlled release properties.<sup>271-273</sup> After gelation, condensation and drying, the molecules are encapsulated and uniformly distributed in the resulting glassy solid

matrix. The encapsulated molecules are released in a time and load dependent manner. Furthermore, an *in vivo* study demonstrated that these controlled release carrier materials are biodegradable.<sup>274</sup> Based on these studies, controlled release, softening/degradation of sol-gel matrix into the ascorbic acid solution were likely the reasons for the decrease of the loaded rhodamine B thiolactone, hence, in the grayscale intensity. On the other hand, no significant change was observed in the grayscale intensities between the control and the membrane stored in a bottle contained oxygen absorber or in the refrigerator. Thus, the membranes stored at low temperatures or in tightly sealed containers without oxygen did not show any effect on their activity.

#### 6.4.4.2. Agar-agar membrane stability and reactivity

In general, compared with sol-gel, the agar-agar membrane was more stable, as shown in Fig. 6.19. When the agar-agar membrane was exposed to air at room temperature, colour change of immobilised rhodamine B thiolactone did not occur for up to one week. After this, a sharp increase in the grayscale intensity was observed as the membrane completely changed to a pink colour. The grayscale intensity after 5 weeks seemed to flatten, which might be due to all of the rhodamine B thiolactone being

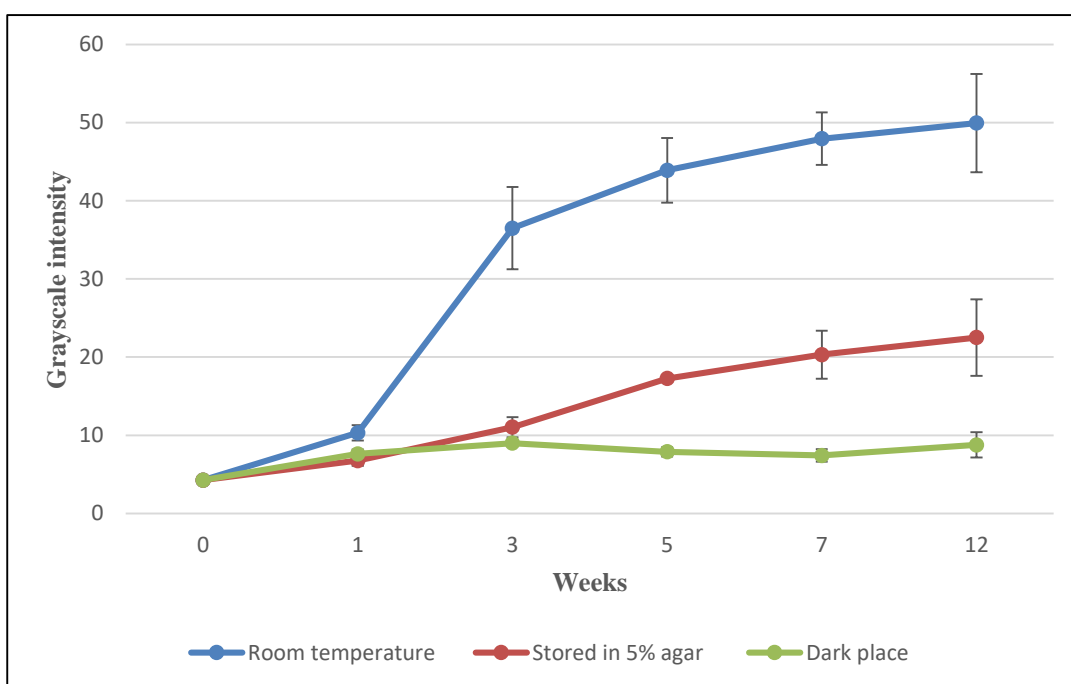


**Figure 6.19: Stability monitoring over time of the agar-agar membranes kept in open air, 5% agar colloid and in dark place for a period up to 12 weeks; error bars represent one standard deviation (n=3).**

converted into a Z form. The membrane stored in 5% (w/v) agar also exhibited an increase in the grayscale intensity compared with the control. Stability of immobilised rhodamine B thiolactone was only detected clearly when the agar-agar membranes were stored in a dark place. Hence, there was no significant difference between the measured grayscale intensities of the stored membranes up to 12 weeks.

The reactivity of the stored agar-agar membrane was also measured as shown in Fig. 6.20. After various time intervals, the sensing activity for 10 µg/L Hg<sup>2+</sup> was measured. Compared with the control (grayscale intensity at 0 weeks) a sharp decline in grayscale intensity was noticed in the membranes stored in 5% (w/v) agar colloid within the first week. In contrast, the agar-agar membranes stored in a dark place were stable for at least 12 weeks.

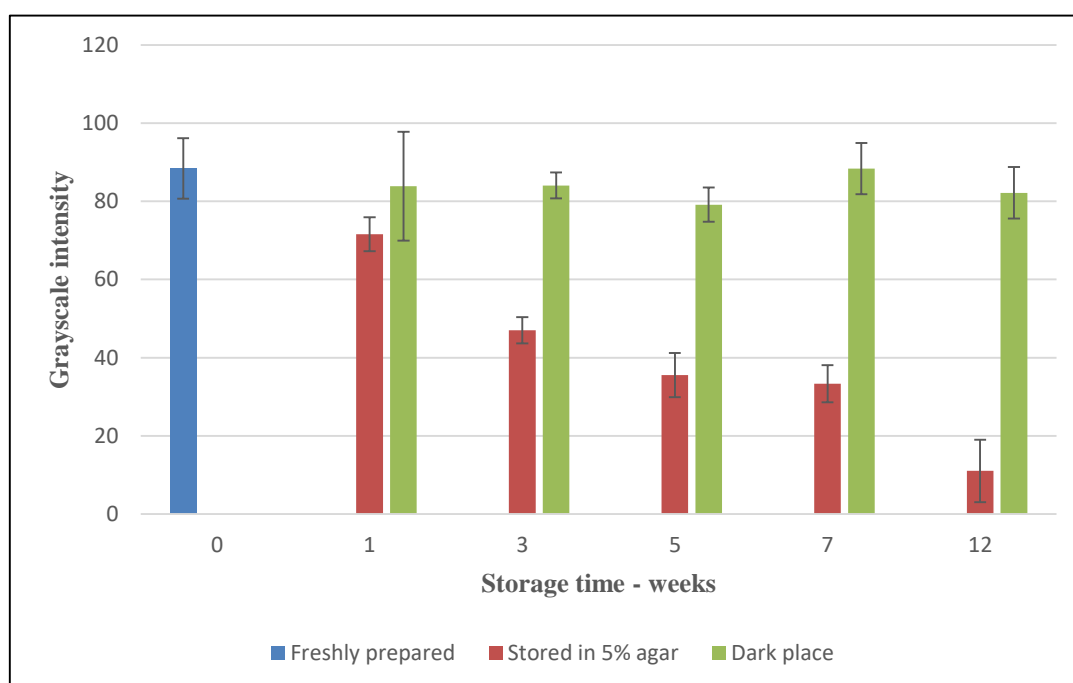


**Figure 6.20: Reactivity at different time intervals of the agar-agar membranes stored in 5% (w/v) agar and in a dark place for a period up to 12 weeks. The membranes exposed to 10 µg/L Hg<sup>2+</sup> solution; error bars represent one standard deviation (n=3).**

There are two potential reasons behind the decrease of the grayscale intensity of the membranes stored in the 5% (w/v) agar; either leakage of the immobilised reagent from the sensing membrane to the carrier support or it might be due to the adhesion of the sensing membrane to the agar colloid. Differences in media concentrations of rhodamine B thiolactone might cause migration of the reagent from the highly loaded

gel to areas of lower concentration, forming a multilayer of the reagent particles within the agar surface. The carrier agar support changed colour to yellowish-pink at the end of the observation period as shown in Fig. 6.21. The second possible reason is the adhesion of the sensing membrane to the wet agar colloid carrier, which may occur when the storage media was peeled off.



**Figure 6.21:** The observation of yellowish-pink coloration of 5% (w/v) agar caused by the leakage of the immobilised reagent from the sensing membrane.

It was concluded from the findings that storing agar-agar membranes in the dark was the best approach since it maintained the stability and reactivity of rhodamine B thiolactone. There was no requirement to store the membrane at low temperature or in an oxygen-free environment, which is a clear advantage over the sol-gel based sensors.

#### **6.4.5. Method application**

The applicability of the proposed agar-agar sensor method for  $\text{Hg}^{2+}$  determination was evaluated by analysing real water samples from a variety of sources (tap water, seawater, stream water and bottled drinking water). When water samples were pumped through the membranes, no significant colour change was observed. This indicated that, as expected, little or no  $\text{Hg}$  was present. The samples were spiked with  $2 \mu\text{g/L}$  of  $\text{Hg}^{2+}$ , after which the sensing experiment was repeated and intensities in  $G_G$  were measured. The  $\text{Hg}^{2+}$  concentrations were obtained from the corresponding regression equations and the percentage spike recoveries were calculated for each spike level using Equation 6.1.

As shown in Table 6.3, the tap water was the only sample where the amount of  $\text{Hg}^{2+}$  detected agreed well with the spiked level. It was found that the measured  $\text{Hg}^{2+}$  values were very low for the spiked seawater, stream water and bottled water samples. The recovery was 106% for spiked tap water. The corresponding value of spiked seawater was only 0.168%. This result confirmed the previous conclusion of poor sensor performance in artificial seawater (see Section 5.4.6). The  $\text{Hg}^{2+}$  concentration determined in stream water was found, however, to be lower than the spiked level (34.7% and 16.5%). The same trend was observed for the spiked bottled water samples, which differ in their dissolved ion content. Recoveries of 43.9%, 32.3% and 20.2% were obtained for bottled water 1, 2 and 3, respectively.

**Table 6.3: Analytical results of  $\text{Hg}^{2+}$  in real water samples and of the spike recovery tests.**

Sample	Spiked $\text{Hg}^{2+}$ concentration $\mu\text{g/L}$	Concentration found $\mu\text{g/L}$ , n=3	Recovery
Tap water	0	ND	106%
	2	$2.13 \pm 0.365$	
Sea water	0	ND	0.168%
	2	$0.003 \pm 0.004$	
Stream water 1	0	ND	34.7%
	2	$0.695 \pm 0.425$	
Stream water 2	0	ND	16.5%
	2	$0.329 \pm 0.447$	
Bottled 1	0	ND	43.9%
	2	$0.878 \pm 0.077$	
Bottled 2	0	ND	32.3%
	2	$0.646 \pm 0.251$	
Bottled 3	0	ND	20.2%
	2	$0.403 \pm 0.158$	

Results are mean  $\pm$  SD, n=number of replicates, ND= not detectable.

Since the analysis was conducted in triplicate, this signal suppression cannot be caused by any failure of the reagent immobilised membranes or the filtration process. Further, the interference study in Section 5.4.4 showed that the rhodamine B thiolactone is selective for  $\text{Hg}^{2+}$  in the presence of major and trace ions typically found in natural water. Thus it was hypothesised that, in the studied waters,  $\text{Hg}^{2+}$  forms species such as complexes with other compounds or ions present, decreasing the amount of free

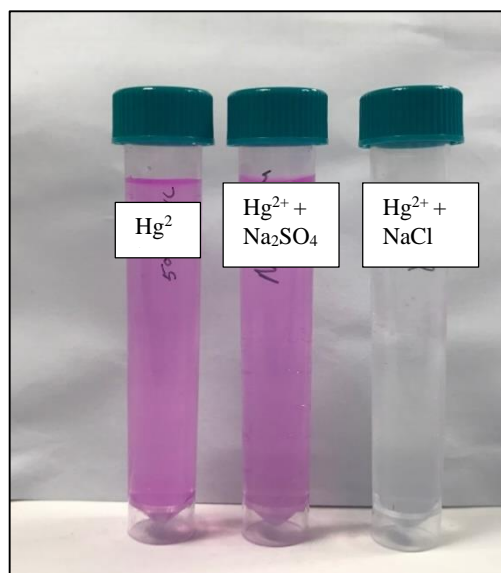
$\text{Hg}^{2+}$  available to react with the sensor. Further investigation of this suggestion is described in the next section.

#### **6.4.5.1. Investigation of the signal suppression**

According to the literature<sup>14, 275</sup>  $\text{Hg}^{2+}$  is not free in natural aquatic systems. It is bound by inorganic or organic molecules found in the environment and forms complexes with hydrosulfide ( $\text{HS}^-$ ) or other thiolate ( $\text{RS}^-$ ) ligands,  $\text{OH}^-$ ,  $\text{Br}^-$  and  $\text{Cl}^-$ . The very strong affinity of S makes it the probable primary competitor for  $\text{Hg}^{2+}$  along with  $\text{Cl}^-$  which is one of the major inorganic anions in seawater and freshwater.

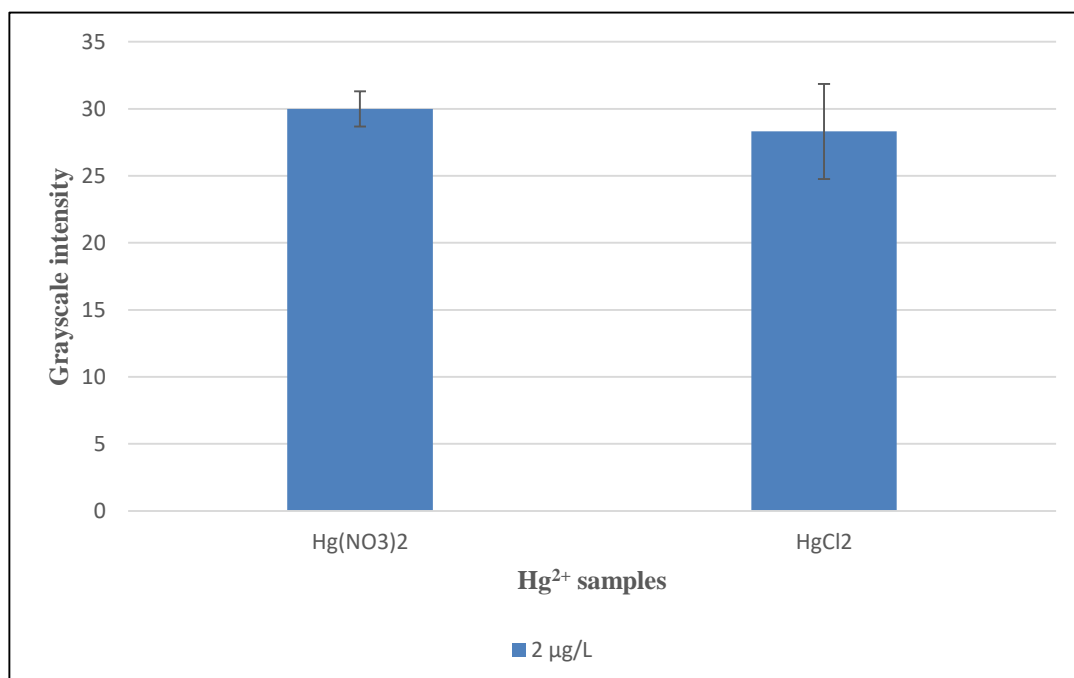
The initial step in this part of the study was to assess the effect of inorganic S ( $\text{SO}_4^{2-}$ ) and  $\text{Cl}^-$  on the amount of  $\text{Hg}^{2+}$  that could be detected. For this purpose, a comparison of the selectivity of rhodamine B thiolactone toward three solutions ( $\text{Hg}^{2+}$  standard in distilled water,  $\text{NaCl}$  and  $\text{Na}_2\text{SO}_4$ ) was investigated. All the measurements were examined under the same conditions, according to the procedure described in Section 3.5.2.3. An aliquot of a 50  $\mu\text{L}$  stock solution of rhodamine B thiolactone (5 mM) was mixed with an appropriate amount of  $\text{Hg}^{2+}$  at pH 5.0, then  $\text{NaCl}$  or  $\text{Na}_2\text{SO}_4$  was added. The final concentrations of  $\text{NaCl}$  and  $\text{Na}_2\text{SO}_4$  were 24.5 g/L and 4.09 g/L, respectively, which corresponding to typical  $\text{Cl}^-$  and  $\text{SO}_4^{2-}$  concentrations in the marine environment.

Fig. 6.22 revealed that the  $\text{Na}_2\text{SO}_4$  did not interfere with the detection of  $\text{Hg}^{2+}$ ; a similar colour intensity was observed with the naked eye between the mixed solution and the solution containing  $\text{Hg}^{2+}$  alone. However, the response was affected significantly in the presence of  $\text{NaCl}$  as no colour change was observed. Because  $\text{Na}^+$  did not show any interference with the detection of  $\text{Hg}^{2+}$  (see Section 5.4.4) it was assumed that the interference was likely to be as a result of  $\text{Cl}^-$  ions reacting with  $\text{Hg}^{2+}$ .



**Figure 6.22: Effect of Na<sub>2</sub>SO<sub>4</sub> and NaCl on the colorimetric response for the detection of 500 µg/L Hg<sup>2+</sup>.**

To further investigate if Cl<sup>-</sup> can affect the sensing response, two Hg<sup>2+</sup> standard solutions with a concentration of 2 µg/L were prepared from different sources; Hg(NO<sub>3</sub>)<sub>2</sub> and HgCl<sub>2</sub>. Each set of solutions was pumped through the agar-agar membrane in triplicate. The result, as illustrated in Fig. 6.23 indicated that there is no



**Figure 6.23: The intensity in G<sub>c</sub> of the agar-agar membranes exposed to 2 µg/L Hg(NO<sub>3</sub>)<sub>2</sub> and HgCl<sub>2</sub> solutions; error bars represent one standard deviation (n=3).**

difference in the grayscale intensity obtained from the scanned membranes exposed to  $\text{Hg}(\text{NO}_3)_2$  and  $\text{HgCl}_2$  solutions.

The explanation of signal suppression in the case of  $\text{NaCl}$  but not when  $\text{HgCl}_2$  was used might be attributed to the  $\text{Cl}^-$  concentration. Depending on the pH and  $\text{Cl}^-$  concentration,  $\text{Hg}^{2+}$  forms more complex compounds with  $\text{Cl}^-$ , which could explain the effects of relatively high  $\text{Cl}^-$  levels on  $\text{Hg}^{2+}$  uptake. Under conditions dominated by  $\text{Cl}^-$  complexation,  $[\text{HgCl}_3]^-$  and  $[\text{HgCl}_4]^{2-}$  complexes may dominate  $\text{Hg}^{2+}$  speciation, thus reduced its availability to uptake by the sensor. Chloride complexes of  $\text{Hg}^{2+}$  in natural aquatic systems include complexes with variable amounts of  $\text{Cl}^-$  ions ( $[\text{HgCl}]^+$ ,  $\text{HgCl}(\text{OH})$ ,  $\text{HgCl}_2$ ,  $[\text{HgCl}_3]^-$ , and  $[\text{HgCl}_4]^{2-}$ ). Furthermore, within a specific range of pH and with an increase in  $\text{Cl}^-$  concentration, the proportion of charged mercuric chloride species  $[\text{HgCl}_3]^-$  and  $[\text{HgCl}_4]^{2-}$  increases gradually as the proportion of  $\text{HgCl}_2$  decreases, as illustrated in Fig. 6.24. Thus, the complexes  $[\text{HgCl}_3]^-$ , and  $[\text{HgCl}_4]^{2-}$  are predominant in seawater,<sup>276</sup> the sample which gave the lowest spike recovery.

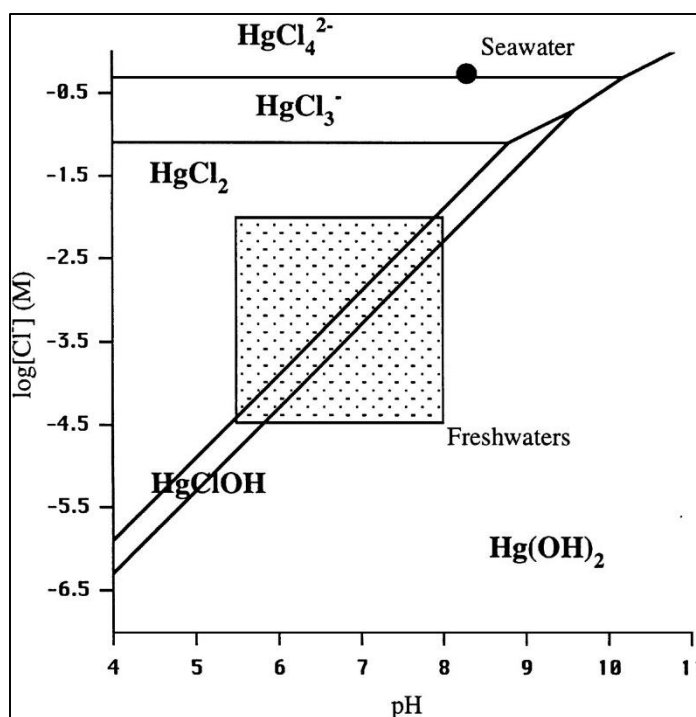
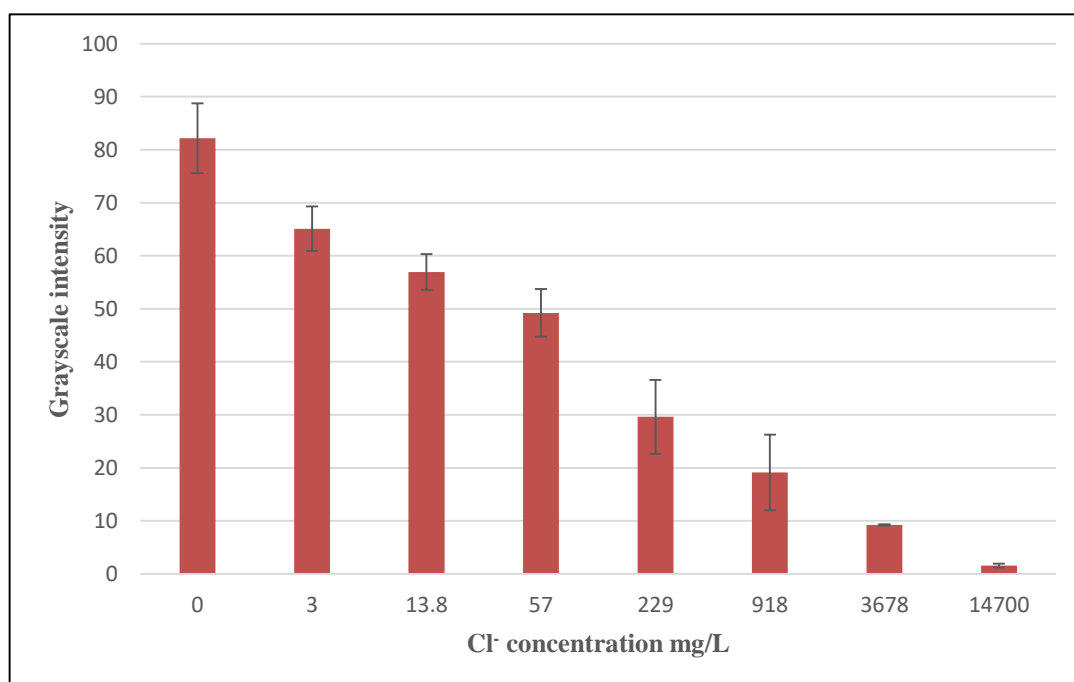


Figure 6.24: Diagram of hydroxo and chloro complexes of  $\text{Hg}^{2+}$  as a function of pH and chloride concentrations.<sup>276</sup>

To investigate how  $\text{Cl}^-$  concentration may affect the availability of  $\text{Hg}^{2+}$  and, hence, the sensor response, a series of  $10 \mu\text{g/L}$   $\text{Hg}^{2+}$  solutions were spiked with  $3 \text{ mg/L}$  to  $14700 \text{ mg/L}$   $\text{Cl}^-$ , a range covering concentrations typical of fresh to marine waters. The rhodamine B thiolactone immobilised agar-based sensor system was used for their analysis. Both naked eye detection and chromogenic analysis in  $G_G$  were conducted on the exposed membranes to study the effect of  $\text{Cl}^-$  concentration on the colorimetric response.

Addition of  $\text{Cl}^-$  up to  $14700 \text{ mg/L}$  critically affected the colorimetric response in  $\text{Hg}^{2+}$  solutions (Fig. 6.25) and suppression was observed even at low  $\text{Cl}^-$  concentrations (Fig. 6.26). The sensing performance was only valid when the  $\text{Cl}^-$  concentration was  $\leq 10 \text{ mg/L}$ , with a  $G_G/G_{G0}$  value of 89.4%. At a concentration of  $229 \text{ mg/L}$   $\text{Cl}^-$  the  $G_G/G_{G0}$  was around 36%. Although  $\text{Cl}^-$  concentration vary considerably in all natural waters at any given area, the sensor may be unsuitable for use in drinking water, where the maximum acceptable concentration of  $\text{Cl}^-$  is  $250 \text{ mg/L}$ .<sup>277</sup>



**Figure 6.25:** The intensity in  $G_G$  of the agar-agar membranes exposed to  $\text{Hg}^{2+}$  solutions of  $10 \mu\text{g/L}$  in the presence of variable concentration of  $\text{Cl}^-$  ranging from 0 to  $14700 \text{ mg/L}$ ; error bars represent one standard deviation ( $n=3$ ).

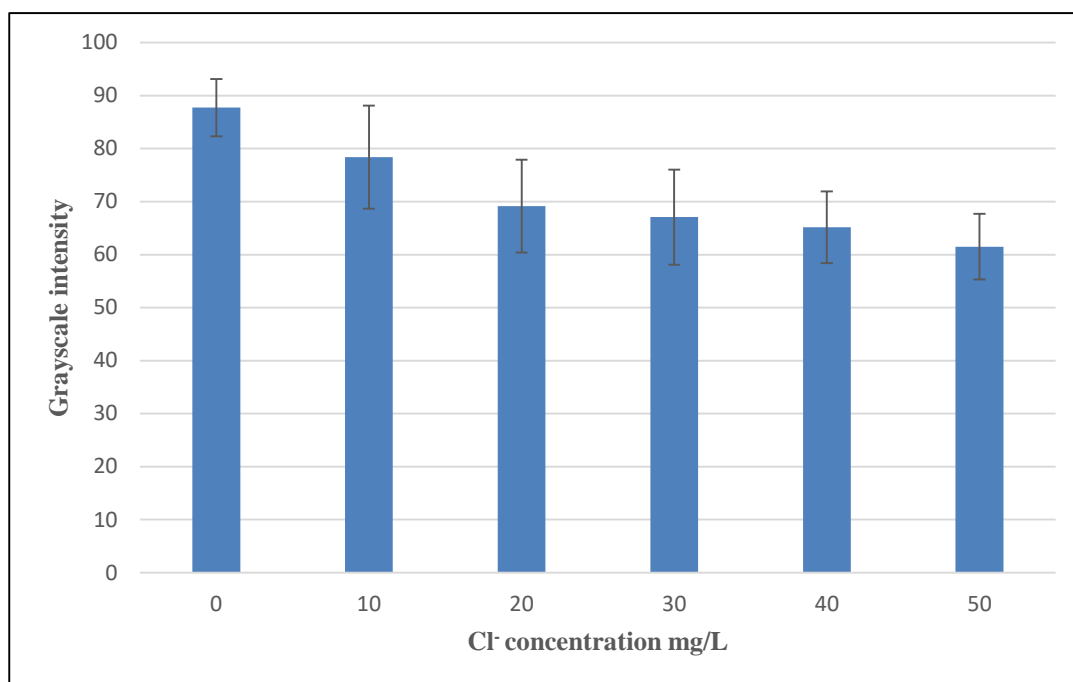


**Figure 6.26:** The intensity in  $G_G$  of the agar-agar membranes exposed to  $Hg^{2+}$  solutions of  $10 \mu g/L$  in the presence of variable concentration of  $Cl^-$  ranging from 0 to 50 mg/L; error bars represent one standard deviation ( $n=3$ ).

Chloride concentrations of the real samples used in Section 6.4.5 were determined using ion chromatography. The samples were analysed in a DIONEX DX-120 ion chromatograph, and the results obtained are shown in Table 6.4.

**Table 6.4:** The effect of  $Cl^-$  ion concentrations on the signal suppression of the real samples.

Sample	$Hg^{2+}$ concentration found $\mu g/L$ , $n=3$	Recovery	$Cl^-$ concentration mg/L
Tap water	$2.13 \pm 0.365$	106%	0.890
Sea water	$0.003 \pm 0.004$	0.168%	16,105
Stream water 1	$0.695 \pm 0.425$	34.7%	18.5
Stream water 2	$0.329 \pm 0.447$	16.5%	25.7
Bottled 1	$0.878 \pm 0.077$	43.9%	5.78
Bottled 2	$0.646 \pm 0.251$	32.3%	7.60
Bottled 3	$0.403 \pm 0.158$	20.2%	12.6

Results are mean  $\pm$  SD,  $n$ =number of replicates.

It can be observed that rhodamine B thiolactone was susceptible to signal suppression effects and that the suppression trends were in the order of the  $\text{Cl}^-$  concentrations. Except for stream water 1, the higher the  $\text{Cl}^-$  concentration the more signal suppression occurred. In particular, the smallest recovery of 0.168% for the seawater and the highest recovery of 106% for the tap water were expected based on the  $\text{Cl}^-$  concentrations of 16105 mg/L and 0.89 mg/L, respectively.

Also, it is worth pointing out that none of the recoveries obtained for real samples matched those expected from analysis of the  $\text{Cl}^-$  spiked standards. All the recoveries in the real samples were less than the expected values from the  $\text{Cl}^-$  spiked standards. For example, the recovery was 0.168% in the real seawater, whereas the corresponding value was 1.87% in the standard spiked with the  $\text{Cl}^-$  concentration typical of seawater. Stream water 2 had a recovery of 16.5% with measured  $\text{Cl}^-$  concentration of 25.7 mg/L; this did not match the recovery values of 78.8% and 76.5% for  $\text{Cl}^-$  concentrations of 20 mg/L and 30 mg/L, respectively. The same phenomena presented in real sample bottled water 3 the recovery was 20.2% whereas in the 10 mg/L spiked standard it was 89.4%. This may be because the real samples contain other halides such as  $\text{Br}^-$  and  $\text{F}^-$ . Complexes of  $\text{Hg}^{2+}$  with  $\text{Br}^-$  ions are also significant in natural waters. Therefore, these halide ions can also react with  $\text{Hg}^{2+}$  reducing the amount of free  $\text{Hg}^{2+}$ , resulting in less being recovered.

As mentioned, it was noticed that the recovery value of stream water 1 did not follow the same trend as the other samples. Chloride concentration of 18.5 mg/L, gave a recovery of 34.7% instead of a projected value of 16-20%. This may be attributed to the presence of other molecules which could affect the observed analytical signal. Therefore, a more in-depth analysis was conducted in order to understand this better.

#### 6.4.5.2. Investigation of the effect of dissolved organic carbon (DOC) on sensor uptake

Stream water 1 was collected from a rural area (Kintyre, Scotland), where peatlands are common, whereas stream water 2 was obtained from an urban area (East Kilbride, Scotland). It is clear from Fig. 6.27 that stream water 1 appeared brownish in colour, and it likely has a high organic carbon load. This brownish colour comes from the leaching of light-absorbing humic and fulvic acid substances from plant and soil organic matter.

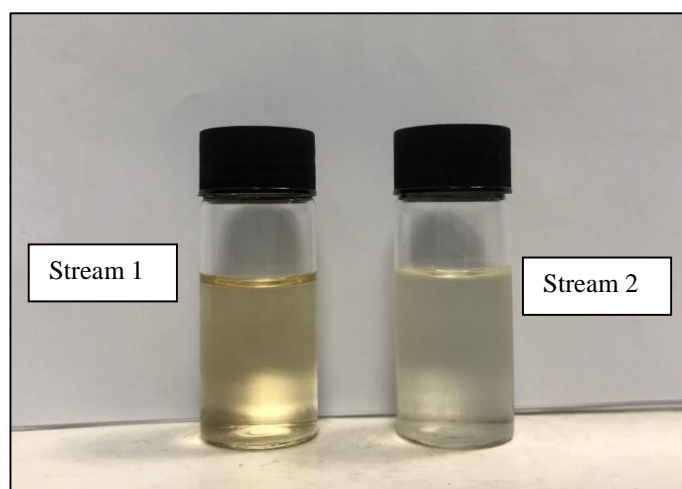


**Figure 6.27: The appearance of dissolved organic carbon (indicated by brown colour) in stream water samples.**

As a result, the organic matter contributes acids to the stream, resulting in the yellow-brown coloration. Dissolved organic carbon is known to bind trace metals strongly, affecting their speciation, solubility, mobility and toxicity.<sup>278</sup>

Although dissolved Hg and DOC concentrations tend to be strongly correlated in many watershed studies,<sup>279-281</sup> the ratio of Hg to DOC is known to vary from site to site.<sup>281</sup> Mercury associates with DOC by binding to reduced S sites within the DOC component. It was found that the aromatic carbon content of DOC with elevated reduced S is responsible for binding the majority of the available Hg.<sup>282</sup> Accordingly, the relative amount of aromatic carbon compound in the DOC will influence the ratio of Hg:DOC.

The primary detection of the presence of the aromatic carbon compounds indicative of DOC quality can be performed using spectrophotometry. Absorbance measurement at a wavelength of 254 nm has been found to strongly correlate with the aromatic carbon content notably through the specific UV absorbance at 254 nm (SUVA<sub>254</sub>).<sup>283, 284</sup> The SUVA<sub>254</sub> values can be calculated as the ratio of the UV absorbance measured at 254 nm to the concentration of DOC and are reported in litre per milligram carbon per meter (L mg-C<sup>-1</sup>m<sup>-1</sup>)

Based on the fact that DOC and salinity control the speciation and bioavailability of Hg<sup>2+</sup> in aqueous solutions,<sup>285, 286</sup> the stream water samples were analysed in duplicate to confirm the presence of DOC. The samples were passed through 0.45 µm cellulose acetate membrane. The filtrate was collected in glass vials, acidified to pH 2.0 with HNO<sub>3</sub> and stored in the dark at 4 °C for analysis of DOC within a few days of sample collection.

UV-vis absorbance measurement of stream waters was performed on a Varian Cary 50 probe visible spectrophotometer (Varian, Inc.) between 200 and 700 nm, with distilled water as reference. A quartz cell with 1.0 cm path length was used. The DOC was measured on Apollo 9000 combustion TOC analyser (Teledyne Tekmar). The stream water SUVA<sub>254</sub> values are reported in Table 6.5.

**Table 6.5: The Cl<sup>-</sup> ion concentrations and DOC in the stream waters.**

Sample	Recovery	Cl <sup>-</sup> concentration mg/L	DOC mg/L n=2	SUVA <sub>254</sub> L mg-C <sup>-1</sup> m <sup>-1</sup>
Stream water 1	34.7%	18.5	30.8	2.36
Stream water 2	16.5%	25.7	29.2	1.65

The recovery is the recovery values of spiked Hg<sup>2+</sup> concentration in the samples.

The DOC concentrations were similar in both stream water samples. However, the stream water 1 concentration of DOC was higher than the Cl<sup>-</sup> concentration, with a high aromatic carbon content (2.36 L mg-C<sup>-1</sup> m<sup>-1</sup>). In contrast, low aromatic carbon content of (1.65 L mg-C<sup>-1</sup> m<sup>-1</sup>) and nearly similar DOC and Cl<sup>-</sup> concentrations were

measured in stream water 2. According to the literature,<sup>285, 286</sup>  $\text{Hg}^{2+}$  binds strongly to reduced S sites within aromatic carbon compounds to form complexes with DOC, resulting in Hg-DOC complexes becoming the dominant Hg species at high DOC levels. In contrast,  $\text{Hg-Cl}^-$  complexes could be the dominating Hg species at high  $\text{Cl}^-$  but low DOC conditions. The results were in agreement with this. Generally, the uptake of  $\text{Hg}^{2+}$  by rhodamine B thiolactone membranes was inhibited by the presence of  $\text{Cl}^-$  ions despite the quantity of DOC. Only in stream water 1, the high aromatic carbon content of DOC and low  $\text{Cl}^-$  levels of 18.5 mg/L were associated with greater  $\text{Hg}^{2+}$  uptake and high recovery (2 times greater than in stream water 2). This might be due to the dominance of Hg-DOC species. In comparison, the  $\text{Hg}^{2+}$  uptake with low aromatic carbon content and high  $\text{Cl}^-$  level of 25.7 mg/L in stream water 2, further confirmed that  $\text{Cl}^-$  ions and DOC competitively controlled the uptake and speciation of  $\text{Hg}^{2+}$ . As a result, an increase of such  $\text{Hg-Cl}^-$  complexes could result in this being the dominating Hg species. However, as the DOC fraction that was present was not chemically characterised, the nature of the Hg-DOC complexes remains unknown.

To sum up, the higher recovery presented in stream water 1 compared with the other samples might be affected by the relatively high DOC concentration, high content of aromatic carbon compounds and low  $\text{Cl}^-$  concentration.

Thus, the variable suppression of colorimetric signal in the presence of high concentration matrix salts is due to:

1. The halide concentrations in the water samples and their interaction with  $\text{Hg}^{2+}$ .
2. The DOC concentrations and their affect on changing the speciation and availability of  $\text{Hg}^{2+}$ .
3. The characteristic of the DOC present, which affects the affinity of Hg for DOC.

#### **6.4.5.3. Treatment of sample with $\text{AgNO}_3$ to remove $\text{Cl}^-$**

Because the presence of  $\text{Cl}^-$  ions significantly affected the membrane's colorimetric analysis, an attempt was made to remove the  $\text{Cl}^-$  from the water samples before the sensing experiment was carried out. A classic method of titration with  $\text{AgNO}_3$  was

conducted. Before the titration, distilled water was spiked with known amounts of NaCl. The molar concentration of NaCl was calculated, and an appropriate volume of AgNO<sub>3</sub> solution added, so that all the Cl<sup>-</sup> ions present in the solution reacted forming a precipitate of AgCl. The white precipitate of AgCl was filtered off, then the samples of filtrate were spiked with 10 µg/L Hg<sup>2+</sup>, diluted up to 300 mL and then pumped through the agar-agar membrane. The membrane was scanned and the colorimetric analysis was conducted against the blank (sample of filtrate diluted up to 300 mL, without Hg<sup>2+</sup> ions).

Formation of the pink colour under these circumstances did still occur, as demonstrated in the blank membrane and Hg<sup>2+</sup> exposed membranes as shown in Fig. 6.28. For the blank membrane, the paper coated with agar-agar immobilised rhodamine B thiolactone also formed a pink colour. This is probably due to reaction with Ag<sup>+</sup> ion (see Section 5.4.4). The presence of AgCl traces can also be observed clearly in the blank image. The AgCl quickly darkens on exposure to light, which caused decomposition to Cl<sub>2</sub> and Ag<sup>0</sup> (signalled by greyish coloration to the membrane).

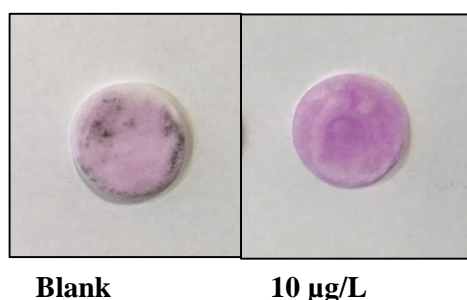


**Figure 6.28: Formation of pink colour on the agar-agar membrane exposed to a blank and 10 µg/L Hg<sup>2+</sup> samples. The samples were treated with AgNO<sub>3</sub> to remove Cl<sup>-</sup>. The appearance of greyish colour indicative of AgCl can be seen on the blank membrane.**

Addition of AgNO<sub>3</sub> did reduce Hg signal suppression by Cl<sup>-</sup>, however, the formation of AgCl on the agar-agar membrane surface may lead to some misleading results. Furthermore, AgNO<sub>3</sub> is expensive and the cost would be prohibitive for routine use.

#### 6.4.6. Recycling of agar-agar membrane with KI

The recycling of agar-agar entrapped rhodamine B thiolactone membrane was determined by re-using the agar-agar membranes for several cycles. For each cycle, agar-agar membrane was exposed to  $10 \mu\text{g/L Hg}^{2+}$ , scanned and then treated with a solution of KI by adding it dropwise on the surface of the exposed membrane. After completion of each KI- $\text{Hg}^{2+}$  reaction cycle, the agar-agar membranes were scanned. This was repeated for the following next cycle.

Results indicated that the spectral sensing was reversible. The pink colour produced by the Hg-rhodamine B thiolactone complex disappeared immediately upon treatment with KI, (possibly due to the formation of  $[\text{HgI}_4]^{2-}$ ) and then was restored again after the treatment with  $\text{Hg}^{2+}$ . As shown in Fig. 6.29, the recycling efficiency is indicated by the grayscale intensity values  $G_G/G_{G0}$  being as high as 99.2%, 101% and 103% for the second, third and fourth cycle, respectively. This regeneration capability makes the sensor much more practical as it can be recycled and reused at least four times.

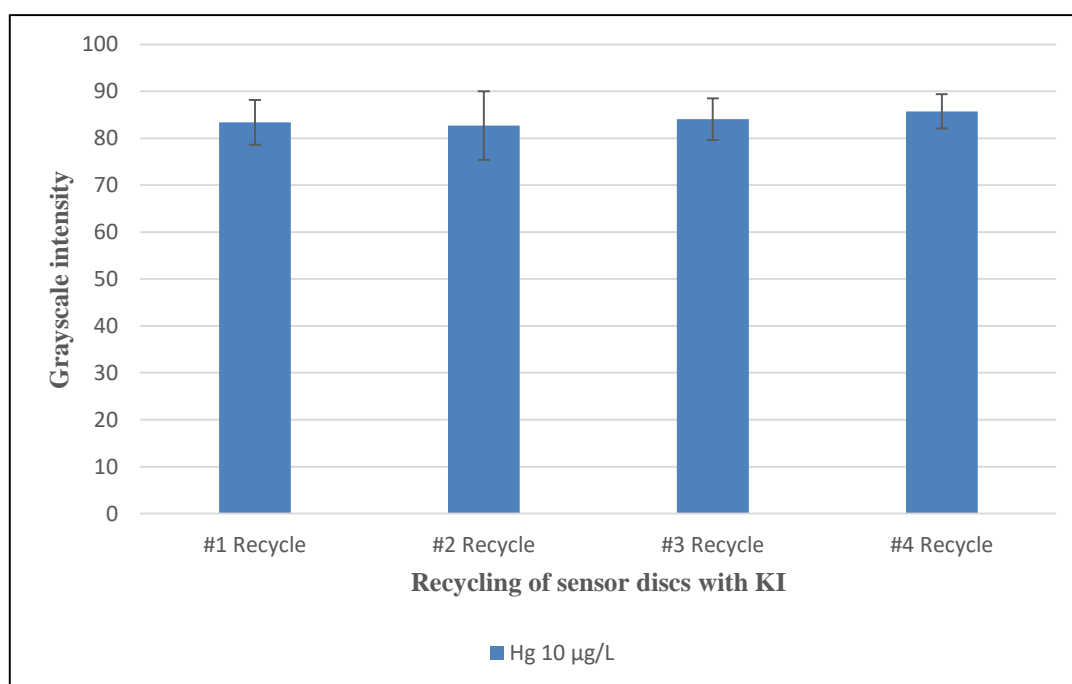


**Figure 6.29: Recycling efficiency of immobilised agar-agar membranes for several cycles. For each cycle, agar-agar membranes were exposed to  $10 \mu\text{g/L Hg}^{2+}$ , then treated with a solution of KI; error bars represent one standard deviation (n=3).**

## 6.5. Conclusion

In this work, along with the sol-gel method, an agar-agar immobilised rhodamine B thiolactone method for a simple colorimetric analysis of  $\text{Hg}^{2+}$  concentration in standard solution samples as well as in real samples were presented. The immobilisation of rhodamine B thiolactone into a solid substrate of filter paper coated with agar-agar colloid was successfully optimised to determine the  $\text{Hg}^{2+}$  in aqueous solutions. This was performed by reducing the preparation time and the chemical reagents used, choosing the strength of the colloid to be 1% (w/v) agar, and reducing the colorant reagent to agar-agar colloid ratio to 1:5 (v/v). To maintain sufficient colorimetric response, the volume of water samples was optimised to be 300 mL.

Filtration of  $\text{Hg}^{2+}$  samples through the membrane, allowed traces of  $\text{Hg}^{2+}$  to be entrapped and colourised simultaneously. The change of colour from white to pink could be discriminated clearly by naked eye with  $\text{Hg}^{2+}$  concentration of 1  $\mu\text{g/L}$  and 0.4  $\mu\text{g/L}$  when the sol-gel matrix and agar-agar colloid were used, respectively.

A simple colorimetric analysis approach using the grayscale intensity values of the coloured membranes for selective  $\text{Hg}^{2+}$  determination was developed. The membrane images were scanned by a flatbed scanner and the colour intensity signal was further analysed using ImageJ software. Under the optimised conditions, the approach showed high sensitivity, low limit of detection and good performance. The proposed agar-agar membrane method allowed for  $\text{Hg}^{2+}$  detection in a range 0.2 to 6  $\mu\text{g/L}$ , with good linear correlation of  $r^2=0.990$  and limit of detection of 0.2  $\mu\text{g/L}$ . The same reaction between  $\text{Hg}^{2+}$  and rhodamine B thiolactone in the sol-gel membrane resulted in a detection range between 0.4 to 5  $\mu\text{g/L}$ ,  $r^2=0.983$  and detection limit of 0.4  $\mu\text{g/L}$ .

Furthermore, the sensory stability and reactivity of membranes during storage was evaluated. The sol-gel membranes were stable for up to 12 weeks when stored at low temperature or kept free from oxygen. The agar-agar showed more stability when exposed to air at room temperature, up to one week. For long term storage, the stability improved further when the membranes were kept in a dark place up to 12 weeks. Regarding the reactivity, only the stored membranes free from oxygen or at low temperature (sol-gel membranes) and the agar-agar membranes stored in a dark place showed the best sensing reactivity and came closest to the control signal.

Practical analysis of real water samples was also demonstrated with an acceptable performance of 106% recovery with spiked tap water. The spike recoveries of other water samples were lower ranging from 0.168% to 43.9%. It was suggested that the suppression of colorimetric signal was due to the presence of a high concentration of  $\text{Cl}^-$  ions. Preliminary evidence suggested this effect might be reduced in water sample with high aromatic content of DOC. Attempts to remove  $\text{Cl}^-$  using  $\text{Ag}^+$  ion were partially successful, but this is not a practical solution for routine use. Therefore, there should be a consideration for alternative approaches to remove  $\text{Cl}^-$  from environment water sample prior analysis.

Finally, the present work indicated the possibility of recycling the rhodamine B thiolactone immobilised agar-agar membranes over the full four cycles during analytical sensing use.

It has been shown that accurate applications will be obtained in water samples with  $\text{Cl}^-$  concentration  $\leq 1$  mg/L (either water that intrinsically contains low levels of  $\text{Cl}^-$  or samples that have had sufficient removal of  $\text{Cl}^-$ ). It would be useful to have the option to apply the method outside the laboratory setting, e.g., at a water treatment facility, reservoir, lake or stream. Therefore, further work in Chapter 7 will explore the use of a battery-powered peristaltic pump, built-in camera portable smartphone and specially designed lightbox. This method was developed to be easily used in the field for  $\text{Hg}^{2+}$  determination in contaminated water samples.

## 7. Development of a portable smartphone colorimetric readout device

### 7.1. Introduction

The development of equipment for digital imaging for quantitative colorimetric detection has occurred very rapidly over recent years. Devices such as high-resolution digital cameras and smartphones have been extended for imaging and sensing *via* the addition of accessories to improve their portability and ease-of-use. Therefore, the requirement for separate detectors and laptop computers for data processing has been eliminated.<sup>287</sup> Smartphones have been used routinely for various purposes outside of basic communication, especially colorimetric detection in different areas such as food safety,<sup>288, 289</sup> environmental monitoring,<sup>290-292</sup> and as point-of-care platforms for healthcare-related applications.<sup>129, 254, 293</sup>

An essential characteristic of smartphones is their cameras. A typical smartphone is commonly provided with at least two high-resolution digital cameras: one on the front and one on the back. The quality of these cameras is in the order of megapixels, which means that each image is divided into millions of monochromatic portions. Furthermore, a camera is not only a lens; several features such as white balance, optical digital zoom, autofocus, ambient light sensors, night-vision filters, and stabilisers are included for image improvement.<sup>294</sup> Therefore, it is generally more convenient for the user to capture images using built-in digital cameras in a mobile phone instead of other high-quality portable digital cameras.

The simplicity of use of smartphones is based on the measurements of the shade, intensity or brightness of coloured samples in a digital image made for this purpose. Furthermore, it is now possible to immediately transmit data to experts in the subject area and access the results without delay *via* wireless connections in remote areas.<sup>295</sup>

The built-in digital camera in smartphones can recognise small differences in colour tone. However, using them for accurate colorimetric measurements requires careful control over parameters such as ambient light and the distance between the camera and the sample. Several studies have reviewed the use of a control housing lightproof

box or phone reader attachment in portable colorimetric assays.<sup>241, 249, 253, 254, 294, 296-300</sup> These studies used an external lamp or an LED as light source to monitor and maintain the illumination of the sample. To avoid the need for any other external elements and simplify the operational design, a few studies have reported an adapted use of the built-in camera, with collimating lenses as a detector and the flash as the light source.<sup>301-303</sup> Alternatively, in other approaches no adapter was needed as the ambient light was controlled with the flash only.<sup>304</sup> However, for validation of these devices complicated image-processing and procedures were conducted; for example, the whole process had to be carried out in a dark environment. These drawbacks make such devices inappropriate for portable colorimetric application in the field.

To provide a field-portable, cost-effective, and wirelessly connected platform to sensitively quantify  $\text{Hg}^{2+}$  ion concentrations in water samples, a battery-powered mobile sensing device was developed. This system consisted of a lightweight homemade lightproof box and a smartphone integrated with a custom-developed data processing application for  $\text{Hg}^{2+}$  quantification.

Chapter 7 investigates whether the built-in digital camera in a mobile phone can be introduced instead of a flatbed scanner to facilitate the development of a portable field device for rapid  $\text{Hg}^{2+}$  quantitative analysis.

## **7.2. Aim**

A mobile phone with built-in digital camera was utilised instead of the scanner in Chapter 6 to analyse  $\text{Hg}^{2+}$ -exposed agar-agar membranes. The built-in camera within the smartphone was selected to meet the requirement of timely and in-field detection. Specific objectives were;

- To use a homemade lightproof box and battery-powered peristaltic pump to create an affordable, accurate, and easy-to-use field-portable method that would enable active screening for  $\text{Hg}^{2+}$  contamination in water.
- To develop a user-friendly Java support application (App) to analyse the images captured by a smartphone built-in camera.

- To compare the performance of the built-in digital camera within a smartphone with that of the scanner, in order to establish the feasibility and comparative accuracy of using the phone as a field-portable detector.
- To assess the reliability and applicability of the method with spiked water samples.

### **7.3. Experimental**

#### **7.3.1. Reagents and apparatus**

The reagents and apparatus used for the determination of  $\text{Hg}^{2+}$  based on filtration through agar-agar membranes were as described in Section 3.6.1.

#### **7.3.2. Solutions preparation**

The stock  $\text{Hg}^{2+}$  standard solution and stock rhodamine B thiolactone solution were prepared as described in Section 3.6.2.1.

#### **7.3.3. Preparation of agar-agar membranes**

The agar-agar membranes were prepared as described in Section 3.6.2.3.

#### **7.3.4. General procedure for colour development and data analysis**

The experimental procedure used for colour development was detailed in Section 3.6.2.4. After completion, the exposed sensors were photographed inside a homemade lightproof box using the built-in digital camera of an iPhone 7.0 Plus (designed by Apple in California, assembled in China). The average intensity of the  $G_G$  for the images obtained from each standard solution was explored using Strathclyde Hg-Sense App software. The concept of the App was initially construed by M Dunlop and K Nshnsh, University of Strathclyde 2017, and written in HTML5/JavaScript by M Dunlop.

## 7.4. Results and discussion

### 7.4.1. Lightproof box design and Hg-Sense App data processing

In order to minimise interference from environmental effects such as ambient light, the analysis performed in this study was carried out in a homemade lightproof box. A 3D model was created using commercial CAD drawing software before being sent to a laser cutter (Fab Lab, University of Strathclyde). As illustrated in Fig. 7.1, the lightproof box consisted of an opaque chest made of 3 mm thick wood with the following dimensions: W 9.8 cm × L 18.5 cm × H 6.8 cm. The internal walls of the box were covered with a layer of matt black paper, in order to provide uniform illumination and to minimise specular reflection.



**Figure 7.1: Homemade lightproof box.**

Coloured agar-agar membrane sensors were photographed inside the lightproof box under the same lighting conditions to obtain the best detection performance. The built-in digital camera of the iPhone 7.0 Plus was adjusted to flash 'on' and 'Auto' high dynamic range (HDR), with the aim of providing a constant light source during the image capturing process. Images were recorded for both the blank and Hg<sup>2+</sup> exposed membranes. Each image was saved as a Portable Network Graphic (PNG) file format on the iPhone's memory at 4032×3024 pixels.

When a new test started, the  $G_G$  of the exposed membrane could be measured by the Hg-Sense App through either directly taking a picture or selecting existing photos which were previously captured by the phones' camera or transferred from other devices *via* Bluetooth, Wi-Fi, *etc.* Once the images were captured, they were cropped to the middle of the image to approximately 2998×3295 pixels, and then opened in the Hg-Sense App to extract the grayscale intensity information. The Hg-Sense App also works off-line on desktops (from photo files) and iOS/Android (from camera or photo files). The grayscale intensities of the cropped area were then acquired by;

- defining the region of the blank sensor area and using the 'background' tool.
- defining the region of the  $Hg^{2+}$  exposed sensor area and using 'filter paper' tool.

The software performed a scan of the pixels in the defined regions, subtracted the blank value and then calculated the  $G_G$  value of each sample. The  $G_G$  intensity value from the sample was reported on the screen. Three replicate images corresponding to three exposed sensors were averaged and used as one point in all graphs presented in this Chapter.

## **7.4.2. Evaluation of the proposed portable method**

### **7.4.2.1. Method performance with and without homemade lightproof box**

To evaluate the performance of the built-in camera as a detector and the phone's flash as a light source, colorimetric detection was performed by comparing the signal intensities in  $G_G$  of a coloured agar-agar sensor under different lighting conditions. Also, comparison was conducted with different distances between the phone's camera and the sensor. The coloured sensor was photographed in triplicate and examined using the Hg-Sense App. The images were captured under different lighting conditions (Fig. 7.2), in room light with different distances between the phone's camera and the coloured sensor (Fig. 7.3), and inside the lightproof box using the phone's flash only (Fig. 7.4).

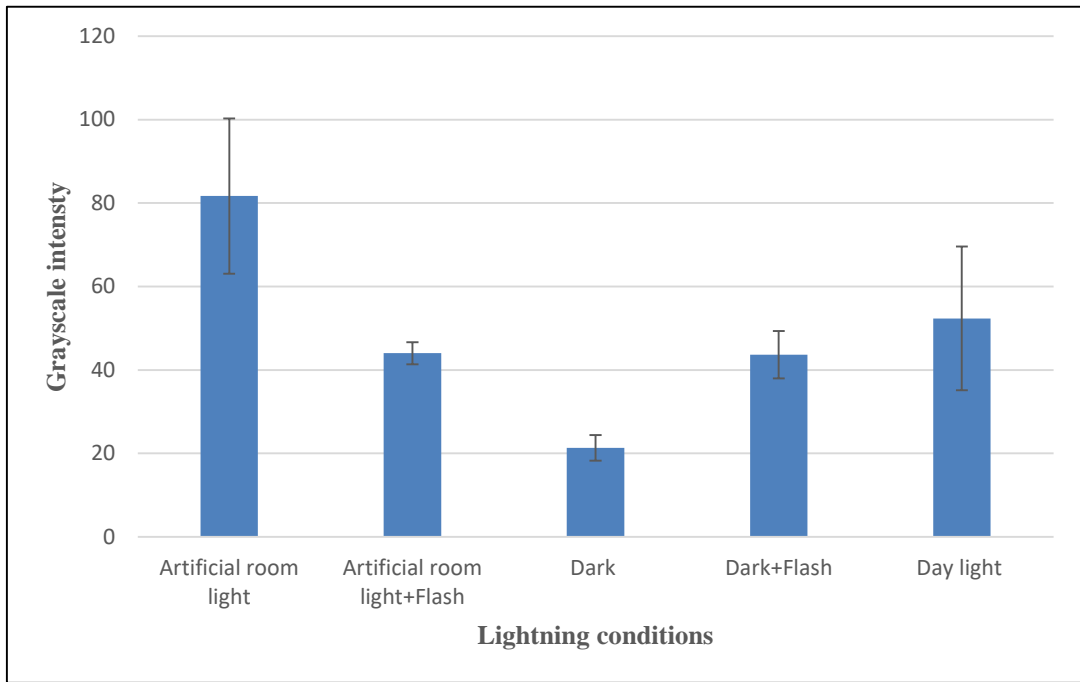


**Figure 7.2: Influence of different lighting conditions on the colorimetric values in the  $G_G$  of the coloured agar-agar membrane captured using the built-in digital camera in an iPhone. Images were captured without a lightproof box; error bars represent one standard deviation (n=3).**

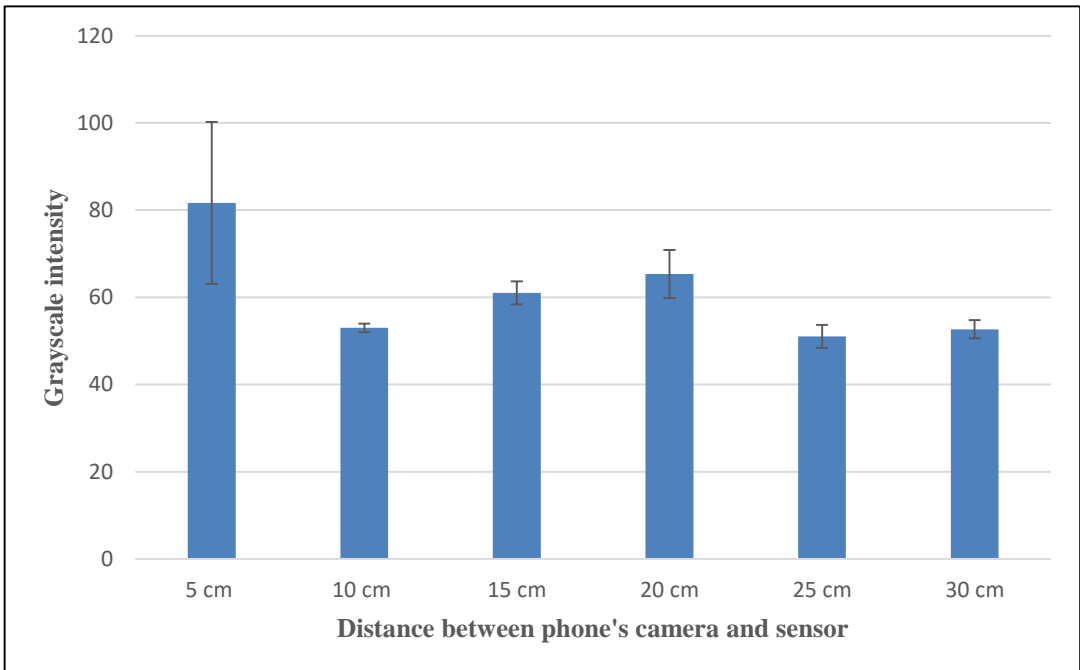


**Figure 7.3: The colorimetric values in the  $G_G$  of the coloured agar-agar membrane captured at different distances between the built-in digital camera in an iPhone and the membrane. Images were captured under artificial room light; error bars represent one standard deviation (n=3).**

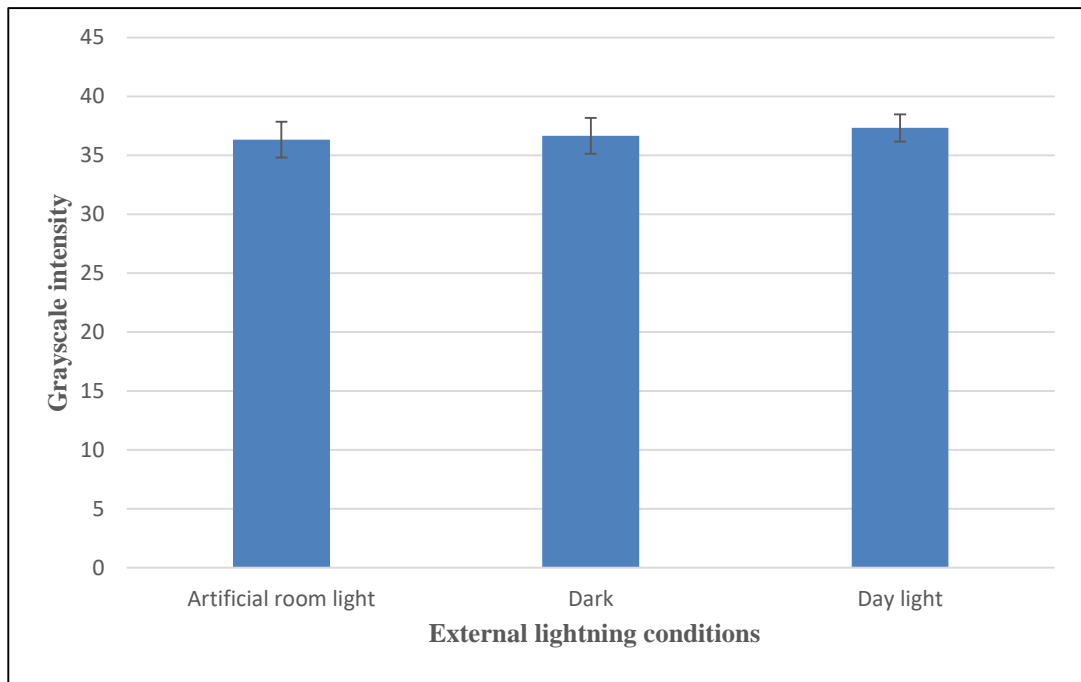


**Figure 7.4: Influence of different external lighting conditions on the colorimetric values in the  $G_G$  of the coloured agar-agar membrane captured using the built-in digital camera in an iPhone. Images were captured inside a lightproof box; error bars represent one standard deviation ( $n=3$ ).**

The results revealed that the signal intensities in  $G_G$  of the coloured sensor under different conditions were varied. For the images captured without the lightproof box, the  $G_G$  measured for the coloured sensor under different lighting conditions were significantly different. The repeatability represented by RSDs varied from 6.01% for images obtained in the artificial room light with flash mode to 32.9% for a daylight images. It seems that the daylight and room light saturated the colour further, resulting in high variation. The slightly better precision values of the  $G_G$  in the room light and the dark images using the camera's flash (6.01% and 13.0%, respectively) may be credited to the constant source of light (flash) saturating the colour equally.

The recorded signals at the different distances between the phone's camera and the coloured sensor were also different. Differences in pixel and focal length among various distances likely affected the measured grayscale intensity.

The use of the flash mode with the lightproof box gave remarkably similar  $G_G$  regardless of the different external lighting conditions. There was no statistical significant difference (t-test at 0.05 significance level). In terms of precision, the RSD values obtained by the proposed lightproof box method were identical regardless of

external lighting. The RSD values were  $\leq 4\%$ , which were better than the corresponding values without the lightproof box. This finding may be attributed again to the constant lighting condition in the lightproof box offered by the camera's flash. Therefore, the developed smartphone colorimetric reader using the built-in flash camera combined with a lightproof box was selected for further use.

#### 7.4.2.2. Comparison of the portable smartphone reader with use of a scanner

In order to demonstrate the use of a smartphone as a field colorimetric readout device, the performance of the built-in digital camera in an iPhone was compared with that of the scanner. To establish this, the results of grayscale intensity in  $G_G$  obtained with the Hg-Sense App for iPhone were compared with those obtained from desktop ImageJ for scanner. Single exposed agar-agar membrane was scanned and photographed by the scanner and the phone-lightproof box ten times each. The images were captured with re-positioning the sensor each time. The grayscale intensity of the ten measurements of the compared methods are shown in Fig. 7.5.

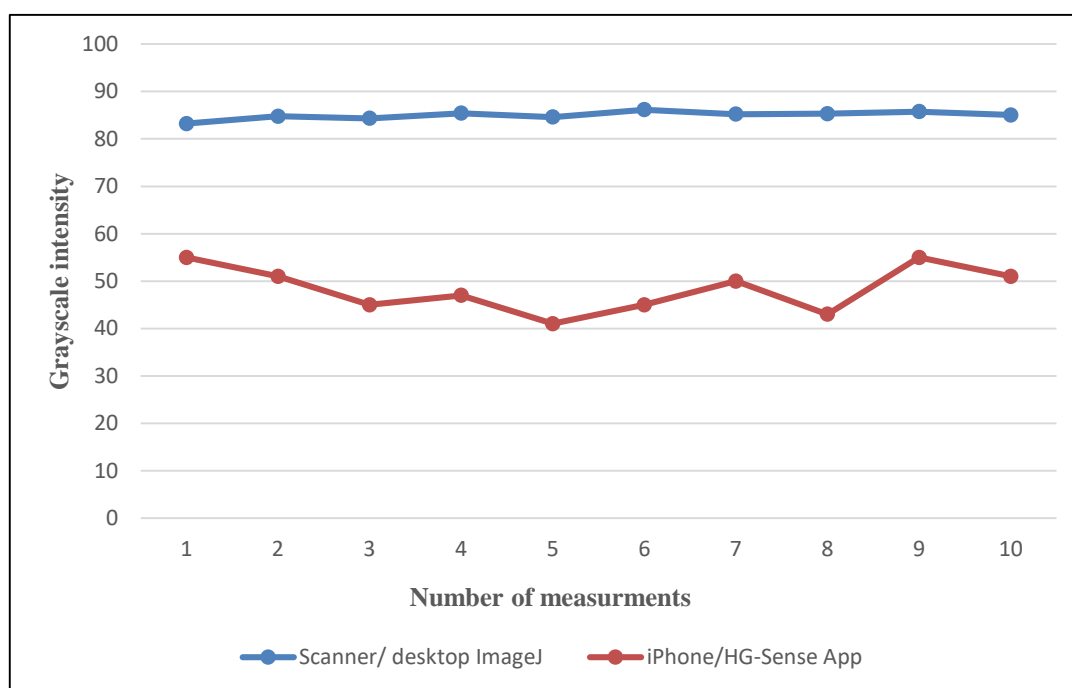


**Figure 7.5: The stability and repeatability of the measurement taken using the Hg-Sense App for iPhone and the desktop ImageJ for flatbed scanner.**

Fig. 7.5 shows that, despite differences in the measured  $G_G$  intensities from the Hg-Sense App and ImageJ, the ratio of the measured values presented are almost equal for the 10 measurements. However, these results were more precise in ImageJ with a standard deviation of  $85.0 \pm 0.815$  and an RSD value of 0.959%, while the standard deviation and RSD for the Hg-Sense App were  $48.3 \pm 4.85$  and 10.1%.

It is worth pointing out that the noticeably high standard deviation that occurred with the Hg-Sense App could be because not all the area of the exposed agar-agar membrane was analysed. Each sampled image was a matrix with  $2998 \times 3295$  pixels and the defined region used by the App was a matrix with about  $20 \times 20$  pixels. The images were cropped to the best-fit within the certain size area frame, as shown in Fig. 7.6.

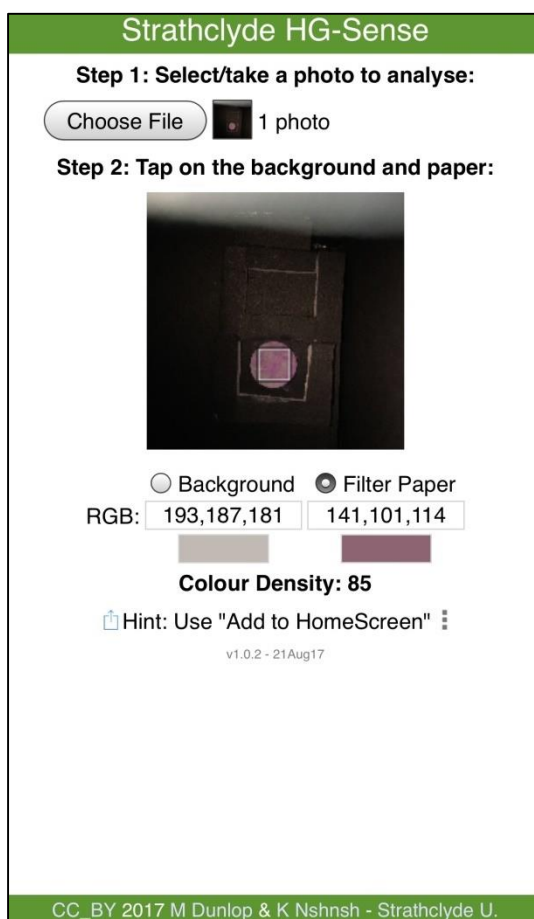


**Figure 7.6: Defined region of a agar-agar membrane image with  $20 \times 20$  pixels that was captured during analysis with the Hg-Sense App.**

The  $G_G$  values were calculated based on the position of the defined region within the sensor paper; only the area in the defined border was measured. Because the defined region did not cover the whole paper and the colour was not distributed equally, the re-positioning of the exposed paper sensor changed the defined area each time.

The grayscale intensity of a number of the agar-agar membranes exposed to different  $Hg^{2+}$  concentrations were then measured using both the iPhone/Hg-Sense App and scanner/desktop ImageJ. The results obtained for these samples by the two devices were plotted against one another. The two sets of measured  $G_G$  values showed a 90% correlation with a  $Hg^{2+}$  range from 0.8 to 10  $\mu g/L$  as illustrated in Fig. 7.7. These results indicate that the performance of the portable Hg-Sense App method were acceptable and could be compared with the laboratory method.

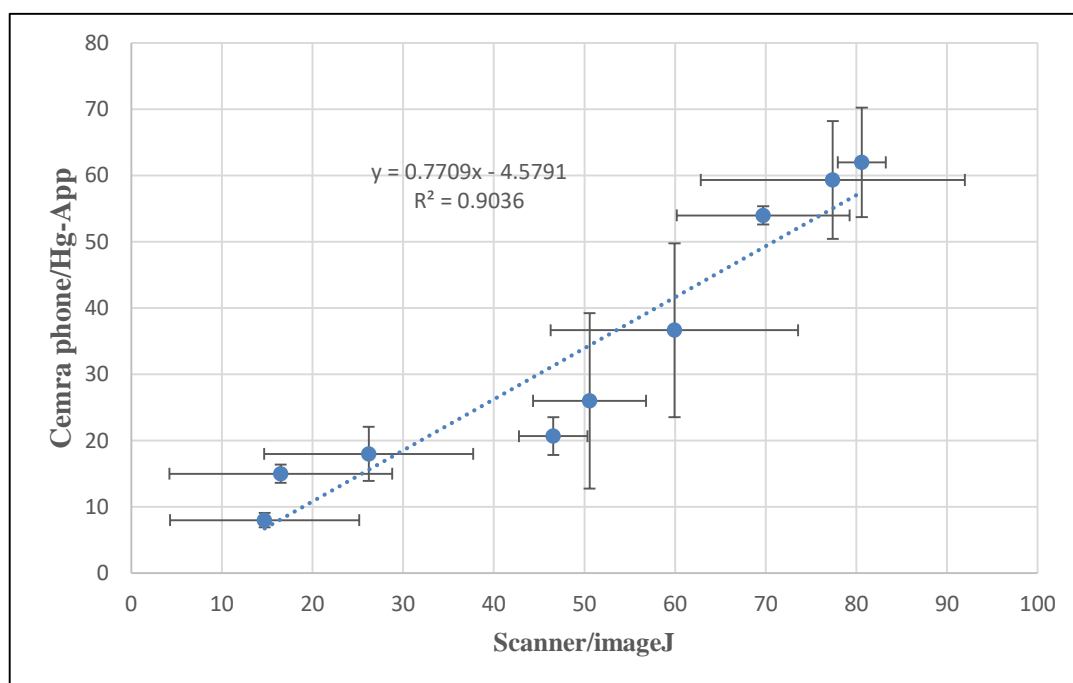


**Figure 7.7:** The correlation between the portable Hg-Sense App method and the laboratory-based ImageJ method; error bars represent one standard deviation ( $n=3$ ).

#### 7.4.2.3. Evaluation of the portable peristaltic pump

For a device to be reliable, the importance of its stability and accuracy is self-evident. In order to use the portable colorimetric method in the field, it is necessary to use a portable peristaltic pump. Different  $Hg^{2+}$  concentrations (low, medium and high) were

pumped in triplicate through agar-agar membranes using two types of peristaltic pumps: a battery-powered, single-channel peristaltic pump (Field-Flow Compact Peristaltic Pump, RVA Synergies Ltd.) and a multi-channel peristaltic pump (laboratory based use). The exposed membranes were scanned and analysed.

The  $G_G$  values for each set of  $Hg^{2+}$  concentration were compared as illustrated in Fig. 7.8. The results of these devices were similar. The statistical analysis (t-test at 0.05 significance level) (see Table A5.8 in Appendix 5) revealed that no differences were found among the measurements of each replicate, indicating that the battery powered peristaltic pump was fit-for-purpose.

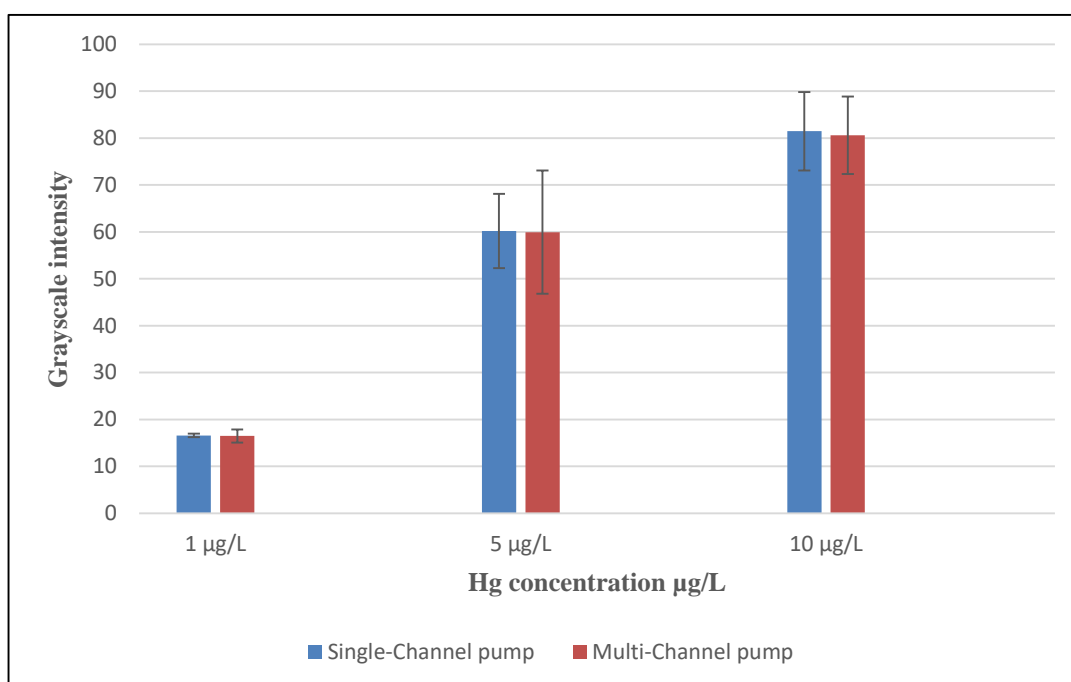


**Figure 7.8:** Comparison between the  $G_G$  values obtained using the battery-powered single-channel peristaltic pump (field based) and the multi-channel peristaltic pump (laboratory based). Concentration of  $Hg^{2+}$  used were 1, 5 and 10  $\mu\text{g/L}$ ; error bars represent one standard deviation ( $n=3$ ).

#### 7.4.3. Sensitivity of $Hg^{2+}$ quantitation using iPhone Hg-Sense App

In order to obtain quantitative information, a calibration curve was constructed by imaging exposed agar-agar membranes at a series of known concentrations of  $Hg^{2+}$ . After capturing a colorimetric image inside the lightproof box using the built-in digital

camera of the iPhone 7.0 Plus, the images were previewed on the screen, and then digitally analysed following the image-processing steps discussed in Section 7.4.1.

The  $G_G$  values generally increased with the increase in  $Hg^{2+}$  concentration ranging from 0.2 to 20  $\mu g/L$  as shown in Fig. 7.9. It was found that  $Hg^{2+}$  concentration range from 0.2 to 0.6  $\mu g/L$  gave negative responses. When the same exposed agar-agar membranes were measured using scanner/desktop ImageJ, they gave notable colorimetric response (see Table A5.5 in Appendix 5). Therefore, the negative response at low  $Hg^{2+}$  concentration was likely due to a systematic error in the portable method. Since strong lighting is critical for generating good photographic performance, the flash light available for illuminating the images may have been insufficient for membranes exposed to low  $Hg^{2+}$  concentration. Thus,  $Hg^{2+}$  concentrations ranging from 0.2 to 0.6  $\mu g/L$  could be considered below the method detection limit. The intensities of  $G_G$  were correlated well over a  $Hg^{2+}$  concentration range of 0.8 to 8  $\mu g/L$ . Above those concentrations, the colorimetric response appeared to be saturated.

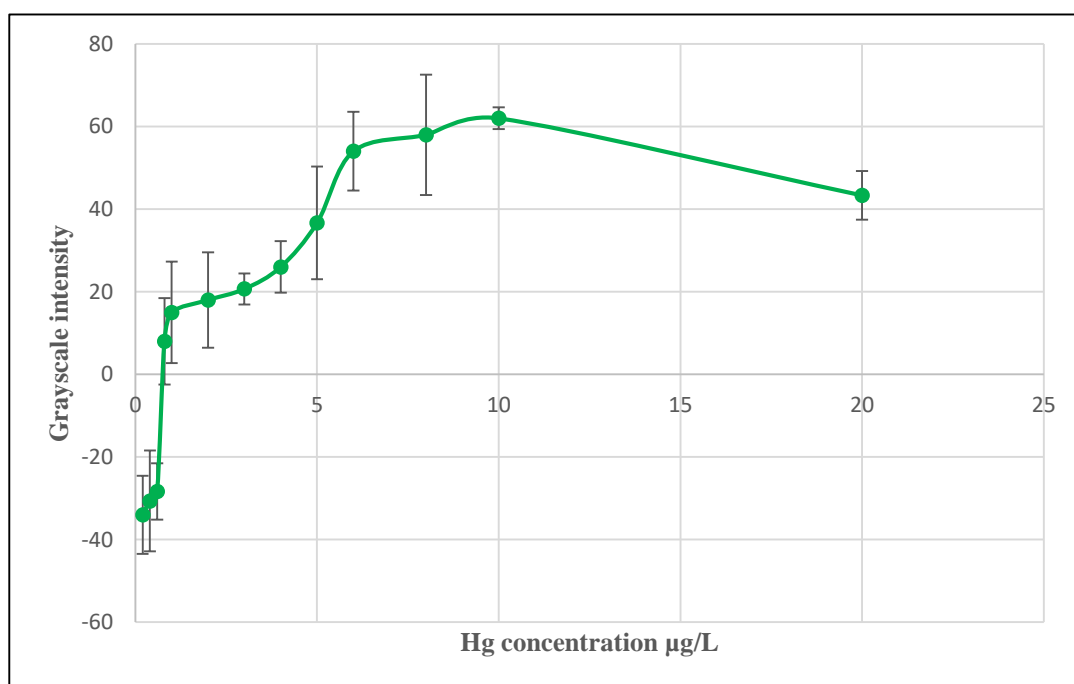


**Figure 7.9:** The relationship between the colorimetric response in  $G_G$  and the concentration of  $Hg^{2+}$  on the exposed agar-agar gel membranes; error bars represent one standard deviation ( $n=3$ ).

A calibration graph was constructed with a good linear fit of  $r^2=0.939$  in the  $\text{Hg}^{2+}$  concentration range of 0.8 to 8  $\mu\text{g/L}$ , as illustrated in Fig. 7.10. The instrumental limit of detection was measured to be 0.8  $\mu\text{g/L}$  with good to moderate precision expressed as RSDs of 2.01% to 26.6% obtained with three experiments (see Table A5.9 in Appendix 5). Each experiment was repeated with three replicate agar-agar sensors at each  $\text{Hg}^{2+}$  concentration tested. The calibration curves of the individual experiments (from 0.8 to 8  $\mu\text{g/L}$ ) each displayed good linear correlation of  $r^2=0.986$ ,  $r^2=0.939$  and  $r^2=0.906$ , as illustrated in Fig. 7.11. Since the repeatability represented by RSDs for the three experiments was acceptable, thus, the results obtained from the proposed readout platform were relatively reasonable and reliable.

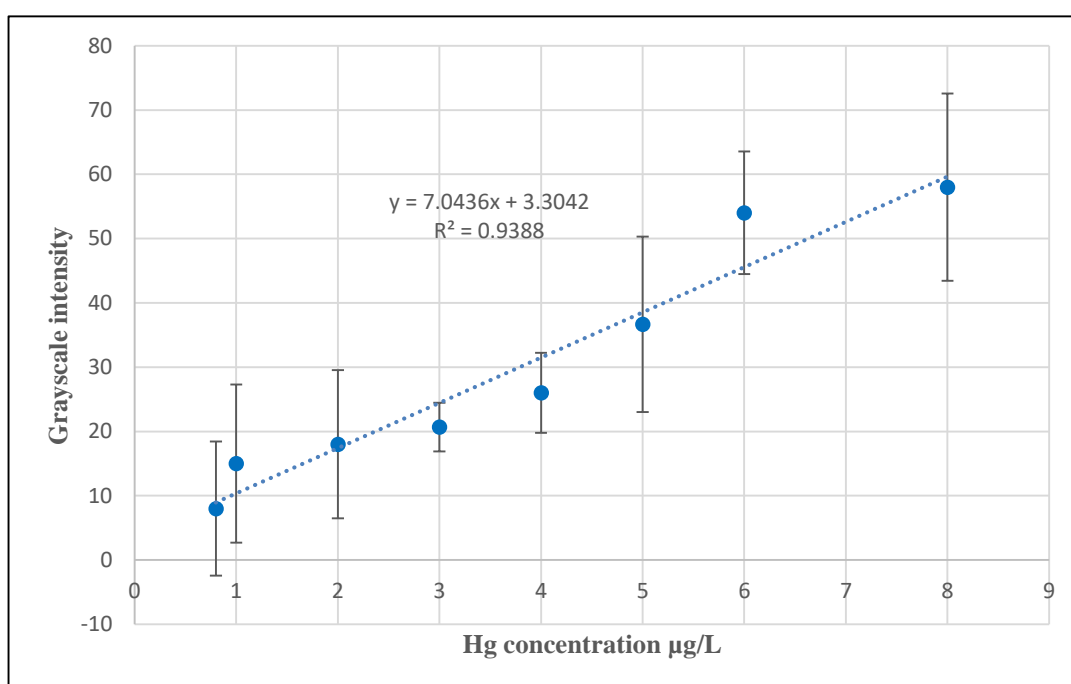


**Figure 7.10:** The linear correlation between the colorimetric response in  $G_G$  recorded by Hg-Sense App of the Hg-rhodamine B thiolactone formed on the agar-agar membranes and  $\text{Hg}^{2+}$  at the concentration range of 0.8 to 8  $\mu\text{g/L}$ ; error bars represent one standard deviation ( $n=3$ ).

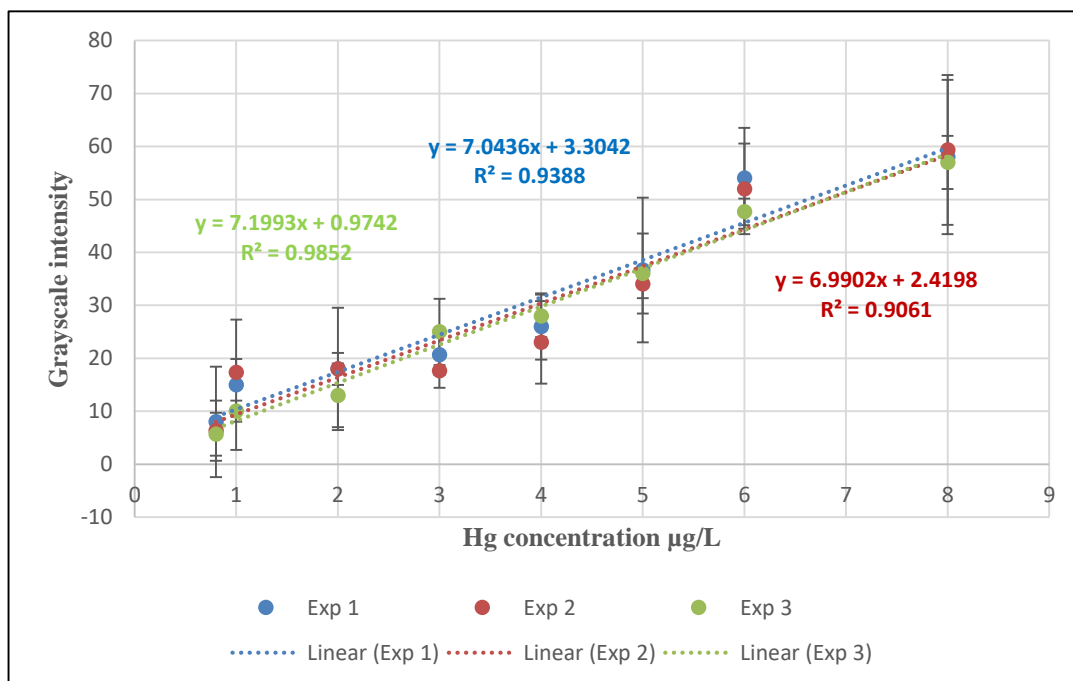


**Figure 7.11: Calibration curves of the colorimetric response in GG recorded by Hg-Sense App of the Hg-rhodamine B thiolactone complex formed on the agar-agar membranes in three repeated experiments (n=3) versus the Hg<sup>2+</sup> concentration range from 0.8 to 8 mg/L; error bars represent one standard deviation (n=3).**

#### 7.4.4. Recovery of developed portable method for Hg<sup>2+</sup> detection

A distilled water sample was spiked with different Hg<sup>2+</sup> concentrations at low, medium and high concentration levels (1, 3 and 5 μg/L) and then pumped through agar-agar membranes. Three repeated measurements were performed at each concentration. The exposed membranes were photographed by the portable method for colorimetric analysis. The G<sub>G</sub> results were read by the Hg-Sense App. The spike values were obtained from the corresponding regression equations and the percentage spike recoveries were calculated for each spike level using Equation 6.1. The results showed that recoveries varied from 88.1% ± 16.2% to 95.0% ± 29.9% (Table 7.1). The measured precision expressed as RSDs from the three replicate indicates that the developed portable method could be a useful tool for the measurement of Hg<sup>2+</sup> concentration.

**Table 7.1: Accuracy Accuracy/recovery study for the triplicate values of the colorimetric response in  $G_G$  recorded at three spiking levels.**

Initial $Hg^{2+}$ $\mu g/L$	$Hg^{2+}$ Spiked $\mu g/L$	$Hg^{2+}$ Found $\mu g/L$ n=3	% Recovery $\pm$ % RSD n=3
0	1	$0.950 \pm 0.284$	$95.0 \pm 29.9$
0	3	$2.61 \pm 0.671$	$86.9 \pm 25.7$
0	5	$4.40 \pm 0.714$	$88.1 \pm 16.2$

Results are mean  $\pm$  SD; n = number of replicates.

## 7.5. Conclusion

The feasibility of utilising a smartphone colorimetric reader as a field detection technique for  $Hg^{2+}$  was demonstrated. Previously reported colorimetric readout platforms used external light source, adapters or other devices to maintain a constant distance between the camera and the sample, separate digital cameras, or sometimes external Apps to measure light intensities of a colorimetric substrate. These approaches were neither portable nor user-friendly. The proposed field-portable method has the following advantages:

1. The colorimetric assay requires only one simple accessory, a lightweight lightproof box, therefore simplifying the procedure design.
2. The developed reader uses simplified built-in flash as a light source to illuminate the images during capture.
3. The simplicity of a user-friendly Hg-Sense App for performing colorimetric detection developed for automatic reading of the  $G_G$  values only.
4. The developed smartphone-based colorimetric reader is compatible with a battery-powered, field-based peristaltic pump to on-site analysis.

The combining of built-in flash mode and the lightproof box gave robust grayscale intensities regardless of the surrounding lighting conditions. The  $Hg^{2+}$  quantitation results obtained using the iPhone Hg-Sense App correlated well with those obtained using a laboratory scanner/desktop ImageJ, confirming the reliability and repeatability of the proposed method. In addition, no differences were found between the results obtained using the field-based and laboratory-based peristaltic pumps, validating the field-portability of the readout platforms. It was found that the quantitation of  $Hg^{2+}$

was achieved with a detection limit of 0.8  $\mu\text{g/L}$ , which is significantly lower than the maximum allowable  $\text{Hg}^{2+}$  level in drinking water of 2  $\mu\text{g/L}$  within EPA guidelines. Practical analysis of spiked samples was also demonstrated, giving 88.1%  $\pm$  16.2% to 95.0%  $\pm$  29.9% recoveries.

The proposed readout platform appears to be relatively portable. Furthermore, it provides both qualitative and quantitative determinations of  $\text{Hg}^{2+}$  with an acceptable error range. However, areas for further research were noted. Each mobile phone has a different size and design; thus, the colorimetric assay requires a lightproof box designed to be universal. Furthermore, the integrated Hg-Sense App requires further development. The function of re-sizing the defined area is not currently available in the App.

## 8. Conclusions and further work

### 8.1. Conclusion

Inexpensive, lightweight, and rapid qualitative naked eye detection approaches have been widely developed for the detection of  $\text{Hg}^{2+}$  in environmental samples. However, the lack of sensitivity, and/or selectivity, complicated synthesis routes, and difficulties in adapting methods to be easily applied in field-portable format are common drawbacks of many recent colorimetric sensors. In an attempt to solve these problems, this thesis had explored the use of small molecule colorimetric sensors for  $\text{Hg}^{2+}$  determination in aqueous solution

In the early stages of this study (Chapter 4), the analytical performance of three commercially available colorimetric sensors was compared. Cuprous iodide, DPC, and R6G were used in solution, in spot test mode (both as wet reagents and when dried onto filter papers), and in a Hg bubbler apparatus.

Reactions between  $\text{Hg}^{2+}$  and CuI, DPC and R6G were observed. Both DPC and R6G produced a colorimetric response in the solution phase. In spot test mode, CuI did not react with  $\text{Hg}^{2+}$ . The original colour of the detecting paper was bleached off upon the addition of  $\text{Hg}^{2+}$  standard solutions. The Hg-DPC compound formed with the coordination of DPC to  $\text{Hg}^{2+}$  was suitable for colorimetric determination of  $\text{Hg}^{2+}$  in wet paper condition. The intensity of the purple coloured complex obtained increased as the concentrations of  $\text{Hg}^{2+}$  in the standards increased. A concentration of 5 mg/L was the lower detection limit that could be observed by the naked eye. However, because of the oxidation of the DPC on the dried test papers, this reagent could not be used in dry paper condition, nor adapted to the Hg bubbler apparatus. The reaction between  $[\text{HgI}_4]^{2-}$  and R6G was successfully achieved by producing  $[(\text{HgI}_4)^{2-}(\text{R6G})^+]_2$  which had a pink colour both in wet and dry spot test mode. However, leaching of R6G was observed upon addition of Hg standards under dry papers condition.

The Hg bubbler apparatus was found to be applicable to R6G as well as the original CuI reagent. The absorbance spectra of Hg-complexes formed were measured directly on the surface of detecting papers using UV-vis reflectance spectroscopy. Linear

calibration between the absorbance and Hg concentrations was obtained with a strong correlation coefficient of  $r^2=0.9726$  and  $r^2=0.923$  for  $\text{Cu}_2[\text{HgI}_4]$  and  $[(\text{HgI}_4)^{2-}(\text{R6G})^+]_2$ , respectively. A concentration of 2  $\mu\text{g/L}$  was considered as the lower limit of detection spectroscopically for both probes.

It was found that the exposed CuI detecting papers should be stored away from light. Direct light caused an increase in colour fading. Also, the comparison of the colour intensity between the standards and environmental samples should be conducted within the first hour of colour development. The CuI detecting papers should be suitable for use worldwide as the coating was not affected by the investigated storage temperatures at 4°C, 25°C and 35°C.

In the second part of this study (Chapter 5), rhodamine B thiolactone, a convenient colorimetric sensor for the visual detection and spectroscopically quantification of  $\text{Hg}^{2+}$ , was successfully synthesised. It was prepared in 48% overall yield from rhodamine B base.  $^1\text{H}$  NMR spectroscopy,  $^{13}\text{C}$  NMR spectroscopy and X-ray crystallography were used to confirm the thiospirocyclic structure of rhodamine B thiolactone.

The stability of solid rhodamine B thiolactone was investigated under different storage environments. It was found that the light yellow needles of the chemosensor changed colour to pink easily at room temperature. The compound was only stable at low temperature -18 °C away from light. It is likely that the action of light and temperature accelerate the ring opening of the product.

The sensing response was based on the ability of  $\text{Hg}^{2+}$  to induce ring opening of rhodamine B thiolactone. The produced Hg-rhodamine B thiolactone complex had a characteristic pink colour. It was found that optimal performance was obtained when the reaction mixture solution contained a minimum of 25  $\mu\text{M}$  chromogenic reagent.

The colorimetric detection provided a rapid, simple detection method both visually, and when quantified *via* spectrophotometry, with detection limits of 50  $\mu\text{g/L}$  and 10  $\mu\text{g/L}$ , respectively. The UV-vis absorbance titration spectra of Hg-rhodamine B thiolactone with a  $\text{Hg}^{2+}$  range from 0 to 1000  $\mu\text{g/L}$  showed a linear calibration with a strong correlation of  $r^2=0.997$ .

Moreover, rhodamine B thiolactone was extremely selective for  $\text{Hg}^{2+}$ . It was found that the presence of even 5 mg/L of  $\text{As}^{3+}$ ,  $\text{Cd}^{2+}$ ,  $\text{Co}^{2+}$ ,  $\text{Cr}^{3+}$ ,  $\text{Cu}^{2+}$ ,  $\text{Fe}^{3+}$ ,  $\text{Mg}^{2+}$ ,  $\text{Mn}^{2+}$ ,  $\text{Na}^+$ ,  $\text{Ni}^{2+}$ ,  $\text{Pb}^{2+}$  and  $\text{Zn}^{2+}$  did not interfere with the detection of  $\text{Hg}^{2+}$ . The exception was that the presence of 1000  $\mu\text{g/L}$   $\text{Ag}^+$  showed a small response.

Rhodamine B thiolactone was successfully tested for the colorimetric analysis of artificial seawater. No significant colour change was observed in the blank sample. The applicability of the rhodamine B thiolactone to detect  $\text{Hg}^{2+}$  in spiked artificial seawater was successfully achieved with a detection limit of 200  $\mu\text{g/L}$ . Furthermore, visual detection in the form of a spot test was successful in wet and dry conditions with a detection limit of 100  $\mu\text{g/L}$ . However, because of the colour change of rhodamine B thiolactone on the dried discs, misleading results could be obtained.

Chapter 6 involved the design of a naked eye membrane sensor for rapid determination of  $\text{Hg}^{2+}$  in water samples. The  $\text{Hg}^{2+}$ -sensing rhodamine B thiolactone was immobilised in agar-agar colloid, as well as the previously-reported sol-gel matrix, to develop chromogenic membranes. The membranes were deposited on filter papers. Pumping  $\text{Hg}^{2+}$  samples through the membranes changed the colour from white to pink. Digital image-based analysis of pink Hg-rhodamine B thiolactone complex was used for the quantification of  $\text{Hg}^{2+}$  using a flatbed scanner and the ImageJ software.

In order to optimise the sensing conditions for the agar-agar membrane, a number of experiments were conducted. The concentration of the agar colloid was chosen to be 1% ( $w/v$ ) agar. The optimal ratio of added chromogenic reagent to agar-agar colloid was 1:5 ( $v/v$ ), and 300 mL was selected as the optimised water sample volume for the reaction.

The coloured Hg-rhodamine B thiolactone could be discriminated clearly by the naked eye with  $\text{Hg}^{2+}$  concentrations as low as of 1  $\mu\text{g/L}$  and 0.4  $\mu\text{g/L}$  when the sol-gel and agar-agar membranes were used, respectively. The correlations between the  $G_R$ ,  $G_G$ , and  $G_B$  values in the RGB colour space and the  $\text{Hg}^{2+}$  concentration were investigated under the optimised conditions. It was found that the  $G_G$  channel captured almost 99% of the total colour change. The membrane-based coloration proved to be a robust and suitable tool for providing a low limit of detection and good performance. The proposed agar-agar membrane allowed for  $\text{Hg}^{2+}$  detection at concentrations as low as

0.2 µg/L. Good linear correlation ( $r^2=0.990$ ) with ImageJ readout was obtained in a  $\text{Hg}^{2+}$  concentration range of 0.2 to 6 µg/L. Good precision (RSDs  $\leq 10\%$ ,  $n=3$ ) was achieved in the analysis of  $\text{Hg}^{2+}$  for spiked water samples. The corresponding values in the sol-gel membrane were in a detection range between 0.4 to 5 µg/L, ( $r^2=0.983$ ) and a detection limit of 0.4 µg/L.

The effects of sol-gel and agar-agar membranes were tested in terms of the sensor stability and their influence on the compound transformation. Furthermore, the reactivity of membranes during storage was evaluated. The most promising performance in terms of preventing colour change and length of storage time was obtained when the agar-agar membranes were kept in a dark place. In contrast, the sol-gel membranes were stable and sensing remained active only when stored at low temperature or kept free of oxygen.

The applicability of the proposed agar-agar membrane was evaluated by determination of  $\text{Hg}^{2+}$  in real water samples. Results indicated that this sensor was suitable for spiked tap water, with a recovery of 106%. However, signal suppression was observed in other water samples, with recoveries ranging from 0.168% to 43.9%. It was suggested that the presence of a high concentration of  $\text{Cl}^-$  ions might contribute to the signal suppression in water samples.

Importantly, it was found that the spectral sensing was reversible. The pink colour produced on the immobilised agar-agar membranes disappeared immediately upon addition of KI and was restored again after exposure to  $\text{Hg}^{2+}$ . This was demonstrated over four cycles.

The final part of the study (Chapter 7), involved successful development of a field-based method for  $\text{Hg}^{2+}$  detection in water samples. A battery-powered peristaltic pump was used to drive the water sample through the agar-agar membranes. The built-in digital camera on a smartphone was used to capture images of the coloured agar-agar membranes inside a homemade lightproof box. The coloured membranes were quantified using a custom developed application (Hg-Sense App), where the relationships between the  $G_G$  intensity and the concentrations of  $\text{Hg}^{2+}$  were obtained. The  $G_G$  intensities were compared to those from a flatbed scanner and ImageJ, confirming the reliability and repeatability of the proposed method.

It was found that the portable platform showed itself to be capable of being used conveniently, while providing acceptable analytical results with low relative errors. The  $\text{Hg}^{2+}$  linear range of 0.8 to 8  $\mu\text{g/L}$ , and low detection limits of 0.8  $\mu\text{g/L}$  achieved were comparable with those from analytical quantification methods. Good linear correlation ( $r^2=0.986$ ,  $r^2=0.939$  and  $r^2=0.906$ ) were obtained with three individual experiments. Good to moderate precision in the range of 2.01% to 26.6% were achieved in the analysis of  $\text{Hg}^{2+}$  standard samples and 16.2% to 29.9% for spiked water samples.

The colorimetric molecule sensors investigated in this work, CuI and R6G (the Hg bubbler apparatus) and rhodamine B thiolactone immobilised membranes (the mechanical flow apparatus) have been successfully used to measure  $\text{Hg}^{2+}$  concentration in water samples. However, rhodamine B thiolactone immobilised agar-agar membrane would be the most fit for purpose. It has been designed and optimised to meet the requirement of inexpensive, readily available, simple and sensitive sensors. The limit of detection achieved was far below the maximum allowable level of  $\text{Hg}^{2+}$  in drinking water (2  $\mu\text{g/L}$  and 6  $\mu\text{g/L}$ ) regulated by the U.S. EPA<sup>44</sup> and WHO,<sup>46</sup> respectively. Therefore, this method can be applied by regulation authorities, not only in developing countries but worldwide. It will be useful where accurate on-site determination of Hg concentration presents a great environmental challenge.

## **8.2. Further work**

In this work, small molecule colorimetric sensors were developed and applied to assess  $\text{Hg}^{2+}$  concentration in water samples. Further experiments could be undertaken using the same sensor systems. For example, the current study has shown CuI detecting papers are a good colorimetric sensor for bubbled  $\text{Hg}^0$ , but further investigation is required to apply the method in the field. In order to avoid using the aquarium pump to carry  $\text{Hg}^0$  to react with the coating, a chemical carrier would be a good substitute. Sodium borohydride ( $\text{NaBH}_4$ ) might be used as reducing/carrier reagent instead of  $\text{SnCl}_2$  and the pump. It is well known that  $\text{NaBH}_4$ , used widely as reductant, reacts with water to form  $\text{H}_2$  gas. The formation of  $\text{H}_2$  gas could be used as the carrier for reduced  $\text{Hg}^0$ . Research effort should be also pointed toward quantification of Hg

formed on the CuI detecting paper. This should be carried out either by using a portable spectrophotometer or a digital imaging device.

Currently, the Hg bubbler apparatus and CuI detecting papers are available in small quantities semi-commercially from the inventors of the approach in Brazil. These can be difficult to obtain in developing countries. Therefore, there is a need to make the approach more easily accessible as a screening tool for academic, industry, and regulatory use.

A clear opportunity for the agar-agar immobilised rhodamine B thiolactone membrane developed in this study would be to explore options to extend the usage to other samples such as sediment pore water and flowing water in the field, without significant sample disturbance.

Sediment systems play an important role in the fate and source of Hg in aquatic bodies. Sediments represent the major sink for  $\text{Hg}^{2+}$  and source for MeHg. Pore water chemistry within the sediment is, thus important to understanding Hg pathways. In this regard, deploying a sampler, e.g., a diffusive gradient in thin-films sampler that incorporates the agar-agar colorant membrane, in sediment or in flowing water for monitoring of Hg concentration would be of interest. Such an approach might estimate accumulated Hg concentration based upon the rate at which the Hg diffuses through a controlled agar-agar membrane. As a result, a more regular water quality monitoring system and background assessment of risk could be conducted. Furthermore, measurement of other Hg species that causes harmful effects to human health, such as MeHg, would be worthwhile in future studies.

For evaluating the impact of  $\text{Cl}^-$  and DOC on the colorimetric sensing, a further in-depth study might be considered. The development of high-performance removal sorbents could be an important issue in sample pre-treatment. For example, the commercially- available OnGuard silver cartridges could be a potential candidate for removing halide species from water samples before colorimetric analysis. Thus, further research in this field is warranted.

It would be also useful to compare the results obtained in this study with alternative molecule sensors that may be more sensitive to Hg, such as Si-rhodamine

thiolactone.<sup>72</sup> The smartphone used for this study was iPhone 7 plus. The effect of using different lenses, cameras, *etc.*, of different smartphones could be investigated. In addition, a universal lightproof box might be designed. In terms of the Hg-Sense App used in this study, it is recommended that further development should be conducted. It is worthwhile to include a function which will permit re-sizing of the defined region, as well as automated calibration of the linear regression. As a result, the App could display more accurate information about Hg<sup>2+</sup> concentration and the suitability of the water to be used.

In addition to Hg contamination, PTE input from anthropogenic sources has been increasing worldwide with rapid industrialisation and urbanisation. Hence, there is a need to extend this type of study to additional PTE, such as As, Cd, and Pb. It would be useful to develop a compact and multi-functional colorimetric sensing platform- a PTE sensor array- to simultaneously measure these elements. Such devices have potential impact to raise public awareness of the possible risk to humans caused by PTE associated with water systems in contaminated areas. They will help government agencies and regulators to make better decisions regarding environmental and public health protection.

## References

1. C. S. C. Wong, X. D. Li and I. Thornton, *Environmental Pollution*, 2006, **142**, 1-16.
2. UNEP, *Global Mercury Assessment Report*, United Nations Environment Programme Chemicals Geneva, Switzerland, 2002.
3. F. M. Morel, A. M. Kraepiel and M. Amyot, *Annual review of ecology and systematics*, 1998, **29**, 543-566.
4. R. P. Mason, A. L. Choi, W. F. Fitzgerald, C. R. Hammerschmidt, C. H. Lamborg, A. L. Soerensen and E. M. Sunderland, *Environmental Research*, 2012, **119**, 101-117.
5. W. C. Li and H. F. Tse, *Environmental Science and Pollution Research*, 2015, **22**, 192-201.
6. UNEP, *Global mercury supply, trade and demand*, United Nations Environment Programme, Chemicals and Health Branch, Geneva, Switzerland, 2017.
7. L. Stokes and R. Saari, Issue Overview: Mercury Emissions and Releases, <http://mercurypolicy.scripts.mit.edu/blog/?p=72>, (accessed December 2016).
8. USEPA, *United States Environmental Protection Agency EPA-452/R-97-005*, 1997.
9. Q. Wang, D. Kim, D. D. Dionysiou, G. A. Sorial and D. Timberlake, *Environmental Pollution*, 2004, **131**, 323-336.
10. G. Compeau and R. Bartha, *Applied and environmental microbiology*, 1985, **50**, 498-502.
11. J. X. Wang, X. B. Feng, C. W. N. Anderson, Y. Xing and L. H. Shang, *Journal of Hazardous Materials*, 2012, **221**, 1-18.
12. R. P. Mason, W. F. Fitzgerald and F. M. M. Morel, *Geochimica et Cosmochimica Acta*, 1994, **58**, 3191-3198.
13. M. E. Andersson, J. Sommar, K. Gårdfeldt and S. Jutterström, *Marine Chemistry*, 2011, **125**, 1-7.
14. N. Batrakova, O. Travnikov and O. Rozovskaya, *Ocean Science*, 2014, **10**, 1047-1063.
15. R. Cesário, L. Poissant, M. Pilote, N. J. O'Driscoll, A. M. Mota and J. Canário, *Science of The Total Environment*, 2017, **603-604**, 279-289.
16. R. P. Mason, in *Methylation-From DNA, RNA and Histones to Diseases and Treatment*, InTech, 2012.
17. E. Lanzillotta and R. Ferrara, *Chemosphere*, 2001, **45**, 935-940.
18. N. L. Bella and A. Hilliker, *Mercury in the Environment*, The Traprock, December 2003.
19. E. Canada, Mercury and the environment, <https://www.ec.gc.ca/mercure-mercury/default.asp?lang=En&n=67E16201-1>, (accessed April 2016).
20. C. J. Moore, A Review Of Mercury In The Environment (Its Occurrence In Marine Fish) [http://www.dnr.sc.gov/marine/img/mm\\_paper.pdf](http://www.dnr.sc.gov/marine/img/mm_paper.pdf), (accessed February 2016).
21. X. H. Cheng, Q. Q. Li, C. G. Li, J. G. Qin and Z. Li, *Chemistry-a European Journal*, 2011, **17**, 7276-7281.
22. K. Leopold, M. Foulkes and P. J. Worsfold, *TrAC Trends in Analytical Chemistry*, 2009, **28**, 426-435.
23. B. Braune, J. Chételat, M. Amyot, T. Brown, M. Clayden, M. Evans, A. Fisk, A. Gaden, C. Girard, A. Hare, J. Kirk, I. Lehnher, R. Letcher, L. Loseto, R. Macdonald, E. Mann, B. McMeans, D. Muir, N. O'Driscoll, A. Poulain, K. Reimer and G. Stern, *Science of The Total Environment*, 2015, **509-510**, 67-90.
24. F. Zahir, S. J. Rizwi, S. K. Haq and R. H. Khan, *Environmental Toxicology and Pharmacology*, 2005, **20**, 351-360.
25. ATSDR, Toxicological Profile for Mercury <http://www.atsdr.cdc.gov/toxprofiles/tp46.pdf>, (accessed February 2016).

26. P. Holmes, K. A. F. James and L. S. Levy, *Science of The Total Environment*, 2009, **408**, 171-182.
27. M. Gochfeld, *Ecotoxicology and Environmental Safety*, 2003, **56**, 174-179.
28. P. B. Tchounwou, W. K. Ayensu, N. Ninashvili and D. Sutton, *Environmental Toxicology*, 2003, **18**, 149-175.
29. J.-D. Park and W. Zheng, *Journal of Preventive Medicine and Public Health*, 2012, **45**, 344-352.
30. J. Ikingura and H. Akagi, *Science of the Total Environment*, 1996, **191**, 59-68.
31. J. a. H. Hopkins, M., *Contaminants in soil: updated collation of toxicological data and intake values for humans. Mercury*, Report 978-1-84911-021-1, Environment Agency, Bristol, 2009.
32. WHO, Mercury and health, <http://www.who.int/mediacentre/factsheets/fs361/en/>, (accessed June 2015).
33. S. Ekino, M. Susa, T. Ninomiya, K. Imamura and T. Kitamura, *Journal of the Neurological Sciences*, 2007, **262**, 131-144.
34. S. B. Skerfving and J. F. Copplestone, *Bulletin of the World Health Organization*, 1976, **54**, 101-112.
35. S. F. Al-Damluji and P. The Clinical Committee on Mercury, *Bulletin of the World Health Organization*, 1976, **53**, 65-81.
36. USEPA, Mercury Compounds, <https://www.epa.gov/sites/production/files/2016-09/documents/mercury-compounds.pdf>, (accessed September 2018).
37. ATSDR, ATSDR's Substance Priority List, <https://www.atsdr.cdc.gov/SPL/>, (accessed August 2018).
38. B. Azevedo, L. Barros Furieri, F. Maciel Peçanha, G. Wiggers, P. Vassallo, M. Simões, J. Fiorim, P. Batista, M. Fioresi, L. Rossoni, I. Stefanon, M. Alonso, M. Salaices and D. Vassallo, *Toxic Effects of Mercury on the Cardiovascular and Central Nervous Systems*, 2012.
39. R. A Bernhoft, *Mercury Toxicity and Treatment: A Review of the Literature*, 2012.
40. S. Bose-O'Reilly, K. M. McCarty, N. Steckling and B. Lettmeier, *Current Problems in Pediatric and Adolescent Health Care*, 2010, **40**, 186-215.
41. L. Jarup, *Br Med Bull*, 2003, **68**, 167-182.
42. S. A. Counter and L. H. Buchanan, *Toxicology and Applied Pharmacology*, 2004, **198**, 209-230.
43. USEPA, *IRIS summary for methylmercury (MeHg) (CASRN 22967-92-6)*, Washington, DC, 2001.
44. USEPA, *National Primary Drinking Water Regulations*, Washington, DC, 2009.
45. USEPA, National Recommended Water Quality Criteria - Aquatic Life Criteria Table, <https://www.epa.gov/wqc/national-recommended-water-quality-criteria-aquatic-life-criteria-table>, (accessed April 2016).
46. G. WHO, *World Health Organization*, 2011, **216**, 303-304.
47. UNEP, *Minamata convention on mercury* United Nations Environment Programme, Geneva, Switzerland, 2013.
48. UNEP, *Report of the Conference of the Parties to the Minamata Convention on Mercury on the work of its first meeting* United Nations Environment Programme Geneva, Switzerland, 2017.
49. L. R. Bravo-Sanchez, B. S. de la Riva, J. M. Costa-Fernandez, R. Pereiro and A. Sanz-Medel, *Talanta*, 2001, **55**, 1071-1078.
50. H. T. Chen, J. G. Chen, X. Z. Jin and D. Y. Wei, *Journal of Hazardous Materials*, 2009, **172**, 1282-1287.

51. D. P. C. de Quadros, B. Campanella, M. Onor, E. Bramanti, D. L. G. Borges and A. D'Ulivo, *Spectrochimica Acta Part B-Atomic Spectroscopy*, 2014, **101**, 312-319.
52. WHO, Mercury Exposure and Health Impacts among Individuals in the Artisanal and Small-Scale Gold Mining (ASGM) Community, [http://www.who.int/ipcs/assessment/public\\_health/mercury\\_asgm.pdf](http://www.who.int/ipcs/assessment/public_health/mercury_asgm.pdf), (accessed February 2016).
53. H. N. Kim, W. X. Ren, J. S. Kim and J. Yoon, *Chemical Society Reviews*, 2012, **41**, 3210-3244.
54. E. M. Nolan and S. J. Lippard, *Chemical Reviews*, 2008, **108**, 3443-3480.
55. Y. W. Choi, G. R. You, M. M. Lee, J. Kim, K. D. Jung and C. Kim, *Inorganic Chemistry Communications*, 2014, **46**, 43-46.
56. J. Liu, D. P. Wu, X. H. Yan and Y. F. Guan, *Talanta*, 2013, **116**, 563-568.
57. J. Kenkel, *Analytical Chemistry for Technicians*, CRC Press LLC, 2000 N.W. Corporate Blvd, Florida, U.S.A., Third Edition edn., 2003.
58. P. Dussubieux, L. S. E. Tsang, J. S. and Tumosa, C. S., *In: Preprints of the 14th Triennial Meeting ICOM Committee for Conservation*, 2005, **2**, 766-773.
59. Z. Yan, M.-F. Yuen, L. Hu, P. Sun and C.-S. Lee, *RSC Advances*, 2014, **4**, 48373-48388.
60. G. Chen, Z. Guo, G. Zeng and L. Tang, *Analyst*, 2015, **140**, 5400-5443.
61. D. Wu, L. Chen, W. Lee, G. Ko, J. Yin and J. Yoon, *Coordination Chemistry Reviews*, 2018, **354**, 74-97.
62. R. R. Avirah, K. Jyothish and D. Ramaiah, *Organic Letters*, 2007, **9**, 121-124.
63. C. Chen, R. Wang, L. Guo, N. Fu, H. Dong and Y. Yuan, *Organic Letters*, 2011, **13**, 1162-1165.
64. C. Chen, H. Dong, Y. Chen, L. Guo, Z. Wang, J.-J. Sun and N. Fu, *Organic & Biomolecular Chemistry*, 2011, **9**, 8195-8201.
65. H. Y. Lee, K. M. K. Swamy, J. Y. Jung, G. Kim and J. Yoon, *Sensors and Actuators B: Chemical*, 2013, **182**, 530-537.
66. M. Wang, F. Y. Yan, Y. Zou, N. Yang, L. Chen and L. G. Chen, *Spectrochimica Acta Part a-Molecular and Biomolecular Spectroscopy*, 2014, **123**, 216-223.
67. S. Lee, B. A. Rao and Y.-A. Son, *Sensors and Actuators B: Chemical*, 2014, **196**, 388-397.
68. Z. Wang, Z. K. Yang, T. Gao, J. W. He, L. J. Gong, Y. B. Lu, Y. Q. Xiong and W. J. Xu, *Analytical Methods*, 2015, **7**, 2738-2746.
69. S. Angupillai, J.-Y. Hwang, J.-Y. Lee, B. A. Rao and Y.-A. Son, *Sensors and Actuators B: Chemical*, 2015, **214**, 101-110.
70. S. K. Kim, K. M. K. Swamy, S.-Y. Chung, H. N. Kim, M. J. Kim, Y. Jeong and J. Yoon, *Tetrahedron Letters*, 2010, **51**, 3286-3289.
71. J. Ni, Q. Li, B. Li and L. Zhang, *Sensors and Actuators B: Chemical*, 2013, **186**, 278-285.
72. J. Tao, X.-C. Wang, X.-Q. Chen, T.-C. Li, Q.-P. Diao, H.-F. Yu and T. Wang, *Dyes and Pigments*, 2017, **137**, 601-607.
73. F. Sancenón, R. Martínez-Máñez and J. Soto, *Tetrahedron Letters*, 2001, **42**, 4321-4323.
74. Z. Zhang, Y. Chen, D. Xu, L. Yang and A. Liu, *Spectrochimica Acta Part A: Molecular and Biomolecular Spectroscopy*, 2013, **105**, 8-13.
75. K. G. Harsha, E. Appalanaidu, N. R. Chereddy, T. R. Baggi and V. J. Rao, *Sensors and Actuators B: Chemical*, 2018, **256**, 528-534.
76. G. G. Vinoth Kumar, M. P. Kesavan, A. Tamilselvi, G. Rajagopal, J. D. Raja, K. Sakthipandi, J. Rajesh and G. Sivaraman, *Sensors and Actuators B: Chemical*, 2018, **273**, 305-315.

77. E. Coronado, J. R. Galan-Mascaros, C. Marti-Gastaldo, E. Palomares, J. R. Durrant, R. Vilar, M. Gratzel and M. K. Nazeeruddin, *Journal of the American Chemical Society*, 2005, **127**, 12351-12356.
78. E. Palomares, R. Vilar and J. R. Durrant, *Chemical Communications*, 2004, DOI: 10.1039/B314138A, 362-363.
79. H.-B. Sun, S.-J. Liu, T.-C. Ma, N.-N. Song, Q. Zhao and W. Huang, *New Journal of Chemistry*, 2011, **35**, 1194-1197.
80. M. Vedamalai and S.-P. Wu, *Organic & Biomolecular Chemistry*, 2012, **10**, 5410-5416.
81. S. Liu, Z. Shi, W. Xu, H. Yang, N. Xi, X. Liu, Q. Zhao and W. Huang, *Dyes and Pigments*, 2014, **103**, 145-153.
82. X.-D. Jiang, J. Zhao, Q. Li, C.-L. Sun, J. Guan, G.-T. Sun and L.-J. Xiao, *Dyes and Pigments*, 2016, **125**, 136-141.
83. W. Ren, Y. Zhang, W. T. Huang, N. B. Li and H. Q. Luo, *Biosensors and Bioelectronics*, 2015, **68**, 266-271.
84. J. Ma, N. Liu, X. Ma, X. Li, Y. Liu, Y. Li, W. Liang and Z. Zhou, *Chinese Journal of Applied and Environmental Biology*, 2015, **21**, 848-853.
85. L. Yu, H. Xu, H. Chen, L. Bai and W. Wang, *Analytical Methods*, 2016, **8**, 7054-7060.
86. J. Chen, J. Pan and S. Chen, *Chemical Communications*, 2017, **53**, 10224-10227.
87. C. Y. Lee, H. Y. Kim, J. K. Ahn, K. S. Park and H. G. Park, *RSC Advances*, 2017, **7**, 47143-47147.
88. T. Yu, T. T. Zhang, W. Zhao, J. J. Xu and H. Y. Chen, *Talanta*, 2017, **165**, 570-576.
89. H. Zhang, Z. lei, X. Fu, X. Deng, Q. Wang and D. Gu, *Sensors and Actuators, B: Chemical*, 2017, **246**, 896-903.
90. T. Li, S. Dong and E. Wang, *Analytical Chemistry*, 2009, **81**, 2144-2149.
91. C. Diez-Gil, A. Caballero, R. Martinez, I. Ratera, A. Tarraga, P. Molina and J. Veciana, 2007.
92. X. Cheng, S. Li, H. Jia, A. Zhong, C. Zhong, J. Feng, J. Qin and Z. Li, *Chemistry – A European Journal*, 2012, **18**, 1691-1699.
93. Y. Chen, H. Bai, W. Hong and G. Shi, *Analyst*, 2009, **134**, 2081-2086.
94. R. Martínez, A. Espinosa, A. Tárraga and P. Molina, *Tetrahedron*, 2010, **66**, 3662-3667.
95. D. Pinheiro, C. S. de Castro, J. S. Seixas de Melo, E. Oliveira, C. Nuñez, A. Fernández-Lodeiro, J. L. Capelo and C. Lodeiro, *Dyes and Pigments*, 2014, **110**, 152-158.
96. R. Shunmugam, G. J. Gabriel, C. E. Smith, K. A. Aamer and G. N. Tew, *Chemistry – A European Journal*, 2008, **14**, 3904-3907.
97. F. Zarlaida and M. Adlim, *Microchimica Acta*, 2017, **184**, 45-58.
98. P. Jarujamrus, M. Amatatongchai, A. Thima, T. Khongrangdee and C. Mongkontong, *Spectrochimica Acta Part A: Molecular and Biomolecular Spectroscopy*, 2015, **142**, 86-93.
99. K. B. A. Ahmed, R. Senthilnathan, S. Megarajan and V. Anbazhagan, *Journal of Photochemistry and Photobiology B: Biology*, 2015, **151**, 39-45.
100. A. Jeevika and D. R. Shankaran, *Materials Research Bulletin*, 2016, **83**, 48-55.
101. S. Maiti, G. Barman and J. Konar Laha, *Applied Nanoscience*, 2016, **6**, 529-538.
102. J. Song, Q. Ma, S. Zhang, Y. Guo and C. Dong, *Journal of Cluster Science*, 2016, **27**, 1203-1212.
103. Y. Wang, F. Yang and X. Yang, *ACS Applied Materials & Interfaces*, 2010, **2**, 339-342.
104. G. L. Wang, X. Y. Zhu, H. J. Jiao, Y. M. Dong and Z. J. Li, *Biosensors & Bioelectronics*, 2012, **31**, 337-342.
105. A. Apilux, W. Siangproh, N. Praphairaksit and O. Chailapakul, *Talanta*, 2012, **97**, 388-394.

106. J.-S. Lee, M. S. Han and C. A. Mirkin, *Angewandte Chemie International Edition*, 2007, **46**, 4093-4096.
107. Y. He, X. Zhang, K. Zeng, S. Zhang, M. Baloda, A. S. Gurung and G. Liu, *Biosensors and Bioelectronics*, 2011, **26**, 4464-4470.
108. J. Wu, L. Li, D. Zhu, P. He, Y. Fang and G. Cheng, *Analytica Chimica Acta*, 2011, **694**, 115-119.
109. Z.-q. Tan, J.-f. Liu, R. Liu, Y.-g. Yin and G.-b. Jiang, *Chemical Communications*, 2009, 7030-7032.
110. Y. L. Zhou, H. Dong, L. T. Liu, M. M. Li, K. X. Xiao and M. T. Xu, *Sensors and Actuators B-Chemical*, 2014, **196**, 106-111.
111. Z. Chen, C. Zhang, H. Ma, T. Zhou, B. Jiang, M. Chen and X. Chen, *Talanta*, 2015, **134**, 603-606.
112. Y. M. Guo, Z. Wang, W. S. Qu, H. W. Shao and X. Y. Jiang, *Biosensors & Bioelectronics*, 2011, **26**, 4064-4069.
113. R. M. Tripathi, R. K. Gupta, P. Singh, A. S. Bhadwal, A. Shrivastav, N. Kumar and B. R. Shrivastav, *Sensors and Actuators B-Chemical*, 2014, **204**, 637-646.
114. Y. Zhu, Y. Cai, Y. Zhu, L. Zheng, J. Ding, Y. Quan, L. Wang and B. Qi, *Biosensors and Bioelectronics*, 2015, **69**, 174-178.
115. J. Tang, P. Wu, X. Hou and K. Xu, *Talanta*, 2016, **159**, 87-92.
116. C. Y. Lin, C. J. Yu, Y. H. Lin and W. L. Tseng, *Analytical Chemistry*, 2010, **82**, 6830-6837.
117. A. Fan, Y. Ling, C. Lau and J. Lu, *Talanta*, 2010, **82**, 687-692.
118. J. Du, Z. Wang, J. Fan and X. Peng, *Sensors and Actuators B: Chemical*, 2015, **212**, 481-486.
119. G. Wang, Z. Chen, W. Wang, B. Yan and L. Chen, *Analyst*, 2011, **136**, 174-178.
120. M. Ariza-Avidad, A. Salinas-Castillo, M. P. Cuellar, M. Agudo-Acemel, M. C. Pegalajar and L. F. Capitan-Vallvey, *Analytical Chemistry*, 2014, **86**, 8634-8641.
121. L. A. Feng, Y. Zhang, L. Y. Wen, L. A. Chen, Z. Shen and Y. F. Guan, *Chemistry-a European Journal*, 2011, **17**, 1101-1104.
122. S. Jayabal, R. Sathiyamurthi and R. Ramaraj, *Journal of Materials Chemistry A*, 2014, **2**, 8918-8925.
123. A. W. Martinez, S. T. Phillips, G. M. Whitesides and E. Carrilho, *Analytical Chemistry*, 2010, **82**, 3-10.
124. A. V. Yallouz, T. Calixto and S. Hacon, *Anais Da Academia Brasileira De Ciencias*, 2002, **74**, 187-191.
125. G.-H. Chen, W.-Y. Chen, Y.-C. Yen, C.-W. Wang, H.-T. Chang and C.-F. Chen, *Analytical Chemistry*, 2014, **86**, 6843-6849.
126. W. Chen, X. Fang, H. Li, H. Cao and J. Kong, *Scientific Reports*, 2016, **6**, 31948.
127. K. S. Min, R. Manivannan and Y.-A. Son, *Sensors and Actuators B: Chemical*, 2018, **261**, 545-552.
128. M. Ponram, U. Balijapalli, B. Sambath, S. K. Iyer, V. B, R. Cingaram and K. Natesan Sundaramurthy, *New Journal of Chemistry*, 2018, **42**, 8530-8536.
129. A. W. Martinez, S. T. Phillips, E. Carrilho, S. W. Thomas, H. Sindi and G. M. Whitesides, *Analytical Chemistry*, 2008, **80**, 3699-3707.
130. X. Li, D. R. Ballerini and W. Shen, *Biomicrofluidics*, 2012, **6**, 011301.
131. D. M. Cate, J. A. Adkins, J. Mettakoonpitak and C. S. Henry, *Analytical Chemistry*, 2015, **87**, 19-41.
132. S. M. Z. Hossain and J. D. Brennan, *Analytical Chemistry*, 2011, **83**, 8772-8778.
133. L. Feng, X. Li, H. Li, W. Yang, L. Chen and Y. F. Guan, *Analytica Chimica Acta*, 2013, **780**, 74-80.

134. L. Feng, H. Li, L. Y. Niu, Y. S. Guan, C. F. Duan, Y. F. Guan, C. H. Tung and Q. Z. Yang, *Talanta*, 2013, **108**, 103-108.
135. M. I. G. S. Almeida, B. M. Jayawardane, S. D. Kolev and I. D. McKelvie, *Talanta*, 2018, **177**, 176-190.
136. C. H. Yin, J. Iqbal, H. L. Hu, B. X. Liu, L. Zhang, B. L. Zhu and Y. P. Du, *Journal of Hazardous Materials*, 2012, **233**, 207-212.
137. M. J. Rand, *Journal of Applied Physics*, 1970, **41**, 787.
138. C. Tams, Enjalbert, N. , PerkinElmer, Inc., United Kingdom, 2009.
139. T. Owen, *Fundamentals of Modern UV-Visible Spectroscopy: A Primer. edit*, Agilent Technologie, German, 2000.
140. RSC, Modern chemical techniques: ultraviolet/visible spectroscopy <http://www.rsc.org/learn-chemistry/resource/res00001300/ultraviolet-visible-spectroscopy?cmpid=CMP00002749>, (accessed February 2016, 2016).
141. M. B. Wallace, A. Wax, D. N. Roberts and R. N. Graf, *Gastrointestinal endoscopy clinics of North America*, 2009, **19**, 233-242.
142. D. Kealey, Haines, P. , *Analytical Chemistry*, Taylor & Francis, London, 2002.
143. W. S. Boyle and G. E. Smith, *Bell System Technical Journal*, 1970, **49**, 587-593.
144. G. F. Amelio, M. F. Tompsett and G. E. Smith, *Bell System Technical Journal*, 1970, **49**, 593-600.
145. M. F. Santillo, *The Physics Teacher*, 2009, **47**, 454-455.
146. J. R. Janesick, T. Elliott, S. Collins, M. M. Blouke and J. Freeman, *Optical Engineering*, 1987, **26**, 268692.
147. J. Janesick and T. Elliott, 1992.
148. E. M. Westbrook and I. Naday, in *Methods in Enzymology*, Academic Press, 1997, vol. 276, pp. 244-268.
149. L. Byrne, J. Barker, G. Pennarun-Thomas, D. Diamond and S. Edwards, *TrAC Trends in Analytical Chemistry*, 2000, **19**, 517-522.
150. J. R. Janesick, *Scientific charge-coupled devices*, SPIE press Bellingham, 2001.
151. A. J. Theuwissen, *Solid-state imaging with charge-coupled devices*, Springer Science & Business Media, 2006.
152. R. Ramanath, W. E. Snyder, G. L. Bilbro and W. A. Sander, *Journal of Electronic imaging*, 2002, **11**, 306-316.
153. R. L. Baer, W. D. Holland, J. M. Holm and P. L. Vora, 1999.
154. B. E. Bayer, *Color imaging array*, U. S. Patent No. 3971065, 1976.
155. A. C. Popescu and H. Farid, *IEEE Transactions on Signal Processing*, 2005, **53**, 3948-3959.
156. G. Themelis, J. S. Yoo and V. Ntziachristos, *Optics letters*, 2008, **33**, 1023-1025.
157. D. Harvey, *Modern analytical chemistry*, McGraw-Hall Companies, Inc., USA, 2000.
158. D. C. Harris, *Quantitative chemical analysis*, W. H. Freeman and Company, New York, 2007.
159. J. N. Miller, and Miller, J. C., *Statistics and Chemometrics for Analytical chemistry*, Pearson Education Limited, sixth edition edn., 2010.
160. P. Patnaik, *Handbook of environmental analysis, second edition edn.*, CRC Press, Taylor & Francis Group, USA, 2010.
161. A. C. Olivieri, *Analytica Chimica Acta*, 2015, **868**, 10-22.
162. A. Hubaux and G. Vos, *Analytical chemistry*, 1970, **42**, 849-855.
163. S. F. James W. Robinson, E., George M. Frame . *Undergraduate Instrumental Analysis*, Taylor & Francis e-Library, New York, 2005.
164. A. V. Yallouz, R. Calixto de Campos and S. Paciornik, *Fresenius' Journal of Analytical Chemistry*, 2000, **366**, 461-465.

165. A. V. Yallouz, R. G. Cesar and S. G. Egler, *Environmental Pollution*, 2008, **151**, 429-433.
166. W. Shi and H. Ma, *Chemical Communications*, 2008, 1856-1858.
167. R. K. Mahajan, R. Kaur, V. Bhalla, M. Kumar, T. Hattori and S. Miyano, *Sensors and Actuators B: Chemical*, 2008, **130**, 290-294.
168. M. B. Gholivand, M. Mohammadi and M. K. Rofouei, *Materials Science and Engineering: C*, 2010, **30**, 847-852.
169. J. Liu, M. Yu, X.-C. Wang and Z. Zhang, *Spectrochimica Acta Part A: Molecular and Biomolecular Spectroscopy*, 2012, **93**, 245-249.
170. A. R. Firooz, A. A. Ensafi, K. Karimi and R. Khalifeh, *Sensors and Actuators B: Chemical*, 2013, **185**, 84-90.
171. K. Bera, A. K. Das, M. Nag and S. Basak, *Analytical Chemistry*, 2014, **86**, 2740-2746.
172. D. Shi, F. Yan, M. Wang, Y. Zou, T. Zheng, X. Zhou and L. Chen, *Materials Research Bulletin*, 2015, **70**, 958-964.
173. S. Y. Lee, J. J. Lee, K. H. Bok, J. A. Kim, Y. K. So and C. Kim, *Inorganic Chemistry Communications*, 2016, **70**, 147-152.
174. Q. Zhang, J. Zhang, H. Zuo, C. Wang and Y. Shen, *Tetrahedron*, 2017, **73**, 2824-2830.
175. C. H. Jeon, C. S. Park, C. S. Lee and T. H. Ha, *Journal of Industrial and Engineering Chemistry*, 2018, **57**, 370-376.
176. S. A. El-Safty, M. A. Shenashen and S. A. El-Safty, *TrAC Trends in Analytical Chemistry*, 2012, **38**, 98-115.
177. C. L. O'Neal, D. J. Crouch and A. A. Fatah, *Forensic Science International*, 2000, **109**, 189-201.
178. H. Miyaji and J. L. Sessler, *Angewandte Chemie*, 2001, **113**, 158-161.
179. A. Perry and D. Miles, *Tetrahedron Letters*, 2016, **57**, 5788-5793.
180. A. O. Gettler and S. Kaye, *Journal of Laboratory and Clinical Medicine*, 1950, **35**, 146-151.
181. C. M. de Almeida Ferreira, S. G. Egler, A. V. Yallouz and Á. R. A. Ignácio, *Chemosphere*, 2017, **174**, 604-612.
182. O. Cavoura, C. M. Davidson, N. Katsiris and H. E. Keenan, *Environmental Monitoring and Assessment*, 2018, **190**, 236.
183. A. Khan, F. Mahmood, M. Y. Khokhar and S. Ahmed, *Reactive and Functional Polymers*, 2006, **66**, 1014-1020.
184. M. Abbasi Tarighat, *Arabian Journal of Chemistry*, 2014, DOI: <https://doi.org/10.1016/j.arabjc.2014.11.042>.
185. J. L. Gerlach and R. G. Frazier, *Analytical Chemistry*, 1958, **30**, 1142-1146.
186. S. Bait and E. Van Dalen, *Analytica Chimica Acta*, 1962, **27**, 416-421.
187. O. Tadao and U. Satori, *Bulletin of the Chemical Society of Japan*, 1967, **40**, 1386-1391.
188. S. Dadfarnia, A. M. Salmanzadeh and A. M. H. Shabani, *Bulletin of the Korean Chemical Society*, 2002, **23**, 1719-1723.
189. G. A. Crespo, F. J. Andrade, F. A. Iñón and M. B. Tudino, *Analytica Chimica Acta*, 2005, **539**, 317-325.
190. L. Mergola, S. Scorrano, E. Bloise, M. P. Di Bello, M. Catalano, G. Vasapollo and R. Del Sole, *Polymer Journal*, 2016, **48**, 73-79.
191. S.-I. Ohira, K. Nakamura, M. Chiba, P. K. Dasgupta and K. Toda, *Talanta*, 2017, **164**, 445-450.
192. F. E. Clarke, *Analytical Chemistry*, 1950, **22**, 553-555.
193. C. S. a. Z. W. S. Odegaard. N, *Material characterization tests for objects of art and archaeology*, Archetype Publications Ltd., London, 2nd edn., 2005.

194. S. P. Asper, O. Schales and S. S. Schales, *Journal of Biological Chemistry*, 1947, **168**, 779-780.
195. T. V. Ramakrishna, G. Aravamudan and M. Vijayakumar, *Analytica Chimica Acta*, 1976, **84**, 369-375.
196. M. Vijayakumar, T. V. Ramakrishna and G. Aravamudan, *Talanta*, 1980, **27**, 911-913.
197. P. Padmaja, N. Balasubramanian and T. V. Ramakrishna, *Talanta*, 1994, **41**, 255-260.
198. P. Padmaja, N. Balasubramanian and T. V. Ramakrishna, *International Journal of Environmental Analytical Chemistry*, 1996, **63**, 47-59.
199. K. R. Prathish, D. James, J. Jaisy and T. P. Rao, *Analytica Chimica Acta*, 2009, **647**, 84-89.
200. L.-t. Fan, M. M. Gharpuray and Y.-H. Lee, in *Cellulose Hydrolysis*, Springer Berlin Heidelberg, Berlin, Heidelberg, 1987, DOI: 10.1007/978-3-642-72575-3\_4, pp. 121-148.
201. H. Sixta, *Handbook of pulp*, 2006, 1009-1067.
202. A. Palme, H. Theliander and H. Brelid, *Carbohydrate Polymers*, 2016, **136**, 1281-1287.
203. N. Strafford and P. F. Wyatt, *Analyst*, 1936, **61**, 528-535.
204. S. Kawamoto, Y. Yokoyama and S. Ikeda, *Bull. Chem. Soc. Jpn.*, 1980, **53**, 391-394.
205. A. Kaparwan, N. Singh, K. Singh and R. S. Dubey, *Asian Journal of Chemistry*, 2012, **24**, 2065-2068.
206. X. Li, X. Gao, W. Shi and H. Ma, *Chemical Reviews*, 2014, **114**, 590-659.
207. S. Panda, A. Panda and S. S. Zade, *Coordination Chemistry Reviews*, 2015, **300**, 86-100.
208. M. Hong, X. Lu, Y. Chen and D. Xu, *Sensors and Actuators B: Chemical*, 2016, **232**, 28-36.
209. X. Chen, F. Wang, J. Y. Hyun, T. Wei, J. Qiang, X. Ren, I. Shin and J. Yoon, *Chemical Society Reviews*, 2016, **45**, 2976-3016.
210. J. Kuchlyan, S. Basak, D. Dutta, A. K. Das, D. Mal and N. Sarkar, *Chemical Physics Letters*, 2017, **673**, 84-88.
211. Q. Lin, Y. Huang, J. Fan, R. Wang and N. Fu, *Talanta*, 2013, **114**, 66-72.
212. H. Zhu, Y. Lin, G. Wang, Y. Chen, X. Lin and N. Fu, *Sensors and Actuators, B: Chemical*, 2014, **198**, 201-209.
213. M. D. Laramie, A. Levitz and M. Henary, *Sensors and Actuators, B: Chemical*, 2017, **243**, 1191-1204.
214. T. Wang, Q. J. Zhao, H. G. Hu, S. C. Yu, X. Liu, L. Liu and Q. Y. Wu, *Chemical Communications*, 2012, **48**, 8781-8783.
215. J. Liu, Y. Q. Sun, P. Wang, J. Zhang and W. Guo, *Analyst*, 2013, **138**, 2654-2660.
216. J. Zhang, J. Wang, W. Zhao and X. Dong, *Chemistry Letters*, 2015, **44**, 952-954.
217. H. Yang, C. Han, X. Zhu, Y. Liu, K. Y. Zhang, S. Liu, Q. Zhao, F. Li and W. Huang, *Adv. Funct. Mater.*, 2016, **26**, 1945-1953.
218. Y. J. Gong, X. B. Zhang, G. J. Mao, L. Su, H. M. Meng, W. Tan, S. Feng and G. Zhang, *Chemical Science*, 2016, **7**, 2275-2285.
219. M. D. Laramie, A. Levitz and M. Henary, *Sensors and Actuators B: Chemical*, 2017, **243**, 1191-1204.
220. J. Wang, W. Li and L. Long, *Sensors and Actuators B: Chemical*, 2017, **245**, 462-469.
221. S. M. Park, M. H. Kim, J.-I. Choe, K. T. No and S.-K. Chang, *The Journal of organic chemistry*, 2007, **72**, 3550-3553.
222. G. Zhang, D. Zhang, S. Yin, X. Yang, Z. Shuai and D. Zhu, *Chemical Communications*, 2005, 2161-2163.
223. S. Yoon, A. E. Albers, A. P. Wong and C. J. Chang, *Journal of the American Chemical Society*, 2005, **127**, 16030-16031.

224. X.-Q. Zhan, Z.-H. Qian, H. Zheng, B.-Y. Su, Z. Lan and J.-G. Xu, *Chemical Communications*, 2008, 1859-1861.
225. M. Beija, C. A. Afonso and J. M. Martinho, *Chemical Society Reviews*, 2009, **38**, 2410-2433.
226. A. A. El-Rayyes, A. Al-Betar, T. Htun and U. K. Klein, *Chemical physics letters*, 2005, **414**, 287-291.
227. C. J. Stephenson and K. D. Shimizu, *Organic & biomolecular chemistry*, 2010, **8**, 1027-1032.
228. D. A. Hinckley and P. G. Seybold, *J. Chem. Educ.*, 1987, **64**, 362.
229. H.-H. Wang, L. Xue, C.-L. Yu, Y.-Y. Qian and H. Jiang, *Dyes and Pigments*, 2011, **91**, 350-355.
230. Y. Jiao, L. Zhang and P. Zhou, *Talanta*, 2016, **150**, 14-19.
231. Z. Guo, W. Zhu, M. Zhu, X. Wu and H. Tian, *Chemistry - A European Journal*, 2010, **16**, 14424-14432.
232. I. Thornton, D. Butler, P. Docx, M. Hession, C. Makropoulos, M. McMullen, M. Nieuwenhuijsen, A. Pitman, R. Rautiu and R. Sawyer, *Final report prepared for European Commission Directorate-General Environment*, 2001.
233. R. G. Pearson, *Journal of Chemical Sciences*, 2005, **117**, 369-377.
234. M. Remelli, V. M. Nurchi, J. I. Lachowicz, S. Medici, M. A. Zoroddu and M. Peana, *Coordination Chemistry Reviews*, 2016, **327-328**, 55-69.
235. I. Sóvágó and K. Várnagy, in *Cadmium: From Toxicity to Essentiality*, eds. A. Sigel, H. Sigel and R. K. O. Sigel, Springer Netherlands, Dordrecht, 2013, DOI: 10.1007/978-94-007-5179-8\_9, pp. 275-302.
236. H. Kozłowski, J. Urbańska, I. Sóvágó, K. Varnagy, A. Kiss, J. Szychta and K. Cherifi, *Polyhedron*, 1990, **9**, 831-837.
237. R. G. Pearson, *Journal of the American Chemical Society*, 1963, **85**, 3533-3539.
238. C. M. McGeough and S. O. Driscoll, *IEEE Transactions on Biomedical Circuits and Systems*, 2013, **7**, 655-659.
239. H. Zhu, I. Sencan, J. Wong, S. Dimitrov, D. Tseng, K. Nagashima and A. Ozcan, *Lab on a Chip*, 2013, **13**, 1282-1288.
240. V. V. Apyari and S. G. Dmitrienko, *Journal of Analytical Chemistry*, 2008, **63**, 530-537.
241. R. Meelapsom, P. Jarujamrus, M. Amatatongchai, S. Chairam, C. Kulsing and W. Shen, *Talanta*, 2016, **155**, 193-201.
242. N. C. Birch and D. F. Stickle, *Clinica Chimica Acta*, 2003, **333**, 95-96.
243. S. Paciornik, A. V. Yallouz, R. C. Campos and D. Gannerman, *Journal of the Brazilian Chemical Society*, 2006, **17**, 156-161.
244. A. Lapresta-Fernández and L. F. Capitán-Vallvey, *Analytica Chimica Acta*, 2011, **706**, 328-337.
245. T. G. Choleva, F. A. Kappi, D. L. Giokas and A. G. Vlessidis, *Analytica Chimica Acta*, 2015, **860**, 61-69.
246. Y. Yao, C. Wang, P. Wang, L. Miao, J. Hou, T. Wang and C. Liu, *Science of The Total Environment*, 2016, **566-567**, 1632-1639.
247. T. Mazzu-Nascimento, P. A. Gomes Carneiro Leao, J. R. Catai, G. G. Morbioli and E. Carrilho, *Analytical Methods*, 2016, **8**, 7312-7318.
248. K. V. Oskolok, E. V. Shults, O. V. Monogarova and A. A. Chaplenko, *Talanta*, 2018, **178**, 377-383.
249. E. d. N. Gaiao, V. L. Martins, W. d. S. Lyra, L. F. d. Almeida, E. C. d. Silva and M. C. U. Araújo, *Analytica Chimica Acta*, 2006, **570**, 283-290.
250. B. M. Jayawardane, I. D. McKelvie and S. D. Kolev, *Talanta*, 2012, **100**, 454-460.

251. B. M. Jayawardane, S. Wei, I. D. McKelvie and S. D. Kolev, *Analytical Chemistry*, 2014, **86**, 7274-7279.
252. A. Choodum, P. Kanatharana, W. Wongniramaikul and N. NicDaeid, *Forensic Science International*, 2012, **222**, 340-345.
253. A. Choodum, P. Kanatharana, W. Wongniramaikul and N. Nic Daeid, *Talanta*, 2013, **115**, 143-149.
254. A. Choodum, K. Parabun, N. Klawach, N. N. Daeid, P. Kanatharana and W. Wongniramaikul, *Forensic Science International*, 2014, **235**, 8-13.
255. N. Pourreza and K. Ghanemi, *Journal of Hazardous Materials*, 2009, **161**, 982-987.
256. M. M. Bradley, L. M. Siperko and M. D. Porter, *Talanta*, 2011, **86**, 64-70.
257. D. B. Gazda, J. S. Fritz and M. D. Porter, *Analytica Chimica Acta*, 2004, **508**, 53-59.
258. H. Filik, D. Aksu, R. Apak and İ. Boz, *Sensors and Actuators B: Chemical*, 2009, **141**, 491-497.
259. A. A. Hill, R. J. Lipert and M. D. Porter, *Talanta*, 2010, **80**, 1606-1610.
260. A. Gałuszka, Z. Migaszewski and J. Namieśnik, *TrAC Trends in Analytical Chemistry*, 2013, **50**, 78-84.
261. O. Prakash and N. Jaiswal, *World Applied Sciences Journal*, 2011, **13**, 572-577.
262. H. Sattar, A. Aman and S. A. U. Qader, *International Journal of Biological Macromolecules*, 2018, **111**, 917-922.
263. W.-K. Lee, Y.-Y. Lim, A. T.-C. Leow, P. Namasivayam, J. Ong Abdullah and C.-L. Ho, *Carbohydrate Polymers*, 2017, **164**, 23-30.
264. M. Matsuo, T. Tanaka and L. Ma, *Polymer*, 2002, **43**, 5299-5309.
265. A. Clark and S. Ross-Murphy, *Structural and mechanical properties of biopolymer gels*, 1987.
266. K. Grudpan, S. D. Kolev, S. Lapanantnopakhun, I. D. McKelvie and W. Wongwilai, *Talanta*, 2015, **136**, 84-94.
267. J. Gille, R. Martin, J. Lubin and J. O. Larimer, *Grayscale/resolution trade-off for text: Model predictions and psychophysical results for letter confusion and letter discrimination*, 1995.
268. W.-K. Lee, Y.-Y. Lim, A. T.-C. Leow, P. Namasivayam, J. O. Abdullah and C.-L. Ho, *Journal of Applied Psychology*, 2017, **29**, 1527-1540.
269. S. S. Singh, H. B. Bohidar and S. Bandyopadhyay, *Colloids and Surfaces B: Biointerfaces*, 2007, **57**, 29-36.
270. M. K. Kang and R. Huang, *Soft Matter*, 2010, **6**, 5736-5742.
271. S. B. Nicoll, S. Radin, E. M. Santos, R. S. Tuan and P. Ducheyne, *Biomaterials*, 1997, **18**, 853-859.
272. D. B. Haddow, P. F. James and R. Van Noort, *Journal of Sol-Gel Science and Technology*, 1998, **13**, 261-265.
273. S. Radin and P. Ducheyne, *Biomaterials*, 2007, **28**, 1721-1729.
274. S. Radin, G. El-Bassyouni, E. J. Vresilovic, E. Schepers and P. Ducheyne, *Biomaterials*, 2005, **26**, 1043-1052.
275. D. Riccardi, H.-B. Guo, J. M. Parks, B. Gu, A. O. Summers, S. M. Miller, L. Liang and J. C. Smith, *The Journal of Physical Chemistry Letters*, 2013, **4**, 2317-2322.
276. F. M. M. Morel, A. M. L. Kraepiel and M. Amyot, *Annual Review of Ecology and Systematics*, 1998, **29**, 543-566.
277. USEPA, *National Secondary Drinking Water Regulations*, United State Environmental Protection Agency, Washington, DC, 2008.
278. M. Ravichandran, *Chemosphere*, 2004, **55**, 319-331.
279. J. A. Dittman, J. B. Shanley, C. T. Driscoll, G. R. Aiken, A. T. Chalmers, J. E. Towse and P. Selvendiran, *Water Resources Research*, 2010, **46**.

280. J. D. Demers, C. T. Driscoll and J. B. Shanley, *Water Resources Research*, 2010, **46**.
281. A. L. Riscassi and T. M. Scanlon, *Water Resources Research*, 2011, **47**.
282. D. A. Burns, G. R. Aiken, P. M. Bradley, C. A. Journey and J. Schelker, *Biogeochemistry*, 2013, **113**, 451-466.
283. E. Tipping, H. T. Corbishley, J.-F. Koprivnjak, D. J. Lapworth, M. P. Miller, C. D. Vincent and J. Hamilton-Taylor, *Environmental Chemistry*, 2009, **6**, 472-476.
284. J. L. Weishaar, G. R. Aiken, B. A. Bergamaschi, M. S. Fram, R. Fujii and K. Mopper, *Environmental Science & Technology*, 2003, **37**, 4702-4708.
285. H. Zhong and W.-X. Wang, *Environmental Science & Technology*, 2009, **43**, 8998-9003.
286. T. Barkay, M. Gillman and R. R. Turner, *Applied and Environmental Microbiology*, 1997, **63**, 4267-4271.
287. D. Zhang and Q. Liu, *Biosensors and Bioelectronics*, 2016, **75**, 273-284.
288. S. Lee, G. Kim and J. Moon, *Sensors*, 2013, **13**, 5109.
289. L. Yu, Z. Shi, C. Fang, Y. Zhang, Y. Liu and C. Li, *Biosensors and Bioelectronics*, 2015, **69**, 307-315.
290. H. El Kaoutit, P. Estevez, F. C. Garcia, F. Serna and J. M. Garcia, *Analytical Methods*, 2013, **5**, 54-58.
291. Q. Wei, R. Nagi, K. Sadeghi, S. Feng, E. Yan, S. J. Ki, R. Caire, D. Tseng and A. Ozcan, *ACS Nano*, 2014, **8**, 1121-1129.
292. S. Vallejos, J. A. Reglero, F. C. Garcia and J. M. Garcia, *Journal of Materials Chemistry A*, 2017, **5**, 13710-13716.
293. J. I. Kenyon, R. Poropatich and M. R. Holtel, *Otolaryngologic Clinics of North America*, 2011, **44**, 1351-1358.
294. D. Quesada-González and A. Merkoçi, *Biosensors and Bioelectronics*, 2017, **92**, 549-562.
295. J. Matthews, R. Kulkarni, M. Gerla and T. Massey, *Mobile Networks and Applications*, 2012, **17**, 178-191.
296. A. I. Barbosa, P. Gehlot, K. Sidapra, A. D. Edwards and N. M. Reis, *Biosensors and Bioelectronics*, 2015, **70**, 5-14.
297. A. Roda, E. Michelini, M. Zangheri, M. Di Fusco, D. Calabria and P. Simoni, *TrAC Trends in Analytical Chemistry*, 2016, **79**, 317-325.
298. W. Xiao, M. Xiao, Q. Fu, S. Yu, H. Shen, H. Bian and Y. Tang, *Sensors*, 2016, **16**, 1871.
299. Z. Liu, Y. Zhang, S. Xu, H. Zhang, Y. Tan, C. Ma, R. Song, L. Jiang and C. Yi, *Analytica Chimica Acta*, 2017, **966**, 81-89.
300. G. Luka, E. Nowak, J. Kawchuk, M. Hoorfar and H. Najjaran, *Royal Society open science*, 2017, **4**, 171025.
301. D. J. You, T. S. Park and J.-Y. Yoon, *Biosensors and Bioelectronics*, 2013, **40**, 180-185.
302. V. Oncescu, D. O'Dell and D. Erickson, *Lab on a Chip*, 2013, **13**, 3232-3238.
303. V. Oncescu, M. Mancuso and D. Erickson, *Lab on a Chip*, 2014, **14**, 759-763.
304. N. Lopez-Ruiz, V. F. Curto, M. M. Erenas, F. Benito-Lopez, D. Diamond, A. J. Palma and L. F. Capitan-Vallvey, *Analytical Chemistry*, 2014, **86**, 9554-9562.
305. Z. Wang, Z. Yang, T. Gao, J. He, L. Gong, Y. Lu, Y. Xiong and W. Xu, *Analytical Methods*, 2015, **7**, 2738-2746.

## Appendix 1

**Table A1.1: Summary of colorimetric sensors used for Hg<sup>2+</sup> determination**

Sensor type	Sensor Molecules	Colour change upon addition Hg <sup>2+</sup>	LOD µg/L	Applied in	Ref.
Organic dye-based sensors	<b>Squaraine</b>				
	SSQ	Deep yellow to colourless	3000	Aqueous solution of Hg <sup>2+</sup> in H <sub>2</sub> O/Acetone (9:1)	62
	SQ-1	Light blue to intense purple	1.40	Aqueous solution of Hg <sup>2+</sup> in AcOH/H <sub>2</sub> O (40:60, v/v)	63
	USQ-1	lilac to brilliant blue	9	Aqueous solution of Hg <sup>2+</sup> in AcOH/H <sub>2</sub> O (10:90, v/v)	64
	<b>Rhodamine</b>				
	Rhodamine hydrazone derivatives	Colourless to pink	30	Aqueous solution of Hg <sup>2+</sup> in CH <sub>3</sub> CN/H <sub>2</sub> O (4:1, v/v), buffer pH 7.4	65
	Rhodamine 6G thiosemicarbazide derivatives	Colourless to pink	2	Aqueous solution of Hg <sup>2+</sup> in DMF/H <sub>2</sub> O (1:1, v/v), buffer pH 7.2	69
	Rhodamine derivative bearing 2, 4-dichloroquinazoline	Colourless to pink	5.40	Aqueous solution of Hg <sup>2+</sup> in buffer solution, immobilisation	66
	Rhodamine pyridine derivative	Colourless to pink	920	Aqueous solution of Hg <sup>2+</sup> in CH <sub>3</sub> CN:H <sub>2</sub> O (7:3, v/v)	67
	Rhodamine 6G	Orang red to pink	15	Aqueous solution of Hg <sup>2+</sup> , buffer pH 5.2	195, 199
Rhodamine 6G-based derivative	Colourless to vermilion	1.36	Aqueous solution of Hg <sup>2+</sup> in micellar solution of DMF	305	

	Rhodamine B combined with boronic acid	Colourless to pink	6000	Aqueous solution of Hg <sup>2+</sup> in CH <sub>3</sub> CN)/H <sub>2</sub> O, buffer pH 7.4	70
	Rhodamine B base 3',6'-bis(diethylamino)-2-(2-oxoethylideneamino)-spiro[isoindoline-1,9'-xanithen]-3-one (RHO)	Colourless to pink	0.54	Aqueous solution of Hg <sup>2+</sup> in EtOH/H <sub>2</sub> O	71
	Si-rhodamine B thiolactone	Colourless to light blue	0.05	Aqueous solution of Hg <sup>2+</sup> in EtOH/H <sub>2</sub> O (2:3, v/v), buffer pH 5.2	72
	<b>Polyether</b>				
	Polyether compound containing azo-oxa binding sites	Yellow to red	20000	Aqueous solution of Hg <sup>2+</sup> in EtOH/H <sub>2</sub> O	73
	4-(bis (2-(ethylthio)ethyl)amino)-N-n-butyl-1,8-naphthalimide	Yellow to colourless	20000	Aqueous solution of Hg <sup>2+</sup> in H <sub>2</sub> O/DMF	74
	2-((E)-(3-(1H-imidazol-1-yl) propylimino) methyl)-5-(diethylamino) phenol	Colourless to yellow	8023	Aqueous solution of Hg <sup>2+</sup> in H <sub>2</sub> O/DMF (5:95, v/v)	55
	Imidazole derivative 6-(Pyren-1-yl)-2-(1,4,5-triphenyl-1H-imidazol-2-yl)quinoline	Colourless to yellow	19.6	Aqueous solution of Hg <sup>2+</sup> in CH <sub>3</sub> CN/buffer (2:1, v/v) pH 5.0	75
	<b>Other organic molecular</b>				
	S1 and S2	Yellow to red	4000	Aqueous solution of Hg <sup>2+</sup>	21
	Pyrazine derived imine	colourless to pink	N/A	Aqueous solution of Hg <sup>2+</sup> in MeOH/H <sub>2</sub> O (3:7, v/v)	76
	<b>Ruthenium</b>				
	N719	Red purple to orange	20	Aqueous solution of Hg <sup>2+</sup> in EtOH	77
	N749	Red purple to orange	150	Aqueous solution of Hg <sup>2+</sup> in EtOH	77
	N719- TiO <sub>2</sub>	Red purple to yellow	4	Aqueous solution of Hg <sup>2+</sup>	78
	<b>BODIPY based sensor</b>				
	BODIPY dye containing a benzo [2, 1, 3] thiadiazole	Purple to yellow	100	Aqueous solution of Hg <sup>2+</sup> in dilute CH <sub>2</sub> Cl <sub>2</sub> solution	79

**Complex-based sensors**

	BODIPY dye containing two triazole units	Blue to purple	45	Aqueous solution of Hg <sup>2+</sup> in CH <sub>3</sub> CN/H <sub>2</sub> O (9:1, v/v), buffer pH 7.0	80
	Aza-BODIPY derivatives	purple to blue	500	Aqueous solution of Hg <sup>2+</sup> in CH <sub>3</sub> CN /CH <sub>2</sub> Cl <sub>2</sub>	81
	Thienyl-containing aza-BODIPY	N/A	120	Aqueous solution of Hg <sup>2+</sup> in CH <sub>3</sub> CN/ buffer (2:8, v/v) pH 7.3	82
	<b>Natural polymer</b>				
	Hairpin DNA probe	Green colour increased	0.2	Aqueous solution of Hg <sup>2+</sup> in H <sub>2</sub> O <sub>2</sub> / ABTS salt	83
	Split DNAzyme fragments	Red to blue	0.002	Aqueous solution of Hg <sup>2+</sup> , DNAzyme integrated with AuNPs	86
	Hairpin DNA and a single strand DNA probe	Red to blue	0.2	Aqueous solution of Hg <sup>2+</sup> , NaCl, AuNPs	88
	Hemin/G-quadruplex (DNAzyme)	N/A	0.0001	Aqueous solution of Hg <sup>2+</sup> . Exonuclease III-assisted DNA cleavages	89
<b>Polymer-based sensors</b>	G-quadruplex-based DNAzymes	N/A	10	Aqueous solution of Hg <sup>2+</sup> in H <sub>2</sub> O <sub>2</sub> / ABTS salt	90
	Cellulose-1,4-disubstituted azine bearing two ferrocene groups	White to purple	10	Aqueous solution of Hg <sup>2+</sup> in CH <sub>3</sub> CN/H <sub>2</sub> O	91
	Cellulose-rhodamine B thiolactone	White to purple red	0.24	Aqueous solution of Hg <sup>2+</sup> pH 5.0, immobilisation	56
	<b>Synthetic polymer</b>				
	Dithioacetals S1, S2 and S3	Blue to green	2	Aqueous solution of Hg <sup>2+</sup> in THF	92
	Oligo(N <sup>1</sup> , N <sup>1</sup> , N <sup>1</sup> ,N <sup>4</sup> ,N <sup>4</sup> ,N <sup>4</sup> -hexamethyl-2-(4-(pyren-1-yl)butanoyloxy)butane-1,4- diaminium bromide	Blue to light yellow	1000	Aqueous solution of Hg <sup>2+</sup> in OHPBDB/poly(dT)	93
	Pyrene derivative	Yellow to pink	N/A	Aqueous solution of Hg <sup>2+</sup> in CH <sub>2</sub> Cl <sub>2</sub> /H <sub>2</sub> O	95

	<i>Bis</i> (pyrenyl)azadiene	Yellow to pink	740	Aqueous solution of Hg <sup>2+</sup> in CH <sub>2</sub> Cl <sub>2</sub> /H <sub>2</sub> O	94
	Terpyridine	Colourless to pink	5	Aqueous solution of Hg <sup>2+</sup> in DMSO/water (1:3, v/v)	96
	<b>AgNPs</b>				
	Citrate AgNPs	Deep yellow to light yellow	8	Aqueous solution of Hg <sup>2+</sup> , the sensing solution contains Cu <sup>2+</sup>	98
	Phyto-protein AgNPs	Yellow to colourless	11030	Aqueous solution of Hg <sup>2+</sup>	99
	Gelatin functionalized AgNPs	Yellow to colourless	5	Aqueous solution of Hg <sup>2+</sup> , hydrogel network and paper substrate	100
	Biosynthesised AgNPs	Yellow to blackish	24070	Aqueous solution of Hg <sup>2+</sup> , 3-mercapto-1, 2-propanediol, pH 10.0	101
<b>Nanoparticles-based sensors</b>	AgNPs reduced by formamidinesulfinic acid	Yellow to colourless	12240	Aqueous solution of Hg <sup>2+</sup> , soluble starch solution as stabiliser/ammonia	102
	Oligonucleotide AgNPs	Yellow to red	3	Aqueous solution of Hg <sup>2+</sup> , NaClO <sub>4</sub> salt	103
	Citrate-AgNPs	Light yellow to deep yellow	0.4	Aqueous solution of Hg <sup>2+</sup> in H <sub>2</sub> O <sub>2</sub>	104
	AgNPs-lab-on-paper	Yellow to light yellow	120	Aqueous solution of Hg <sup>2+</sup> , the sensing solution contains Cu <sup>2+</sup> , Immobilisation	105
	<b>AuNPs</b>				
	<i>Nucleotide-functionalised AuNPs</i>				
	DNA-AuNPs	Purple to red	20	Aqueous solution of Hg <sup>2+</sup> at 47°C	106

Hairpin oligonucleotide-AuNPs	Colourless to red	0.02	Aqueous solution of Hg <sup>2+</sup> , buffer pH 8.0, immobilisation	107
Mercury-specific DNA-functionalized AuNPs	Red to purple	12	Aqueous solution of Hg <sup>2+</sup> , buffer pH 8.0, fish samples	108
<b><i>Thiol-functionalised AuNPs</i></b>				
AuNPs functionalised with mercaptopropionic acid and homocystine	Colourless to red	5	Aqueous solution of Hg <sup>2+</sup> in the presence of 2,6 pyridinedicarboxylic acid	109
AuNPs functionalised with 4-mercaptophenylboronic acid	Red to blue	1.60	Aqueous solution of Hg <sup>2+</sup> , buffer pH 4.0	110
Citrate-AuNPs	Red to blue	0.10	Aqueous solution of Hg <sup>2+</sup> , thiocyanuric acid, buffer pH 7.0	111
<b><i>Au-amalgam based-sensors</i></b>				
Amalgam Tween 20-AuNPs	Red to purple	20	Aqueous solution of Hg <sup>2+</sup> , buffer pH 12.0	116
Surfactants Tween 80- AuNPs	Red to purple	2	Aqueous solution of Hg <sup>2+</sup> , buffer pH 7.0	117
Surfactants Tween 20- AuNPs	Red to purple	0.160	Aqueous solution of Hg <sup>2+</sup> , Thymine, buffer pH 7.0	118
<b><i>Protein-functionalised AuNPs</i></b>				
Papain-AuNPs	Pink to blue	40	Aqueous solution of Hg <sup>2+</sup>	112
AuNPs- <i>Trichoderma harzianum</i> fungal	Pink red to greyish blue	0.5	Aqueous solution of Hg <sup>2+</sup>	113
AuNPs-cationic polymer/DNA interaction	Red to blue/purple	1	Aqueous solution of Hg <sup>2+</sup> , phthalic diglycol diacrylate, buffer pH 7.0	114
Citrate-AuNPs	Red to purple	2	Aqueous solution of Hg <sup>2+</sup> , N- acetyl-L-cysteine	115

## Appendix 2

**Table A2.1: The absorbance values vs. Hg<sup>2+</sup> concentration for Cu<sub>2</sub>[HgI<sub>4</sub>] at 434 nm**

<b>Hg<sup>2+</sup> concentration µg/L</b>	<b>Absorbance n=3</b>
<b>2</b>	0.028 ± 0.021
<b>5</b>	0.044 ± 0.013
<b>25</b>	0.115 ± 0.018
<b>45</b>	0.159 ± 0.019
<b>65</b>	0.193 ± 0.012

Results are mean ± SD; n = number of replicates.

**Table A2.2: The absorbance values of Cu<sub>2</sub>[HgI<sub>4</sub>] at 434 nm in a 48-hour period. A number of Hg<sup>2+</sup> concentrations have been investigated**

<b>HOURS</b>	<b>25 µg/L n=3</b>	<b>75 µg/L n=3</b>
<b>0</b>	0.161 ± 0.006	0.208 ± 0.005
<b>1</b>	0.159 ± 0.006	0.205 ± 0.009
<b>2</b>	0.149 ± 0.007	0.194 ± 0.006
<b>3</b>	0.148 ± 0.002	0.194 ± 0.005
<b>4</b>	0.130 ± 0.016	0.173 ± 0.021
<b>5</b>	0.126 ± 0.022	0.169 ± 0.020
<b>6</b>	0.119 ± 0.027	0.165 ± 0.018
<b>7</b>	0.112 ± 0.016	0.160 ± 0.026
<b>8</b>	0.115 ± 0.013	0.157 ± 0.020
<b>24</b>	0.104 ± 0.003	0.149 ± 0.020
<b>48</b>	0.086 ± 0.018	0.139 ± 0.019

Results are mean ± SD; n = number of replicates.

**Table A2.3: F-test for the absorbance values of Cu<sub>2</sub>[HgI<sub>4</sub>] at 434 nm in a 48-hour period**

<b>Hg<sup>2+</sup> concentration µg/L</b>	<b>Between 0 and 1 hr, v=2</b>		<b>Between 0 and 2 hr, v=2</b>		<b>Between 0 and 3 hr, v=2</b>		<b>Between 0 and 4 hr, v=2</b>		<b>Between 0 and 5 hr, v=2</b>		<b>Between 0 and 6 hr, v=2</b>		<b>Between 0 and 7 hr, v=2</b>		<b>Between 0 and 8 hr, v=2</b>		<b>Between 0 and 24 hr, v=2</b>		<b>Between 0 and 48 hr, v=2</b>	
	F calculated	F critical	F calculated	F critical	F calculated	F critical														
<b>25</b>	1.09	19	1.60	19	6.41	19	8.54	19	15.3	19	<u>23.7</u>	19	8.82	19	5.25	19	2.81	19	10.9	19
<b>75</b>	3.16	19	1.17	19	1.02	19	17.3	19	15.0	19	12.7	19	<u>26.1</u>	19	15.9	19	14.9	19	14.5	19

v = degree of freedom; A significance level (α) =0.05

**Table A2.4: t-test for the absorbance values of Cu<sub>2</sub>[HgI<sub>4</sub>] at 434 nm in a 48-hour period**

<b>Hg<sup>2+</sup> concentration µg/L</b>	<b>Between 0 and 1 hr, v=4</b>		<b>Between 0 and 2 hr, v=4</b>		<b>Between 0 and 3 hr, v=4</b>		<b>Between 0 and 4 hr, v=4</b>		<b>Between 0 and 5 hr, v=4</b>		<b>Between 0 and 6 hr, v=4</b>		<b>Between 0 and 7 hr, v=4</b>		<b>Between 0 and 8 hr, v=4</b>		<b>Between 0 and 24 hr, v=4</b>		<b>Between 0 and 48 hr, v=4</b>	
	t calculated	t critical	t calculated	t critical	t calculated	t critical														
<b>25</b>	0.523	2.78	2.44	2.78	<u>3.80</u>	2.78	<u>3.16</u>	2.78	2.77	2.78	2.68	4.30	<u>4.96</u>	2.78	<u>5.77</u>	2.78	<u>15.3</u>	2.78	<u>6.79</u>	2.78
<b>75</b>	0.464	2.78	<u>3.35</u>	2.78	<u>3.47</u>	2.78	<u>2.83</u>	2.78	<u>3.30</u>	2.78	<u>3.92</u>	2.78	3.17	4.30	<u>4.22</u>	2.78	<u>5.04</u>	2.78	<u>5.94</u>	2.78

v = degree of freedom; A significance level (α) =0.05

**Table A2.5: The absorbance values of Cu<sub>2</sub>[HgI<sub>4</sub>] at 434 nm. The CuI detecting papers have been stored at different temperatures for up to 20 weeks before exposure to 75 µg/L Hg<sup>2+</sup> standard solution**

<b>Time elapsed</b>	<b>control n=3</b>	<b>~ 4 °C n=3</b>	<b>~ 25 °C n=3</b>	<b>~ 35 °C n=3</b>
<b>0 week</b>	0.192 ± 0.002			
<b>After 4<sup>th</sup> weeks</b>		0.190 ± 0.002	0.191 ± 0.005	0.191 ± 0.003
<b>After 8<sup>th</sup> weeks</b>		0.191 ± 0.005	0.190 ± 0.005	0.185 ± 0.002
<b>After 12<sup>th</sup> weeks</b>		0.192 ± 0.003	0.192 ± 0.002	0.191 ± 0.005
<b>After 16<sup>th</sup> weeks</b>		0.192 ± 0.002	0.191 ± 0.003	0.192 ± 0.004
<b>After 20<sup>th</sup> weeks</b>		0.192 ± 0.002	0.190 ± 0.002	0.191 ± 0.003

Results are mean ± SD; n = number of replicates.

**Table A2.6: The absorbance values of [HgI<sub>4</sub>][R6G]<sub>2</sub> complex in the solution phase with the associated Hg<sup>2+</sup> concentrations**

<b>Hg<sup>2+</sup> concentration µg/L</b>	<b>530 nm n=3</b>	<b>570 nm n=3</b>
<b>2</b>	0.044 ± 0.001	0.0004 ± 0.0004
<b>4</b>	0.013 ± 0.003	0.009 ± 0.002
<b>8</b>	0.022 ± 0.003	0.086 ± 0.001
<b>12</b>	0.026 ± 0.003	0.023 ± 0.0004
<b>16</b>	0.011 ± 0.002	0.025 ± 0.001
<b>32</b>	0.002 ± 0.001	0.033 ± 0.001
<b>48</b>	-0.015 ± 0.001	0.037 ± 0.0004
<b>64</b>	-0.031 ± 0.003	0.045 ± 0.0003
<b>80</b>	-0.039 ± 0.002	0.057 ± 0.002

Results are mean ± SD; n = number of replicates.

**Table A2.7: The absorbance values of [HgI<sub>4</sub>][R6G]<sub>2</sub> complex in the spot test mode with the associated Hg<sup>2+</sup> concentrations**

<b>Hg<sup>2+</sup> concentration µg/L</b>	<b>570 nm n=3</b>
<b>2</b>	0.021 ± 0.022
<b>5</b>	0.042 ± 0.092
<b>25</b>	0.051 ± 0.019
<b>50</b>	0.066 ± 0.017
<b>75</b>	0.073 ± 0.028
<b>100</b>	0.091 ± 0.059

Results are mean ± SD; n = number of replicates.

## Appendix 3

Table A3.1: Crystallographic data of rhodamine B thiolactone

<b>Identification code</b>	<b>COBCUS</b>
<b>Empirical formula</b>	$C_{28}H_{30}N_2O_2S$
<b>formula weigh</b>	458.60
<b>crystal system</b>	orthorhombic
<b>space group</b>	P n a 21
<b>cell dimensions</b>	a = 16.0424 (9) Å $\alpha = 90^\circ$ b = 12.1440 (5) Å $\beta = 90^\circ$ c = 12.1109 (5) Å $\gamma = 90^\circ$
<b>volume</b>	2359.43 Å <sup>3</sup>
<b>Temperature</b>	294(2) K
<b>Density</b>	1.236 g/cm <sup>3</sup>

The supplementary crystallographic data for this compound can be obtained free of charge via [www.ccdc.cam.ac.uk/data\\_request/cif](http://www.ccdc.cam.ac.uk/data_request/cif)

### <sup>1</sup>H NMR and <sup>13</sup>C NMR spectra

NMR spectra in CDCl<sub>3</sub> were recorded on a Bruker AV3 400 spectrometer. <sup>1</sup>H NMR (CDCl<sub>3</sub>)  $\delta$  1.17 (t, J = 7.0 Hz, 12H, NCH<sub>2</sub>CH<sub>3</sub>), 3.34 (q, J = 7.2 Hz, 8H, NCH<sub>2</sub>CH<sub>3</sub>), 6.30 (d, J = 8.8 Hz, 2H, xanthene H), 6.34 (d, J = 8.4 Hz, 2H, xanthene H), 6.72 (d, J = 8.8 Hz, 2H, xanthene H), 7.22 (d, J = 7.6 Hz, 1H, ArH), 7.46 (t, J = 7.4 Hz, 1H, ArH), 7.54 (t, J = 7.6 Hz, 1H, ArH), 7.86 (d, J = 7.6 Hz, 1H, ArH). <sup>13</sup>C NMR (CDCl<sub>3</sub>)  $\delta$  12.8, 44.6, 63.0, 97.8, 108.5, 108.8, 122.8, 127.5, 128.4, 130.1, 134.4, 135.8, 148.7, 152.5, 158.2, 198.0

**Table A3.2: The absorbance values for Hg-rhodamine B thiolactone complex at 559 nm vs. Hg<sup>2+</sup> concentration**

<b>Hg<sup>2+</sup>concentration µg/L</b>	<b>Absorbance n=3</b>
<b>10</b>	0.012±0.0003
<b>20</b>	0.016±0.001
<b>30</b>	0.021±0.001
<b>40</b>	0.027±0.0003
<b>50</b>	0.031±0.001
<b>100</b>	0.038±0.0004
<b>200</b>	0.085±0.0001
<b>300</b>	0.143±0.001
<b>400</b>	0.204±0.002
<b>500</b>	0.264±0.001
<b>600</b>	0.318±0.001
<b>700</b>	0.375±0.0001
<b>800</b>	0.433±0.0004
<b>900</b>	0.470±0.0003
<b>1000</b>	0.525±0.001

Results are mean ± SD; n = number of replicates.

**Table A3.3: Sea salt composition used to prepare the artificial seawater**

<b>Sea salt ASTM D1141-98</b>	<b>Gradient %</b>	<b>Concentration in seawater g/L</b>
<b>NaCl</b>	58.5	24.5
<b>MgCl<sub>2</sub>-6H<sub>2</sub>O</b>	26.5	5.20
<b>Na<sub>2</sub>SO<sub>4</sub></b>	9.75	4.09
<b>CaCl<sub>2</sub></b>	2.77	1.16
<b>KCl</b>	1.65	0.695
<b>NaHCO<sub>3</sub></b>	0.477	0.201
<b>KBr</b>	0.238	0.101
<b>H<sub>3</sub>BO<sub>3</sub></b>	0.071	0.027
<b>SrCl<sub>2</sub>-6H<sub>2</sub>O</b>	0.095	0.025
<b>NaF</b>	0.007	0.003

## Appendix 4

**Table A4.1: Characteristic data of the chromatic analysis in  $G_R$ ,  $G_G$  and  $G_B$  colour measures for determination of  $Hg^{2+}$  on the exposed sol-gel membranes with ImageJ software**

<b>Hg<sup>2+</sup>concentration μg/L</b>	<b>G<sub>R</sub> n=3</b>	<b>G<sub>G</sub> n=3</b>	<b>G<sub>B</sub> n=3</b>
<b>0.4</b>	3.18 ± 0.664	3.06 ± 0.659	4.38 ± 0.889
<b>0.6</b>	1.68 ± 0.535	3.52 ± 0.524	1.95 ± 0.574
<b>0.8</b>	2.84 ± 0.195	5.28 ± 0.454	3.51 ± 0.768
<b>1</b>	3.34 ± 0.757	9.41 ± 0.789	5.88 ± 0.256
<b>2</b>	4.16 ± 0.416	13.3 ± 2.83	6.18 ± 1.73
<b>3</b>	4.86 ± 0.859	22.2 ± 2.37	6.69 ± 0.863
<b>4</b>	4.40 ± 0.659	26.6 ± 3.19	6.12 ± 0.896
<b>5</b>	7.96 ± 2.68	38.9 ± 0.648	9.61 ± 4.05
<b>10</b>	9.51 ± 1.16	47.3 ± 1.64	10.8 ± 1.32
<b>20</b>	11.8 ± 0.599	50.9 ± 6.17	12.6 ± 1.59

Results are mean ± SD; n = number of replicates.

**Table A4.2: Characteristic data of the chromatic analysis in  $G_R$ ,  $G_G$  and  $G_B$  colour measures for determination of  $Hg^{2+}$  on the exposed agar-agar membranes with ImageJ software**

<b>Hg<sup>2+</sup>concentration μg/L</b>	<b>G<sub>R</sub> n=3</b>	<b>G<sub>G</sub> n=3</b>	<b>G<sub>B</sub> n=3</b>
<b>0.2</b>	3.34 ± 0.823	7.13 ± 1.05	4.99 ± 1.21
<b>0.4</b>	4.46 ± 0.417	10.8 ± 1.24	4.64 ± 0.655
<b>0.6</b>	4.37 ± 0.612	13.2 ± 2.26	5.89 ± 0.967
<b>0.8</b>	5.33 ± 1.12	17.0 ± 4.27	6.93 ± 1.11
<b>1</b>	7.86 ± 0.593	22.4 ± 2.97	8.74 ± 0.669
<b>2</b>	10.9 ± 4.78	33.4 ± 5.32	12.4 ± 4.12
<b>3</b>	13.6 ± 1.17	45.3 ± 6.23	12.3 ± 0.757
<b>4</b>	12.6 ± 2.66	54.8 ± 9.44	11.5 ± 1.21
<b>5</b>	14.2 ± 4.82	62.5 ± 6.70	12.9 ± 2.96
<b>6</b>	15.1 ± 0.669	75.1 ± 2.38	12.5 ± 0.857
<b>8</b>	17.2 ± 1.15	80.2 ± 9.12	15.3 ± 0.519
<b>10</b>	16.7 ± 0.920	88.4 ± 7.76	14.3 ± 1.11
<b>20</b>	20.2 ± 0.768	113 ± 5.64	16.8 ± 1.86

Results are mean ± SD; n = number of replicates.

**Table A4.3: Grayscale intensity in  $G_G$  of the immobilised agar-agar membranes kept in open air for different time intervals**

<b>Agar-agar concentration (w/v)</b>	<b>0 week n=3</b>	<b>1 week n=3</b>	<b>2 weeks n=3</b>	<b>3 weeks n=3</b>
<b>1%</b>	4.34 ± 0.368	10.1 ± 1.08	25.2 ± 0.706	37.8 ± 3.08
<b>2%</b>	4.60 ± 2.34	10.7 ± 1.81	16.4 ± 1.19	28.5 ± 1.90
<b>3%</b>	3.60 ± 2.11	10.3 ± 1.27	14.1 ± 0.992	30.1 ± 1.40
<b>4%</b>	3.92 ± 2.04	10.5 ± 1.33	15.8 ± 1.03	18.9 ± 1.00
<b>5%</b>	4.58 ± 1.42	10.5 ± 1.80	11.2 ± 0.534	17.8 ± 1.89

Results are mean ± SD; n = number of replicates.

**Table A4.4: Effect of water sample volumes on the colorimetric response in  $G_G$  of the immobilised agar-agar membranes. Typical  $Hg^{2+}$  concentration was 5 µg/L**

<b>Hg<sup>2+</sup> Sample volume (mL) (nmole)</b>	<b>Concentration of rhodamine B thiolactone in the agar-agar membranes mole, n=3</b>		
	<b>5.0×10<sup>-6</sup></b>	<b>7.5×10<sup>-6</sup></b>	<b>1.0×10<sup>-5</sup></b>
<b>50 (1.25)</b>	11.5 ± 7.48	12.4 ± 3.61	12.2 ± 2.83
<b>100 (2.5)</b>	25.9 ± 5.66	22.2 ± 10.7	22.5 ± 7.01
<b>150 (3.75)</b>	35.7 ± 3.35	28.8 ± 9.97	29.5 ± 11.9
<b>200 (5)</b>	43.9 ± 4.41	40.4 ± 4.52	37.6 ± 6.97
<b>300 (7.5)</b>	53.7 ± 8.96	53.3 ± 4.94	47.5 ± 6.11
<b>500 (12.5)</b>	66.6 ± 8.30	61.3 ± 2.63	56.3 ± 7.17
<b>700 (17.5)</b>	75.4 ± 7.44	-	-
<b>1000 (25)</b>	81.1 ± 8.17	-	-

Results are mean ± SD; n = number of replicates.

**Table A4.5: Effect of water sample volumes on the colorimetric response in  $G_G$  of the immobilised agar-agar membranes. Typical  $Hg^{2+}$  concentration was 10  $\mu g/L$**

<b>Hg<sup>2+</sup> Sample volume (mL) (nmole)</b>	<b>Concentration of rhodamine B thiolactone in the agar-agar membranes mole, n=3</b>		
	<b>5.0×10<sup>-6</sup></b>	<b>7.5×10<sup>-6</sup></b>	<b>1.0×10<sup>-5</sup></b>
<b>50 (2.5)</b>	30.9 ± 7.06	24.6 ± 8.02	39.1 ± 11.6
<b>100 (5)</b>	46.5 ± 6.58	41.2 ± 9.09	57.4 ± 10.2
<b>150 (7.5)</b>	62.6 ± 2.83	53.9 ± 11.1	73.6 ± 6.06
<b>200 (10)</b>	70.6 ± 5.00	71.4 ± 7.06	85.1 ± 7.36
<b>300 (15)</b>	89.9 ± 9.33	88.5 ± 1.67	102 ± 9.87
<b>500 (25)</b>	101 ± 9.29	97.3 ± 6.31	116 ± 9.67
<b>700 (35)</b>	110 ± 8.39	-	-
<b>1000 (50)</b>	117 ± 10.9	-	-

Results are mean ± SD; n = number of replicates.

**Table A4.6: Effect of colorant reagent volume on the colorimetric response in  $G_G$  of the immobilised agar-agar membranes**

<b>Colorant reagent volume added to each 5 mL Agar-agar (mole)</b>	<b>Hg<sup>2+</sup> concentration <math>\mu g/L</math>, n=3</b>	
	<b>5</b>	<b>10</b>
<b>0.5 mL (2.5×10<sup>-6</sup>)</b>	37.2 ± 8.67	68.1 ± 6.91
<b>1 mL (5×10<sup>-6</sup>)</b>	50.8 ± 9.37	89.1 ± 5.19
<b>1.5 mL (7.5×10<sup>-6</sup>)</b>	51.2 ± 3.85	88.5 ± 1.67
<b>2 mL (1×10<sup>-5</sup>)</b>	54.6 ± 8.25	102 ± 9.87

Results are mean ± SD; n = number of replicates

**Table A4.7: F-test for the colorimetric response in  $G_G$  of the different colorant reagent concentrations loaded in the agar-agar membranes**

<b>Hg<sup>2+</sup> concentration µg/L</b>	<b>Between 2.5×10<sup>-6</sup> and 5×10<sup>-6</sup>, v=2</b>		<b>Between 2.5×10<sup>-6</sup> and 7.5×10<sup>-6</sup>, v=2</b>		<b>Between 2.5×10<sup>-6</sup> and 1×10<sup>-5</sup>, v=2</b>		<b>Between 5×10<sup>-6</sup> and 7.5×10<sup>-6</sup>, v=2</b>		<b>Between 5×10<sup>-6</sup> and 1×10<sup>-5</sup>, v=2</b>		<b>Between 7.5×10<sup>-6</sup> and 1×10<sup>-5</sup>, v=2</b>	
	F calculated	F critical	F calculated	F critical	F calculated	F critical	F calculated	F critical	F calculated	F critical	F calculated	F critical
<b>5</b>	1.17	19	5.07	19	1.10	19	5.92	19	1.29	19	4.59	19
<b>10</b>	1.77	19	17.0	19	2.04	19	9.60	19	3.61	19	<u>34.7</u>	19

v = degree of freedom; A significance level ( $\alpha$ ) = 0.05

**Table A4.8: t-test of the colorimetric response in  $G_G$  of the different colorant reagent concentrations loaded in the agar-agar membranes**

<b>Hg<sup>2+</sup> concentration µg/L</b>	<b>Between 2.5×10<sup>-6</sup> and 5×10<sup>-6</sup>, v=4</b>		<b>Between 2.5×10<sup>-6</sup> and 7.5×10<sup>-6</sup>, v=4</b>		<b>Between 2.5×10<sup>-6</sup> and 1×10<sup>-5</sup>, v=4</b>		<b>Between 5×10<sup>-6</sup> and 7.5×10<sup>-6</sup>, v=4</b>		<b>Between 5×10<sup>-6</sup> and 1×10<sup>-5</sup>, v=4</b>		<b>Between 7.5×10<sup>-6</sup> and 1×10<sup>-5</sup>, v=4</b>	
	t calculated	t critical	t calculated	t critical	t calculated	t critical	t calculated	t critical	t calculated	t critical	t calculated	t critical
<b>5</b>	1.84	2.78	2.56	2.78	2.51	2.78	0.076	2.78	0.525	2.78	0.636	2.78
<b>10</b>	<u>4.20</u>	2.78	<u>4.96</u>	2.78	<u>4.92</u>	2.78	0.196	2.78	2.06	2.78	2.40	4.30

v = degree of freedom; A significance level ( $\alpha$ ) = 0.05

**Table A4.9: The grayscale intensity of the exposed sol-gel membranes vs. Hg<sup>2+</sup> concentration**

<b>Hg<sup>2+</sup> concentration µg/L</b>	<b>G<sub>G</sub> n=3</b>
<b>0.4</b>	3.06 ± 0.659
<b>0.6</b>	3.52 ± 0.524
<b>0.8</b>	5.28 ± 0.454
<b>1</b>	9.41 ± 0.789
<b>2</b>	13.3 ± 2.83
<b>3</b>	22.2 ± 2.37
<b>4</b>	26.6 ± 3.19
<b>5</b>	38.9 ± 0.648

Results are mean ± SD; n = number of replicates.

**Table A4.10: The precision (%RSD) of the calibration curves of the colorimetric response in  $G_G$  of the Hg-rhodamine B thiolactone formed on the agar-agar membranes obtained with three repeated experiments (n=3) vs.  $Hg^{2+}$  concentration**

No. of Exp.	$Hg^{2+}$ concentration $\mu g/L$ , n=3									
	0.2	0.4	0.6	0.8	1	2	3	4	5	6
<b>Exp. 1</b>	7.13 ± 1.05	10.8 ± 1.24	13.3 ± 2.26	17.0 ± 4.27	22.4 ± 2.97	33.4 ± 5.32	45.3 ± 6.23	54.8 ± 9.44	62.5 ± 6.70	75.1 ± 2.38
<b>Exp. 2</b>	5.98 ± 1.76	10.6 ± 0.760	13.6 ± 2.01	15.1 ± 1.80	21.1 ± 1.95	28.0 ± 3.77	37.2 ± 1.55	45.4 ± 2.56	52.7 ± 6.74	79.4 ± 2.59
<b>Exp. 3</b>	5.80 ± 0.726	10.3 ± 0.708	12.0 ± 0.656	14.7 ± 1.08	16.5 ± 1.39	26.2 ± 4.07	46.6 ± 2.85	50.6 ± 13.2	59.9 ± 13.1	69.7 ± 1.39
<b>Total</b>	<b>6.30 ± 0.724</b>	<b>10.6 ± 0.257</b>	<b>12.9 ± 0.851</b>	<b>15.6 ± 1.25</b>	<b>20.0 ± 3.10</b>	<b>29.2 ± 3.74</b>	<b>43.0 ± 5.06</b>	<b>50.3 ± 4.69</b>	<b>58.4 ± 5.08</b>	<b>74.7 ± 4.84</b>
<b>%RSD</b>	<b>11.5</b>	<b>2.43</b>	<b>6.58</b>	<b>7.99</b>	<b>15.5</b>	<b>12.8</b>	<b>11.8</b>	<b>9.33</b>	<b>8.71</b>	<b>6.48</b>

Results are mean ± SD; n = number of replicates; %RSD = relative standard deviation.

**Table A4.11: The grayscale intensity in  $G_G$  of the sol-gel membranes kept in different storage conditions**

Weeks	Room temperature n=3	Ascorbic acid n=3	Oxygen absorber n=3	Fridge n=3	Dark place n=3
0	3.71 ± 0.077	3.71 ± 0.077	3.71 ± 0.077	3.71 ± 0.077	3.71 ± 0.077
1	28.0 ± 2.41	9.96 ± 0.144	4.47 ± 0.323	4.02 ± 0.081	20.9 ± 1.68
3	54.3 ± 0.716	10.9 ± 0.412	3.60 ± 0.159	3.28 ± 0.116	22.3 ± 3.10
5	65.2 ± 0.700	15.7 ± 0.662	8.34 ± 1.38	4.75 ± 0.160	24.3 ± 1.64
7	69.5 ± 1.05	17.6 ± 0.356	8.41 ± 0.987	5.49 ± 1.04	26.0 ± 2.61
12	70.8 ± 5.23	26.1 ± 2.05	10.2 ± 1.52	5.21 ± 1.57	29.3 ± 1.63

Results are mean ± SD; n = number of replicates.

**Table A4.12: The grayscale intensity in  $G_G$  of the stored sol-gel membranes. The membranes were exposed to 10 µg/L  $Hg^{2+}$  standard solution**

Weeks	Ascorbic acid n=3	Oxygen absorber n=3	Fridge n=3
0	67.6 ± 3.15	67.6 ± 3.15	67.6 ± 3.15
1	71.2 ± 0.946	65.9 ± 3.42	64.2 ± 1.01
3	65.1 ± 3.91	65.4 ± 1.54	63.9 ± 6.16
5	55.6 ± 1.78	66.0 ± 1.04	62.3 ± 5.75
7	35.9 ± 8.68	63.1 ± 4.88	60.5 ± 13.5
12	30.2 ± 10.3	66.2 ± 2.61	57.3 ± 9.77

Results are mean ± SD; n = number of replicates.

**Table A4.13: The grayscale intensity in  $G_G$  of the agar-agar membranes kept in different storage conditions**

Weeks	Room temperature n=3	Stord in 5%(w/v) agar n=3	Dark place n=3
0	4.26 ± 0.157	4.26 ± 0.157	4.26 ± 0.157
1	10.3 ± 0.974	6.76 ± 0.652	7.61 ± 0.576
3	36.5 ± 5.28	11.0 ± 1.28	8.98 ± 0.196
5	43.9 ± 4.13	17.3 ± 0.465	7.89 ± 0.604
7	47.9 ± 3.36	20.3 ± 3.07	7.42 ± 0.796
12	49.9 ± 6.29	89.8 ± 3.93	8.77 ± 1.61

Results are mean ± SD; n = number of replicates.

**Table A4.14: The grayscale intensity in  $G_G$  of the stored agar-agar membranes. The membranes were exposed to 10  $\mu\text{g/L}$   $\text{Hg}^{2+}$  standard solution**

<b>weeks</b>	<b>Stored in 5%(w/v) agar n=3</b>	<b>Dark place n=3</b>
<b>0</b>	88.4 $\pm$ 7.76	88.4 $\pm$ 7.76
<b>1</b>	71.6 $\pm$ 4.33	83.9 $\pm$ 13.9
<b>3</b>	47.0 $\pm$ 3.35	84.0 $\pm$ 3.32
<b>5</b>	35.5 $\pm$ 5.65	79.2 $\pm$ 4.37
<b>7</b>	33.3 $\pm$ 4.75	88.3 $\pm$ 6.55
<b>12</b>	11.0 $\pm$ 7.96	82.2 $\pm$ 6.58

Results are mean  $\pm$  SD; n = number of replicates.

**Table A4.15: The grayscale intensity in  $G_G$  of the agar-agar membranes exposed to 2  $\mu\text{g/L}$   $\text{Hg}^{2+}$  solutions**

<b><math>\text{Hg}(\text{NO}_3)_2</math> n=3</b>	<b><math>\text{HgCl}_2</math> n=3</b>
30.0 $\pm$ 1.31	28.3 $\pm$ 3.54

Results are mean  $\pm$  SD; n = number of replicates.

**Table A4.16: The grayscale intensity of the agar-agar membranes exposed to  $\text{Hg}^{2+}$  solutions of 10  $\mu\text{g/L}$  with a spike amount of  $\text{Cl}^-$  concentration ranging from 0 to 14700 mg/L**

<b><math>\text{Cl}^-</math> concentration mg/l</b>	<b><math>G_G</math>, n=3</b>
<b>0</b>	82.2 $\pm$ 6.57
<b>3</b>	65.1 $\pm$ 4.19
<b>13.8</b>	56.9 $\pm$ 3.39
<b>57</b>	49.2 $\pm$ 4.50
<b>229</b>	29.6 $\pm$ 6.98
<b>918</b>	19.1 $\pm$ 7.12
<b>3678</b>	9.24 $\pm$ 0.108
<b>14700</b>	1.53 $\pm$ 0.374

Results are mean  $\pm$  SD; n = number of replicates.

**Table A4.17: The grayscale intensity of the agar-agar membranes exposed to Hg<sup>2+</sup>solutions of 10 µg/L with a spike amount of Cl<sup>-</sup> concentration ranging from 0 to 50 mg/L**

<b>Cl<sup>-</sup> concentration mg/l</b>	<b>G<sub>G</sub>, n=3</b>
<b>0</b>	87.7 ± 5.38
<b>10</b>	78.4 ± 9.72
<b>20</b>	69.1 ± 8.74
<b>30</b>	67.1 ± 8.98
<b>40</b>	65.2 ± 6.75
<b>50</b>	61.5 ± 6.18

Results are mean ± SD; n = number of replicates.

**Table A4.18: The UV absorbance measurement at a wavelength of 254 nm for the real water samples analysed. Absorbance values were recorded before and after acidifying to pH 2.0 with HNO<sub>3</sub>**

<b>Bottled water n=3</b>		<b>Tap water n=3</b>		<b>Stream water 1 n=3</b>		<b>Stream water 2 n=3</b>	
Before	After	Before	After	Before	After	Before	After
-0.001 ± 0.0002	-0.001 ± 0.001	-0.062 ± 0.0004	-0.061 ± 0.001	0.727 ± 0.001	0.714 ± 0.001	0.483 ± 0.001	0.520 ± 0.001

Results are mean ± SD; n = number of replicates.

**Table A4.19: The grayscale intensity of immobilised agar-agar membranes exposed to 10 µg/L Hg<sup>2+</sup>, then treated with a solution of KI for several cycles.**

<b>No. of cycles</b>	<b>G<sub>G</sub>, n=3</b>
<b>#1 Recycle</b>	83.4 ± 4.78
<b>#2 Recycle</b>	82.7 ± 7.30
<b>#3 Recycle</b>	84.1 ± 4.43
<b>#4 Recycle</b>	85.8 ± 3.66

Results are mean ± SD; n = number of replicates.

## Appendix 5

**Table A5.1: The grayscale intensity of the coloured agar-agar membrane captured using the built-in digital camera in an iPhone/HG-Sense App. Images were captured without a lightproof box**

<b>Lighting condition</b>	<b>G<sub>G</sub>, n=3</b>	<b>%RSD</b>
<b>Artificial room light</b>	81.6 ± 18.6	22.8
<b>Artificial room light + Flash</b>	44.0 ± 2.65	6.01
<b>Dark place</b>	21.3 ± 3.06	14.3
<b>Dark + Flash</b>	43.6 ± 5.68	13.0
<b>Day light</b>	52.3 ± 17.2	32.9

Results are mean ± SD; n = number of replicates; %RSD = relative standard deviation.

**Table A5.2: The grayscale intensity of the coloured agar-agar membrane captured at different distances between the built-in digital camera in an iPhone and the membrane. Images were captured under artificial room light**

<b>Distance, cm</b>	<b>G<sub>G</sub>, n=3</b>	<b>%RSD</b>
<b>5</b>	81.7 ± 18.6	22.8
<b>10</b>	53.0 ± 1.00	1.89
<b>15</b>	61.0 ± 2.65	4.34
<b>20</b>	65.3 ± 5.51	8.43
<b>25</b>	51.0 ± 2.65	5.19
<b>30</b>	52.7 ± 2.08	3.95

Results are mean ± SD; n = number of replicates; %RSD = relative standard deviation.

**Table A5.3: The grayscale intensity of the coloured agar-agar membrane captured using the built-in digital camera in an iPhone/HG-Sense App. Images were captured inside a lightproof box**

<b>Lighting condition</b>	<b>G<sub>G</sub>, n=3</b>	<b>%RSD</b>
<b>Room light</b>	36.3 ± 1.53	4.20
<b>Dark place</b>	36.6 ± 1.53	4.16
<b>Day light</b>	37.3 ± 1.15	3.09

Results are mean ± SD; n = number of replicates; %RSD = relative standard deviation.

**Table A5.4: The grayscale intensity of the measurements taken using the HG-Sense App for iPhone and ImageJ for desktop scanner**

<b>Hg<sup>2+</sup> concentration µg/L, n=1</b>	<b>Scanner/ImageJ GG</b>	<b>iPhone/HG-Sense App GG</b>
<b>10</b>	83.2	55.0
	84.8	51.0
	84.4	45.0
	85.4	47.0
	84.6	41.0
	86.2	45.0
	85.2	50.0
	85.3	43.0
	85.7	55.0
	85.0	51.0
<b>Total GG</b>	<b>85.00 ± 0.815</b>	<b>48.3 ± 4.85</b>
<b>%RSD</b>	<b>0.959</b>	<b>10.1</b>

Results are mean ± SD; n = number of replicates; %RSD = relative standard deviation.

**Table A5.5: The correlation of the grayscale intensities between the portable HG-Sense App method and the lab-based ImageJ method**

<b>Hg<sup>2+</sup> concentration µg/L</b>	<b>Scanner/ImageJ GG, n=3</b>	<b>iPhone/HG-Sense App GG, n=3</b>
<b>0.2</b>	5.80 ± 0.725	-34.0 ± 9.46
<b>0.4</b>	10.3 ± 0.708	-30.6 ± 12.2
<b>0.6</b>	11.9 ± 0.656	-28.3 ± 6.81
<b>0.8</b>	14.7 ± 1.08	8.00 ± 10.4
<b>1</b>	16.5 ± 1.39	15.0 ± 12.3
<b>2</b>	26.2 ± 4.07	18.0 ± 11.5
<b>3</b>	46.5 ± 2.85	20.6 ± 3.79
<b>4</b>	50.6 ± 13.2	26.0 ± 6.25
<b>5</b>	59.9 ± 13.1	36.7 ± 13.7
<b>6</b>	69.2 ± 1.39	54.0 ± 9.54
<b>8</b>	77.4 ± 8.90	58.0 ± 14.6
<b>10</b>	80.6 ± 8.26	62.0 ± 2.65
<b>20</b>	98.5 ± 4.31	43.3 ± 5.86

Results are mean ± SD; n = number of replicates.

**Table A5.6: Comparison between the  $G_G$  values obtained using the HG-Sense App from two pumps**

$Hg^{2+}$ concentration $\mu g/L$	Single-Channel pump	Multi-Channel pump
<b>1</b>	$16.6 \pm 0.379$	$16.5 \pm 1.39$
<b>5</b>	$60.2 \pm 7.91$	$59.9 \pm 13.1$
<b>10</b>	$81.5 \pm 8.36$	$80.6 \pm 8.26$

Results are mean  $\pm$  SD; n = number of replicates.

**Table A5.7: F-test for the colorimetric response in  $G_G$  of the two used pumps at different  $Hg^{2+}$  concentrations**

Between $Hg^{2+}$ concentration of 1 $\mu g/L$ , $v=2$		Between $Hg^{2+}$ concentration of 5 $\mu g/L$ , $v=2$		Between $Hg^{2+}$ concentration of 10 $\mu g/L$ , $v=2$	
F calculated	F critical	F calculated	F critical	F calculated	F critical
13.4	19	2.75	19	1.02	19

$v$  = degree of freedom; A significance level ( $\alpha$ ) = 0.05

**Table A5.8: t-test for the colorimetric response in  $G_G$  of the two used pumps at different  $Hg^{2+}$  concentrations**

Between $Hg^{2+}$ concentration of 1 $\mu g/L$ , $v=4$		Between $Hg^{2+}$ concentration of 5 $\mu g/L$ , $v=4$		Between $Hg^{2+}$ concentration of 10 $\mu g/L$ , $v=4$	
t calculated	t critical	t calculated	t critical	t calculated	t critical
0.135	2.78	0.026	2.78	0.127	2.78

$v$  = degree of freedom; A significance level ( $\alpha$ ) = 0.05

**Table A5.9: Calibration curves of the colorimetric response in  $G_G$  using the HG-Sense App of the Hg-rhodamine B thiolactone formed on the agar-agar membranes obtained with three repeated experiments (n=3) vs.  $Hg^{2+}$  concentration.**

No. of Exp.	$Hg^{2+}$ concentration $\mu g/L$ , n=3							
	0.8	1	2	3	4	5	6	8
<b>Exp. 1</b>	8.00 $\pm$ 10.4	15.0 $\pm$ 12.3	18.0 $\pm$ 11.5	20.6 $\pm$ 3.79	26.0 $\pm$ 6.24	36.6 $\pm$ 13.7	54.0 $\pm$ 9.54	58.0 $\pm$ 14.6
<b>Exp. 2</b>	6.33 $\pm$ 5.69	17.3 $\pm$ 2.51	18.0 $\pm$ 3.00	17.6 $\pm$ 3.21	23.0 $\pm$ 7.81	34.0 $\pm$ 2.65	52.0 $\pm$ 8.54	59.3 $\pm$ 14.2
<b>Exp. 3</b>	5.66 $\pm$ 4.04	10.0 $\pm$ 2.00	13.0 $\pm$ 6.00	25.0 $\pm$ 6.24	28.0 $\pm$ 4.00	36.0 $\pm$ 7.55	47.7 $\pm$ 2.51	57.0 $\pm$ 5.00
<b>Total</b>	<b>6.67 <math>\pm</math> 1.20</b>	<b>14.1 <math>\pm</math> 3.75</b>	<b>16.3 <math>\pm</math> 2.89</b>	<b>21.1 <math>\pm</math> 3.69</b>	<b>25.7 <math>\pm</math> 2.52</b>	<b>35.6 <math>\pm</math> 1.38</b>	<b>51.2 <math>\pm</math> 3.23</b>	<b>58.1 <math>\pm</math> 1.17</b>
<b>%RSD</b>	<b>18.0</b>	<b>26.6</b>	<b>17.7</b>	<b>17.5</b>	<b>9.80</b>	<b>3.90</b>	<b>6.32</b>	<b>2.01</b>

Results are mean  $\pm$  SD; n = number of replicates; %RSD = relative standard deviation.